CSIRO LAND AND WATER
www.csiro.au

Hydroclimate of the Pilbara: past, present and future

A technical report to the Government of Western Australia and industry partners from the CSIRO Pilbara Water Resource Assessment

Stephen Charles, Guobin Fu, Richard Silberstein, Freddie Mpelasoka, Don McFarlane, Geoff Hodgson, Jin Teng, Christina Gabrovesk, Riasat Ali, Olga Barron, Santosh Aryal and Warrick Dawes

CSIRO Land and Water

7 October 2015

Department of Water
Department of Regional Development
PILBARA DEVELOPMENT COMMISSION
PILBARA CITIES
ROYALTIES FOR REGIONS
bhpbilliton resourcing the future

CSIRO Land and Water

CSIRO Land and Water provides the science to underpin Australia's economic, social and environmental prosperity through stewardship of land and water resources, ecosystems, and urban areas.

For more information visit <http://www.csiro.au/Research/LWF>.

Citation

Charles SP, Fu G, Silberstein RP, Mpelasoka F, McFarlane D, Hodgson G, Teng J, Gabrovsek C, Ali R, Barron O, Aryal SK and Dawes W (2015) Hydroclimate of the Pilbara: past, present and future. A report to the Government of Western Australia and industry partners from the CSIRO Pilbara Water Resource Assessment. CSIRO Land and Water, Australia.

ISBN 978-1-4863-0546-9

Copyright and disclaimer

© 2015 CSIRO To the extent permitted by law, all rights are reserved and no part of this publication covered by copyright may be reproduced or copied in any form or by any means except with the written permission of CSIRO.

Important disclaimer

CSIRO advises that the information contained in this publication comprises general statements based on scientific research. The reader is advised and needs to be aware that such information may be incomplete or unable to be used in any specific situation. No reliance or actions must therefore be made on that information without seeking prior expert professional, scientific and technical advice. To the extent permitted by law, CSIRO (including its employees and consultants) excludes all liability to any person for any consequences, including but not limited to all losses, damages, costs, expenses and any other compensation, arising directly or indirectly from using this publication (in part or in whole) and any information or material contained in it.

Pilbara Water Resource Assessment acknowledgments

This report was prepared by CSIRO for the West Australian Government and industry partners – BHP Billiton, West Australian Department of Water, Water Corporation, Pilbara Development Commission, and the Department of Regional Development.

The project was led by a Steering Committee that consisted of Greg Claydon (DoW, Chair), Blair Douglas (BHP Billiton), Warwick McDonald (CSIRO), Hamid Mohsenzedah (DoW), Paul Vanderwal (Water Corporation) and Gus Tampalini (PDC). People who served on the Committee in early stages of the project were Patrick Seares (DoW, Chair), Glen Walker (CSIRO), Keith Anthonisz (DRDL, PDC), Kevin Lee (PDC), Paul Trotman (PDC) and Richard Bairstow (PDC).

The interim version of this report benefited from formal reviews by Glenn Cook and Mohammed Bari, Bureau of Meteorology, and Cuan Petheram and Mike Pook, CSIRO. It also benefited from review comments from the three Technical Advisory Committees (Surface Water Hydrology, Groundwater and Water Dependant Ecosystems). Helpful input was also received from Richard Dare, Bureau of Meteorology; Tom van Neil, Francis Chiew, Deborah Abbs and Sally Lavender, CSIRO; and Pauline Grierson, UWA.

Foreword

As the leading iron ore mining region of Australia and the base of some of the nation's largest offshore oil and gas fields, the Pilbara has been undergoing significant growth and development.

With this economic growth has come an increased demand for water to support industry and a growing population.

The Pilbara economy is dominated by the extraction, processing and export of minerals and gas. Industrial water use includes dust suppression associated with bulk handling of ore and other uses at the coastal ports of Port Hedland, Dampier, Cape Lambert and Ashburton, and oil and gas, salt and ammonium nitrate production.

The Pilbara is also home to a number of groundwater-dependent ecosystems and riverine pools, which have enormous ecological, Aboriginal cultural, social and tourism values, given that they occupy less than half of one percent of a semi-arid area in one of the hottest parts of Australia.

The Western Australian Government is committed to delivering a sustainable water future that provides certainty for business investment in the Pilbara, and supports the Pilbara Regional Investment Blueprint objectives and Pilbara Cities vision of Karratha and Port Hedland transforming into regional centres of 50,000 people. It is also working to use water availability to lift the productivity of irrigated agriculture and livestock in the region by expanding existing precincts and starting new ones under the $40 million Royalties for Regions funded Water for Food initiative.

To do this, we need the confidence to set out how much water is available to support the region's growth, as well as to meet the environmental needs of the Pilbara's surface water and groundwater resources and their dependent values.

To date, groundwater investigations, water allocation planning and water supply planning have been undertaken about the water available in the Pilbara to meet sustainable development objectives of Pilbara coastal towns and industry.

Water use in the Pilbara is dominated by mining, with current water abstraction for the mining sector estimated to be around 550 GL/year, with around 250 GL/year of this water used for ore processing, dust suppression, consumption and other purposes. Through Pilbara water supply planning work undertaken by the Western Australian Department of Water, projected total water demand for the Pilbara region is expected to more than double by 2042 under a medium growth scenario.

The Pilbara has a highly variable climate with rain coming mainly from unpredictable thunderstorms and tropical cyclones over summer. The historical records show that there can be long periods of drought when summer rains fail and there is no wet season.

Understanding how future climate scenarios may change climatic conditions and consequently alter surface water volumes and groundwater recharge is an important piece to the jigsaw puzzle that will enable sustainable and effective management of water in the region.

The Department of Water, the Pilbara Development Commission and BHP Billiton agreed to partner with CSIRO to do this work and continue building the knowledge base to underpin future water resource management in the Pilbara. CSIRO had been involved in similar assessments throughout Australia, including in the south-west of Western Australia, so a nationally consistent, but regionally calibrated, approach was taken in this assessment. Funding for the $3.5 million project came from $1.5 million contributions each by CSIRO and the State Government through Royalties for Regions, and $0.5 million from BHP.

A Steering Committee consisting of representatives from the Department of Water, Pilbara Development Commission, BHP Billiton, CSIRO and Water Corporation, and several specialist technical committees,

provided substantial guidance to CSIRO throughout the project which had an assessment area of almost 300,000 km^2.

The Pilbara Water Resource Assessment project required several innovative assessment methods to be used, including remote sensing methods for groundwater-dependent ecosystems, hydrological interpretations, landscape and water resources characterisations, updated numerical modelling and the latest climate science.

The assessment indicates that the Pilbara is likely to be even hotter in the future, while rainfall patterns will continue to be highly variable with no clear wetting or drying trends. Even so, the assessment has increased our understanding of the climate and the water resources of the region in an otherwise uncertain environment and with otherwise uncertain changes to the climate.

Among other things, the reports and products from the assessment will be valuable for future decisions about water supplies and allocations in the region, and for carrying out strategic water and environmental assessments for new mining and other developments.

As Chairman of the Steering Committee of partners, I recommend these reports to you. The information will be helpful to the management of water in one of the hottest, driest and most economically important regions of Australia.

Greg Claydon

Chairman, Pilbara Water Resource Assessment Steering Committee

Contents

Figures

Tables

Contributors to the Pilbara Water Resource Assessment

Project Director	Warwick McDonald
Project Manager	Don McFarlane
Climate	Steve Charles, Guobin Fu, Freddie Mpelesoka, Jin Teng, Francis Chiew BoM: Glenn Cook
Data Management	Geoff Hodgson, Christina Gabrovsek DoW: Lindsay Preece, John Patten, Goran Alibegovic
Surface Water Hydrology	Richard Silberstein, Santosh Aryal DoW: Jacqui Durrant, Simon Rogers BoM: Mohammad Bari Water Corporation: Charles Jeevaraj BHP Billiton: Iain Rea RPS Australia Asia Pacific: Vince Piper
Groundwater	Riasat Ali, Warrick Dawes, Phil Commander, Rodrigo Rojas, Glen Walker DoW: Hazli Koomberi, Gary Humphreys, Hamid Mohsenzedah, Scott Macaulay BHP Billiton: Blair Douglas, Damien Janssen, Jed Youngs HydroConcept Pty Ltd: Seth Johnson MWH: Gary Clark
Groundwater-Dependent Ecosystems	Olga Barron, Irina Emelyanova DoW: Mike Braimbridge, Penny Wallace-Bell DPaW: Stephen van Leeuwen, Adrian Pinder Equinox Environmental Pty Ltd: Dan Huxtable UWA: Pauline Grierson WRM: Andrew Storey BHP Billiton: Lucinda Ransom ECU: Masoomeh Alibakhsh
Reporting	Maryam Ahmad, Daniel Aramini, Sonja Chandler, Cuan Petheram, Becky Schmidt
Communications	Leane Regan, Rebecca Jennings, Anne McKenzie, Chris McKay DoW: Verity Klemm, Peter Collins BHP Billiton: Robert Carruthers, Leanne Franco PDC: Lisa Mayne, Rebecca Jarvis Water Corporation: Emily Hunter

Note: all contributors are affiliated with CSIRO unless indicated otherwise. Activity Leaders are underlined. Many members contribute to more than one activity but are only listed once.

Shortened forms

BOM	Bureau of Meteorology
CCAM	Conformal-Cubic Atmospheric Model
CSIRO	Commonwealth Scientific and Industrial Research Organisation
DJF	December January February
DMI	Dipole Mode Index
DTD	Dew-point temperature depression
ENSO	El Niño Southern Oscillation
EPI	East Pole index
ESIO	East southern Indian Ocean
GCM	Global Climate Model
GDE	Groundwater-dependent ecosystems
GDV	Groundwater-dependent terrestrial vegetation
IFD	Intensity-frequency-duration
IOCI	Indian Ocean Climate Initiative
IOD	Indian Ocean Dipole
IPCC	Intergovernmental Panel on Climate Change
JJA	June July August
MAM	March April May
MJO	Madden-Julian Oscillation
MSLP	Mean sea-level pressures
NHMM	Non-homogeneous hidden Markov model
OLR	Outgoing Longwave Radiation
PE	Potential evaporation
PPD	Patched Point Data
RAMS	Regional Atmospheric Modelling System
RCP	Representative concentration pathways
SAM	Southern Annular Mode
SILO	Queensland Government Climate database
SLP	Sea-Level Pressure
SON	September October November
SST	Sea surface temperature
TC	Tropical cyclone
WRF	Weather Research and Forecasting

Units

UNIT	DESCRIPTION
L	litre
kL	kilolitre (1,000 litres)
ML	megalitre or 1000 kilolitres (kL)
GL	gigalitre or 1000 megalitres (ML)
m	metres
km	kilometres
m^3/second	cubic metres per second or 'cumecs'
Ma	million years
mAHD	metres above Australian Height Datum
mBGL	metres below ground level
Mt	mega tonne

Executive summary

Key findings

- The Pilbara is a semi-arid region that is significantly surface water limited, given annual potential evaporation can exceed annual rainfall by more than an order of magnitude.
- There is an apparent enhancement in annual rainfall over the Hamersley Range with corresponding lower potential evaporation, relative to the surrounding plains.
- The Assessment area mean rainfall for the baseline Historical climate period from October 1960 (shown as water year 1961) to September 2012 (water year 2012) was 334 mm/year, compared to the long-term (1911 to 2012) mean of 299 mm/year. About 60% of annual rainfall falls between January and March.
- An exceptionally wet 7-year period from 1995 to 2001 had a mean annual rainfall of 500 mm/year. Western Australia experienced more tropical cyclones than average during this period.
- The majority of climate change projections indicate tropical cyclones may become less frequent overall but that the strongest tropical cyclones may increase in intensity and size and travel further south.
- There are linear trends of increasing annual rainfall, extreme rainfall, number of rainfall days and mean rain day intensity for the 1961 to 2012 period in the east of the Assessment area, with opposing decreasing trends in the western third.
- Winter rainfall has decreased in the West Pilbara because cold fronts have progressively reached less far north since the mid-20th century on.
- The cause for the increase in summer rainfall in recent decades may be climate change, natural variability, aerosols emanating from south-east Asia, or some combination of these.
- On balance, projections indicate that the Pilbara may become slightly drier by 2030 and 2050 although wetter projections cannot be discounted. There is not sufficient confidence in the projections to allow quantification of the probabilities of the wet or dry scenarios occurring in the future.
- The median projected warming relative to the Historical climate (mid-point in 1986) is 1.5 to 1.6 °C for 2030 and 2.1 to 2.9 °C for 2050, for a medium greenhouse gas emission scenario (representative concentration pathway (RCP) 4.5), and for a high greenhouse gas emission scenario (RCP8.5), respectively.
- The corresponding median projected annual rainfall changes are –0.1 to –1.8% for 2030 and –0.1 to –2.5% for 2050, for RCP4.5 and RCP8.5, respectively.
- The selected future wet scenarios have projected annual rainfall increases ranging from 3.2% (2030, RCP4.5) to 7.8% (2050, RCP8.5).
- The selected future dry scenarios have projected annual rainfall decreases ranging from –4.2% (2030, RCP4.5) to –17% (2050, RCP8.5).
- The corresponding projected areal potential evaporation changes range from annual increases of 3 to 4% for 2030 and from 4 to 7% for 2050.
- Annual rainfall deficits increase for all future climate scenarios because of projected increases in areal potential evaporation.

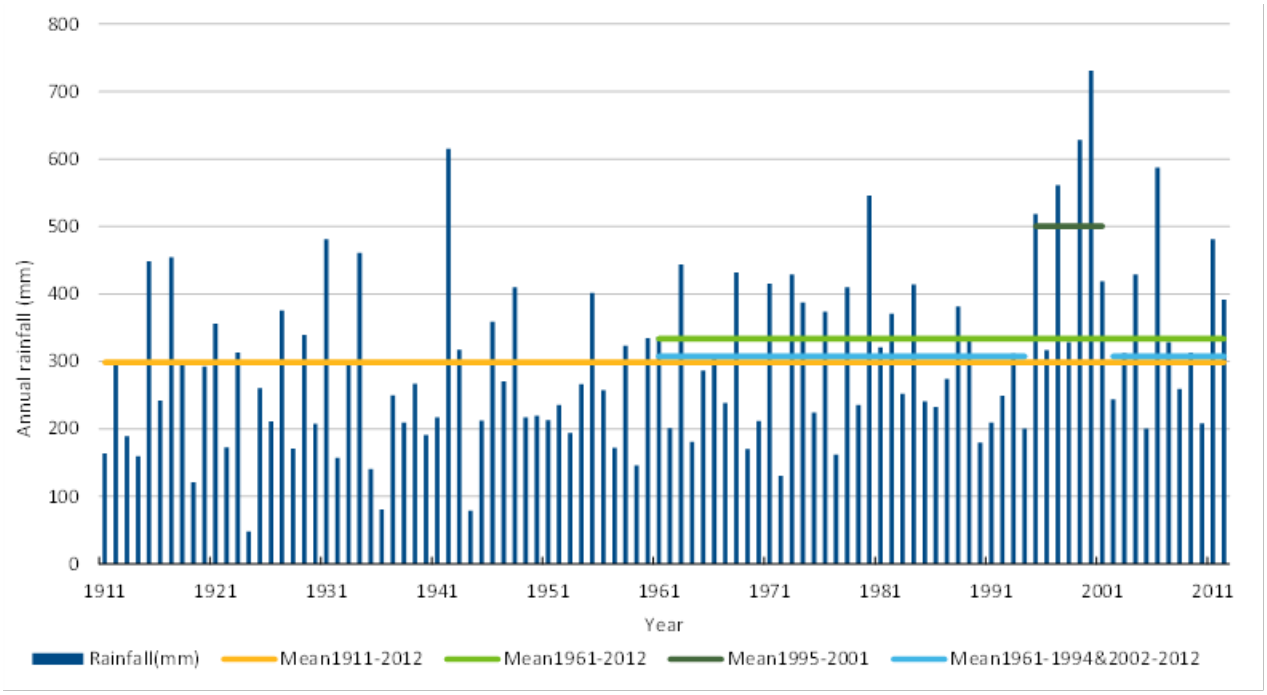

Figure 1 Average annual (October to September water year) total rainfall for the Assessment area for 1911 to 2012, showing means for certain periods

Summary

This summary assesses changes to climate that have a direct and immediate effect on hydrology, as the magnitude and timing of rainfall influence both runoff and recharge rates. Increased evaporative losses, predominantly as a result of increased temperatures, also result in greater aridity. Analyses of climate processes and data were undertaken to summarise and interpret the climate drivers influencing observed climate variability and trends. The Assessment area is influenced by the Australian monsoon to the north-east and the adjacent warm northern seas that generate tropical cyclones and tropical depressions. The marked seasonality and large year-to-year variability of these and associated processes, together with the strong seasonality in the temperature contrast between land and ocean, result in highly seasonal and variable rainfall. This ranges from local-scale intermittent intense rainfall to large-scale persistent rainfall.

The Pilbara is a semi-arid region that is significantly water limited, given that annual PE can exceed annual rainfall by an order of magnitude. The Assessment area's 1911 to 2012 mean annual rainfall is 299 mm (Figure 1). There is large year-to-year variability, with annual rainfall ranging from 48 mm in 1924 to 731 mm in 2000. The wettest months are January to March, producing 60% of annual rainfall. February is the wettest month with an average of 71 mm, or 24% of the annual rainfall, and September is the driest with an average 2 mm, or 0.6% of the annual rainfall. There are also strong spatial gradients with higher annual rainfall over the Hamersley Range (up to 500 mm) and 100 km inland of the north-east coast (Figure 2). This is indicative of trough line, which is preferential to thunderstorms, with advection and convergence of moist sea breezes together with uplift from orography (Hamersley Range) and heating (e.g. the Marble Bar region). The rainfall of the recent 1990–2012 period shows a large increase, relative to the long term, over the north-east Canning Basin, as well as an extended region of enhanced rainfall over the Hamersley Range (Figure 3). This shorter period contains the very wet 7-year period 1995 to 2001, and hence the increased magnitudes reflect the influence of these extreme years.

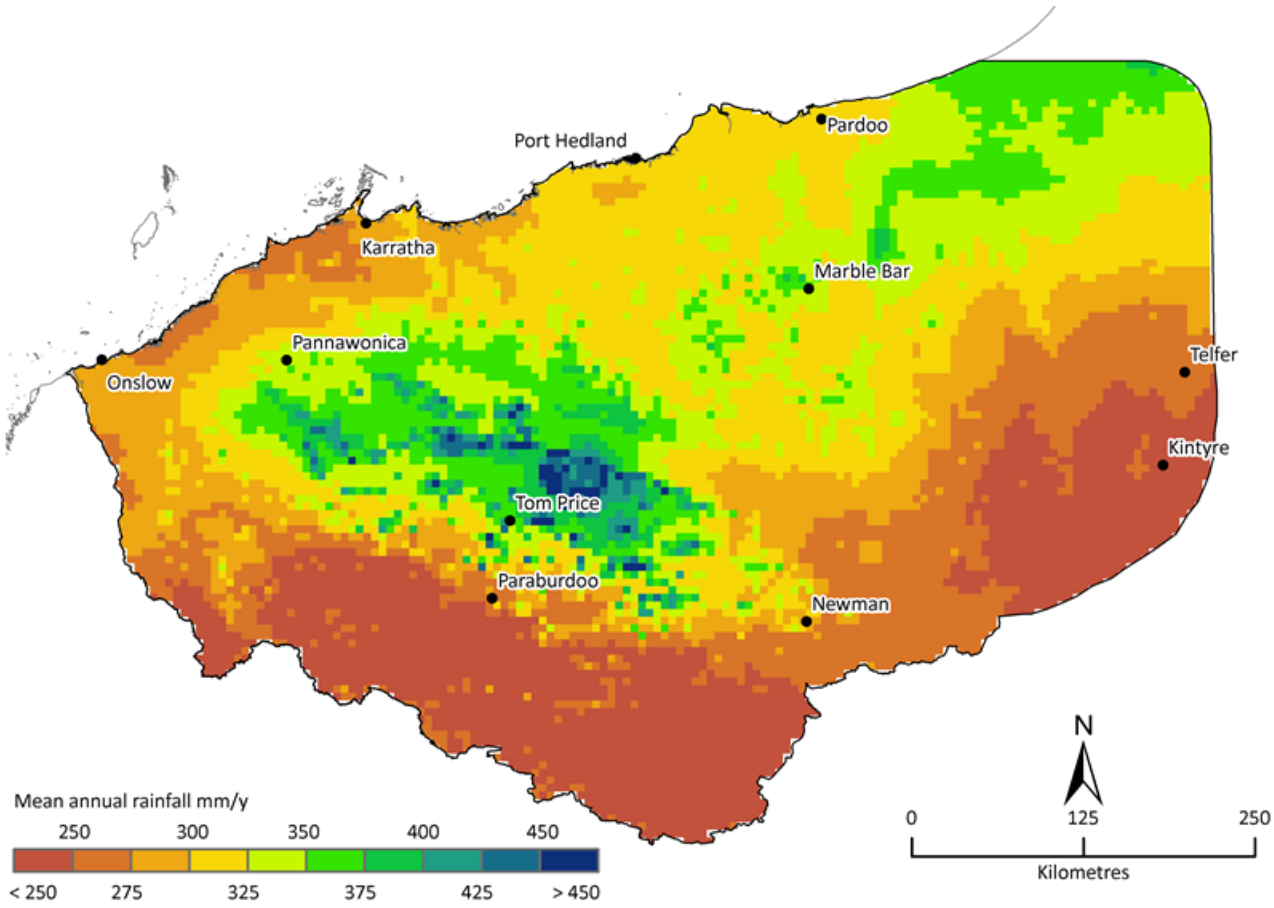

Figure 2 Mean annual rainfall (mm/year) for the period 1911 to 2012

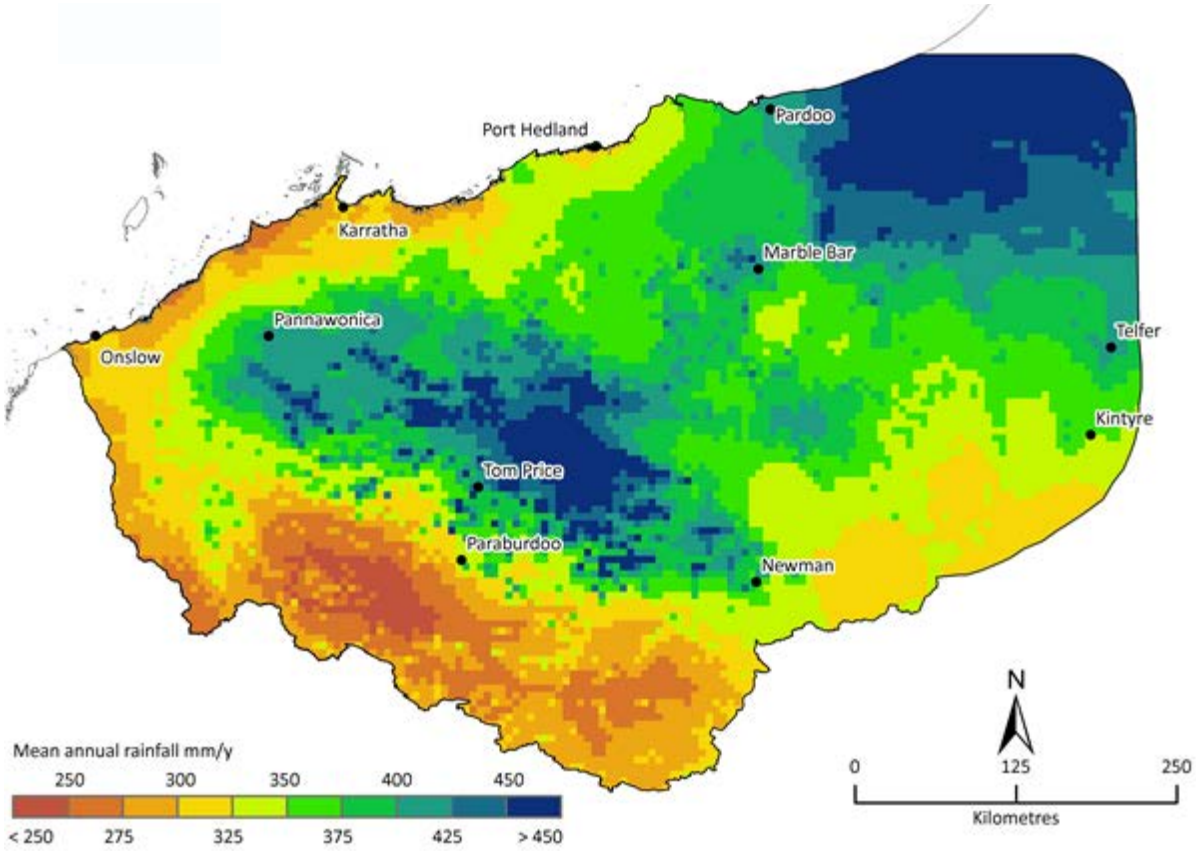

Figure 3 Mean annual rainfall (mm/year) for the period 1990 to 2012

Mean annual PE across the Assessment area, calculated using Morton's wet areal formula, ranges from 1700 mm in the south-east to over 2000 mm in the northern coastal parts (Figure 4). It most probably underestimates the inland potential as it does not account for advection due to dry and hot inland winds. PE varies seasonally from an average of 7.3 mm/day in December and January to 2.8 mm/day in June and July. This results in a calculated mean annual rainfall deficit ranging between 1200 mm over the Hamersley Range to 1750 mm along the coastline and eastern inland parts of the Assessment area. PE estimated from Class A pan evaporation is much higher than that estimated by Morton's formula because it is measured from a small water body with a dry surrounding environment and accounts for wind-induced advection. Morton's wet areal formula is used for modelling because it can be readily estimated across the Assessment area using available climate data. Class A pan evaporation is more applicable for estimating evaporation from isolated water bodies such as dams and mine pit lakes.

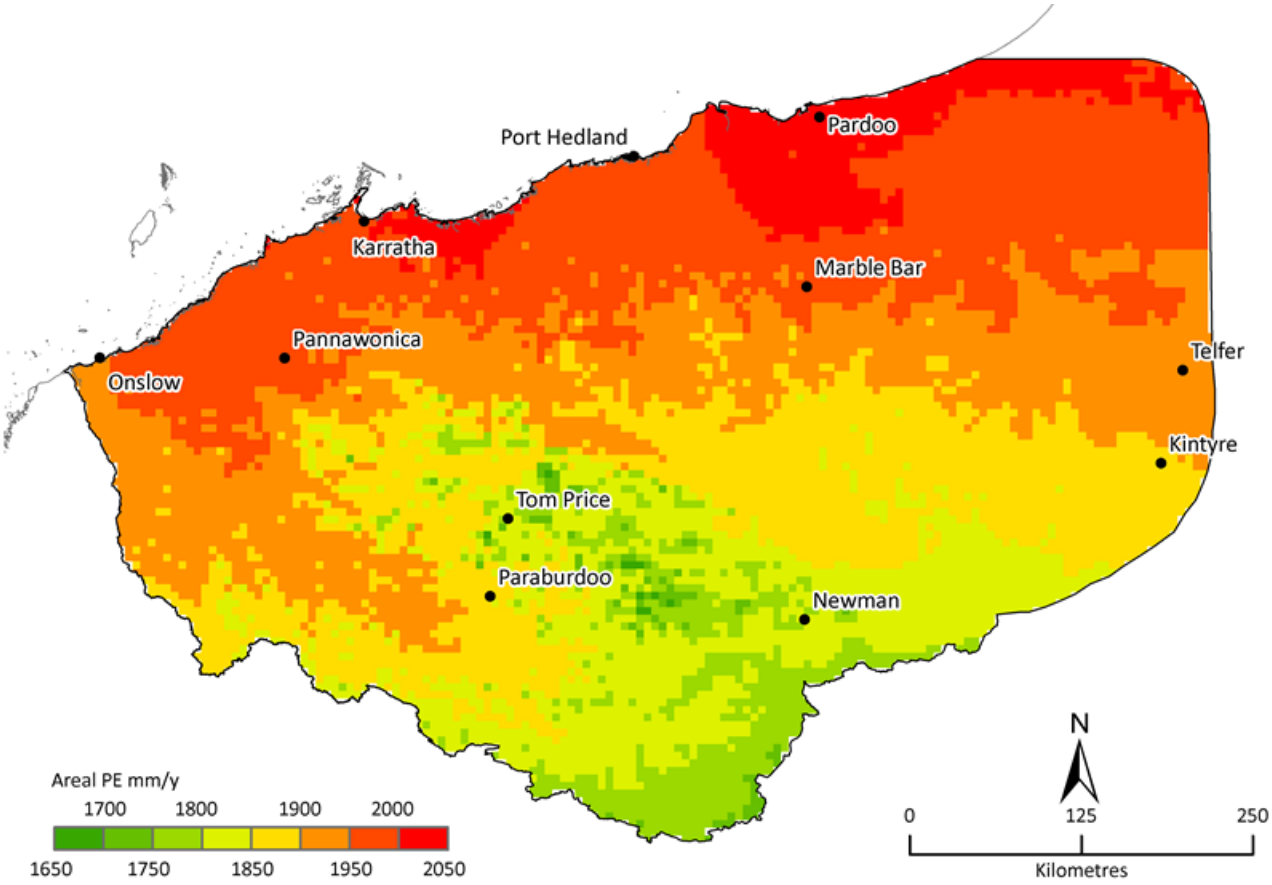

Figure 4 Mean annual potential evaporation (mm/year) calculated using Morton's areal wet environment method for the period 1911 to 2012

The magnitude and direction of long-term trends in rainfall varies across the Assessment area. Overall, annual rainfall trends have strengthened over more recent periods compared with the long-term trends, as highlighted by the spatial distribution of trends across different periods (Figure 5).

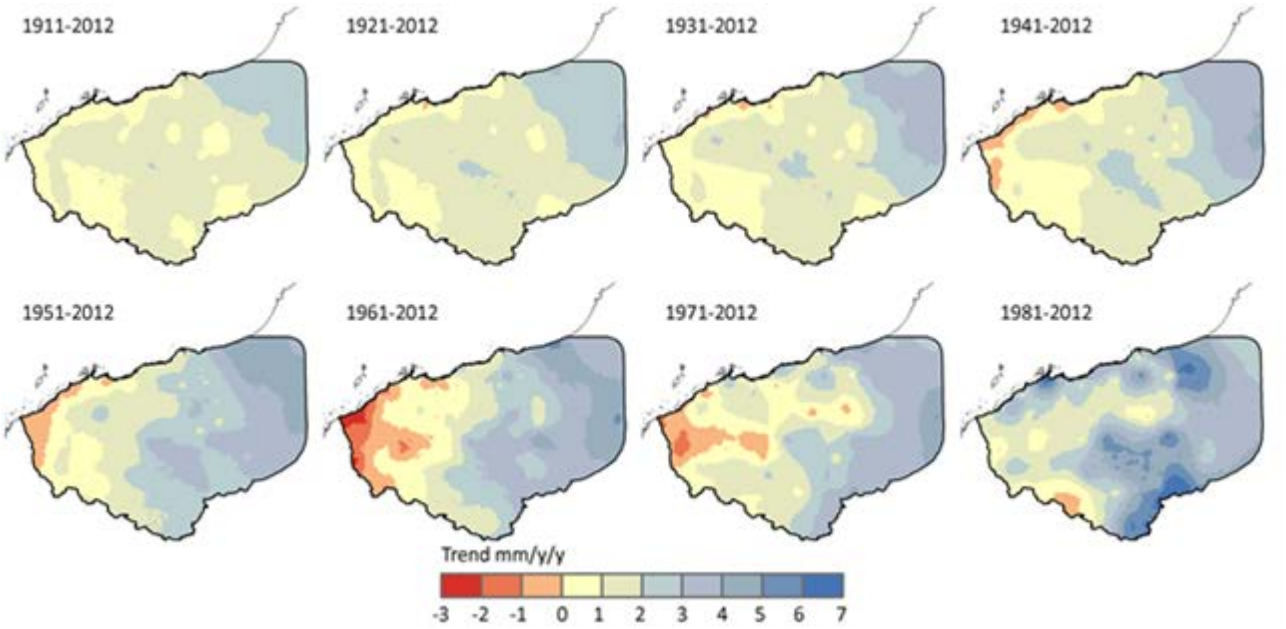

Figure 5 Trends in annual rainfall (mm/year/year) for periods ranging from the last 102 years (1911 to 2012) through to the last 32 years (1981 to 2012) for the Assessment area

The 1961 to 2012 period was identified as having somewhat larger trends than most other periods, with rainfall increasing in the eastern parts and decreasing in the western parts of the Assessment area (Figure 6). The decrease in the west is partially attributed to a decrease in winter rainfall due to cold fronts being displaced to the south as high pressure systems in the mid-latitude ridge intensify. There is some indication that the trends in total rainfall are more related to trends in high intensity rainfall (particularly 99th percentile daily rainfall) than to the number of rain days or the average rain day intensity (Figure 6).

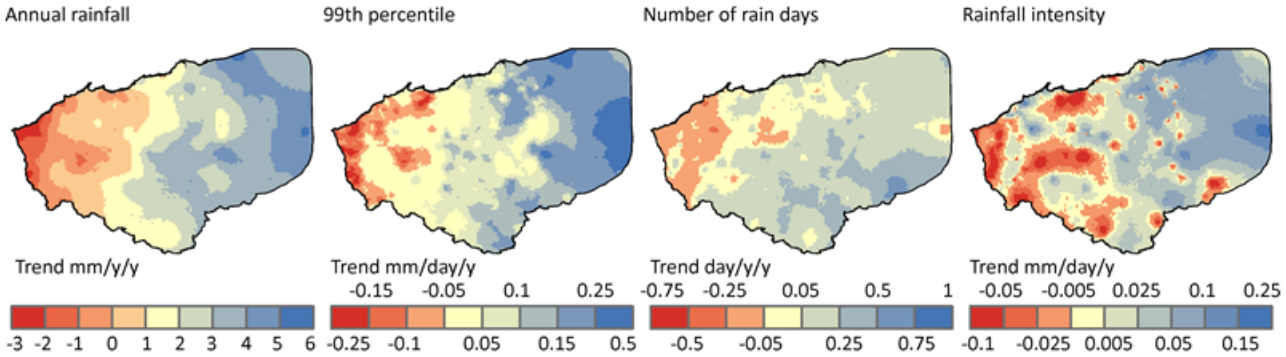

Figure 6 Trends for 1961 to 2012 (a) annual rainfall, (b) 99th percentile daily rainfall, (c) number of rain days >1 mm, and (d) rainfall intensity for the Assessment area

Time trends at individual stations are shown as the cumulative difference from the mean for five high-quality stations (Figure 7). These highlight the progressive drying (falling trend) over the early part of the record, followed by consistent and ongoing wetting (rising trend) since the 1960s for most stations, with particularly rapid wetting since the 1990s for the inland east (Bonney Downs) and inland central (Mount Florance) stations. The wetting trends continue in the most recent years for three eastern and central stations (Bonney Downs, Roebourne and Mount Florance), whereas the two westerly stations (Mardie, on the coast, and Mount Augustus, to the south-west) show recent declines.

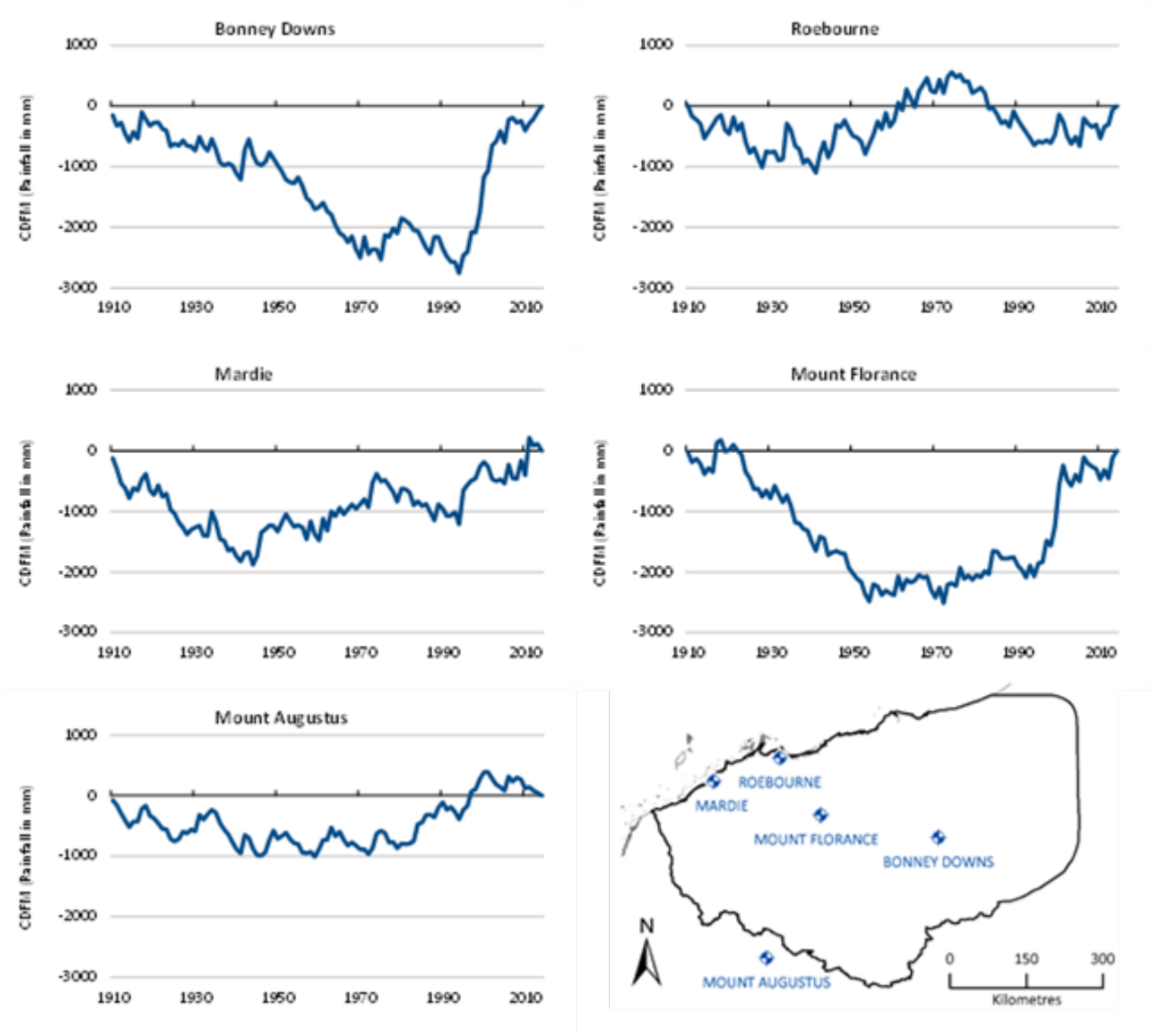

Figure 7 Cumulative difference from the mean time series for five stations with high-quality long-term records. Locations of stations shown in bottom right panel

The significantly wetter period of seven years from 1995 to 2001, with an average annual rainfall of 500 mm (Figure 1), experienced more frequent tropical cyclones than average. The largest increases in monthly rainfall in the 1961 to 2012 period occurred in February, March and December – months with the highest historical frequency of tropical cyclones.

Palaeoclimatological research indicates that the Pilbara has experienced past periods of intense aridity, and that the recent wetter decades may be unprecedented within the last several hundred years. Past analogues can not be directly related to current changes, however, as the rate of change caused by current climate change is much faster than that of past natural changes.

Because many climate processes interact to affect climate across the Assessment area, the spatial variability and trends are complex and not easily attributed to simple cause and effect. There is no scientific consensus as to the specific cause(s) of the increasing wet-season rainfall observed in recent decades over the north-west of Australia, including the eastern Pilbara. Possible causes of observed circulation, wind and moisture flow changes include: (i) expansion of the tropical zone, (ii) increased atmospheric aerosol loads over the Asian region, and (iii) sea surface temperature changes both remotely, from the tropical Atlantic or tropical western Pacific, and regionally from the warming Indian Ocean. Changes to the future frequency and intensity of tropical cyclones (TCs) and monsoon depressions will be relevant to the continuation of observed trends. While one recent study concluded that the frequency of TCs could increase throughout

the 21st century, many more studies concur with CSIRO findings of fewer but more intense TCs in the future. Thus the weight of current understanding supports decreases in the frequency of TCs impacting the Assessment area as more likely than increases. Several studies also show that the intensity of TCs may increase in the future.

Global climate models (GCMs) are used for climate change projection. However, even if GCMs were able to adequately represent all large-scale processes and their interactions, the climatic changes affecting the Assessment area over the next several decades can not be predicted with certainty. This is because (i) it is not easy to predict the factors influencing the rate of global change in greenhouse gas emissions, such as the rates of economic and technological growth and their resulting emissions profiles, are not easy to predict; and (ii) the regional response to global forcing is still highly variable across the latest GCMs. Given this uncertainty in future climate trends, a scenario approach using projections of plausible climate futures from many GCMs is used to account for the range of possible changes to climate baselines. The Assessment used the latest GCM scenarios from the Fifth Coupled Model Intercomparison Project (CMIP5), as used in the most recent Intergovernmental Panel on Climate Change Fifth Assessment Report, for medium (RCP4.5) and high (RCP8.5) changes to radiative forcing. The RCP numbers refer to the approximate radiative forcing levels by 2100 – that is, 4.5 W/m^2 and 8.5 W/m^2, respectively. RCP4.5 represents increased emissions of greenhouse gases until about 2040 and then reductions due to the implementation of mitigation, whereas RCP8.5 represents a future with little curbing of emissions and rapidly rising greenhouse gas concentrations.

Scenarios of daily rainfall and PE on 0.05° grid cells across the Assessment area were developed for climate inputs into hydrological models. The historical baseline (Scenario A) is the daily data rainfall and areal PE for the period 1961 to 2012. These series are modified according to a scaling approach to produce perturbed versions (Scenario C), representing 2030 and 2050 climates as projected by 18 CMIP5 GCMs (Table 1).

The projections from the GCMs indicate that the largest rainfall changes result from projected decreases in December to February rainfall under the RCP8.5 scenario in 2050. Overall the majority of GCMs project changes within 5% of the current climate mean for both 2030 and 2050. From the ensemble of Scenario C time series for 2030 and 2050, the RCP8.5 and RCP4.5 ensemble members that produced the 90th, 50th and 10th percentile rainfall changes for the Assessment area are identified as the Cwet, Cmid and Cdry scenarios, respectively.

Table 1 Coupled Model Intercomparison Project Phase 5 (CMIP5) global climate models and institutions

GLOBAL CLIMATE MODEL	INSTITUTION	INSTITUTION ID
ACCESS1.0 ACCESS1.3	Commonwealth Scientific and Industrial Research Organisation (CSIRO) and Bureau of Meteorology (BOM), Australia	CSIRO-BOM
BCC-CSM1.1	Beijing Climate Center, China Meteorological Administration, China	BCC
CanESM2	Canadian Centre for Climate Modelling and Analysis, Canada	CCCMA
CCSM4	National Center for Atmospheric Research, USA	NCAR
CNRM-CM5	Centre National de Recherches Meteorologiques / Centre Européen de Recherche et Formation Avancée en Calcul Scientifique, France	CNRM-CERFACS
CSIRO-Mk3.6.0	Commonwealth Scientific and Industrial Research Organisation in collaboration with Queensland Climate Change Centre of Excellence, Australia	CSIRO-QCCCE
GFDL-ESM2G GFDL-ESM2M	NOAA Geophysical Fluid Dynamics Laboratory, USA	NOAA GFDL
HadGEM2-ES	Met Office Hadley Centre, UK	MOHC
IPSL-CM5A-LR IPSL-CM5A-MR IPSL-CM5B-LR	Institut Pierre-Simon Laplace, France	IPSL
MIROC-ESM MIROC-ESM-CHEM	Japan Agency for Marine-Earth Science and Technology, Atmosphere and Ocean Research Institute (The University of Tokyo), and National Institute for Environmental Studies, Japan	MIROC
MIROC5	Atmosphere and Ocean Research Institute (The University of Tokyo), National Institute for Environmental Studies, and Japan Agency for Marine-Earth Science and Technology, Japan	MIROC
MRI-CGCM3	Meteorological Research Institute, Japan	MRI
NorESM1-M	Norwegian Climate Centre, Norway	NCC

The projected changes to Assessment area temperature range from 1.2 to 1.8 °C for 2030 and 1.8 to 2.9 °C for 2050 (Table 1). Although the median projected rainfall change (relative to the 1961 to 2012 baseline) is a relatively small 2% reduction by 2050, some scenarios project much larger changes ranging from reductions of 17% to increases of 8% by 2050 (Table 2). Median PE projections are for increases of 3% for 2030, rising to increases of 7% for 2050 (Table 3). Thus, on balance the projections indicate that the Pilbara may become slightly drier by 2030 and 2050. A small rainfall reduction may have a larger proportional impact on the region's hydrology given the known sensitivity of hydrology to small changes in rainfall as well as the projected higher temperatures and PE. While a slight majority of models project drier and warmer conditions, several indicate that the Pilbara could become wetter and warmer. Even though the wetter models are in the minority, they should not be discounted, as they are often better than the drier models at reproducing some of the large-scale climate processes influencing Pilbara hydroclimate. Thus, as well as using the median projected scenarios, wet and dry scenarios were used to investigate the hydrological impacts of a range of projected changes for 2030 and 2050.

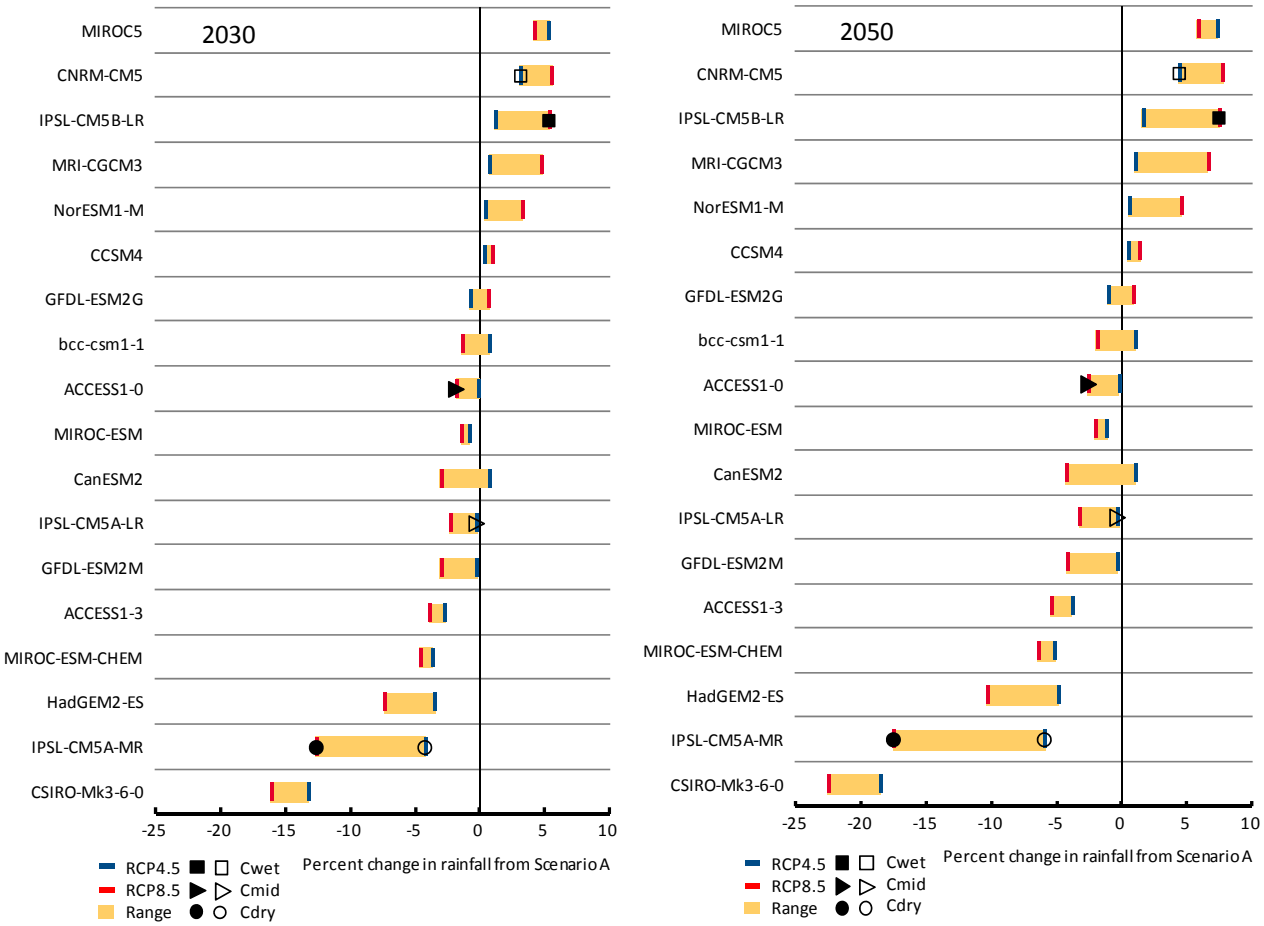

Figure 8 Assessment area mean annual rainfall change (%, relative to Scenario A) for RCP4.5 and RCP8.5 projections from 18 CMIP5 GCMs for 2030 and 2050. The second wettest (driest) scenarios from RCP4.5 and RCP8.5 are designated Cwet (Cdry). The median, selected from the 9th and 10th ranked GCM closest to the respective RCP4.5 and RCP8.5 mean, is designated Cmid. Solid symbols are used for RCP8.5, open symbols for RCP4.5

Table 2 Assessment area mean annual temperature changes (relative to Scenario A) under Cwet, Cmid and Cdry future climate scenarios from 18 GCM's RCP4.5 and RCP8.5 emissions scenario projections for 2030 and 2050

PERIOD	SCENARIO C	RCP4.5 EMISSIONS SCENARIO CHANGE (°C)	RCP8.5 EMISSIONS SCENARIO CHANGE (°C)
2030	C30wet	1.4	1.2
2030	C30mid	1.5	1.6
2030	C30dry	1.6	1.8
2050	C50wet	1.8	2.1
2050	C50mid	2.1	2.9
2050	C50dry	1.8	2.7

Table 3 Assessment area mean annual rainfall changes (relative to Scenario A) under Cwet, Cmid and Cdry future climate scenarios from 18 GCM's RCP4.5 and RCP8.5 emissions scenario projections for 2030 and 2050

PERIOD	SCENARIO C	RCP4.5 EMISSIONS SCENARIO		RCP8.5 EMISSIONS SCENARIO	
		(%)	(MM)	(%)	(MM)
2030	C30wet	3.2	11	5.6	19
2030	C30mid	–0.1	0	–1.8	–6
2030	C30dry	–4.2	–14	–12.6	–42
2050	C50wet	4.5	15	7.8	26
2050	C50mid	–0.1	0	–2.5	–8
2050	C50dry	–5.9	–20	–17.4	–58

Table 4 Assessment area mean annual areal PE changes (relative to Scenario A) under Cwet, Cmid and Cdry future climate scenarios from 18 GCM's RCP4.5 and RCP8.5 emissions scenario projections for 2030 and 2050

PERIOD	SCENARIO C	RCP4.5 EMISSIONS SCENARIO		RCP8.5 EMISSIONS SCENARIO	
		(%)	(MM)	(%)	(MM)
2030	C30wet	3.0	57	2.2	42
2030	C30mid	3.2	60	3.1	59
2030	C30dry	3.8	72	3.8	72
2050	C50wet	4.0	76	4.1	77
2050	C50mid	4.7	89	6.6	125
2050	C50dry	4.4	83	6.5	123

1 Introduction

1.1 Overview

This report is one of a series of reports that form part of the Pilbara Water Resource Assessment (Table 1.1) that provides a review of the current and possible future water resources of this very important part of Australia.

Table 1.1 Reports that comprise the Pilbara Water Resource Assessment

TITLE	TYPE	APPROXIMATE LENGTH (PAGES)
Proposed project methods	Technical	120
Hydroclimate of the Pilbara: past, present and future	Technical	120
Hydroclimate of the Pilbara: past, present and future	Summary	12
Hydroclimate of the Pilbara: past, present and future	Factsheet	4
Water Resource Assessment for the Pilbara	Regional	200–300
Pilbara Water Resource Assessment: Ashburton Robe Region	Regional	200–300
Pilbara Water Resource Assessment: Upper Fortescue Region	Regional	200–300
Pilbara Water Resource Assessment: Lower Fortescue Hedland Region	Regional	200–300
Pilbara Water Resource Assessment: De Grey Canning Region	Regional	200–300
Water Resource Assessment for the Pilbara	Summary	16
Pilbara Water Resource Assessment: Ashburton Robe Region	Summary	12
Pilbara Water Resource Assessment: Upper Fortescue Region	Summary	8
Pilbara Water Resource Assessment: Lower Fortescue Hedland Region	Summary	16
Pilbara Water Resource Assessment: De Grey Canning Region	Summary	16
Water Resource Assessment for the Pilbara	Factsheet	4
Pilbara Water Resource Assessment: Ashburton Robe Region	Factsheet	4
Pilbara Water Resource Assessment: Upper Fortescue Region	Factsheet	4
Pilbara Water Resource Assessment: Lower Fortescue Hedland Region	Factsheet	4
Pilbara Water Resource Assessment: De Grey Canning Region	Factsheet	4

In addition to reports, the Assessment has developed a number of datasets on future climate, hydrology and environmental variables in a format that takes account of their accessibility and usefulness for later use. Other outputs include new and updated rainfall-runoff and groundwater models. The purpose of this report is to present background information on the climate of the Pilbara and to develop future climate scenarios that can be compared with a defined historical baseline period. A scenario approach is used because there is considerable uncertainty about what the future climate of the Pilbara may be, despite recent research carried out by the Indian Ocean Climate Initiative stage 3 (IOCI, 2012). A broad stakeholder assessment of the vulnerabilities and potential impacts of climate change on the Pilbara has identified water resources as an issue of concern under warmer and drier climate scenarios (Loechel et al., 2011).

The historical record is also limited in some areas and time periods due to a paucity of meteorological recording stations. This report synthesises what is currently known from a number of sources and identifies deficiencies in data, its interpretation and overall knowledge. It is recognised that the review of the region's climate has uses beyond hydrological understanding and modelling so additional climate variables are included for completeness.

Similar reports on the climate and possible future scenarios have been produced for the Murray–Darling Basin by Chiew et al. (2008), for northern Australia by Li et al. (2009), for Tasmania by Post et al. (2009) and for the south-west of Western Australia by Charles et al. (2010).

1.2 Geographic scope

For the purposes of the Assessment, the Pilbara has been defined as comprising the Ashburton, Onslow Coast, Fortescue, Port Hedland Coast and De Grey River Basins (as defined by the Australian Water Resources Council) as well as the western part of the Canning Basin and sections of the Great Sandy Desert that includes the Telfer and Kintyre mineral deposits and Karlamilyi National Park (Figure 1.1).

This includes all major river drainages and mineral deposits in the Pilbara. It also takes in the West Canning Basin and the recharge areas to the main aquifer which is prospective for providing a water supply to towns and mines in the East Pilbara.

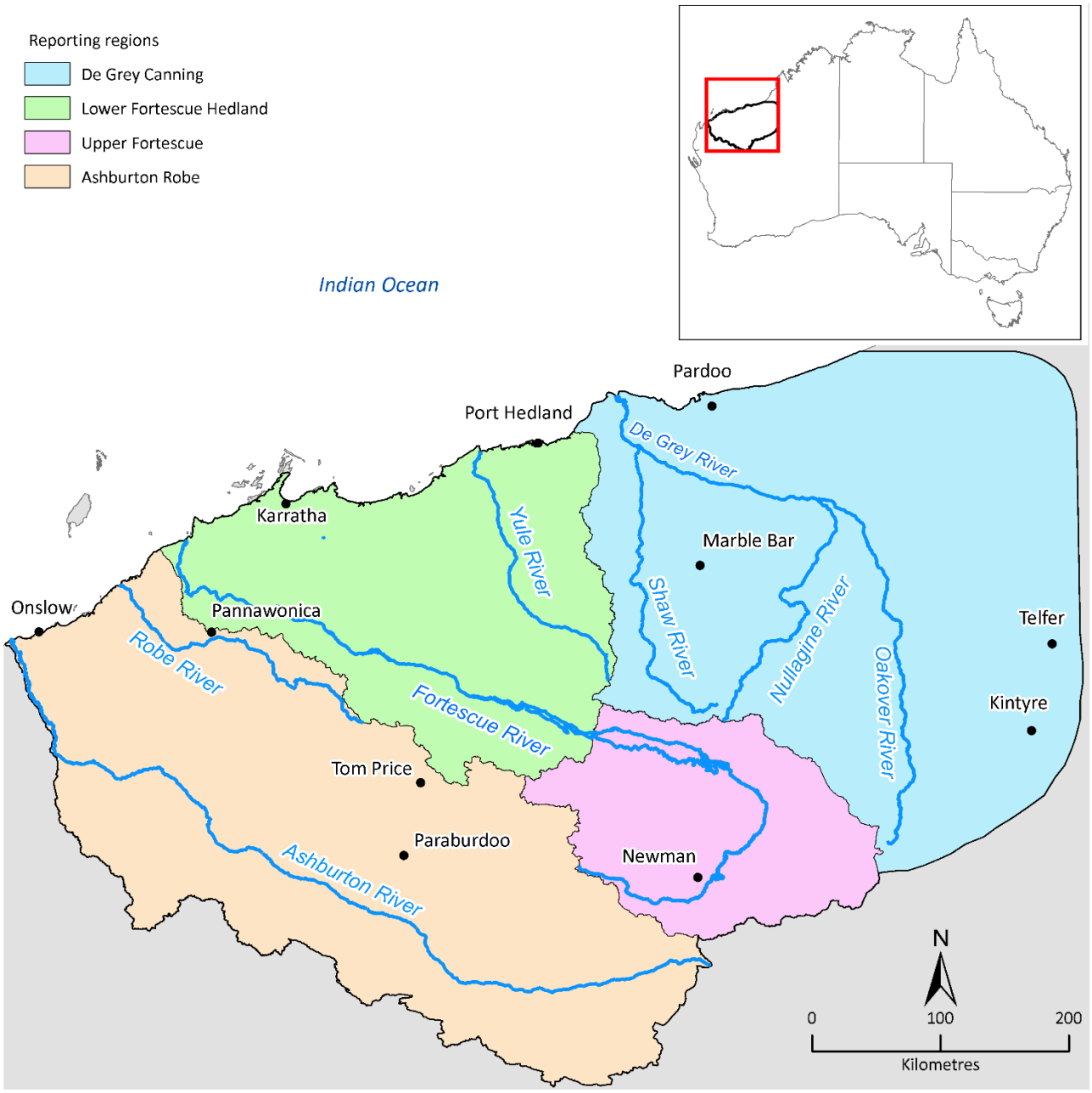

Figure 1.1 Geographic scope and reporting regions for the Pilbara Assessment area

While most climate data that have been analysed in this report lie within the area shown in Figure 1.1, climatic influences are exerted from outside this region and climate stations close to the boundary provide important information. Oceans are an especially important influence on the area's climate. Depending on the purpose therefore the geographic scope of the analysis can extend well into Asia, and the Pacific and Indian Oceans. Greenhouse gases are important forcing agents on future climate and these have a global reach.

1.3 Temporal scope

Analyses of the historical Pilbara climate cover the period since 1911 (Chapter 2), as meteorological measurements from this point are comparable and easily accessible, and extend until the end of the 2011–12 water year (i.e. 30 September 2012). Data is available from about 1880 in the Pilbara, however it is not necessarily comparable and some is not digitised and so is not easily accessible until about 1910 when comprehensive digitised data is available. Some palaeo-climatic data are also reviewed in Chapter 2

because this provides a valuable perspective on long-term changes that have affected the current soils, drainages, and biota.

Future climate projections focus on the periods centred on 2030 and 2050 which is the planning period for many developments, management plans and mine closures. Longer-term projections can be made using GCMs but there is increasing uncertainty the further out these projections go, especially around the level of global emissions and the nature and extent of global feedback mechanisms.

1.4 Climate types

The Pilbara has a hot and arid climate classified, according to Köppen-Geiger climate classification, as mainly BWh (Arid, desert, hot), with the inland eastern Pilbara BSh (Arid, steppe, hot) (Crosbie et al., 2012). Climate zones such as these are dominated by the influence of subtropical anticyclones (or highs) caused by descending air, which are located on the descending arm of the Hadley Cell circulation (to the south of the Pilbara). Over 80% of annual precipitation falls in the summer-autumn half of the year (December to May), when the subtropical anticyclone has migrated further southward, and annual precipitation is much less than annual potential evaporation in these zones.

While these climate zones are mainly hot regions around the world, some west coast deserts can be relatively cool because of airflow from nearby cold ocean currents (e.g. the Atacama Desert in Chile which is close to the north flowing Humboldt Current). In the Pilbara, warm waters in the neighbouring eastern Indian Ocean from the Indonesian Throughflow and associated Leeuwin Current results in the region being hot. Although arid, extreme rainfall can occur in the Pilbara as the result of a number of mechanisms, explained in detail in Chapter 2.

1.5 Objectives

The objectives of the climate component of the Assessment include:

1. providing a review of historical Pilbara climate averages and trends using Bureau of Meteorology data and the Stage 3 Indian Ocean Climate Initiative (IOCI) findings, including:
    a. drivers of changes to recent rainfall
    b. intensity and frequency of tropical cyclones
    c. climate extremes
2. developing 2030 and 2050 climate scenarios of daily rainfall and areal potential evaporation (areal PE) to run surface water and recharge/groundwater models
3. summarising the range of possible future climates of relevance to sectors outside hydrology where possible.

1.6 References

Charles S, Silberstein R, Teng J, Fu G, Hodgson G, Gabrovsek C, Crute J, Chiew F, Smith I, Kirono D, Bathols J, Li L, Yang A, Donohue R, Marvanek S, McVicar T, Van Niel T and Cai W (2010) Climate analyses for south-west Western Australia. A report to the Australian Government from the CSIRO South-West Western Australia Sustainable Yields Project. CSIRO, Australia.

Chiew F, Teng J, Kirono D, Frost A, Bathols J, Vaze J, Viney N, Young W, Hennessy K and Cai W (2008) Climate data for hydrologic scenario modelling across the Murray-Darling Basin. A report to the Australian Government from the CSIRO Murray-Darling Basin Sustainable Yields Project. CSIRO.

Crosbie RS, Pollock DW, Mpelasoka FS, Barron OV, Charles SP and Donn MJ (2012) Changes in Köppen-Geiger climate types under a future climate for Australia: hydrological implications. Hydrol. Earth Syst. Sci. 16(9), 3341-3349. Doi: 10.5194/hess-16-3341-2012.

IOCI (2012) Western Australia's Weather and Climate: A Synthesis of Indian Ocean Climate Initiative Stage 3 Research. Australia. Available online: <http://www.ioci.org.au/publications/ioci-stage-3/cat_view/17-ioci-stage-3/23-reports.html>.

Li L, Donohue R, McVicar T, Van Niel T, Teng J, Potter N, Smith I, Kirono D, Bathols J, Cai W, Marvanek S, Gallant S, Chiew F and Frost A (2009) Climate data and their characterisation for hydrological scenario modelling across northern Australia. A report to the Australian Government from the CSIRO Northern Australia Sustainable Yields Project. CSIRO Water for a Healthy Country Flagship, Australia.

Loechel B, Hodgkinson JH and Moffat K (2011) Pilbara Regional Mining Climate Change Adaptation Workshop: Report on workshop outcomes. Available online: <http://www.csiro.au/~/media/CSIROau/Flagships/Climate%20Adaptation/CAF_MiningReports/PilbaraRegionalMiningClimateChangeAdaptationWorkshop_OutcomesReport.pdf>.

Post D, Chiew F, Teng J, Vaze J, Yang A, Mpelasoka F, Smith I, Katzfey J, Marston F, Marvanek S, Kirono D, Nguyen K, Kent D, Donohue R, Li L and McVicar T (2009) Production of climate scenarios for Tasmania. A report to the Australian Government from the CSIRO Tasmania Sustainable Yields Project. CSIRO Water for a Healthy Country Flagship, Australia.

2 Pilbara climatology

2.1 Large-scale processes

The Pilbara's hydroclimate (i.e. the climatology of the variables influencing the hydrological cycle) is characterised by extremes and high variability both spatially and temporally. According to Köppen-Geiger climate classification the Pilbara is mainly BWh (Arid, desert, hot), with the inland eastern Pilbara BSh (Arid, steppe, hot) (Crosbie et al., 2012). Rainfall and temperature exhibit high variability between the seasons (i.e. high within-year, or intra-annual, variability) with occasional intense rainfall and consistently high temperatures in summer (December to February), an autumn (March to May) transition to dry and warm conditions throughout winter (June to August) and spring (September to November), with the western Pilbara receiving rain in winter from southern sources. The Pilbara often records temperatures of 43 °C or above in summer months and has recorded Australia's highest temperature in 12 of the 20 years in the period 1996 to 2015 (<http://www.bom.gov.au/cgi-bin/climate/extremes/annual_extremes.cgi>). The highest maximum daily temperature recorded in the Pilbara to date is 50.5 °C at Mardie Station on 19 February 1998. There is also large year-to-year rainfall variation (i.e. high inter-annual variability) and spatial heterogeneity with longitudinal, latitudinal and coastal to inland contrasts, influenced by the complex topography of the Hamersley Ranges. Combined with consistently high potential evaporation, this results in significant hydrological variability (intra- and inter-annually) and large annual water deficits across the Assessment area. Detailed analyses of these hydroclimate characteristics are presented in Section 2.2.

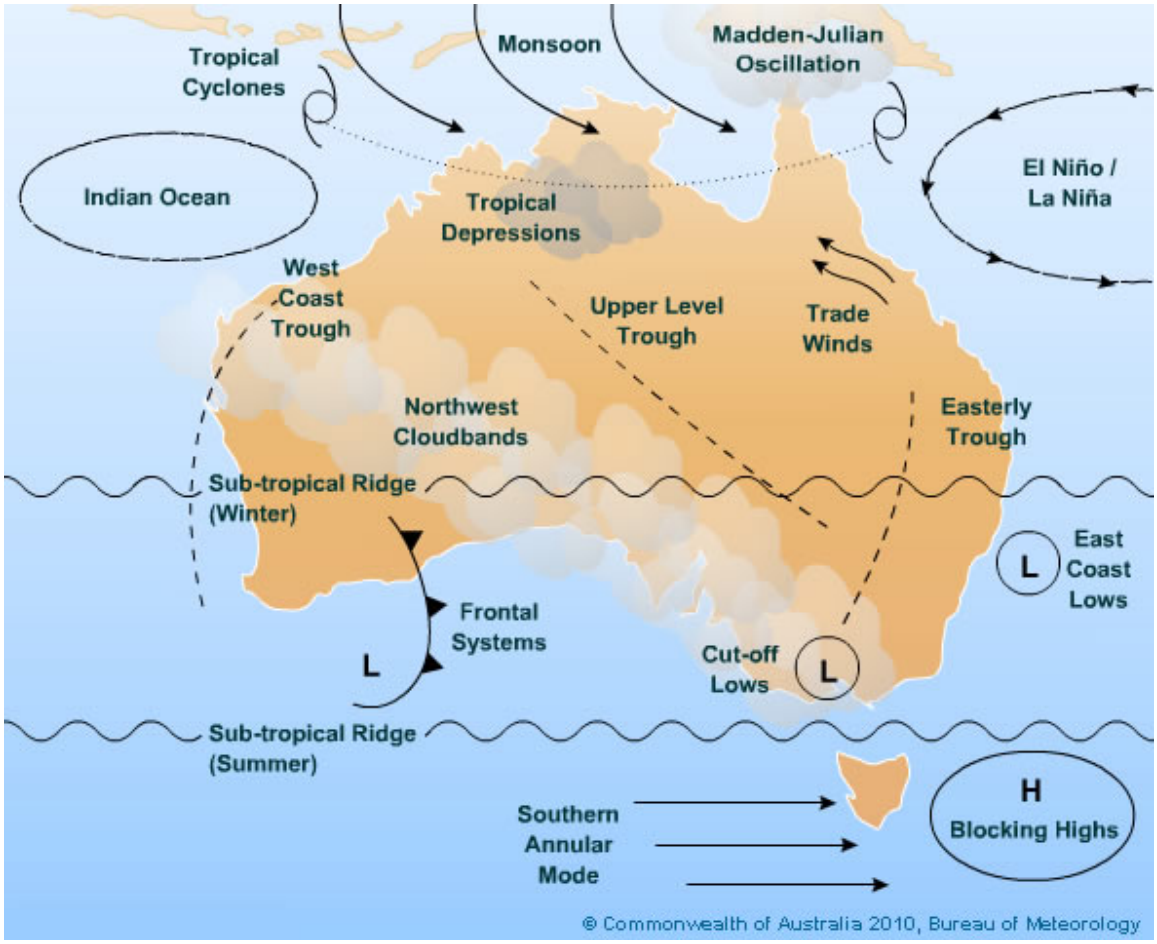

Figure 2.1 Main influences on Australian climate and year-to-year variability

Source: (Bureau of Meteorology, 2010)

Many large-scale atmospheric and oceanic processes interact at a range of spatial and temporal scales to influence the seasonality, inter-annual and spatial variability of climate (particularly rainfall) across the Assessment area (Figure 2.1). The most influential processes are outlined in the following sections.

2.1.1 Subtropical ridge, frontal systems and north-west cloudbands

In winter and spring the subtropical ridge and associated belt of high pressure systems (anticyclones) are positioned over the Australian continent directing dry easterly or south-easterly winds across the Pilbara. This is the predominant climatic influence on the region and is responsible for the pronounced aridity. The seasonal southward movement of the subtropical ridge sees it positioned south of the continent during late spring, summer, and early autumn, allowing tropical systems to dominate the Pilbara's climate in the summer wet season.

Southern cold fronts can extend north to the Pilbara in late autumn, winter, and early spring, bringing rains to the region, most commonly to western parts. However, the northward extent of fronts shows a long-term decreasing trend in recent decades, possibly related to the observed southward expansion of the Hadley Cell (Frederiksen et al., 2014; Risbey et al., 2009). Cold fronts can also interact with mid-level moisture in the eastern Indian Ocean to create rain-bearing north-west cloudbands (NWCBs) (Tapp and Barrell, 1984; Telcik and Pattiaratchi, 2014; Wright, 1997) although there is observational evidence that NWCBs have reduced in frequency and influence in recent decades (G. Cook (BoM), 2013, pers. comm.) and not all NWCBs are rain-producing systems.

2.1.2 Heat lows and thunderstorms

During the spring, summer and autumn a significant localised feature of Pilbara climate is the prevalence of a semi-permanent low pressure 'heat low'. The heat low is the result of location of the region and the resulting temperature gradients, declining both to the north as a result of the relatively cooler oceanic influence, and the south as a result of decreased solar heating. For a lot of the time it is a shallow system not directly associated with rainfall. The persistence of these heat lows, that form preceding the monsoon season, exhibits a coupled relationship between the strength of the monsoonal circulation and associated heavy rainfall and (Suppiah, 1992).

The thermal uplift associated with heat lows influences the formation of convective thunderstorms of varying size and intensity that are a frequent feature during the late-afternoon to night, occasionally resulting in heavy rainfall and localised flooding. Thunderstorm development also depends on inland penetration and convergence of sufficient moisture, often entrained by the afternoon sea breeze. There has to be a sufficient depth of moisture in a conditionally unstable atmosphere to produce thunderstorms with a low enough base for rainfall to reach the ground given the overall dry atmospheric background (M. Pook (CSIRO), 2013, pers. comm.).

The eastern Pilbara is more prone to thunderstorms during the December to March period (Allen and Karoly, 2013), with an annual average of more than 30 thunder-days northwest of Newman (Kuleshov et al., 2002). There are no published studies quantifying the relative contributions of thunderstorms to Pilbara rainfall totals, however the contribution is expected to be significant, particularly in the drier years (Rouillard et al., 2014). Although climate model projections do not resolve such features, projected changes in climatology indicate the potential for an increased propensity for thunderstorms to form (Allen and Karoly, 2013; Allen et al., 2014a; 2014b). A recent international study has observed an increase in convective rainfall with increasing temperature (Berg et al., 2013).

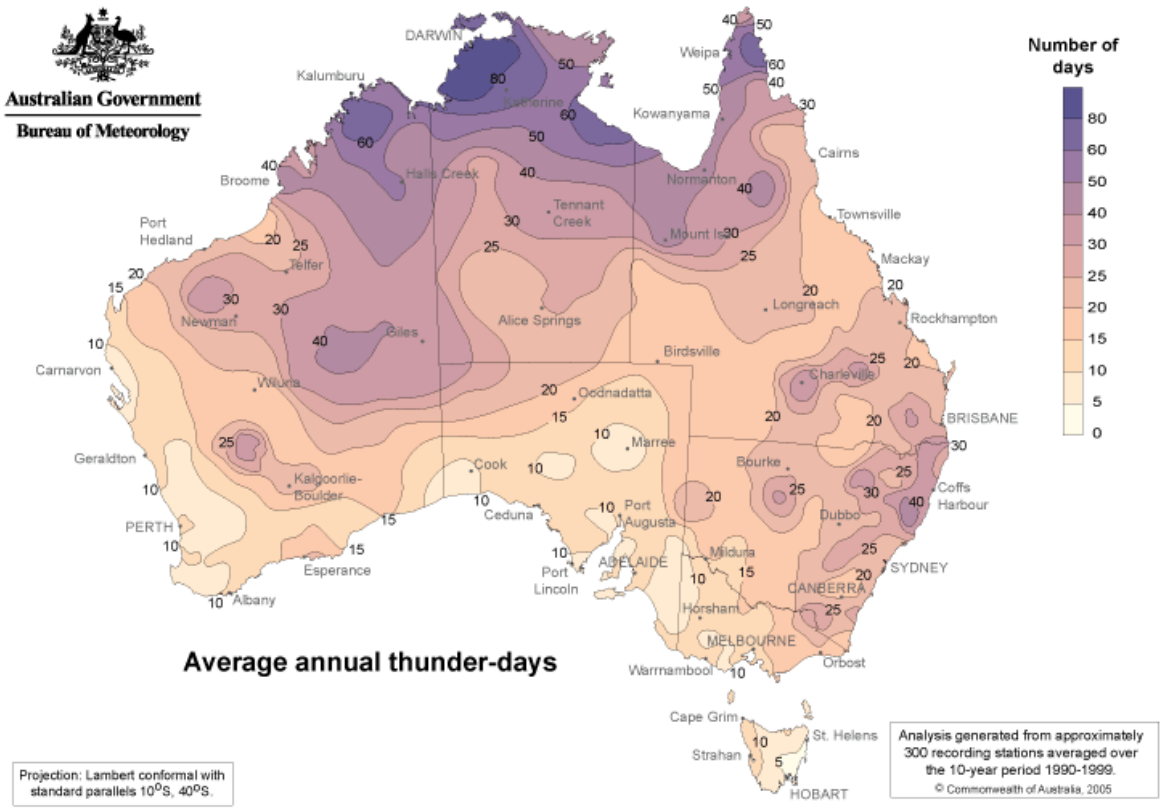

Figure 2.2 Australian thunder-days for the 10-year period 1990 to 1999

Source: (Bureau of Meteorology, 2012a)

2.1.3 El Niño Southern Oscillation

El Niño Southern Oscillation (ENSO) is a coupled oceanic-atmospheric process originating in the equatorial Pacific producing sea surface temperature (SST) and wind anomalies that influence climate variability globally on multi-year (sub-decadal) timescales (Trenberth, 1997). ENSO is commonly quantified as the strength of atmospheric pressure gradients across the Pacific (e.g. Southern Oscillation Index, SOI) and/or SST anomalies in certain regions of the equatorial or near-equatorial Pacific. It has three phases – the warm El Niño phase, cold La Niña phase and a neutral phase.

The large-scale variations in SST patterns related to ENSO directly influence the climate of the Assessment area, as do indirect impacts through its influence on the variability or intensity of the other large-scale processes interacting across tropical and subtropical Australia. The relationship between ENSO and Australian rainfall variability is much studied, as summarised in Risbey et al. (2009) and discussed in more detail with respect to the Assessment area in section 2.1.9.

2.1.4 Monsoon

The Australian Monsoon is the predominant annual variation in tropical large-scale circulation that brings the wet season to northern Australia. It results from the seasonal oscillation of warm tropical oceans across the equator following the cycle of solar radiation maximum. This changes the wind direction from the south-easterly tradewinds of the dry season to a north-westerly flow that draws in moisture to northern Australia (McBride, 1998).

The monsoon season is most commonly observed across northern Australia from December to March, with high variability in the timing, extent and intensity of rain due to oscillations between ‘active’ and ‘break’ monsoon phases. Low pressure systems, ‘monsoon depressions’, are frequently generated along the trough line and these systems are dominant rainfall producing systems commonly associated with heavy rain.

Monsoon depressions contribute to summer rainfall in the Pilbara more frequently in the east than the west, are often modulated by the Madden-Julian Oscillation, as well as frequently influencing tropical cyclone genesis (Wheeler and McBride, 2005).

A stronger monsoon circulation is associated with an increased frequency of monsoon depressions and tropical cyclones and rainfall variability is strongly tied to the active/break cycle of the monsoon on intra-seasonal scales and large-scale influences, such as ENSO, on inter-annual timescales. Smith et al. (2008) found that long-term trends in total wet season rainfall and average intensities coincide (i.e. either both are going up or both going down together) across northern Australia, bit found no evidence that these trends were related to changing monsoon season lengths.

2.1.5 Madden-Julian Oscillation

A dominant feature of rainfall variability in the tropics is a global-scale atmospheric circulation and moist convection wave that propagates eastward across the equatorial Indian and Pacific oceans with an average speed of 400 km/day, resulting in a local periodicity of 30 to 60 days (Zhang, 2005). It was first documented by Madden and Julian (1972) and hence is known as the Madden-Julian Oscillation (MJO). The MJO interacts at various scales to influence ENSO, the monsoon circulation, and tropical cyclone genesis.

Over northern (tropical and subtropical) Australia during the monsoon season, the MJO produces 'active' and 'break' phases in convective activity that respectively enhance or suppress rainfall. The enhanced convection of the active phase increases the probability of extreme weekly rainfall (i.e. upper 20th percentile) by a factor of three compared to non-active phases for far northern Australia in summer (Wheeler and Hendon, 2004). Wheeler et al. (2009) produced composite maps of the MJO contribution to enhanced rainfall (upper tercile weekly rainfall) across Australia for all seasons, showing active MJO phases in December-January-February (DJF) enhance rainfall across most of the Pilbara (for the western, coastal and eastern but not central inland Pilbara) and in the March-April-May (MAM) period for the western coastal Pilbara only. Hall et al. (2001) investigated the influence of MJO on tropical cyclone activity, concluding that particularly for the Western Australian region there is enhanced genesis of tropical cyclones corresponding with enhanced MJO convection (i.e. the active phase of MJO). The relationship is stronger still during El Niño events. As well as enhanced convection, the MJO cycle also enhances large-scale processes influencing TC formation such as enhanced low-level vorticity (Hall et al., 2001). Figure 2.3 shows fluctuations in Outgoing Longwave Radiation (OLR) associated with periods of above and below average cloudiness caused by MJO 'pulses' as they move across northern Australia.

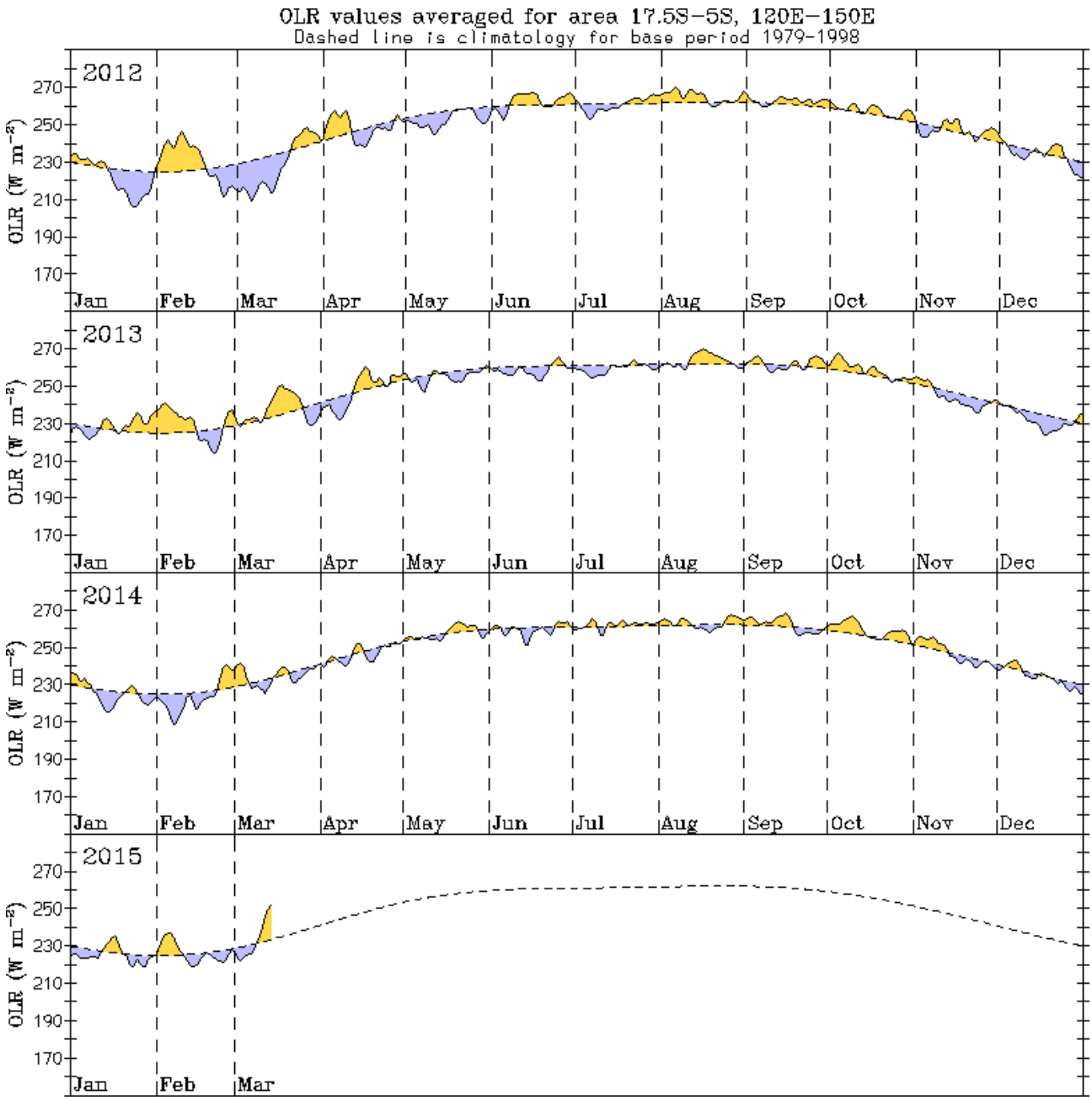

Figure 2.3 Outgoing longwave radiation anomalies (3-day moving average in W/m^2) showing fluctuations in cloudiness related to MJO. Below average (blue) represents more cloud and above (yellow) less cloud

Source: (Bureau of Meteorology, 2015)

Zhang (2005) noted the poor performance of the then current (circa 2005, i.e. CMIP3) climate models in simulating realistic MJO characteristics. An updated assessment of CMIP5 GCMs by Hung et al. (2013) concluded that although there has been general improvement with greater realism in CMIP5 models than in CMIP3 models, only one-third reproduce realistic MJO periodicity and they also tend to overestimate precipitation persistence (i.e. wet periods last too long). Only one of the 20 GCMs assessed, CNRM-CM5, reproduced a realistic eastward propagation of the MJO.

2.1.6 Tropical cyclones and depressions

Tropical cyclones (TCs), i.e. intense tropical depressions, are a major source of large-scale rainfall across the Pilbara (Lavender and Abbs, 2013). The largest volumes of rainfall received by the Assessment area are invariably a result of TCs crossing the Pilbara coast (Dare, 2013) [although there are also many localised

flooding events that are not directly correlated with the incidence of TCs; ~50% according to Rouillard et al. (2014)].

Kuleshov (2012) emphasised the dominant role that ENSO exerts on the year-to-year variability in TC genesis and development through influencing SST distribution, relative humidity and vorticity. Analysing a 1969 to 2006 database, Kuleshov (2012) observed increased TC genesis during La Niña episodes off the coast of northwest Australia (centred around 15 °S, 120 °E) resulting from positive SST and relative humidity anomalies and cyclonic vorticity anomalies. Ramsay et al. (2008) also concluded that ENSO-related Pacific SST anomalies influence TC frequency in the Australian region through an 'atmospheric bridge' resulting in enhanced low-level vorticity and reduced vertical wind shear.

The TC season in the southern hemisphere is generally from November to April (Kuleshov, 2012). For the east southern Indian Ocean (ESIO, defined by the longitude range 80 to 135 °E) during La Niña episodes there is a double peak, in December and March, in the number of days with TC activity ('TC days') 50 to 100% higher than in El Niño or neutral phases. TC frequency peaks in March for all three ENSO phases. Within the ESIO, there is a 'hot spot' in TC genesis and TC days to the north of the Pilbara and west of the Kimberley (Dowdy and Kuleshov, 2012). Liu and Chan (2012) also found that the tropical Indian Ocean off the Western Australian coast has more prominent TC activity than other regions and that the inter-annual variability is related to ENSO with a doubling of the annual number of TCs in La Niña years from the frequency in El Niño years. A relationship with the Indian Ocean Dipole (IOD) was also found for the eastern Australian region (due to enhanced negative cyclonic relative vorticity when La Niña and negative IOD events coincide) but not for the Western Australian region.

Although TC records can be considered complete and reliable since the introduction of meteorological satellites in the late 1960s, trend analysis is problematic due to this limited record, changes in observation technologies and analysis techniques (Kuleshov, 2012). Harper et al. (2008) reanalysed the TC dataset for the north-west region (for Woodside Petroleum Ltd.) and concluded that earlier northwest Australian records (circa 1970s) contain underestimation biases in central pressure deficit of the order of 20%, leading to false trends. They concluded that there is no evidence of a trend in TC intensity over the last 30 years for northwest Australia. Goebbert and Leslie (2010) used the TC dataset compiled by Harper et al. (2008) to investigate trends and possible predictors of TC inter-annual variability for the northwest. They found that commonly assessed global modes (including Niño-3.4, Niño-4, Southern Oscillation Index, Northern Oscillation Index, North Atlantic Oscillation, Pacific-North American pattern, Pacific decadal oscillation, Arctic Oscillation, Quasi-Biennial Oscillation, IOD index) were not significantly correlated with the variability of TC frequency or duration. Kuleshov et al. (2010) used nonparametric Monte Carlo techniques to determine whether there were trends in TC occurrence and intensity for the 1981/82 to 2006/07 seasons, in addition to those attributable to inter-annual variability or changes in observing practise, and also concluded that there were no significant trends in TC numbers in the Australian region. Dowdy (2014) examined TC frequency in the Australian region for the seasons 1981/82 to 2012/13 and, after accounting for the variability associated with ENSO, determined that there has been a significant decrease in TC numbers over this period (at a 0.93 to 0.98 confidence level).

Dare et al. (2012) undertook a detailed analysis of the influence of tropical cyclones on Australian rainfall, investigating both the magnitude and variability of spatial influence for TCs that crossed the coast and those that came within 500 km of the coast without crossing. Investigating TC counts for 5° longitudinal bands across the northern Australian coastline over 41 seasons (1969/70 to 2009/10) showed that the Pilbara coast has experienced the greatest number of TCs of any region in Australia, on average four per year with three crossing the coast. While the contribution of TCs to Pilbara rain rates is not the highest across the continent in absolute terms it is the highest in percentage terms, contributing 25 to 34% of mean November to April rainfall. TCs that make landfall in the Pilbara have the greatest inland penetration nationally, contributing up to 21% of November to April rainfall up to 450 km inland. The 115 to 120 °E band has the largest distance at which the inland TC rain rate falls to half the coastal rain rate (~250 km).

The seven-year period with the highest rainfall across the Pilbara (1994/5 to 2000/1) contains several seasons with above average numbers of TCs. The rainfall and number of TCs influencing the Pilbara during this exceptionally wet period are summarised in Table 2.1.

Table 2.1 Summary of 1994/5 to 2000/1 Pilbara rainfall and tropical cyclone characteristics

WATER YEAR (Oct-Sep)	WATER YEAR RAINFALL (mm)[1]	NOV-APR ALL RAINFALL (mm)[2]	NOV-APR TC RAINFALL (mm)[2]	% TC RAINFALL OF ALL (%)[2]	TC COUNT[2]
1994/95	500.5	392.1	107.0	27	2
1995/96	301.5	202.6	118.9	59	6
1996/97	543.6	434.0	52.3	12	3
1997/98	316.1	90.8	2.7	3	2
1998/99	611.0	552.2	132.4	24	5
1999/00	708.4	656.6	236.1	36	8
2000/01	391.0	326.1	76.7	24	4

1 SILO datadrill averaged over Pilbara Assessment area; 2: for TCs contributing to rainfall in the 115-120 °E by 20-25 °S grid box.
Source: 115-120 °E by 20-25 °S grid box TC rainfall and TC count from R. Dare (BoM, 2013, pers. comm.)

The consecutive seasons of 1998/99 and 1999/00 saw the highest rainfall totals on record and are also both La Niña years. Given that rainfall in these years would have undoubtedly produced a large hydrological impact in the region, it is of interest to summarise the TCs that influenced the Pilbara during these two seasons.

The 1998/1999 season has been noted as particularly active, with Leslie et al. (2002) concluding that the above average number of TCs and the number of unusually intense TCs making landfall (three Category 5 TCs) can be attributed to favourable precursors to the development of tropical cyclones (cyclogenesis). These include anomalies in mean sea-level pressures (MSLP) (lower than average), SSTs (warmer than average), relative humidity (higher than average) and weak wind shears in the genesis regions. Five TCs contributed 24% of November to April rainfall in the 115 to 120 °E by 20 to 25 °S grid box encompassing most of the Pilbara Assessment area (R Dare (BoM), 2013, pers. comm.).

The BoM Western Australia Tropical Cyclone Season Summary for 1998/1999 (http://www.bom.gov.au/cyclone/history/wa/1999.shtml) notes that moderate La Niña conditions had been preceded by El Niño conditions. The TCs of note, in chronological order, were:

1. 02/12/1998 to 07/12/1998. Severe Tropical Cyclone *Billy* formed north of Port Hedland reaching cyclone intensity as it tracked southwest towards the west Pilbara coastline, weakening to cross as a tropical low near Onslow.
2. 06/12/1998 to 12/12/1998. Severe Tropical Cyclone Thelma was the most intense TC in the Northern Region in the last 35 years reaching its peak as a Category 5 in the Timor Sea before weakening as it crossed the northwest Kimberley coast.
3. 15/03/1999 to 20/03/1999. Severe Tropical Cyclone Elaine intensified to severe cyclone strength well off the WA coast before moving south and weakening, crossing the coast between Geraldton and Kalbarri on 20 March, then flooding Moora.
4. 16/03/1999 to 23/03/1999. Severe Tropical Cyclone Vance reached Category 5 overnight 20 March, and crossed 25 km to the east of Exmouth on the morning of 22 March causing severe beach erosion. Learmonth Meteorological Office, 35 km south of Exmouth, recorded a record wind speed gust for the Australian mainland of 267 km/hour.
5. 02/04/1999 to 07/04/1999. Severe Tropical Cyclone Gwenda was near Category 5 on the 6 April before weakening when within 100 km of Port Hedland, crossing 50 km to the east of Port Hedland.

The tracks of these TCs are shown in Figure 2.4.

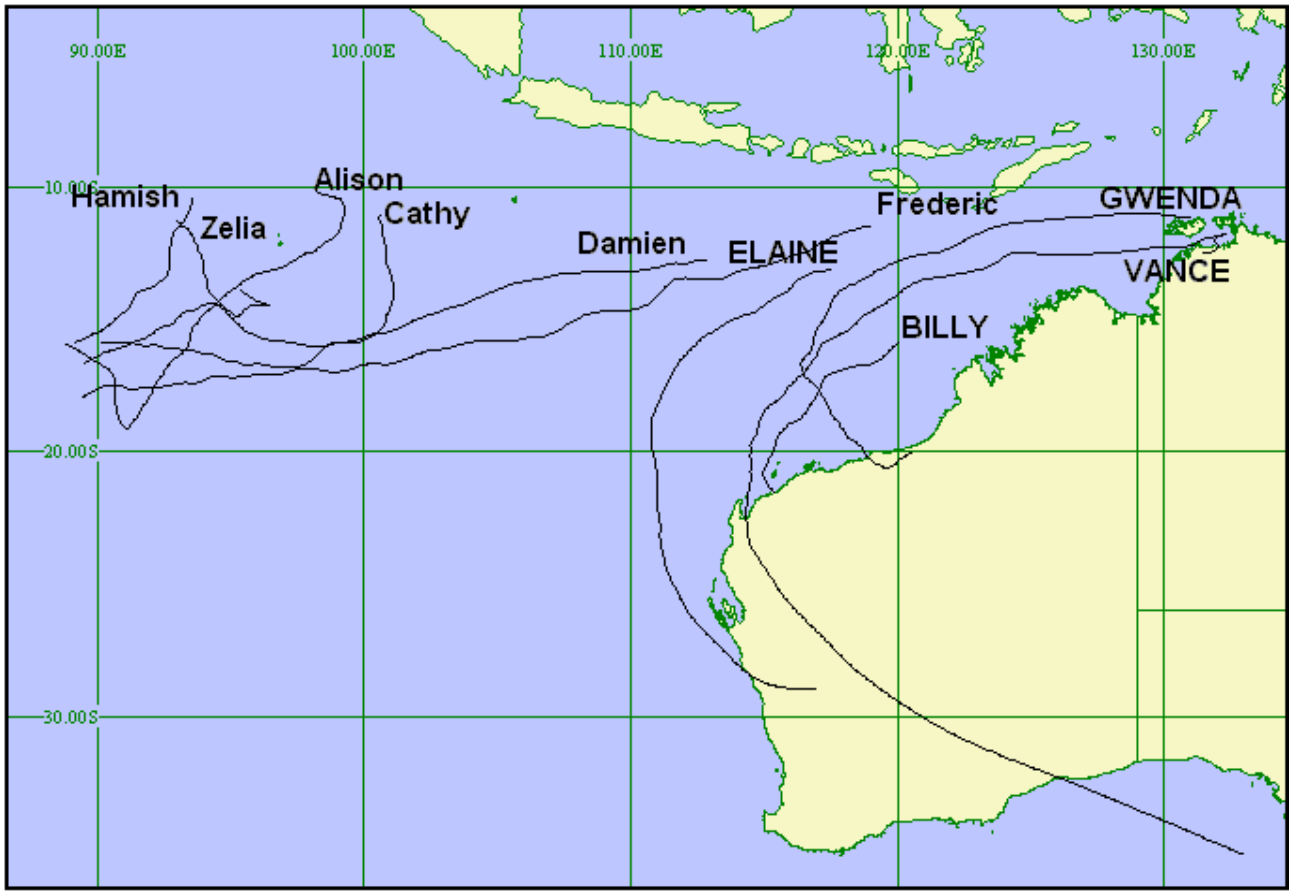

Figure 2.4 1998/99 tropical cyclone tracks influencing Western Australia (NB: TC Thelma not shown)

Source: (Bureau of Meteorology, 2013b)

The 1999/2000 season was even more active than the previous 1998/99 season, with 8 TCs contributing to the wettest year on record for the Pilbara. These 8 TCs contributed 36% of November to April rainfall in the 115 to 120 °E by 20 to 25 °S grid box encompassing most of the Pilbara Assessment area (R. Dare, *pers. comm.*, 2013).

The BoM Western Australia Tropical Cyclone Season Summary for 1999/2000 (http://www.bom.gov.au/cyclone/history/wa/2000.shtml) notes the rapid onset of (moderate) La Niña conditions from October 1999 influenced both the number of TCs and the overall wet season rainfall. The TCs (and one significant tropical low that did not develop into a TC) in chronological order were as follows (with their tracks shown in Figure 2.5):

1. 09/12/1999 to 17/12/1999. Tropical Cyclone Ilsa crossed at Eighty Mile Beach on 17 December 1999 after a long track eastwards across the Indian Ocean.
2. 09/12/1999 to 16/12/1999. Severe Tropical Cyclone *John* was Category 5 just before it crossed the coast between Port Hedland and Karratha on 15 December 1999. A maximum wind gust of 210 km per hour was recorded at Cape Lambert.
3. 21/01/2000 to 23/01/2000. Tropical low tracked towards Pilbara coast but did not develop into a TC.
4. 24/01/2000 to 01/02/2000. Tropical Cyclone *Kirrily* moved towards the WA coast reaching Category 2 before turning and tracking southwest before weakening below TC strength.
5. 29/02/2000 to 08/03/2000. Severe Tropical Cyclone *Norman* formed from a Kimberley low and reached Category 5 on 2 March during its 3-day westward track approximately 250 km from the Pilbara coast.
6. 05/03/2000 to 09/03/2000. Tropical Cyclone *Steve* reformed west of Broome on 5 March after crossing the continent. It tracked very close to the Pilbara coast before crossing in the western Pilbara near Mardie at midnight on 6 March. Very heavy rainfall resulted in widespread flooding including the

Fitzroy, De Grey, Gascoyne and Murchison River catchments. Rainfall totals ranged from 200 to 300 mm for parts of the western Pilbara and northern Gascoyne. Several sites reported daily rainfall amounts that were the highest on record such as Mandora (281.0 mm on 6 March) and Mount Narryer (152.0 mm on 10 March).

7. 15/03/2000 to 19/03/2000. Tropical Cyclone *Olga* tracked west southwest parallel to the Kimberley and Pilbara coasts reaching Category 2 before weakening well to the west.
8. 13/04/2000 to 20/04/2000. Severe Tropical Cyclone *Paul* tracked westerly 1000 km north of the Pilbara coast reaching Category 5 on 15 April then continuing west slowing and weakening.
9. 17/04/2000 to 21/04/2000. Severe Tropical Cyclone *Rosita* crossed the west Kimberley coast as a Category 5 cyclone 40 km south of Broome on 20 April 2000 then moved southeast.

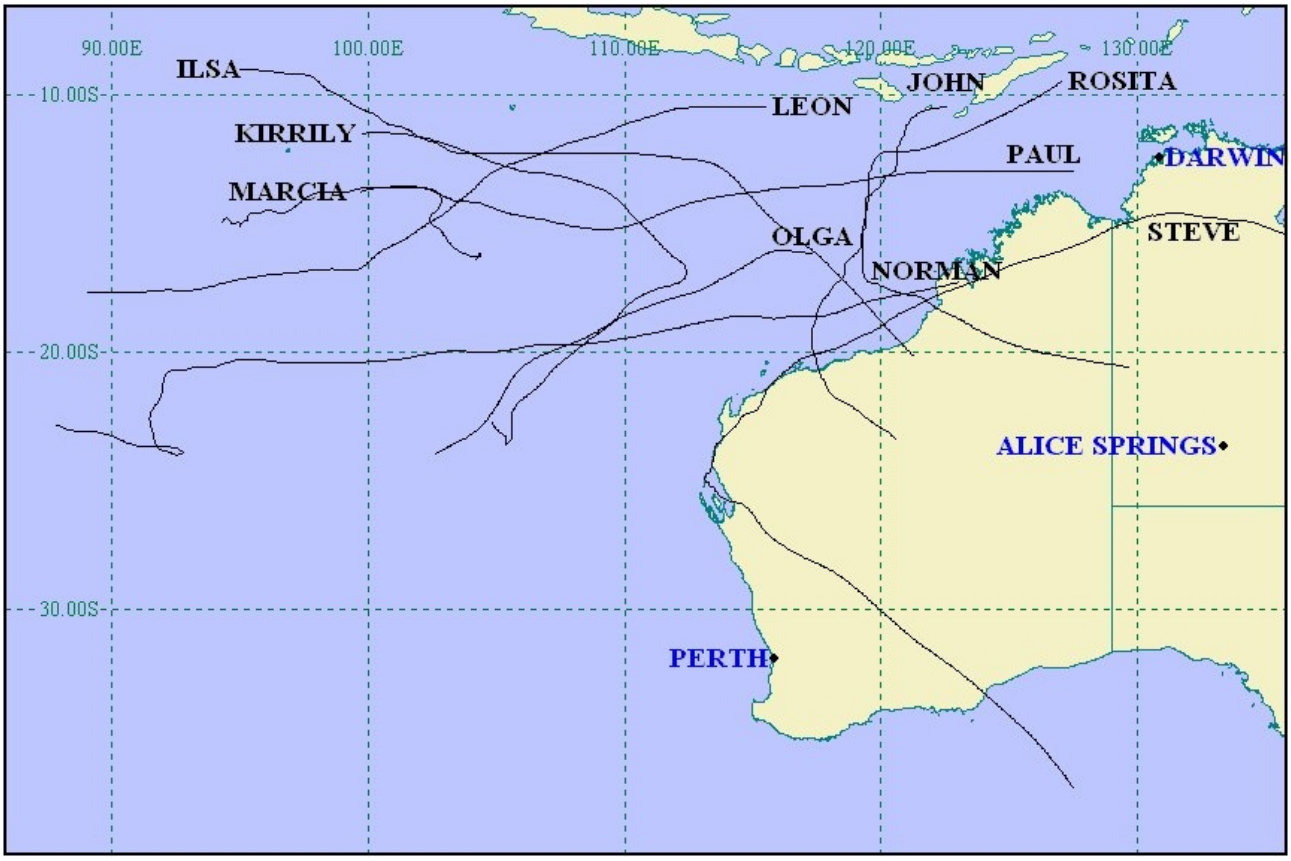

Figure 2.5 1999/00 tropical cyclone tracks influencing Western Australia

Source: (Bureau of Meteorology, 2013c)

Although there is a relationship between the number of cyclones per season and rainfall totals, there is not a strong linear correlation as shown in Figure 2.6. While there is little long-term trend in the inter-annual variability in the frequency or intensity of TCs in the Pilbara region in the most recent decades (Goebbert and Leslie, 2010; Hassim and Walsh, 2008) there is large inter-annual variability in the proportion of Pilbara rain that comes from TCs, ranging from 0% to 86% of November to April total rain from TCs for the 110 to 115 °E and 115 to 120 °E longitudinal bands analysed by Dare et al. (2012), the highest variability nationally. However given that on average only a third of November to April rainfall in the Pilbara results from TCs, it is not always the case that a season with a low contribution from TCs is necessarily a drier year. For example, the coefficient of determination (R^2) between November to April total rainfall and TC rainfall for the 5° x 5° grid box over the Pilbara (115 to 120 °E and 20 to 25 °S) for 1969/70 to 2010/11 is only 0.08. Thus while TC rainfall may dominate in some years the non-TC contributions to total rainfall are on average greater, be they large-scale tropical depressions or smaller scale convective storms.

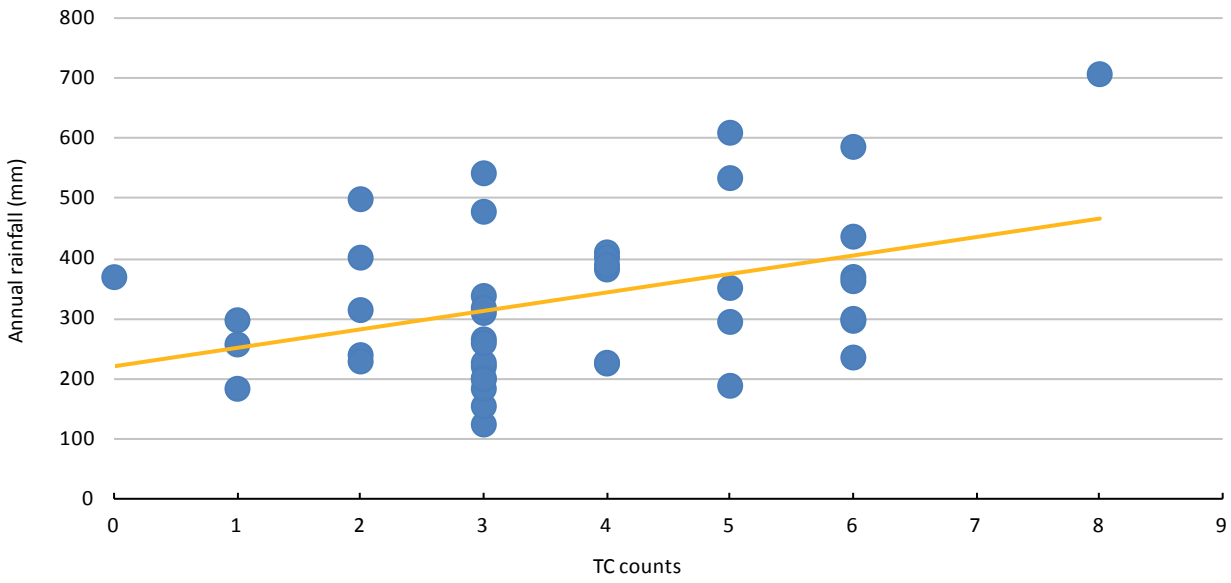

Figure 2.6 Assessment area annual rainfall (water year, mm) versus tropical cyclone (TC) counts for 1969/70 to 2010/11

Lavender and Abbs (2013) compared the contribution of tropical cyclones and closed-lows[1] to Australian rainfall trends by analysing precipitation efficiency (i.e. amount of rainfall per TC or closed-low day) for TCs for 1970-2009 and closed-lows for 1989-2009. Detailed descriptions of the databases used to determine TC and closed-low rainfall are given in Lavender and Abbs (2013). They found TC-days contributed between 20 to 35% of annual rainfall and over 40% of extreme rainfall events (i.e. above the 99th percentile) for the Pilbara coastline with maxima of TC influence on extreme rainfall centred near Port Hedland. Consistent with other studies they find no trends in frequency of TCs over northwest Australia and very little trend in the percentage of annual rainfall contributed by TCs with some areas showing a slight increase and some a slight decrease. Thus the increasing trend in total rainfall in the northwest, of 2.85 mm per year across the 1970 to 2009 period, is mostly contributed by non-TC rain (2.25 mm per year). The closed-low analysis of the shorter 1989 to 2009 period found a much larger trend, 8.22 mm per year, from combined TCs and closed-lows, in annual rainfall of which 5.79 mm per year was contributed by closed-lows. As there was little trend in closed-low days (i.e. frequency of closed-lows) there was necessarily an increase in rainfall per closed-low day, i.e. an increase in rainfall efficiency, over the northwest as a whole. For the Pilbara region there was a small positive trend in TC precipitation efficiency (although not statistically significant at the 90% level) and no apparent trend in closed-low efficiency (for non-TC closed-lows or all closed-lows, i.e. including TCs).

Anthropogenic climate change is warming the atmosphere and the oceans and thus is expected to increase the theoretical upper intensity of TCs due to warmer SSTs. A global review by Knutson et al. (2010) summarised the current state of knowledge:

> ***Detection and attribution***:
>
> *It remains uncertain whether past changes in any tropical cyclone activity (frequency, intensity, rainfall, and so on) exceed the variability expected through natural causes, after accounting for changes over time in observing capabilities.*
>
> ***Tropical cyclone projections****:*
>
> *Frequency: It is likely that the global frequency of tropical cyclones will either decrease or remain essentially unchanged owing to greenhouse warming. We have very low confidence in projected*

[1] Defined by Lavender and Abbs (2013) as systems with a low-pressure centre at any of five atmospheric levels (the surface, 850, 700, 500 and 300 hPa) that last for more than 48 hours. Include tropical cyclones, tropical depressions, cut-off lows and mid-latitude lows.

changes in individual basins. Current models project changes ranging from -6 to -34% globally, and up to ±50% or more in individual basins by the late twenty-first century.

Intensity: Some increase in the mean maximum wind speed of tropical cyclones is likely (+2 to +11% globally) with projected twenty-first century warming, although increases may not occur in all tropical regions. The frequency of the most intense (rare/high-impact) storms will more likely than not increase by a substantially larger percentage in some basins.

Rainfall: Rainfall rates are likely to increase. The projected magnitude is on the order 20% within 100 km of the tropical cyclone centre.

Genesis, tracks, duration and surge flooding: We have low confidence in projected changes in tropical cyclone genesis-location, tracks, duration and areas of impact. Existing model projections do not show dramatic large-scale changes in these features. The vulnerability of coastal regions to storm-surge flooding is expected to increase with future sea-level rise and coastal development, although this vulnerability will also depend on future storm characteristics.

Modelling studies of projected changes in TC climatology undertaken for the Australian region by CSIRO (Abbs, 2012; IOCI, 2012) have used multiple levels of dynamical downscaling. Firstly, CSIRO Conformal-Cubic Atmospheric Model (CCAM), a stretched-grid global atmospheric model with a 65 km horizontal resolution over Australia, downscaled from GCM projections and subsequently the Regional Atmospheric Modelling System (RAMS) down to 5 km resolution was nested in these CCAM runs. The finer spatial scale of dynamic downscaling is required as typical GCM spatial resolutions of 200 to 500 km are larger than TCs, hence GCM-modelled TCs are wider and less intense than observed TCs. The CCAM simulations account for projected changes in TC occurrence, genesis and decay characteristics but are still too coarse to adequately assess changes to TC intensity as they do not resolve the TC eyewall where the strongest winds and heaviest rainfalls occur. RAMS was applied to one of the CCAM results at a 5 km resolution to resolve such characteristics on an event basis for 120 tropical cyclone-like vortices in current and future periods.

CCAM reproduced the historical patterns of spatial TC occurrence in the Australian region, accounting for the different spatial patterns seen during El Niño and La Niña events. Although the spatial patterns are reproduced, too few TCs are simulated by CCAM so that the frequencies are underestimated by approximately 40%. CCAM downscaling for seven CMIP3 GCMs for the A2 scenario consistently simulate fewer TCs in the northwest region for the period 2051 to 2090 than in 1971 to 2000, on average a 50% decline in the number of TCs. These simulations also show a small decrease in duration (0.6 days) and an approximately 100 km southward shift in genesis and decay regions.

Assessment of the projected intensity changes simulated by the RAMS 5 km downscaling for 2051 to 2090, relative to 1961 to 2000, focussed on the storm characteristics for the 12 hours centred on the period of maximum TC intensity (i.e. minimum pressure). These show projected increases in the size and intensity of TCs with the proportion of TCs with a maximum wind speed greater than 40 m per second (approximately Category 3 to 5), the integrated kinetic energy (a measure of TC size and wind speed), the radius of maximum winds, and the radius to gale-force winds all increasing. Rainfall intensity in the 12-hour periods simulated increased 33% in within 300 km of the TC centre and 23% within 200 km (IOCI, 2012).

While one recent study, downscaling six CMIP5 GCMs, concluded the frequency of TCs could increase throughout the 21st Century (Emanuel, 2013) many more CMIP3 and CMIP5 studies concur with CSIRO findings of fewer but more intense TCs in the future (Bell et al., 2013; Gleixner et al., 2014; Murakami et al., 2014; Roberts et al., 2015; Scoccimarro et al., 2014; Tory et al., 2013). Thus the weight of current understanding supports decreases in the frequency of TCs impacting the Assessment area as more likely than increases. However uncertainties remain, for example research investigating Atlantic TCs suggests atmospheric aerosols from industrial pollution may have suppressed storm development in the 20th Century and thus decreasing pollution could lead to an increased frequency of TCs in the future (Dunstone et al., 2013). There are currently no equivalent studies of aerosol impacts on TCs for the Australian region.

2.1.7 Indian Ocean Dipole

As a moisture source and as the source of thermal energy for tropical cyclone growth a warmer Indian Ocean (positive SST anomalies) is associated with enhanced rainfall and cooler SSTs (negative anomalies) are associated with reduced rainfall. The IOD is a major pattern of Indian Ocean SST variability that impacts on Australia's rainfall. The IOD is expressed as contrasting SST anomalies between the western and eastern equatorial Indian Ocean (Saji et al., 1999). The IOD is calculated using the Dipole Mode Index (DMI) which is the difference between SSTs in a western box (50 to 70 °E and 10 °N to 10 °S) and an eastern box (90 to 110 °E and 0 to 10 °S). A positive DMI occurs when the eastern SSTs are anomalously cool and western SSTs are anomalously warm (Figure 2.7). This contributes to drier conditions over central and southern Australia. In contrast a negative DMI occurs when the eastern SSTs are anomalously warm and western SSTs are anomalously cool, contributing to wetter conditions over parts of southern Australia.

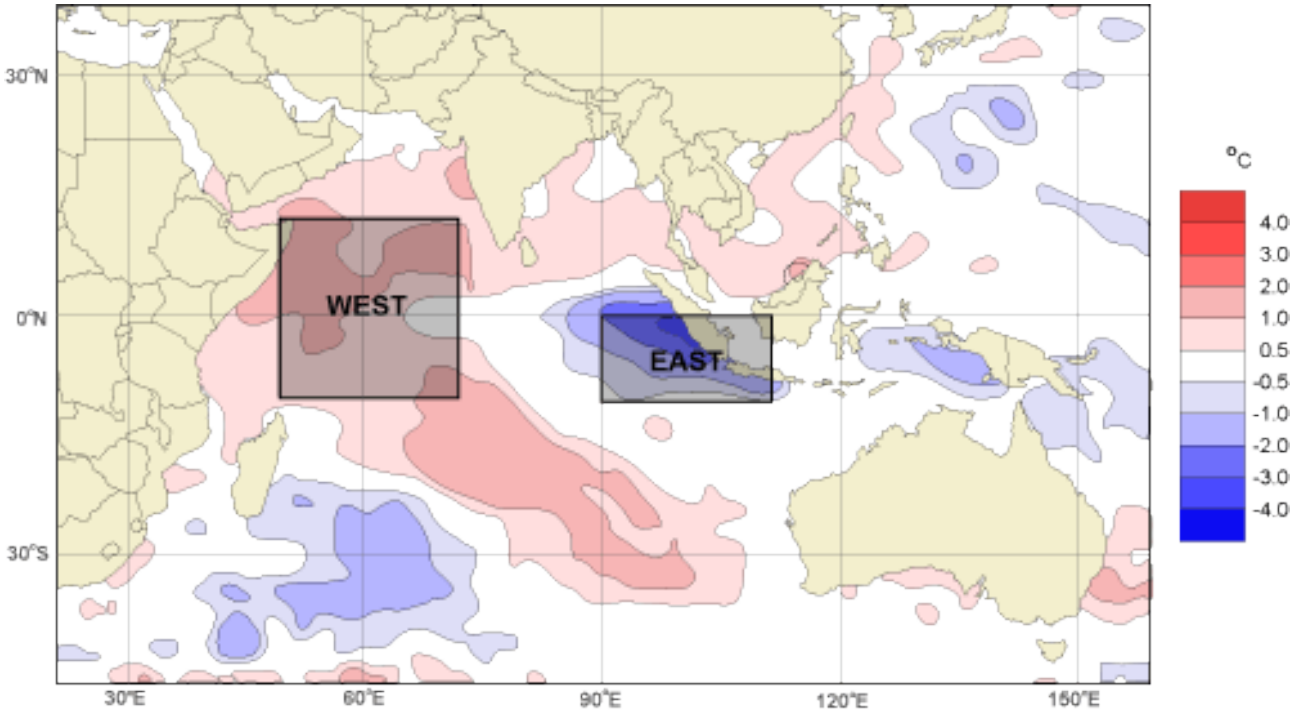

Figure 2.7 Positive IOD event peaking in November 1997, showing departures from average SSTs with the east and west poles used to calculate the Dipole Mode Index represented by boxes

Source: (Bureau of Meteorology, 2013a)

The IOD interacts with ENSO to further enhance or suppress rainfall but the relationship is complicated and the key dependencies have yet been fully resolved. As IOD events typically develop through winter (JJA) and peak in spring (SON) they have some correlation with Pilbara rainfall in winter but little correlation with spring (see Figure 3 in Cai et al. (2009); Figures 3 and 6 in Cai et al. (2011b)). However as these seasons contribute a small proportion of total annual rainfall the influence of IOD is likewise small. The shift towards a greater frequency of positive IOD events during the last 30 years is hypothesised to be a causal factor in the drying trend seen in south-eastern Australia's winter and spring rainfall (Cai et al., 2009).

2.1.8 Other drivers

Recent research linking tree-ring chronology to increased summer-autumn rainfall over the Pilbara (O'Donnell AJ et al., 2015 (submitted)) suggests there is a signal from the Southern Annular Mode (SAM, the north–south movement of the westerly wind belt that circles Antarctica). A mechanism by which SAM influences storm tracks leading to increased spring-autumn precipitation in the Australian subtropics is described by Hendon et al. (2014).

2.1.9 Rainfall relationships with large-scale processes

The rainfall climatology of the Pilbara results from interactions between the large-scale processes (described above) and localised features such as convective storms. There are trends of increasing rainfall across a significant proportion of northern and central parts of the western half of the Australian continent, including the eastern Pilbara region, since the middle of the twentieth century (Berry et al., 2011). In contrast, the western Pilbara has experienced long-term rainfall declines (predominantly in the May to October half-year since the 1960s, as shown later) linked to reduced frontal rainfall from southern sources. These historical spatial and temporal rainfall properties are presented in detail in sections 1.1.1 and 2.2.3.

An Australia-wide study by Schepen et al. (2011) is insightful when examining the key climatic drivers of regional rainfall variability of relevance to the Pilbara region. Thirteen monthly climate indices of atmospheric or oceanic conditions (Table 1 in Schepen et al.) were assessed as potentially useful predictors for seasonal rainfall. There was little predictive power for the Pilbara from any of the indices for the MAM, JJA or SON seasons whereas DJF showed a positive to very strong supportive evidence from two Indian Ocean SST indices, the Indonesia index 'II' of SST anomalies over the Indonesian Seas (defined as average SST anomaly over 120 to 130 °E and 0 to 10 °S), and the Indian Ocean East Pole index (EPI), defined as average SST anomaly over 90 to 110 °E and 0 to 10 °S.

Taschetto and England (2009) reviewed rainfall trends in Australia for the period 1970 to 2005. Trends in OLR, Sea-Level Pressure (SLP) and divergence at the 200 hPa level indicated increased convection consistent with the increased DJF rainfall over the eastern Pilbara. Daily rainfall distributions were found to shift to higher intensities in DJF and MAM during the 1990s compared to the 1970s. Very heavy events in particular have positive trends in the eastern Pilbara for DJF and MAM, which they suggest result from convective systems rather than large-scale rainfall systems. Changes to the monsoon trough are hypothesised to be the cause of these rainfall changes.

Risbey et al. (2009) emphasise IOD, MJO and ENSO as the dominant drivers of rainfall variability on seasonal to inter-annual timescales in the Australian tropics and that these drivers are not independent, with ENSO influencing the others (particularly IOD). Using long-term records (1889-2006) they find ENSO (SOI) is positively correlated with Pilbara rainfall in DJF, eastern Pilbara rainfall in JJA, and uncorrelated in MAM and SON. IOD was found to be not significant for Pilbara rainfall variability given its season of influence is June to October, and MJO has its strongest influence on monsoonal rains.

Most studies of northwest rainfall trends have focussed on the regions to the north of the Pilbara (e.g. Kimberley and Northern Territory), where the rainfall trends are stronger and thus there have been few studies that have investigated Pilbara rainfall directly. Fierro and Leslie (2012) analysed correlations between rainfall for a larger region including the Pilbara (an box between latitudes 20° and 30°S, and longitude 120°E and the coast) and indices related to climate drivers such as ENSO and related atmospheric circulation anomalies. Five of their ten stations were in, or close to, the Pilbara, i.e. coastal stations Port Hedland and Exmouth Gulf and inland stations Coolawanyah, Mulga Downs and Mount Augustus. They determined ENSO has been the dominant factor in the summer (November to April) rainfall increase, consistent with La Niña years being more frequent in the period with increased rainfall (as noted above, La Niña years are associated with an increased frequency of tropical cyclones). For winter (May to October) rainfall, they found the strongest relationship with IOD phase (i.e. greater rainfall during negative phases of IOD and vice versa). Investigating associated circulation anomalies, Fierro and Leslie (2012) attribute the increasing Pilbara summer rainfall to increased onshore advection of moist tropical air as a result of a shift from once strong anticyclonic anomalies to now weak cyclonic anomalies. For winter, the recent marginal drying trend was attributed to winds shifting from a strong onshore component in the 1960s and 1970s to a weak offshore component during the decade to 2010. These regional scale circulations anomalies can, in turn, be related to hemispherical scale trends in circulation processes that are consistent with forcing from external factors (i.e., external radiative forcing, including anthropogenic greenhouse gases, ozone, aerosols and land use change) as proposed by Frederiksen and Grainger (2015).

Rotstayn et al. (2012) used a GCM (CSIRO Mk3.6) to model the role that aerosols (more specifically, the Asian aerosol haze) may have had on northwest Australian rainfall trends, proposing a mechanism by which

the cooling effect of aerosols across the South-East Asian region increases cyclonic (clockwise) circulation over the Indian Ocean, leading to more moisture being transported towards northwest Australia by strengthened monsoonal winds. However, given the results were only based on one GCM, they state this interpretation should be treated as a hypothesis at this stage until tested by multiple models.

Lin and Li (2012) suggest that the observed increase in north-west Australian summer rainfall may be partially explained by a remote teleconnection with the tropical Atlantic. The mechanism involves increased tropical Atlantic sea surface temperatures producing enhanced atmospheric accent, promoting the south-eastward propagation of a Rossby wave train that produces anomalies in upper tropospheric geopotential heights over Australia. This results in enhanced ascent and convergence in the lower troposphere over Australia, with associated increased rainfall in north-west Australia. In addition to this tropical Atlantic teleconnection, a relationship has also been proposed between warming sea surface temperatures in the tropical western Pacific to the north of Australia and north-west Australian summer rainfall increases since 1979 (Li et al., 2013). In this process, tropical western Pacific sea surface temperature warming results in the formation of a large cyclonic anomaly across the whole of northern Australia with the resulting low sea-level pressure correlated with more rainfall, cloud and surface evaporation (and hence land surface cooling) over the region. Li et al. (2013) conclude that this increase in tropical western Pacific sea surface temperatures is the dominant driver of increasing northern Australia summer rainfall trends over the 1979 to 2010 period. As yet there is no clear understanding as to how these proposed driving factors have combined to produce the observed trends, or which are likely to dominate in the future (Cai et al., 2011a; Li et al., 2013; Lin and Li, 2012; Rotstayn et al., 2012).

The majority of CMIP3 GCMs project a drying trend over NWA, at odds with the recently observed trends. Cai et al. (2011a) determined that of 24 CMIP3 models only nine projected an increasing rainfall trend with all modelled trends found to be much weaker that the observed trends (for 1950 to 2008). Cai et al. (2011a) also cautioned against the use of the driest projections as they are a result of model biases in the location of ENSO. That is, the observed teleconnection between ENSO and northeast Australia is shifted too far west in some models, erroneously affecting NWA rainfall trends, and thus these models produce unrealistically strong future NWA rainfall reductions. Whether this issue is still a problem with CMIP5 simulations is yet to be assessed. Catto et al. (2012) concluded that most CMIP5 models fail to reproduce the strong correlation between ENSO (Niño 3.4) and northern Australia SST seasonal cycles (two exceptions were NorESM1-M and CNRM-CM5). Some aspects of simulated ENSO are improved over CMIP3, whereas north Australian SST evolution has not, indicating that the CMIP5 models '*are still missing some underlying process or mechanism*' (Catto et al., 2012).

In summary, the above studies emphasis that Pilbara rainfall variability is driven by interactions between the key large-scale processes described above and these interactions are complicated and not fully understood. ENSO, the monsoon, MJO, and tropical cyclones appear to be the main factors that combine to produce the observed frequency and intensity of wet years. Their variability and trends are thus the dominant drivers of the observed rainfall trends discussed later.

2.2 Climate variable characteristics and trends

2.2.1 Datasets

The Bureau of Meteorology only classifies six stations as providing high-quality rainfall data in the Pilbara region (<http://www.bom.gov.au/climate/change/hqsites/>). As six stations would not be sufficient to explore the climate variability and trends for such a large area, more stations are used to explore the spatial differences using the SILO dataset, a comprehensive archive of Australian rainfall and climate data constructed from ground-based observational data (Jeffrey et al., 2001). Station-based datasets are available for approximately 4600 locations across Australia, commencing in 1890 for rainfall and 1957 for other climate variables. The network of stations recording daily weather has changed over time, with rainfall recorded at more stations than other climate variables. Automatic weather stations were introduced into the Bureau's network from the early 1990s, and the associated tipping bucket rain gauges

(TBRG) generally augmented the network, though the network of TBRGs is much sparser than that of the manual gauges. The reliability of extreme daily rainfall recordings can be questionable due to the overflow of gauges and potential undercatch because of high winds during tropical cyclone events, though the former problem is not an issue with the more recent TBRGs. Thus it is important that trends in extreme daily rainfall in the SILO data are interpreted with caution due to these observational concerns. That is, trends in extreme daily rainfall in the SILO data may be a result of observational equipment changes rather than any intensification due to climate trends.

The station data have been used to produce interpolated surfaces on a regular 0.05° grid extending from latitude 10 °S to 44 °S and longitude 112 °E to 154 °E. A thin plate smoothing spline was used to interpolate daily climate variables, and ordinary kriging was used to interpolate daily and monthly rainfall (Jeffrey et al., 2001). Thus two datasets are available from SILO: the Patched Point Dataset (PPD) for locations and the Data Drill gridded data at 0.05**°** resolution (http://www.longpaddock.qld.gov.au/silo/). The PPD are observed data when available from BoM stations with missing or suspect values 'patched' with interpolated data. Patched data is valuable for modelling studies, saving the user the task of dealing with missing data. The missing data are filled ('patched') with interpolated values from other stations nearby. The PPD would typically be used when an analysis or simulation is needed at or close to a meteorological station. However, if an analysis is required for a location that has no meteorological station nearby or for spatial analysis, then the Data Drill is the more useful product.

There are 93 PPD stations within or around the Assessment area (Figure 2.8) and about 10,000 0.05**°** grid cells. Daily rainfall comes with a source code to indicate its source (Table 2.2). The ideal situation is to investigate the trends and variability with 'real' observations only, i.e. a source code 0. An exploratory data-quality check (Figure 2.9) shows that: 1) it is very hard to detect trends using observed rainfall only; and 2) it is better to investigate starting from 1910, instead of 1900, as there are very limited observations before 1910.

Limitations in the data due to the changes in the observational network (i.e. stations opening and closing over time), changes in observational practises (such as the move from manual to automated weather stations) mean that the trends and spatial patterns presented in the following sections should be interpreted with caution as they could be influenced by data availability and quality changes rather than solely changes in climate. For example, trends in the east of the Assessment area are derived from very few stations east of the Nullagine River (Figure 2.8).

Table 2.2 SILO data source code values and meanings

VALUE	MEANING
0	Official observation as supplied by Bureau of Meteorology (may come from a volunteer)
13	Official observation that was from a period > 1 day, redistributed to daily data using daily observations from a comparable station
15	As for 13, but redistributed using interpolated data (see code 25)
23	Comparable station, official observation supplied by the Bureau of Meteorology
25	Interpolated from daily observations for that date
26	Synthetic Class A pan evaporation, calculated from interpolated temperatures, radiation and vapour pressure
35	Interpolated from daily observations using anomaly interpolation method for CLIMARC data
75	Interpolated from the long-term averages of daily observations for that day of year

Source: (The Long Paddock, 2011)

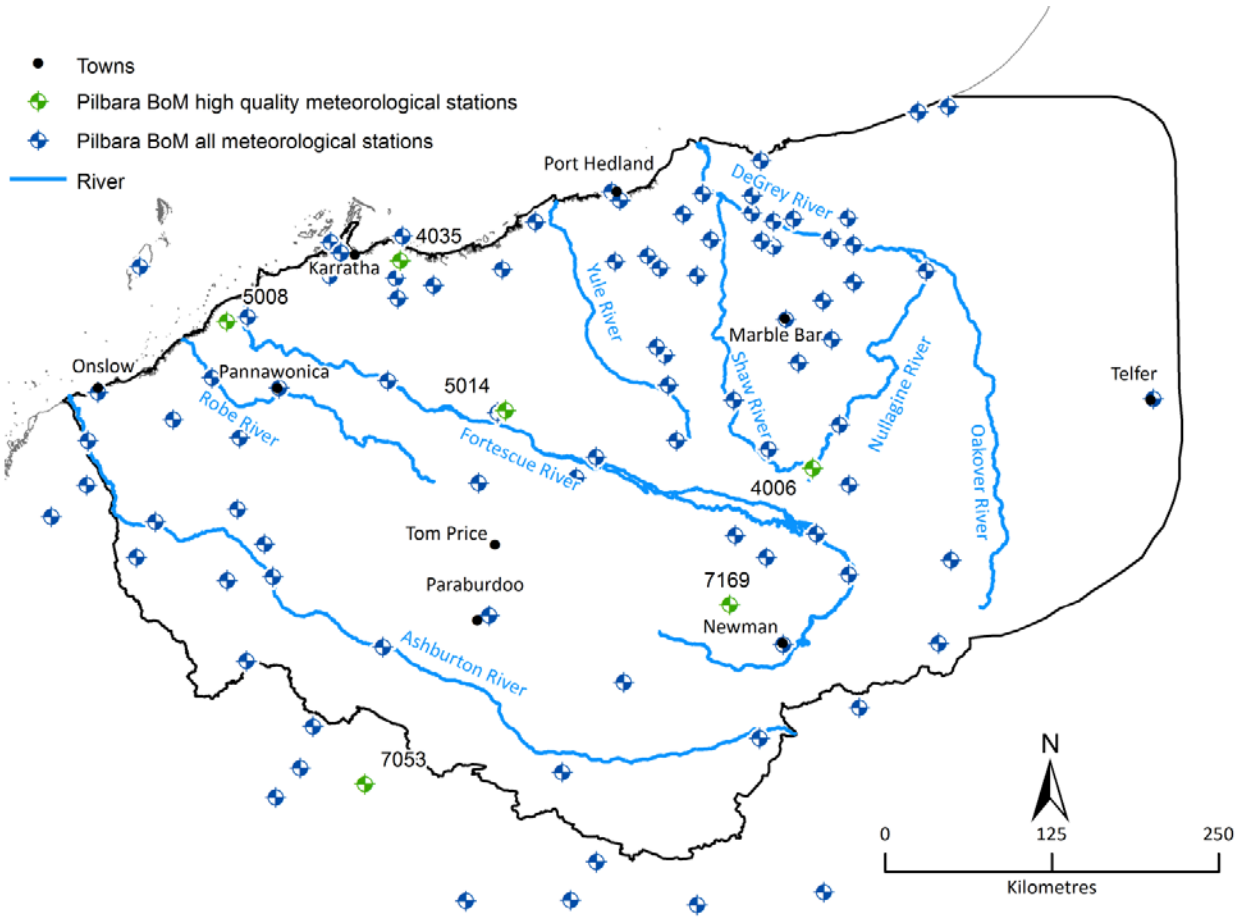

Figure 2.8 Assessment area showing the six high-quality Bureau of Meteorology stations and 93 PPD stations

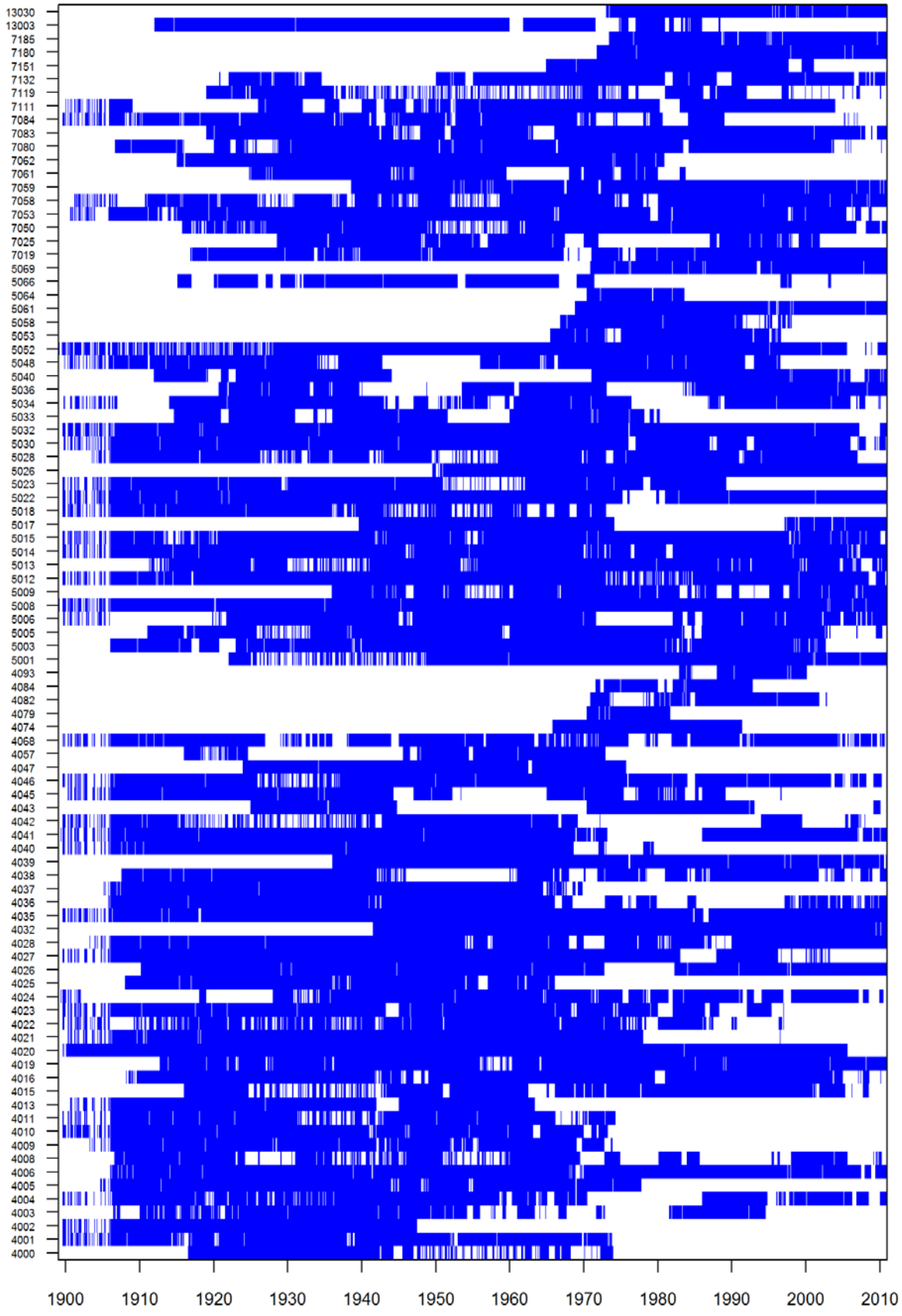

Figure 2.9 PPD daily rainfall data availability with official observations (source code 0)

2.2.2 Climate variable characteristics

Rainfall

The mean annual rainfall in the Pilbara region generally decreases from 300 to 350 mm in the north to less than 250 mm in the south (Figure 2.10, 1911 to 2012 average). However, elevated inland areas tend to receive higher annual totals with some locations in the Hamersley Ranges averaging over 500 mm per year (Figure 2.10). A comparison with elevation emphasises the orographic influence (Figure 2.11). Orography combines with high temperatures and moisture convergence to produce preferential conditions for thunderstorm activity, as was seen in the location of maximum thunder-days in Figure 2.2. A line of higher rainfall from the northeast corner of the Assessment area to the Hamersley Ranges is probably also related to favourable conditions for evening thunderstorm development, following daily advection of low-level moisture from the coast and high temperatures producing uplift.

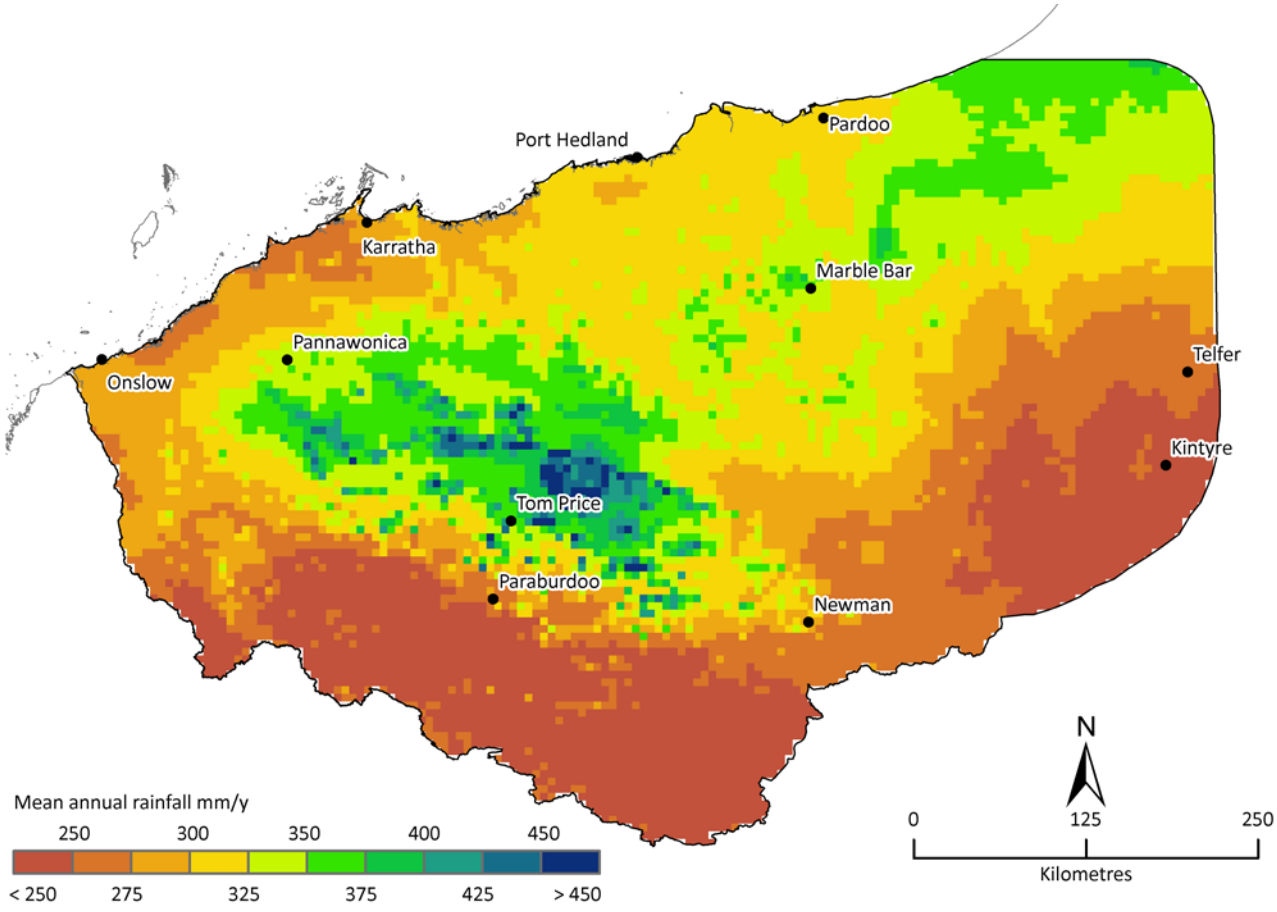

Figure 2.10 Mean annual rainfall (mm/year) for the period 1911 to 2012

The January to March period receives 60% of the annual total rainfall (Figure 2.12), with February the wettest month (with an average of 71.4 mm, or 23.9% of the annual total) and September the driest month (1.8 mm or 0.6% of the annual total). This monthly distribution supports the use of the 1st October to 30th September as the water year for the Assessment as discussed later. The western and south-western sub-regions may have a double peak in their monthly rainfall distribution (e.g. station 5017 Onslow Airport - Figure 2.13).

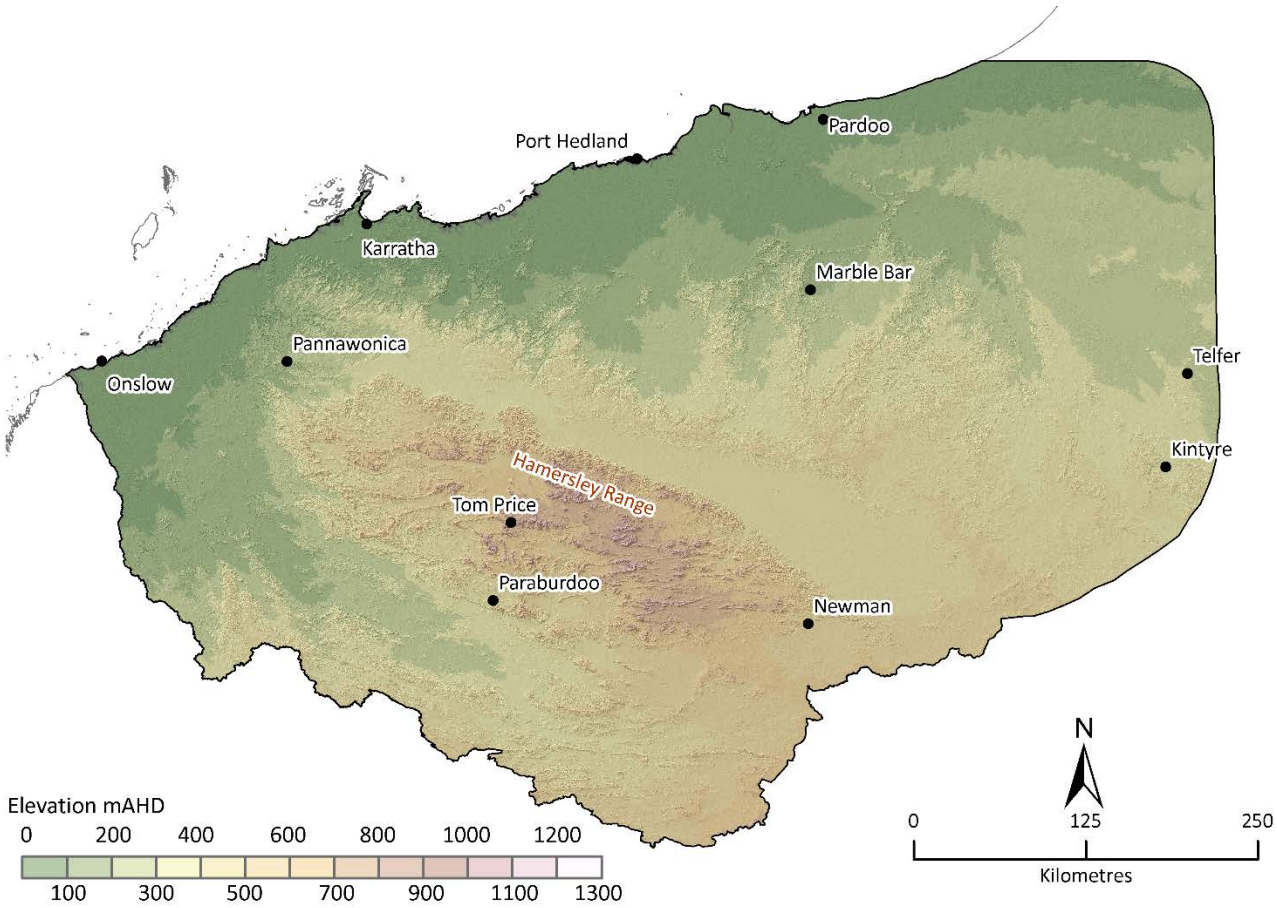

Figure 2.11 Elevation of Assessment area (m)

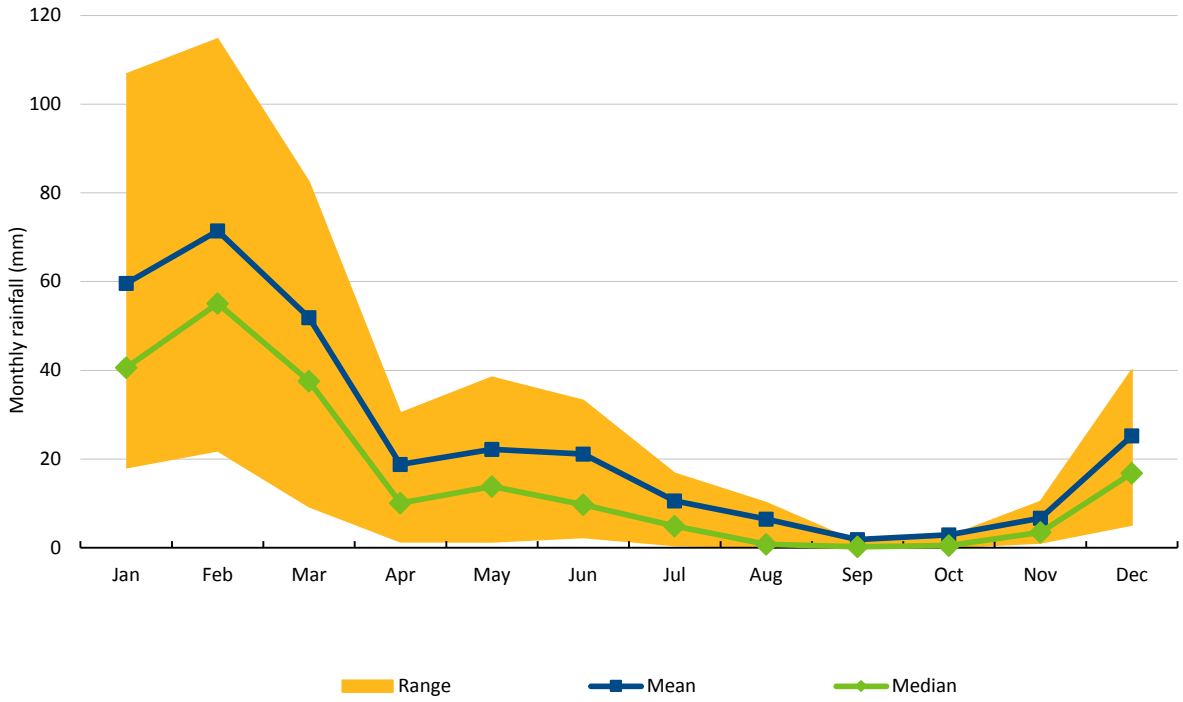

Figure 2.12 Assessment area monthly rainfall (mm) for the period 1911 to 2012 (range is the 20th to 80th percentile monthly rainfall)

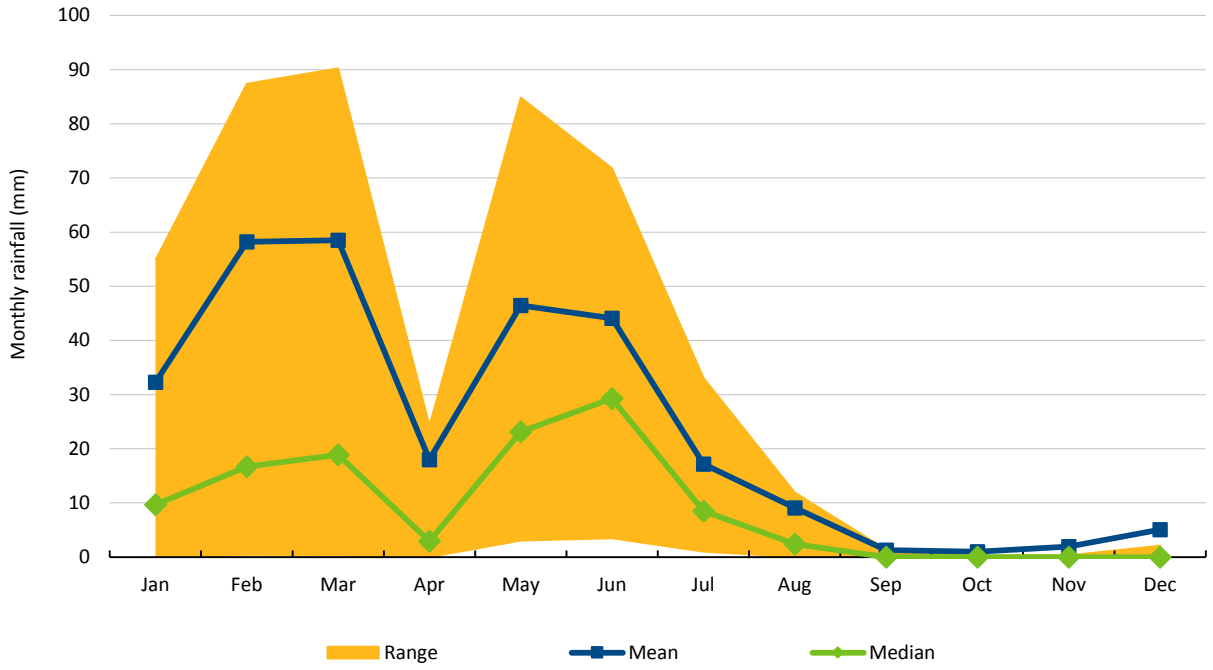

Figure 2.13 Onslow airport (Station 5017) monthly rainfall (mm) for the period 1911 to 2012 (range is the 20th to 80th percentile monthly rainfall)

Temperature

Temperature is important for hydroclimate assessment as it influences the evaporation rate. January is generally the hottest month of the year in the Pilbara, although in some northern inland and coastal parts December has the highest mean maximum temperature (Figure 2.14). Monthly means of daily maximum temperature for January in southwest and eastern portions are mostly greater than 39 °C, and at Marble Bar the average is 41 °C (Figure 2.15). Elevated and near-coastal locations have slightly lower monthly mean daily maximum temperatures; however, these are still generally above 35°C (Figure 2.15). The temperature is several degrees lower in the Hamersley Ranges, corresponding with its increased rainfall (Figure 2.11).

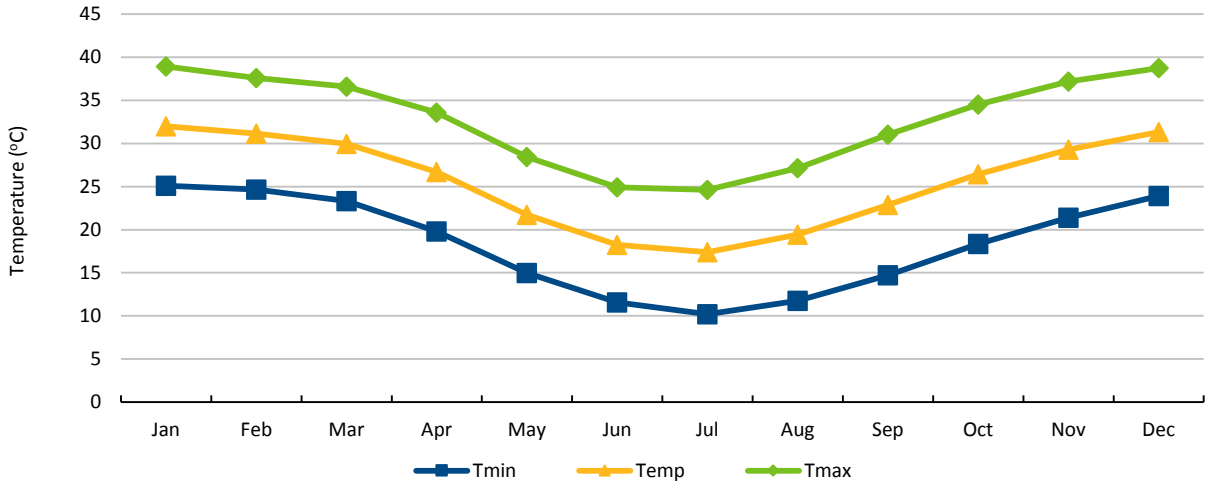

Figure 2.14 Monthly means of daily minimum (Tmin), mean (Temp) and maximum (Tmax) temperatures for the period 1911 to 2012

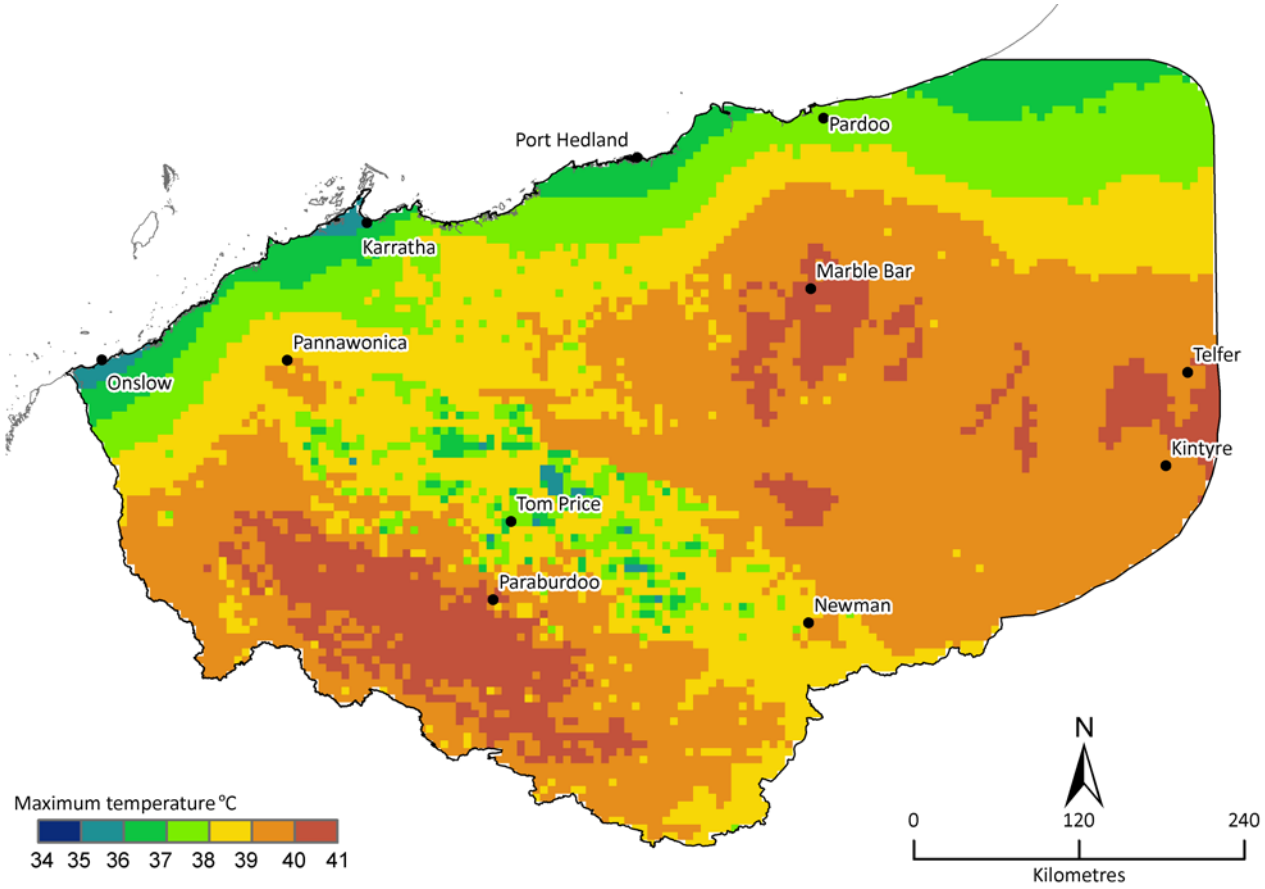

Figure 2.15 Monthly mean of January daily maximum temperature for the period 1911 to 2012

Temperatures above 45 °C have been recorded at most sites in the months from November to February and the highest official temperature recorded in the region, as well as in Western Australia, is 50.5 °C at Mardie on 19 February 1998. Although Marble Bar does not hold the record for the highest temperature in the state, its 160 consecutive days with maximum temperatures equal to or greater than 37.8 °C (or 100 °F) from 31st October 1923 to 17th April 1924 supports its claim of being the hottest town in Australia.

The monthly mean of daily minimum temperatures is lowest in July, when the minima range from 5 to 6 °C in the south of the Assessment area, and increase northward to between 13 and 15 °C in near-coastal parts (Figure 2.16). The Hamersley Ranges experience a modest cooling effect.

Temperatures below zero are generally confined to the far south of the Pilbara. Newman Airport, with six years of observations, has an average of eight days per year with minimum temperatures below zero. The lowest recorded temperature in the Assessment area has been –2.2 °C, at Nullagine on 20 July 1965.

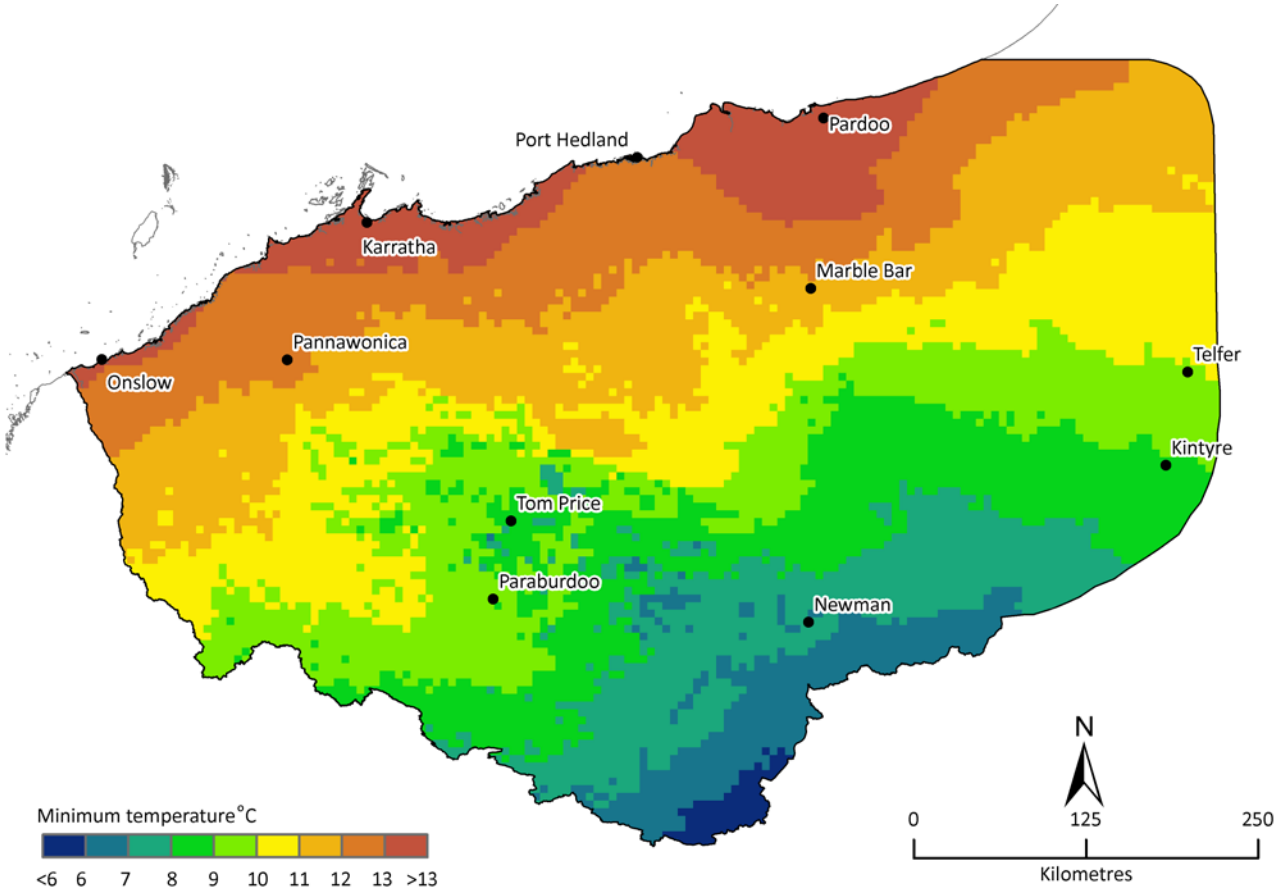

Figure 2.16 Monthly mean of July daily minimum temperature for the period 1911 to 2012

Wind

For much of the year, particularly in the cooler months, the region is under the influence of the east to south-easterly trade winds, but during spring, these winds weaken as the semi-permanent inland heat low develops in the Pilbara. Thus through the warmer months, inland winds tend to be variable whereas in near-coastal parts afternoon sea breezes are dominant. Sea breezes can occur all year round but are most pronounced in the warmer months. This can be seen in the contrasting wind roses for Port Hedland (a coastal location) and Newman (an inland location), with the 3 pm Port Hedland winds dominated by onshore north or north-west winds whereas Newman experiences dominant east and south-east winds at 9 am and 3 pm in both winter and summer half-years (Figure 2.17).

Strong winds can occur in the afternoon summer sea breezes and also in east to south-easterly wind surges in the winter months. These surges are more likely to occur in the morning when a high pressure system quickly moves eastward into the Great Australian Bight. The highest wind gust recorded in the Assessment area is 267 km per hour at both Varanus Island on 10 April 1996, from Tropical Cyclone *Olivia*, and at Learmonth on 22 March 1999 from Tropical Cyclone *Vance*.

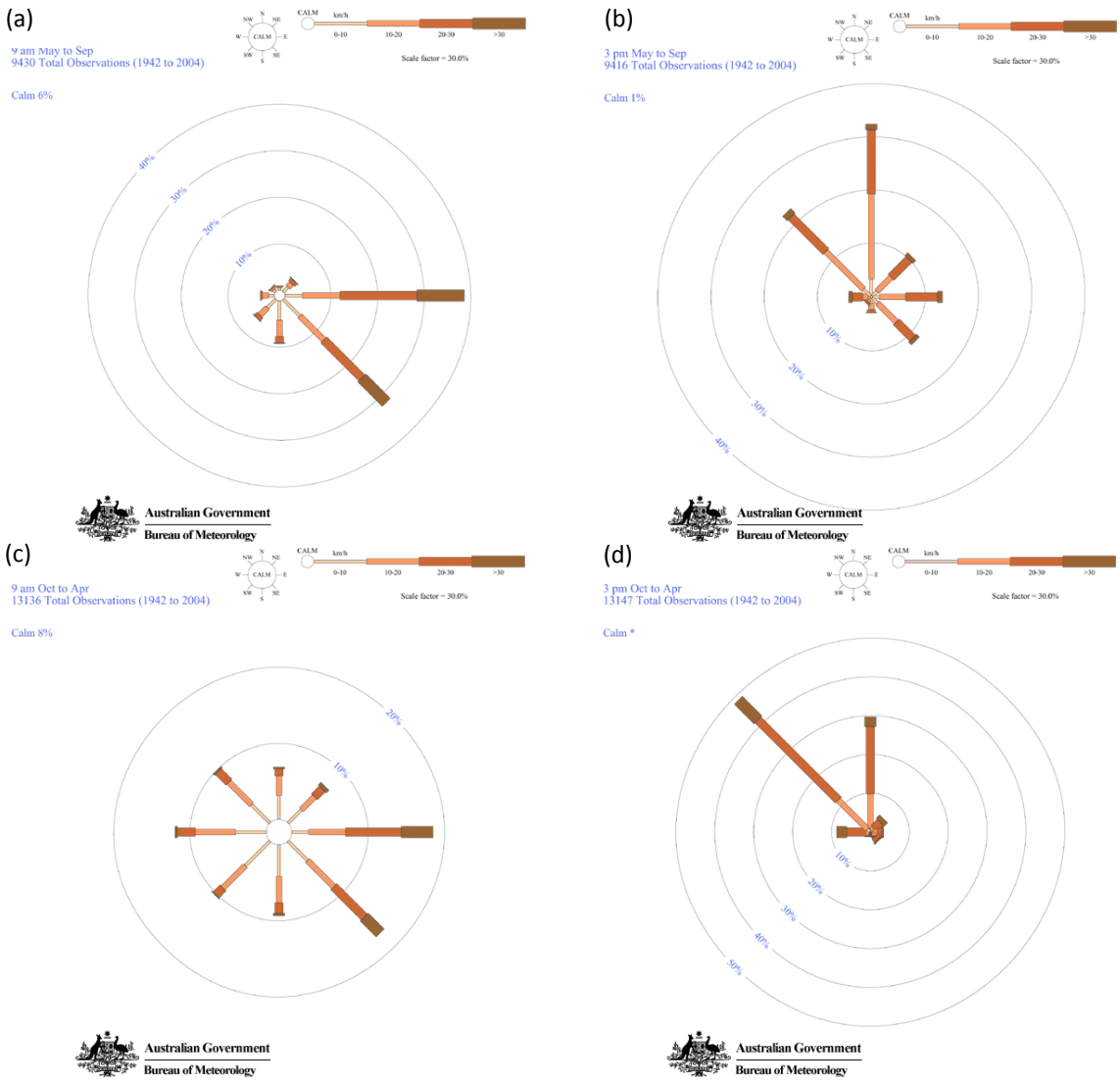

Figure 2.17 Wind roses for Port Hedland (a to d) and Newman (e to h). (a/e) and (b/f) are 9am and 3pm for May to September and (c/g) and (d/h) are 9am and 3pm for October to April for the respective stations

Source: (Bureau of Meteorology, 2012b)

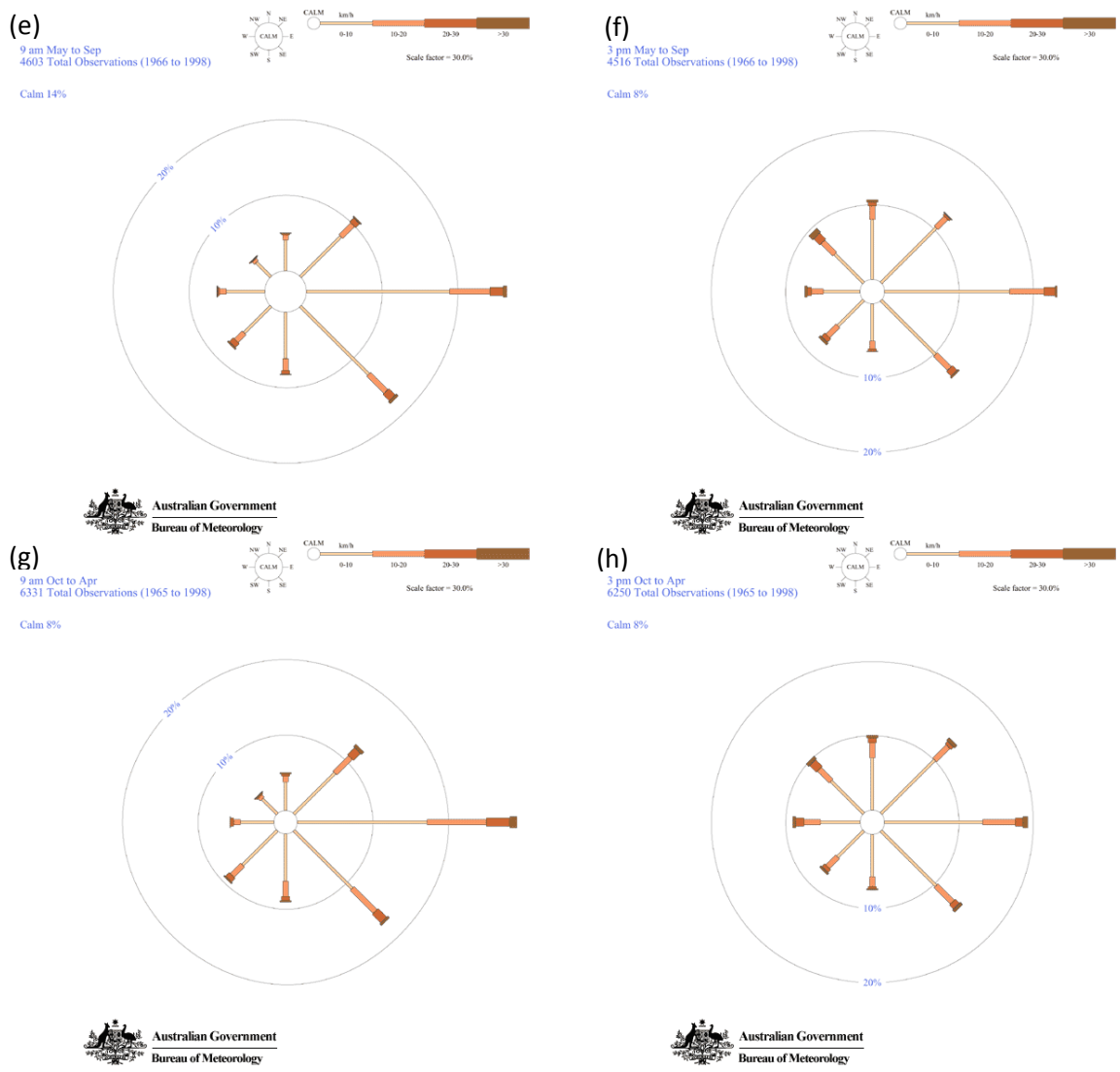

Figure 2.17 Wind roses for Port Hedland (a to d) and Newman (e to h). (a/e) and (b/f) are 9am and 3pm for May to September and (c/g) and (d/h) are 9am and 3pm for October to April for the respective stations (continued)

Source: (Bureau of Meteorology, 2012a)

Relative humidity

The Pilbara region is one of the driest areas of Australia in terms of the lack of water vapour in the air. The mean relative humidity is 35 to 40% for more than half of the Assessment area (Figure 2.18). The relative humidity can be 50 to 55% along the coast decreasing to less than 40% in most inland areas (Figure 2.18). The mean annual relative humidity at 3pm is generally 10 to 15% lower than the corresponding 9 am readings.

Average relative humidity has a double peak in February (48%) and June (47%), and is lowest in October (32%). This winter peak is more a function of the cooler temperatures rather than increased atmospheric moisture. The fluctuation between the highest and lowest monthly values is about 15 to 20% (Figure 2.19).

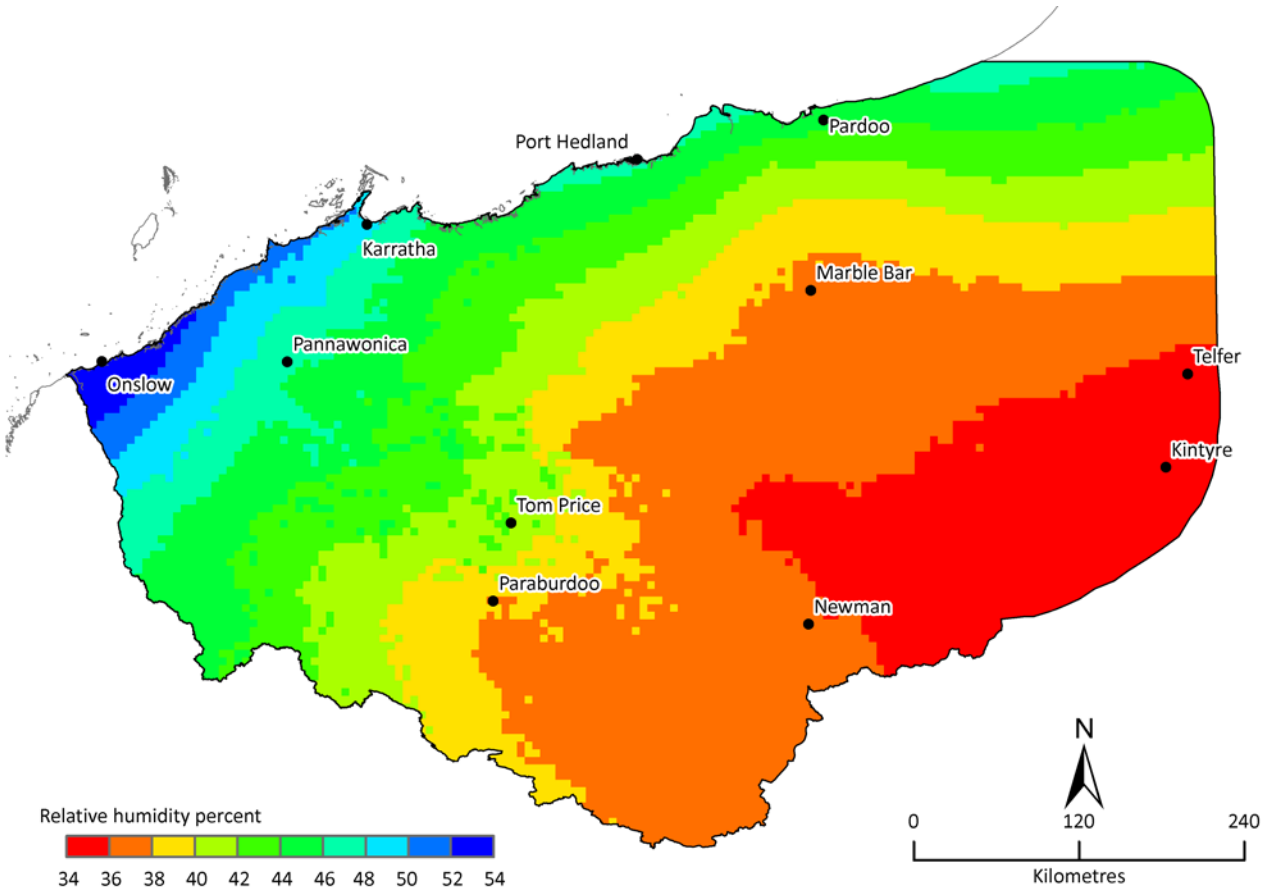

Figure 2.18 Mean relative humidity (%) for the period 1911 to 2012

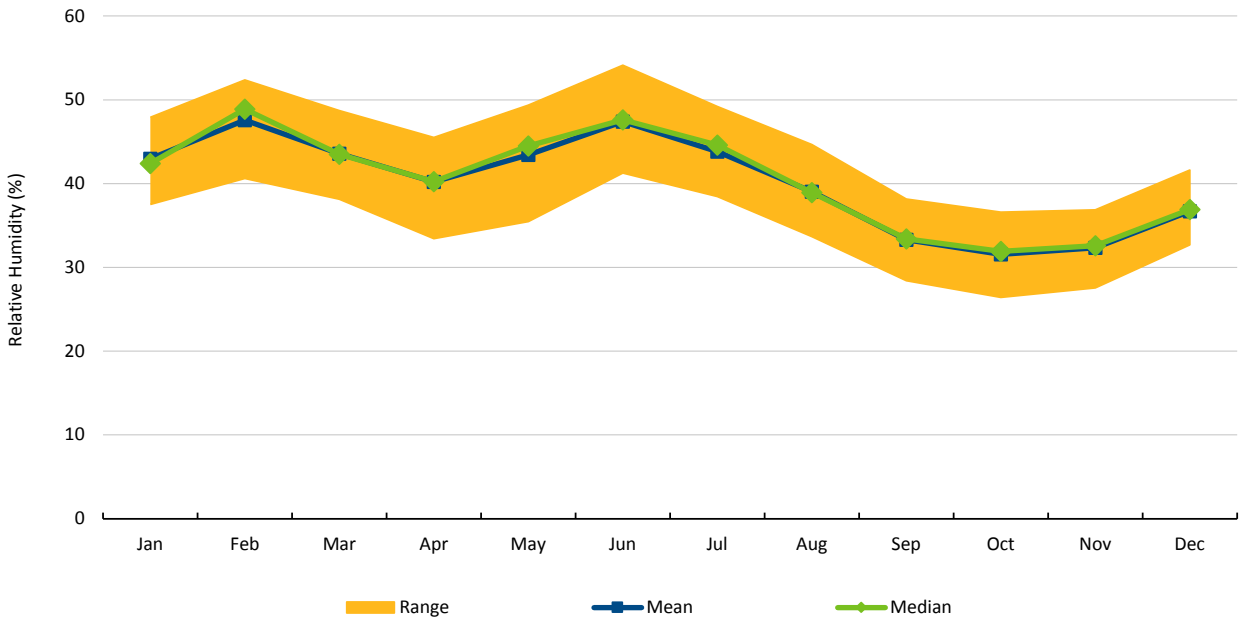

Figure 2.19 Monthly relative humidity (%) for the period 1911 to 2012 (range is the 20th to 80th percentile monthly relative humidity)

Solar radiation

Western parts of the Pilbara have the highest number of sunshine hours in the country with an average of over 10 hours/day while southern and eastern parts average over 9 hours. The average daily solar radiation ranges from 20.5 MJ/m^2 in the southern mountain regions to 22.5 MJ/m^2 along the coast (Figure 2.20).

Solar radiation reaches its maximum rate in November at 27 MJ/m^2/day and its minimum in June at 15 MJ/m^2 (Figure 2.21). Mean daily sunshine hours show a much smaller variation across the Assessment area from a mean of over 10 hours in November to 8 to 9 hours in June.

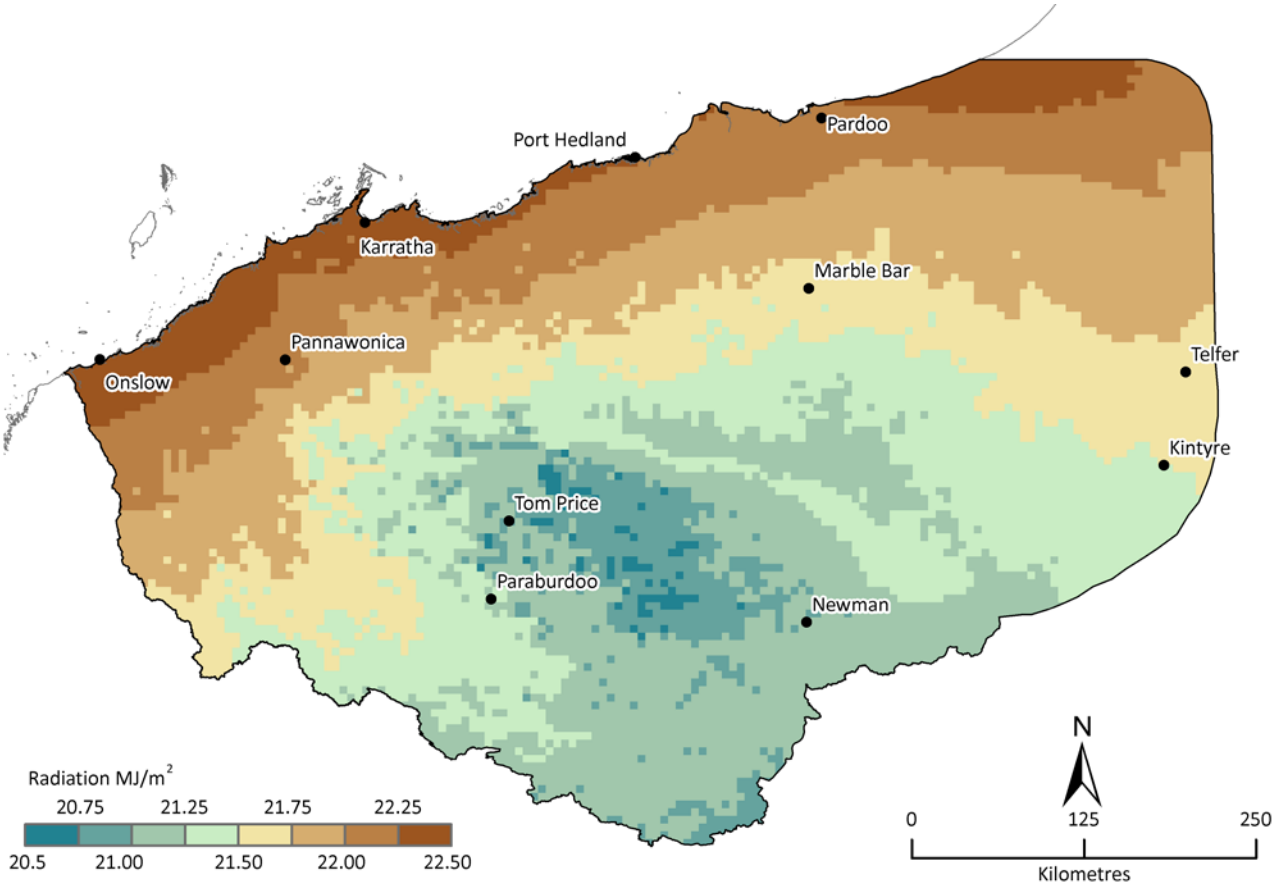

Figure 2.20 Mean daily solar radiation (MJ/m^2) for the period 1911 to 2012

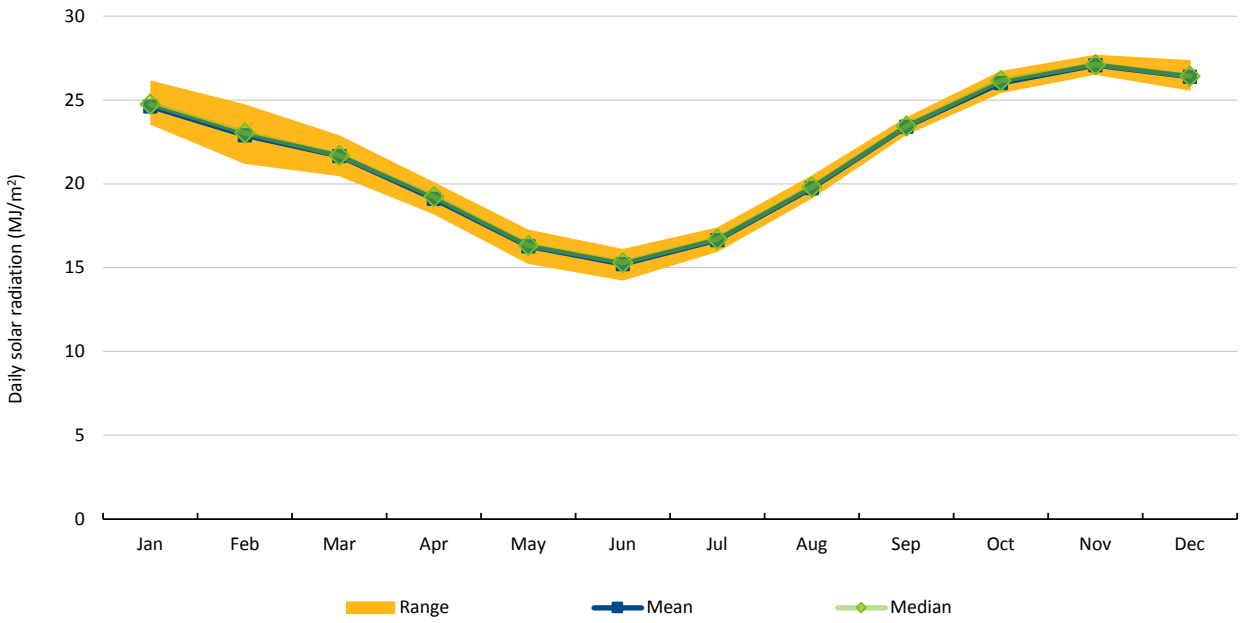

Figure 2.21 Monthly mean of daily solar radiation (MJ/m^2/day) (range is the 20th to 80th percentile daily solar radiation) for the period 1911 to 2012

Cloud

The seasonal variations of cloudiness in the Pilbara obviously relate to those of rainfall, showing a tendency to be cloudier in the first half of the calendar year than the second as it is the time of the higher rainfall over summer and of NWCBs in the spring and early winter. Generally, coastal locations show little diurnal variation while inland locations have higher cloud cover in the afternoon during summer months due to convective storms.

Throughout the Pilbara, October has the peak number of clear days (defined as days when the average of the 9 am and 3 pm cloud amounts is less than or equal to two-eighths of the sky obscured) with monthly averages above 25 days on the coast, decreasing inland to less than 20 days in some locations. The lowest number of clear days generally occurs in February with an average of 12 days on the western coast, decreasing eastward to between 6 and 8 days on the eastern coast and inland, given this is when the monsoon, tropical depressions (including TCs), and heat low generated convective storms have a higher occurrence. Jovanovic et al. (2011) examined cloudiness trends for the 1957 to 2007 period, finding decreasing trends for the Pilbara in winter.

Potential evaporation

Areas of the Pilbara have the highest average annual potential evaporation in Australia. Morton's areal potential evaporation (areal PE), calculated using SILO temperature, solar radiation and vapour pressure as input to Morton's wet environment formula (Morton, 1983), ranges from about 1700 mm/year in the southeast to more than 2000 mm/year in the northern coastal parts (Figure 2.22). The effects of elevation on potential evaporation result in lower values along the Hamersley Ranges (Figure 2.22) possibly due to greater cloud cover and slightly lower temperatures.

Monthly areal PE reaches a maximum in December to January (7.2 mm/day) and minimum in June to July (2.8 mm/day) (Figure 2.23). However, SILO interpolated Class A pan evaporation (Jeffrey et al., 2001) show both different magnitudes and spatial distributions, ranging from about 3500 mm in the east to about 2860 mm in the elevated regions (Figure 2.24). However due to the sparse network of stations recording daily Class A pan evaporation the magnitudes and spatial patterns are not necessarily realistic, hence they are shown here for purposes of comparison but not used further in hydrological modelling. Although Morton's areal PE and pan evaporation show different spatial distributions, annual rainfall deficit maps

(rainfall minus potential evaporation) obtained using these two evaporation estimates show spatial similarities in some regions, such as lower deficit values in the Hamersley Range (Figure 2.25 and Figure 2.26).

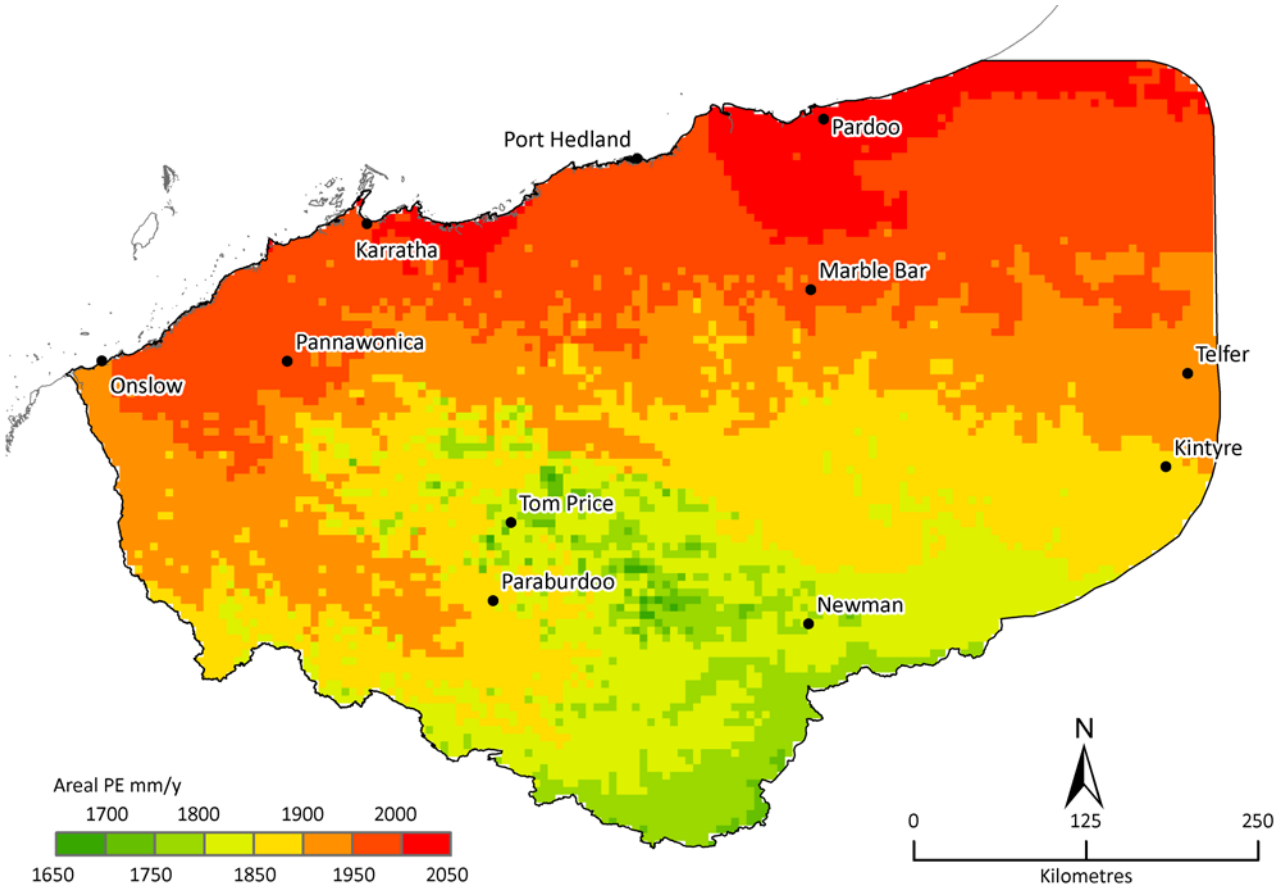

Figure 2.22 Mean annual potential evaporation (mm/year) calculated using Morton's areal wet environment method for the period 1911 to 2012

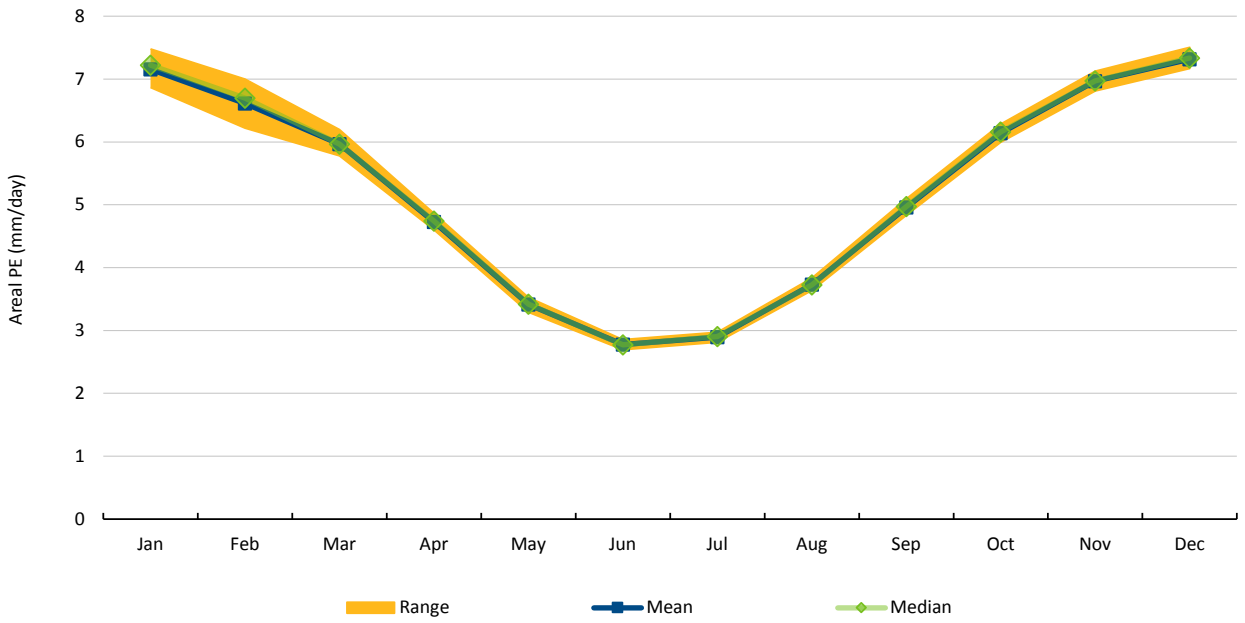

Figure 2.23 Monthly mean of daily potential evaporation (mm/day) calculated using Morton's areal wet environment method (range is the 20th to 80th percentile daily potential evaporation) for the period 1911 to 2012

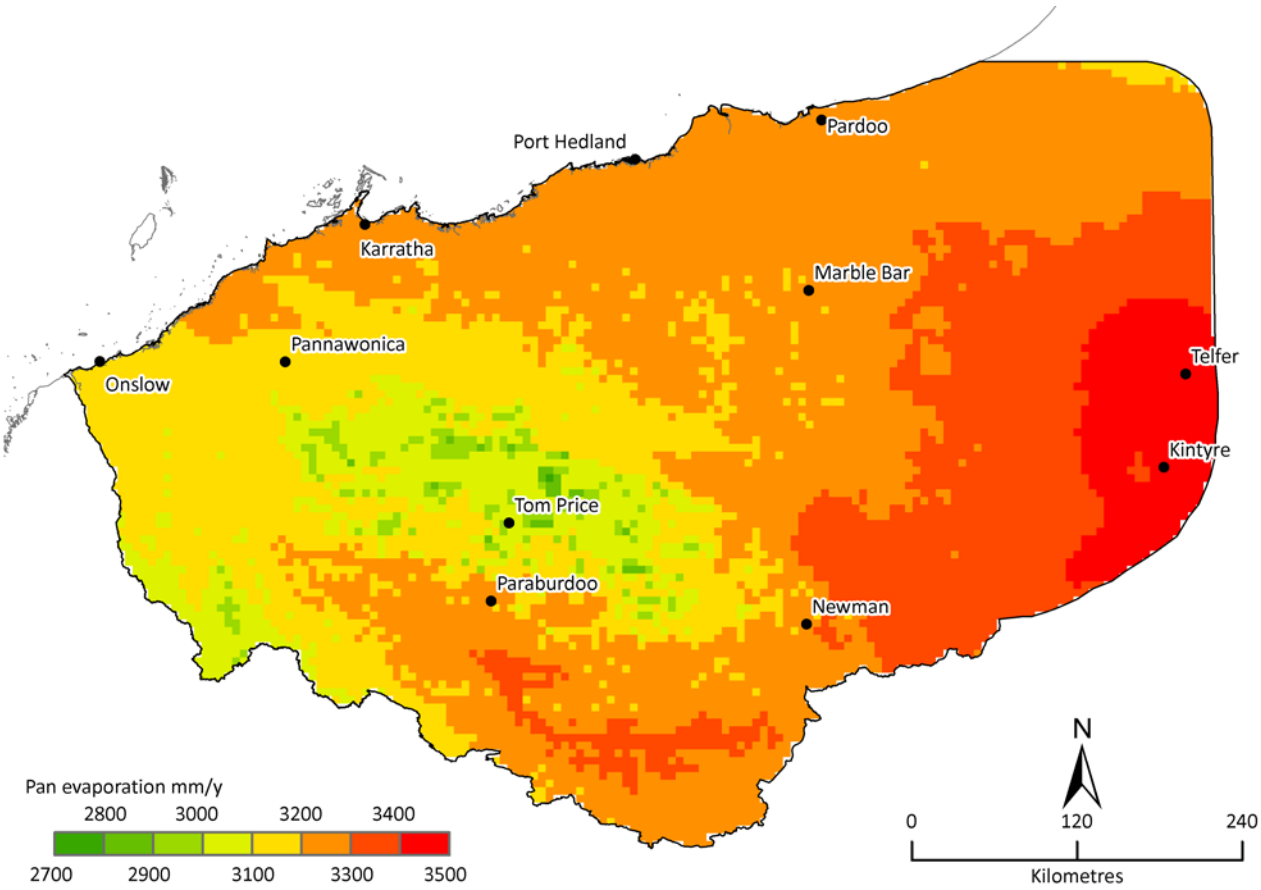

Figure 2.24 Mean annual Class A pan evaporation (mm/year) for the period 1971 to 2012

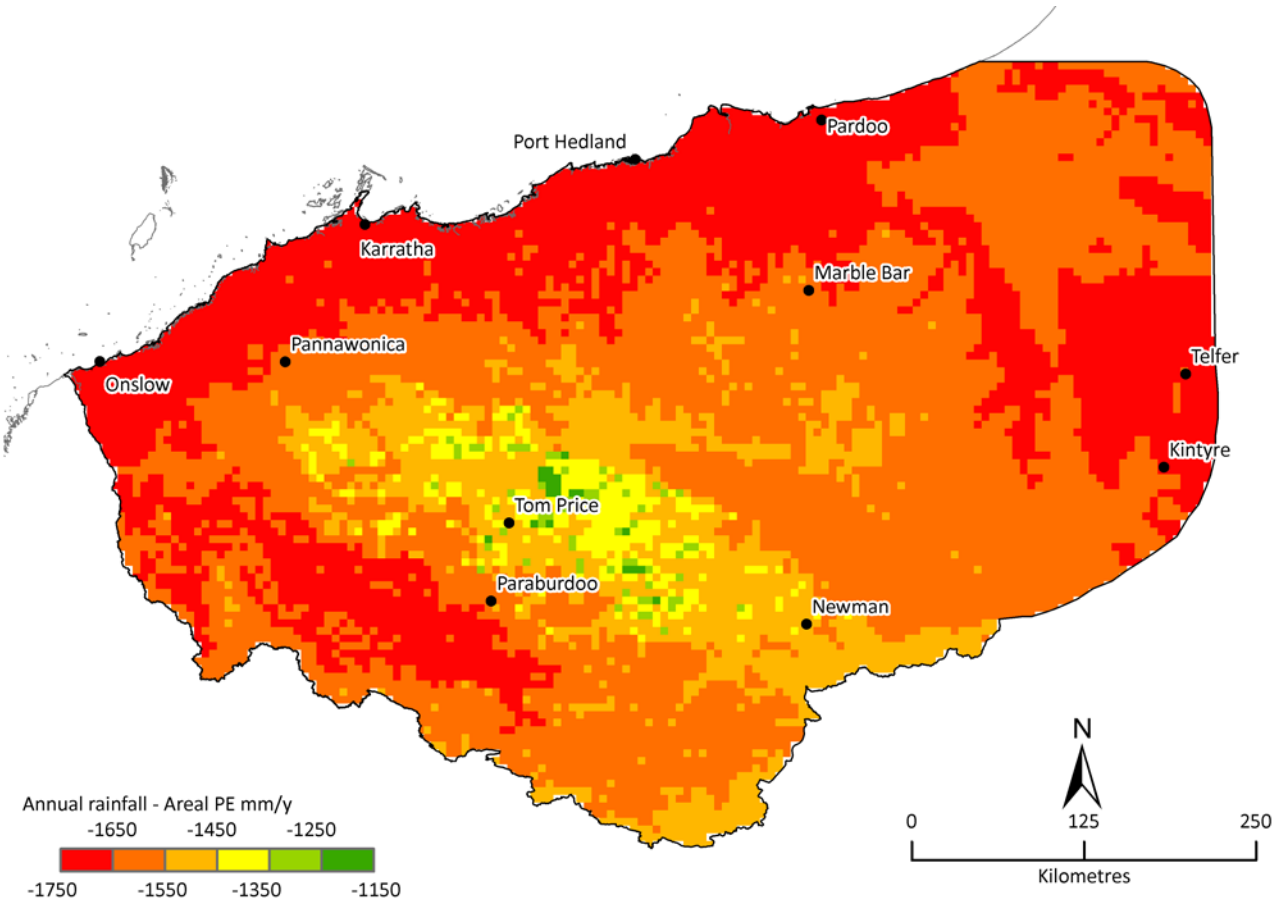

Figure 2.25 Mean annual rainfall deficit (mm/year) using Morton's areal wet environment estimate of APET

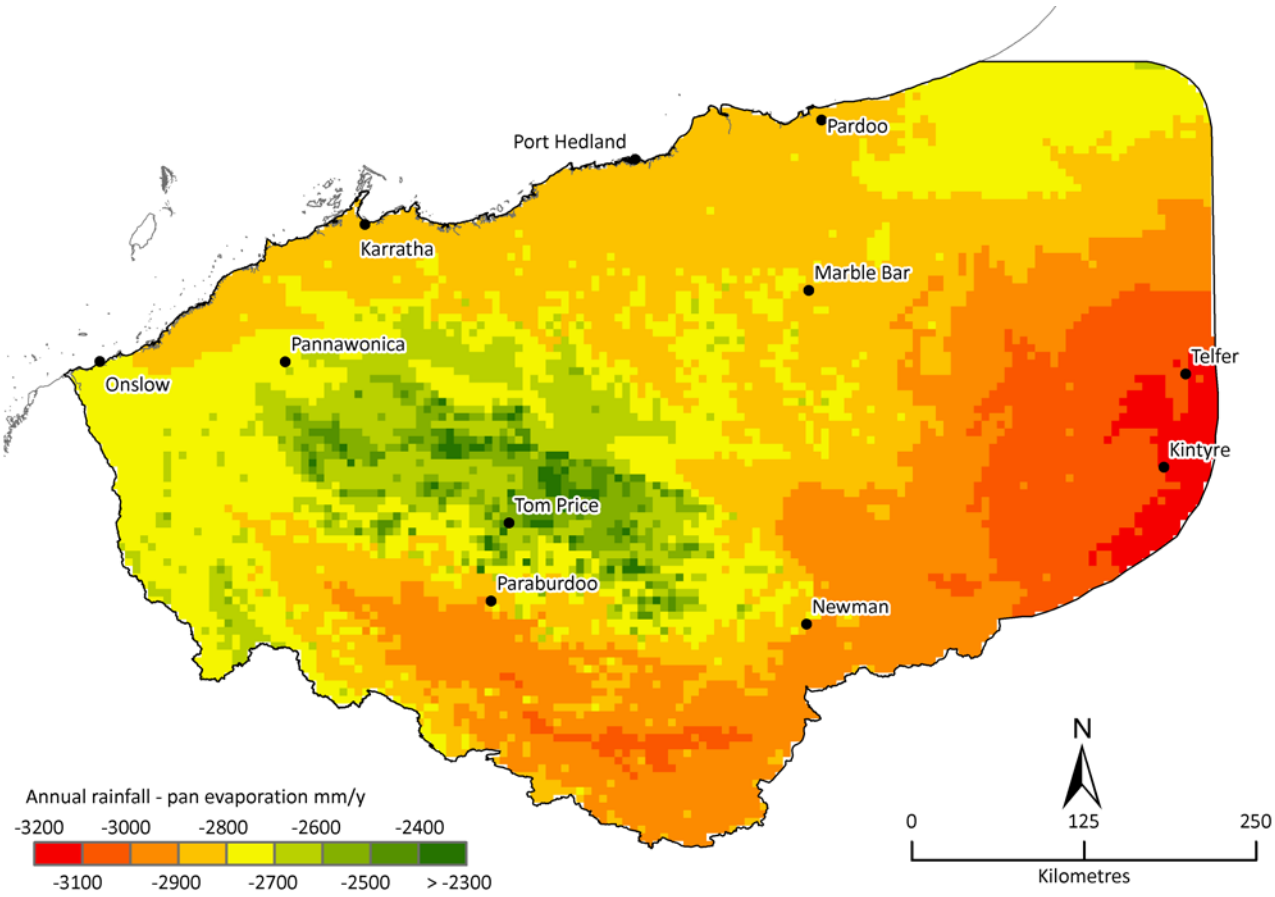

Figure 2.26 Mean annual rainfall deficit (mm/year) using Class A Pan evaporation estimate

2.2.3 Climate variable variability and trends

Rainfall variability and trends

A characteristic of rainfall in the Pilbara is its large inter-annual variability. Figure 2.27 shows the annual rainfall anomaly (calculated as the difference between each year's rainfall and the long-term mean, expressed as a proportion of the 1911 to 2011 water year long-term mean) for the entire Assessment area from both PPD stations and SILO drilled data. The two datasets show similar annual variability. The maximum annual rainfall in 2000 was about 140% larger than the long-term mean, while the minimum annual rainfall in 1924 was about 83% less than the long-term mean. That is to say, the annual rainfall in 2000 across the Assessment area was about 14.5 times greater than that in 1924. In the context of the rest of Australia, this variability is larger than all regions with the exception of central Australia (see: <http://www.bom.gov.au/jsp/ncc/climate_averages/rainfall-variability/index.jsp>).

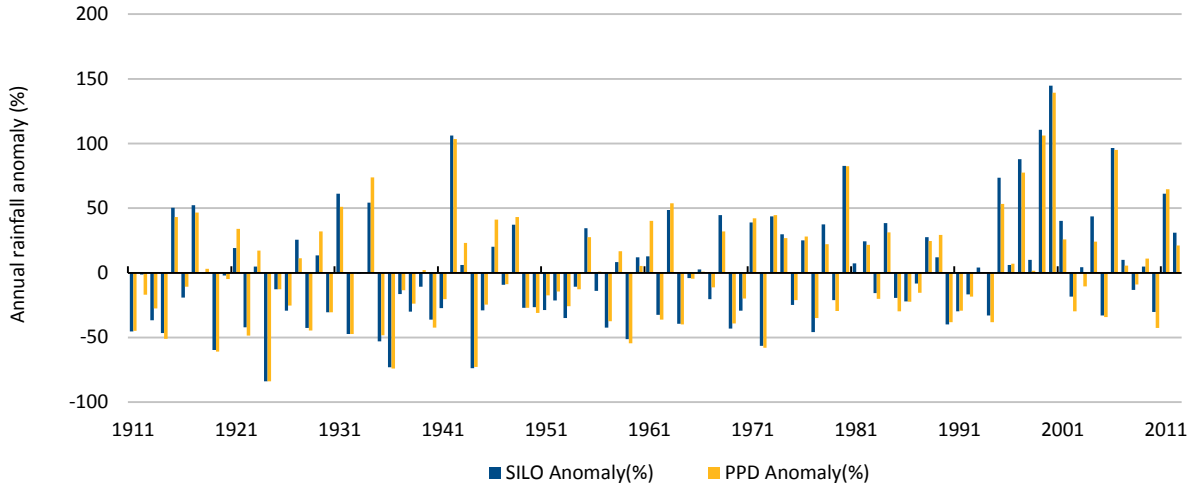

Figure 2.27 Water year rainfall anomaly (%) for 1911 to 2012 for the Assessment area

For the individual grid points, this ratio is considerably larger (Figure 2.28). For example, it is greater than 50 along the majority of the Pilbara coast. The greater rainfall variability along the coast is attributed to the 'hit or miss' nature of tropical cyclones producing very high localised rainfall in certain years (Dare et al., 2012). In an extreme case (near Karratha, for the gridpoint 118 °E 20.75 °S) this ratio reaches 1840 with a minimum annual rainfall of only 0.4 mm and maximum annual rainfall of 737.1 mm.

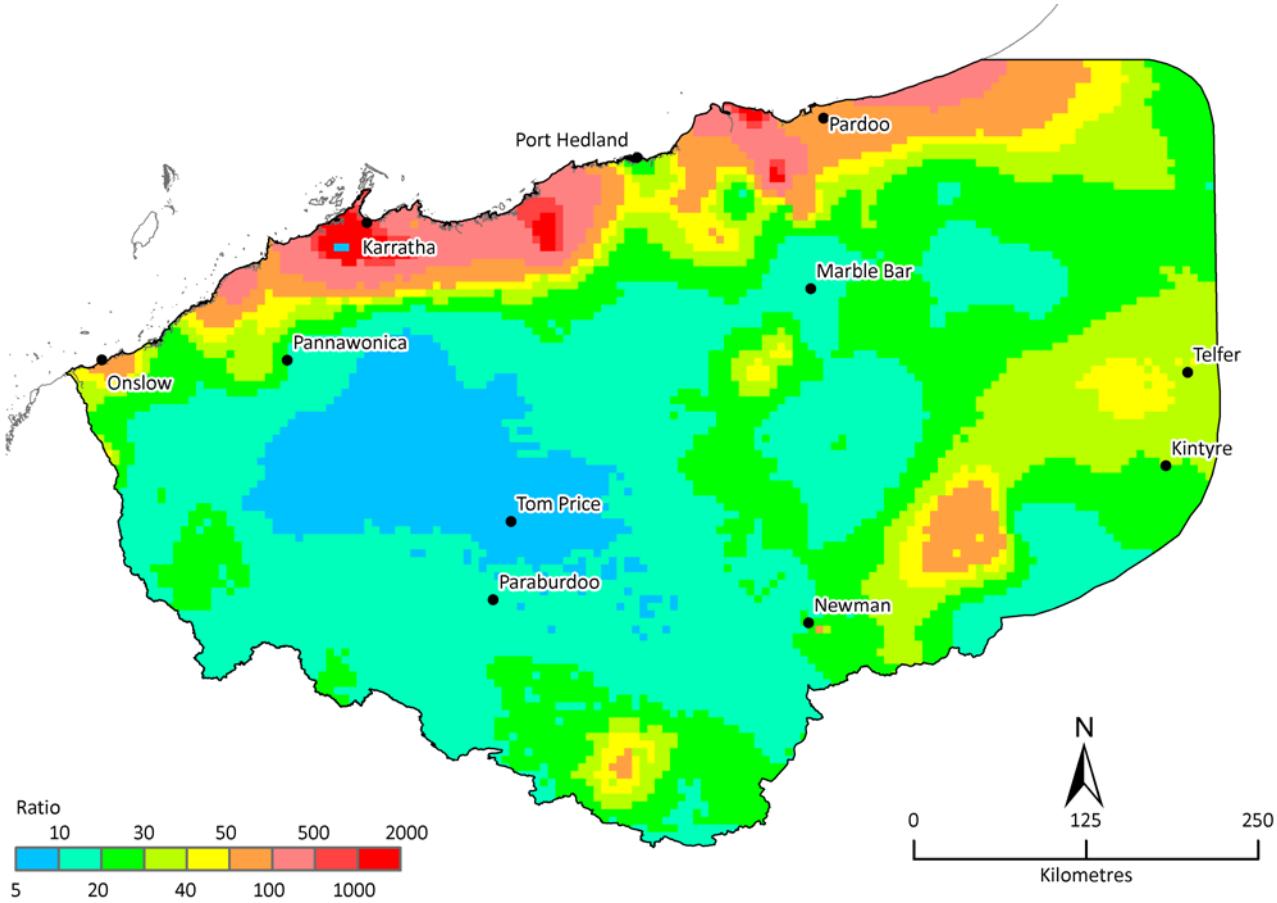

Figure 2.28 Ratio of the annual maximum to minimum rainfalls

While the annual rainfall in the Pilbara region has been increasing in recent decades this is not consistent across sub-regions (Figure 2.29). The 1961 to 2012 period (the baseline period selected in Chapter 4) shows a decreasing trend in the west and larger increasing trend in the east. This emphasises the spatial heterogeneity of rainfall trend and variability. Mapping the trends on a half-year seasonal basis (Figure 2.30 and Figure 2.31) highlights that the increasing trends only occur in the November to April period that contains the tropical wet season whereas decreasing trends are almost completely restricted to the April to May period that experiences southern rainfall influences.

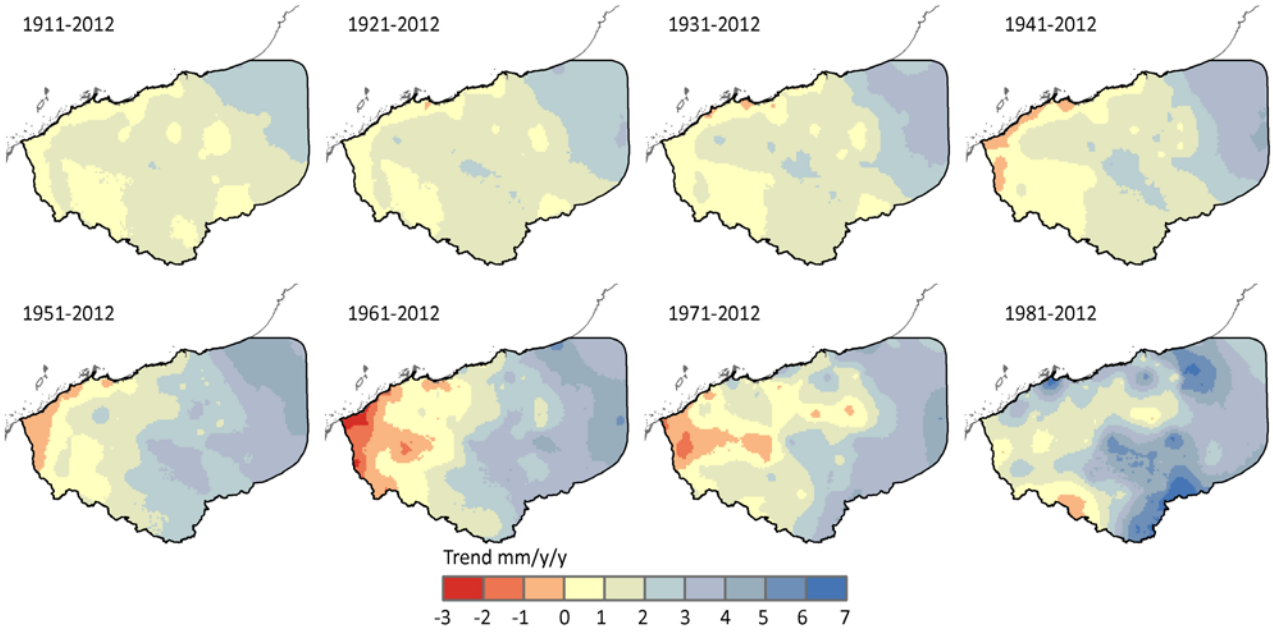

Figure 2.29 Trends in annual rainfall (mm/year/year) for periods ranging from the last 102 years (1911 to 2012) through to the last 32 years (1981 to 2012)

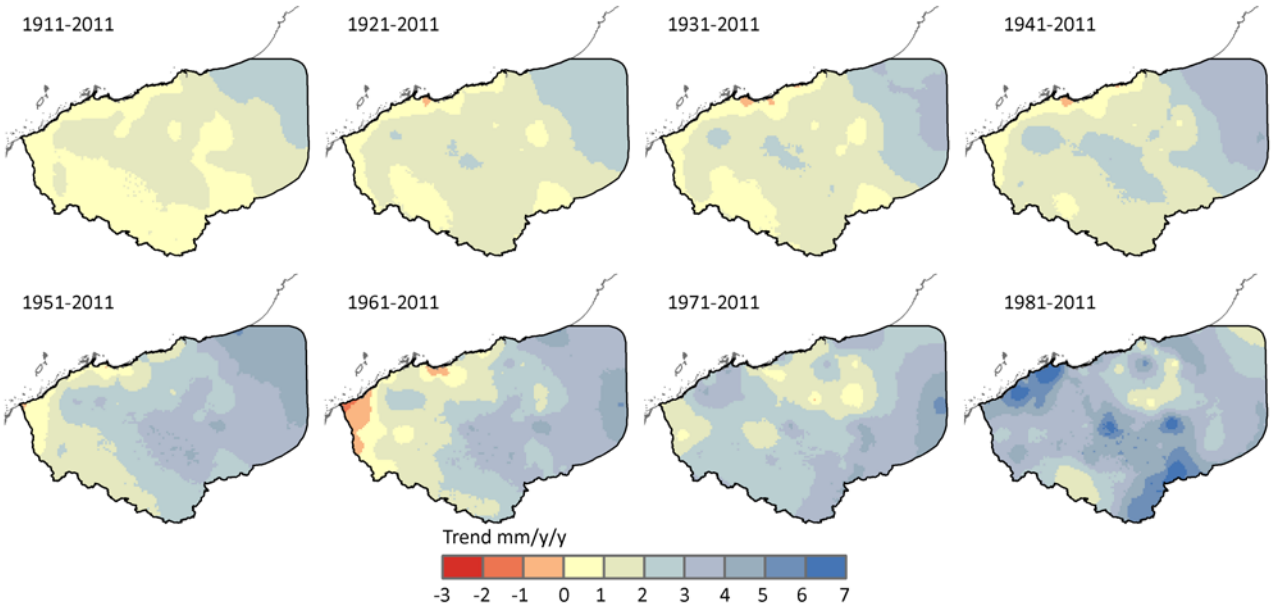

Figure 2.30 Trends in November to April rainfall (mm/year/year) for periods ranging from the last 101 years (1911 to 2011) through to the last 31 years (1981 to 2011) (to 2011, as October 2012 not extracted)

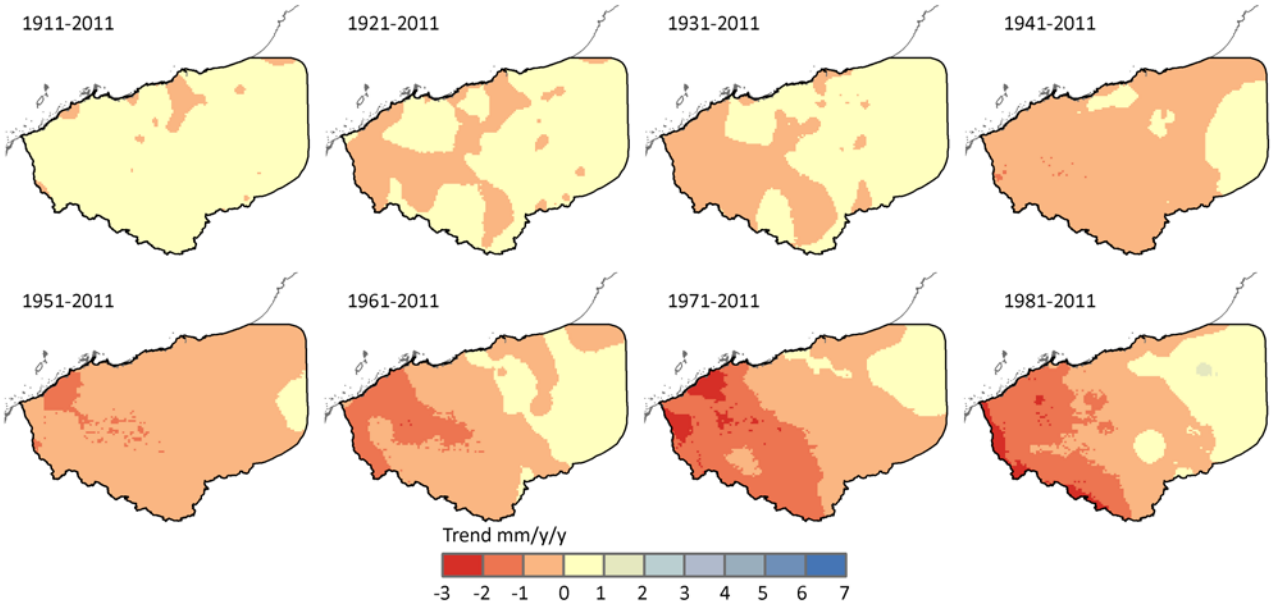

Figure 2.31 Trends in May to October rainfall (mm/year/year) for periods ranging from the last 101 years (1911 to 2011) through to the last 31 years (1981 to 2011) (to 2011, as October 2012 not extracted)

A cluster analysis was used to group stations with similar seasonal rainfall cycles across the Assessment area. To avoid the effects of rainfall magnitude, each annual rainfall time series was standardized before cluster analysis. The results show that the 93 PPD stations can be grouped into eight clusters (Figure 2.32) and the stations within each cluster are spatially coherent (Figure 2.33). This implies the cluster results identify areas influenced by similar underlying physical processes.

The time series of annual rainfall for these eight clusters show differences (Figure 2.34). There is an east-west contrast between clusters 1 to 5 that have a maximum annual rainfall in either 2000 or 2006, which gives their time series an increasing trend, contrasting with clusters 6 to 8 that have maximum annual rainfall in 1961, 1934 and 1942 respectively.

Temporal trends at individual stations are shown as the time series of the cumulative difference from the mean for five high-quality stations (Figure 2.35). These highlight the progressive drying over the early part of the record followed by consistent and on-going wetting since the 1960s for most stations, with particularly rapid wetting since the 1990s for the inland east (Bonney Downs) and inland central (Mount Florance) stations. The wetting trends continue in the most recent years for three eastern and central stations (Bonney Downs, Roebourne and Mount Florance) whereas the two westerly stations (Mardie, on the coast, and Mount Augustus to the southwest) show recent declines.

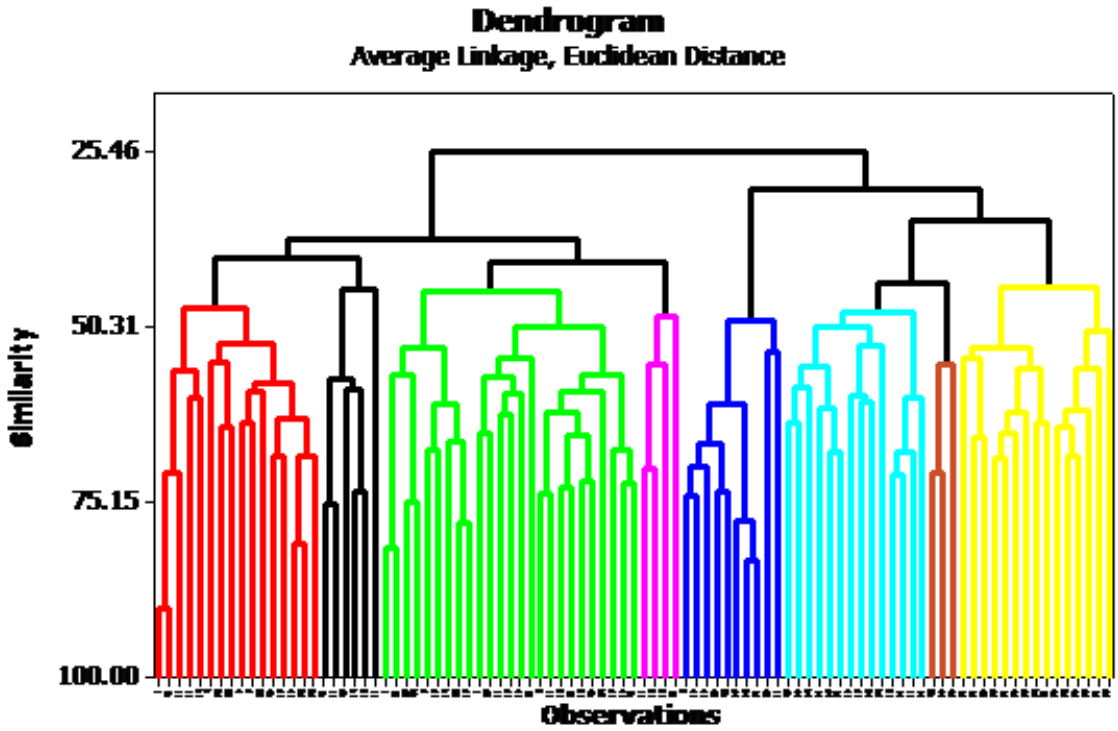

Figure 2.32 Cluster results of 93 PPD stations (order, left to right, is 1. Upper Fortescue, 2. Lower-Mid Fortescue, 3. Port Hedland-De Grey coastline, 4. West Canning-Sandy Desert, 5. Karratha coastline, 6. Lower Ashburton Robe, 7. Fortescue coast, and 8. Upper Ashburton)

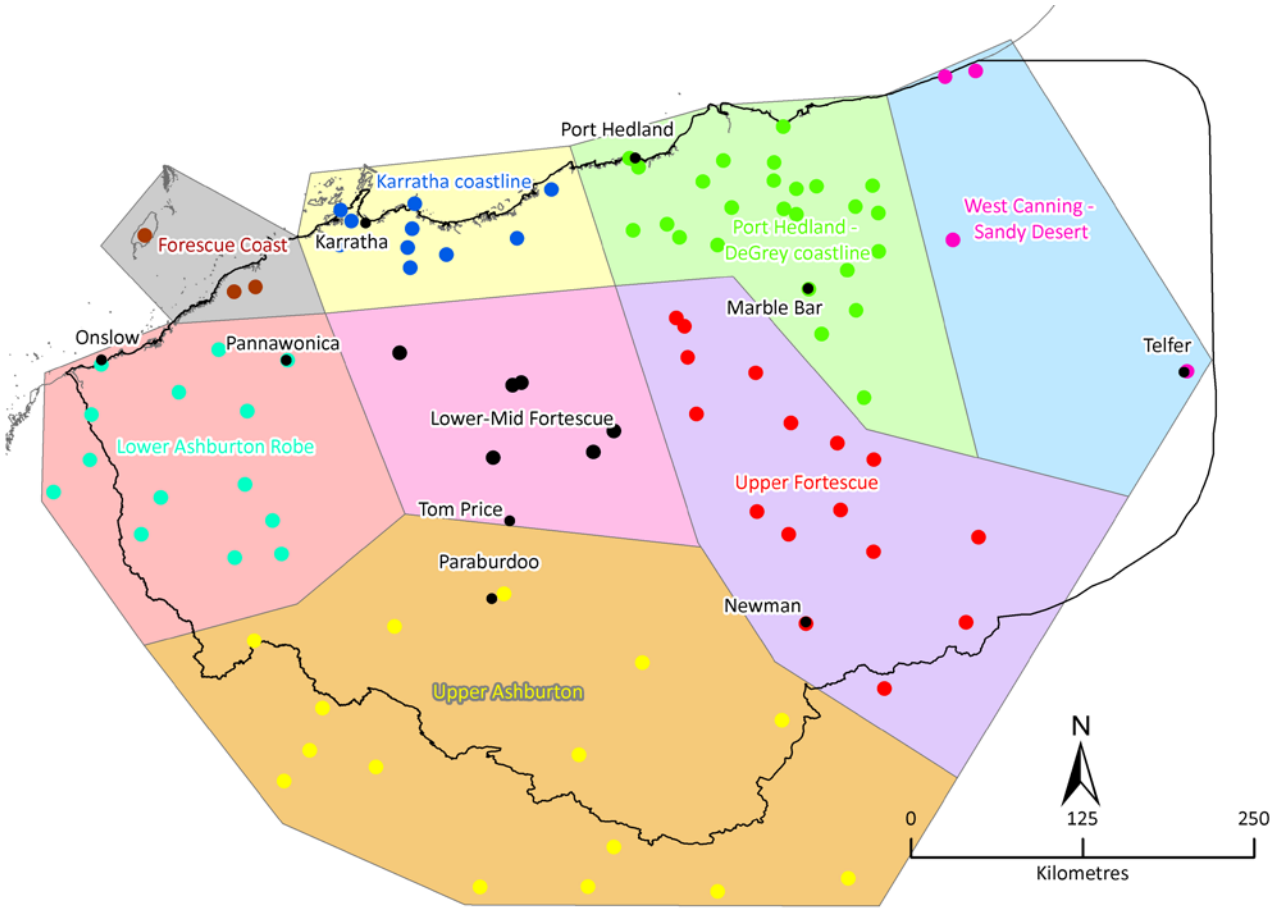

Figure 2.33 Spatial distribution of the eight rainfall clusters with station colours matching those in the dendogram

Figure 2.34 Time series of 1911 to 2012 water year rainfall for the clusters with 11-year moving average

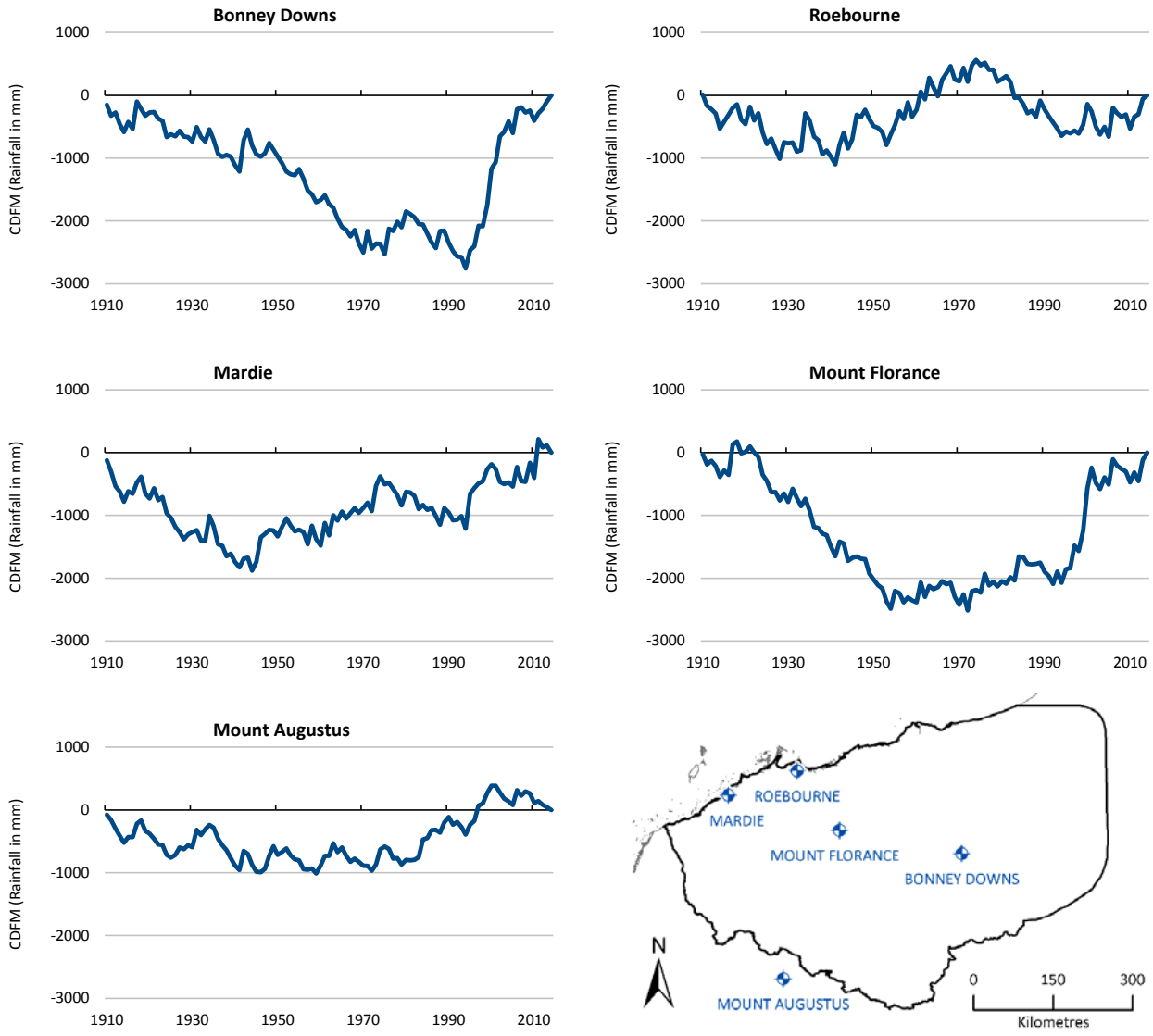

Figure 2.35 Cumulative difference from the mean time series for five stations with high-quality long-term records. Locations of stations shown in bottom right panel

The trends of rainfall also vary from month to month (Figure 2.36). December, January February, and March have an increasing trend of rainfall over the last 102 years (1911–2012) and the last 52 years (1961–2012). This is consistent with increased rainfall from summer systems: monsoonal, tropical cyclone and tropical depression processes as well as enhanced convection. May and June have had a decreasing trend for the last 52 years but almost no-trend for the full 102 years. This is consistent with decreased frontal systems since the 1960s, a documented change that has also contributed to the SWWA rainfall decline in autumn and early winter (IOCI, 2012). The rainfall trends in July, August, September, October and November are minimal and probably not significant, given the limited rainfall in these months (Figure 2.12).

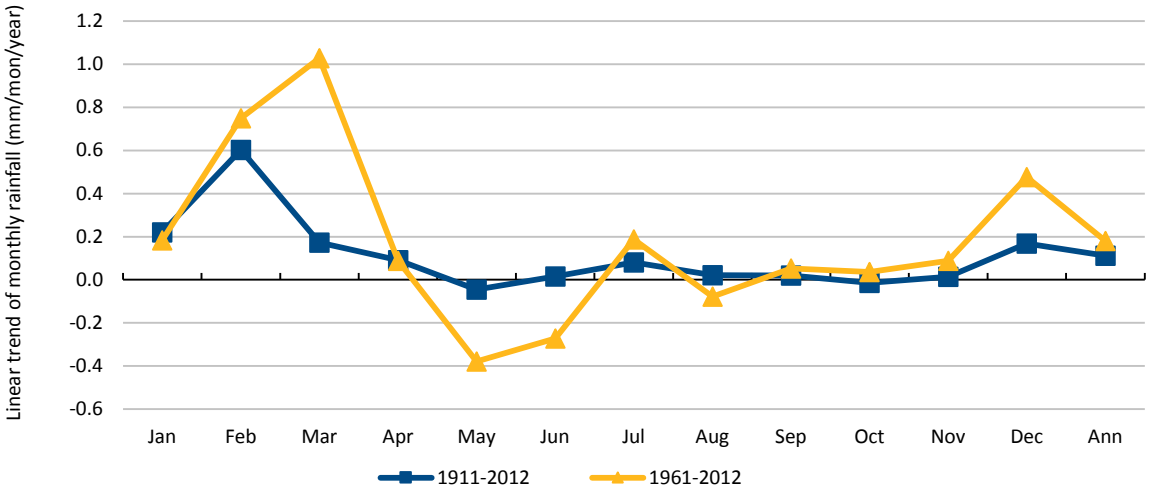

Figure 2.36 Linear trends in Assessment area monthly rainfall (mm/month/year) for the 1911 to 2012 and 1961 to 2012 periods

The annual anomalies in daily extreme rainfall (maximum daily rainfall, 99th and 95th percentiles of daily rainfall), the numbers of rainfall days (using thresholds 0 and 1 mm to define a rain day), and the average rainfall intensity (ratio of annual rainfall to the number of rainfall days) show similarities as well as differences when plotted side by side with annual total rainfall anomalies (Figure 2.37). Using linear correlation to quantify the temporal similarities between the annual total rainfall anomalies and the other anomaly time series, the 99th percentile daily rainfall has the highest correlation coefficient of 0.97. The 95th daily rainfall ranks second with a correlation coefficient of 0.96, and the average rainfall intensity has the smallest correlation coefficient of 0.74 (Figure 2.37). Thus intensity, rather than number of rain days, is more relevant to extremes in annual rainfall totals. The average number of rain days (>0 mm) in the last 102 years is 60.6 days which reduces to 34.2 days if a 1 mm threshold is used. This means that 43.7% of rain days (26.5/60.6) have a daily rainfall of less than 1 mm, and they only contribute about 3.5% of the annual total rainfall.

The spatial heterogeneity of the linear trends in daily maximum rainfall is shown for different time periods in Figure 2.38 and for 99th percentile daily rainfall in Figure 2.39, 95th percentile daily rainfall in Figure 2.40, number of rainfall days (>1 mm) in Figure 2.41 and average rainfall intensity in Figure 2.42. To determine the spatial coherence between these trends and total annual rainfall, Figure 2.43 plots the correlation of the linear trends of these rainfall statistics and annual total rainfall calculated for each individual gridcell and then averaged. This shows the highest correlation for the 99th and 95th percentile daily rainfall. Thus although spatially heterogeneous, the gridcell trends are consistent with the areal averages shown in Figure 2.37. However, differences in the strength of the linear relationship are evident for several different periods examined. For example, the correlation between the 99th percentile daily rainfall and the annual rainfall has decreased from about 0.9 to only 0.6 in the last 30 years (Figure 2.43). This means the similarities in the spatial distribution of trends across the Assessment area has weakened between these two variables. The spatial correlation between average rainfall intensity and annual rainfall is slightly stronger than that between the number of rainfall days and annual rainfall (Figure 2.43).

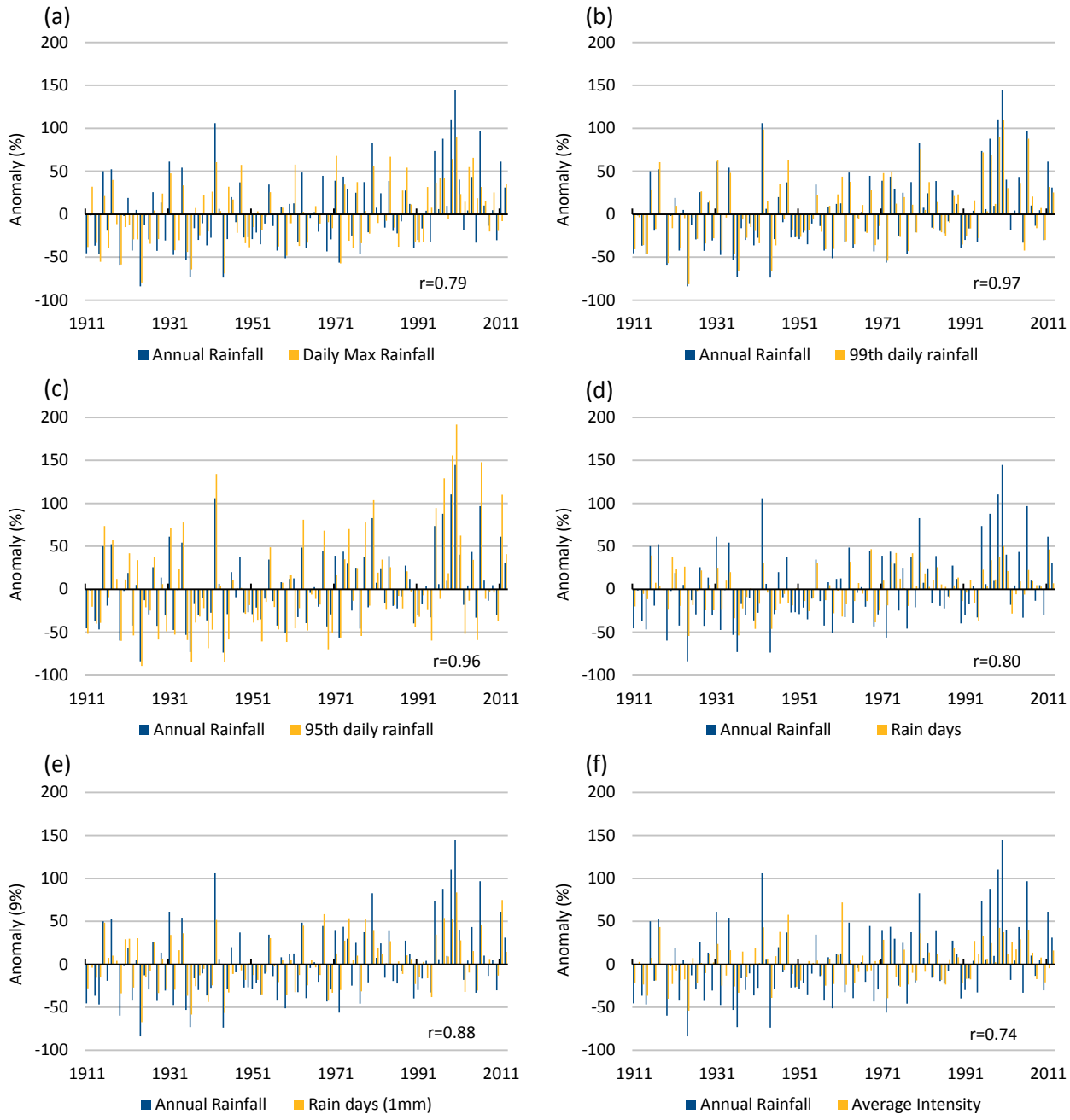

Figure 2.37 Annual anomaly (%) of annual rainfall and (a) daily maximum, (b) 99th percentile daily rainfall, (c) 95th percentile daily rainfall, (d) the number of rain days, (e) the number of rain days >1 mm and (f) average rainfall intensity

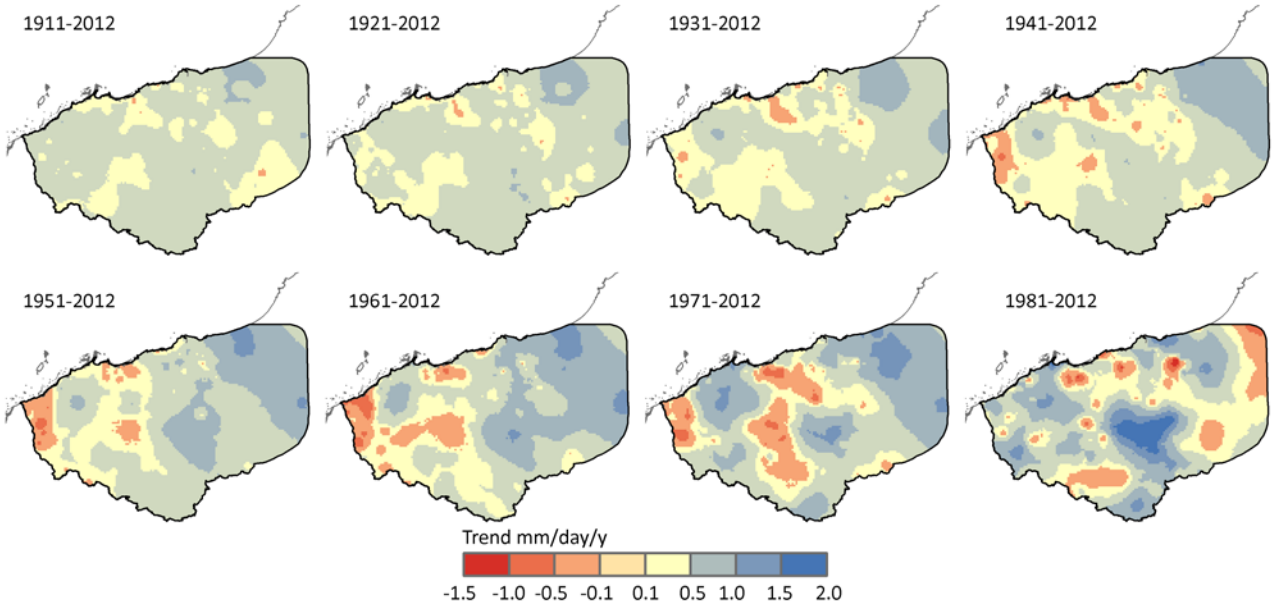

Figure 2.38 Trend of annual maximum daily rainfalls (mm/day/year)

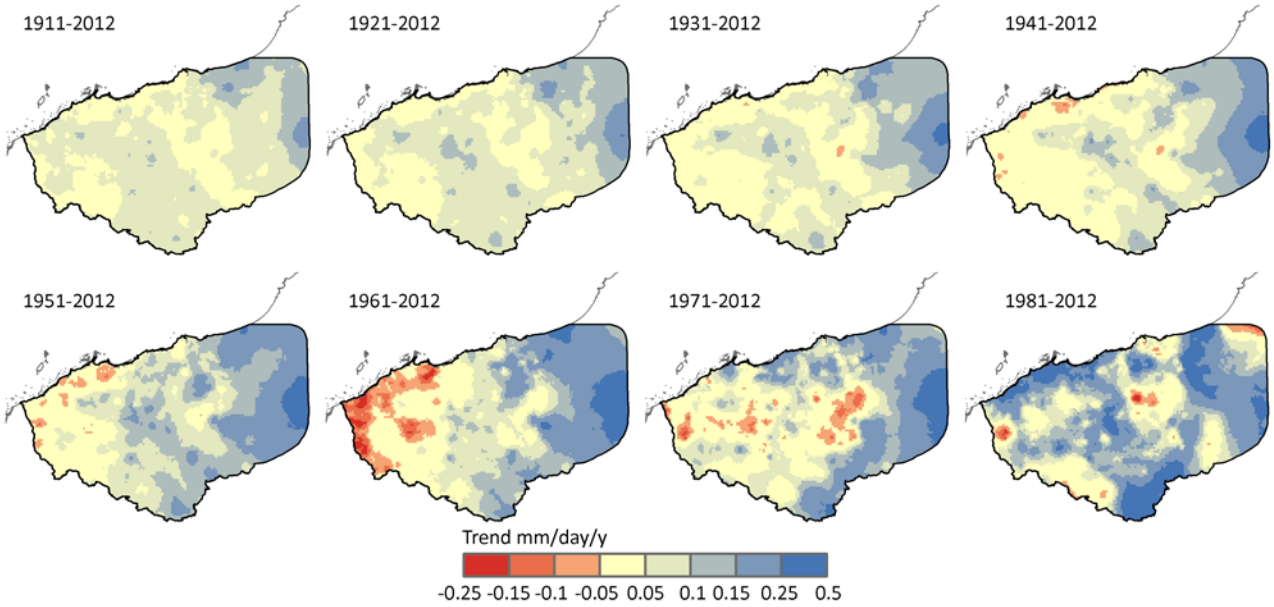

Figure 2.39 Trend of 99th percentile daily rainfall (mm/day/year)

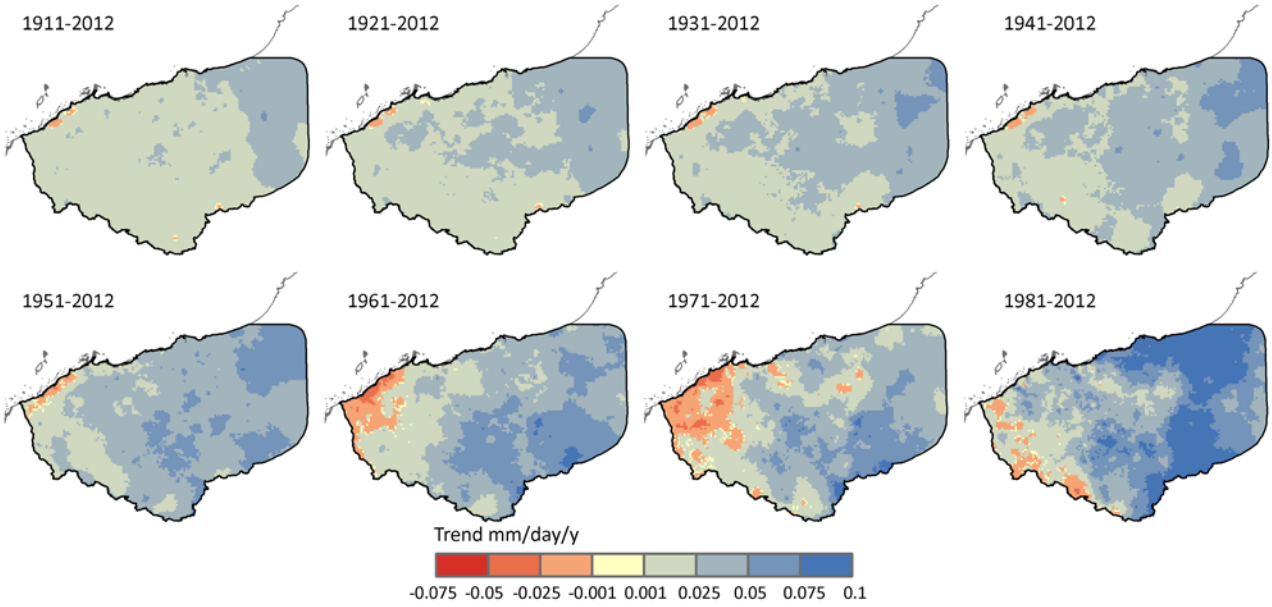

Figure 2.40 Trend of 95th percentile daily rainfall (mm/day/year)

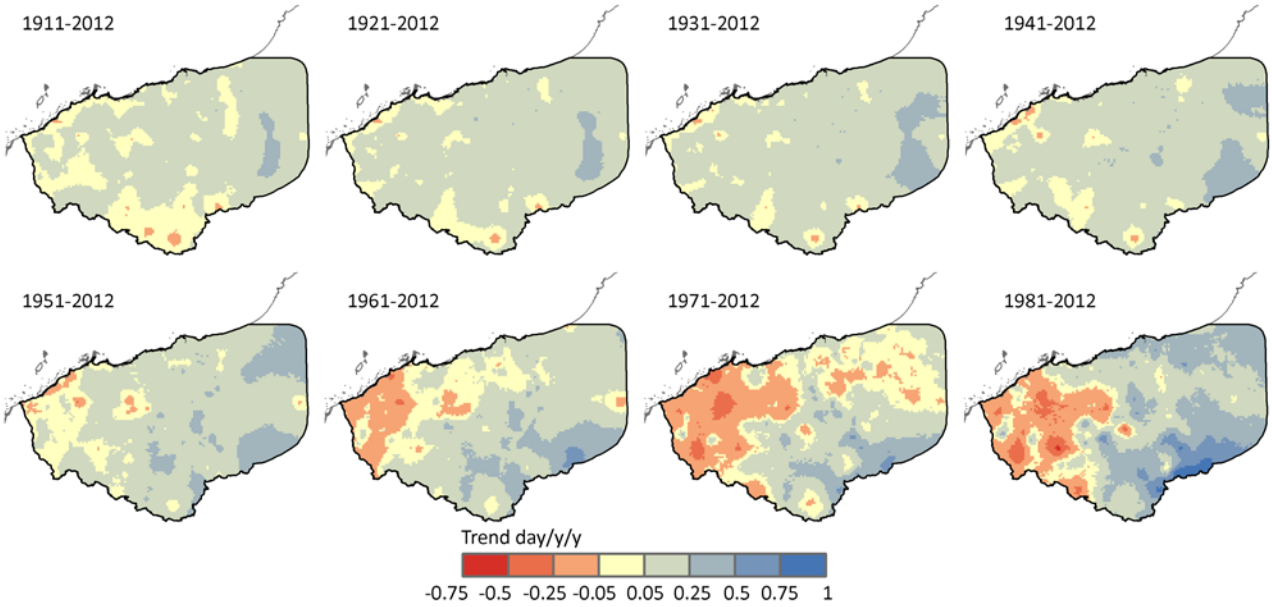

Figure 2.41 Trend of the number of rainfall days over 1 mm (day/year/year)

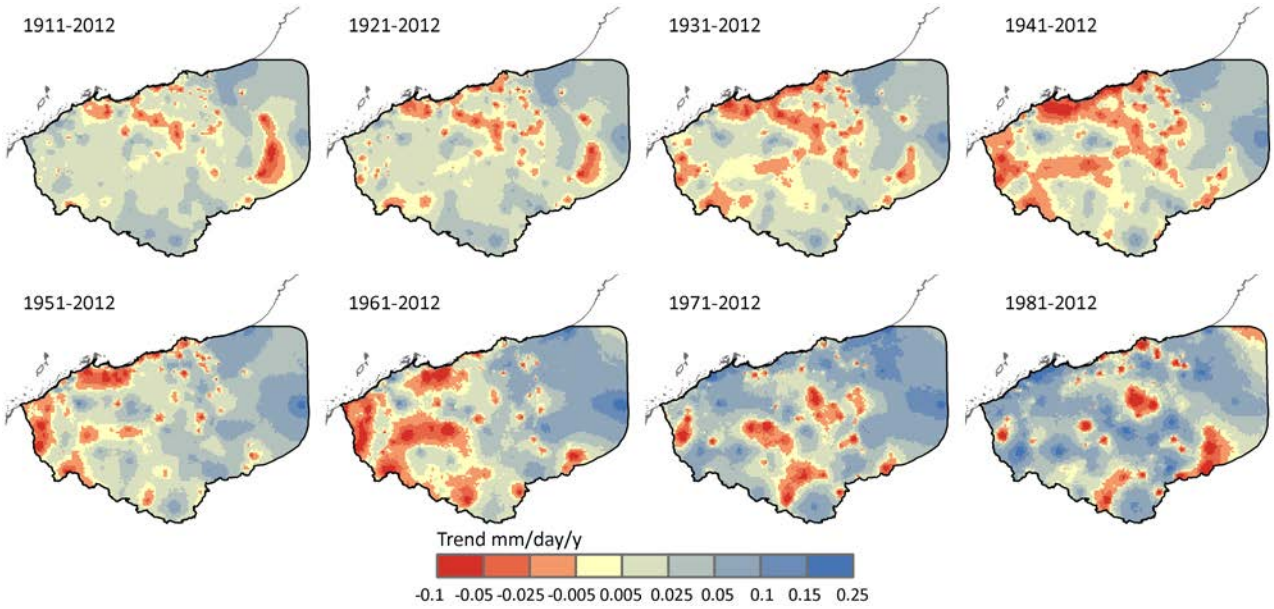

Figure 2.42 Trend of average rainfall intensity (mm/day/year)

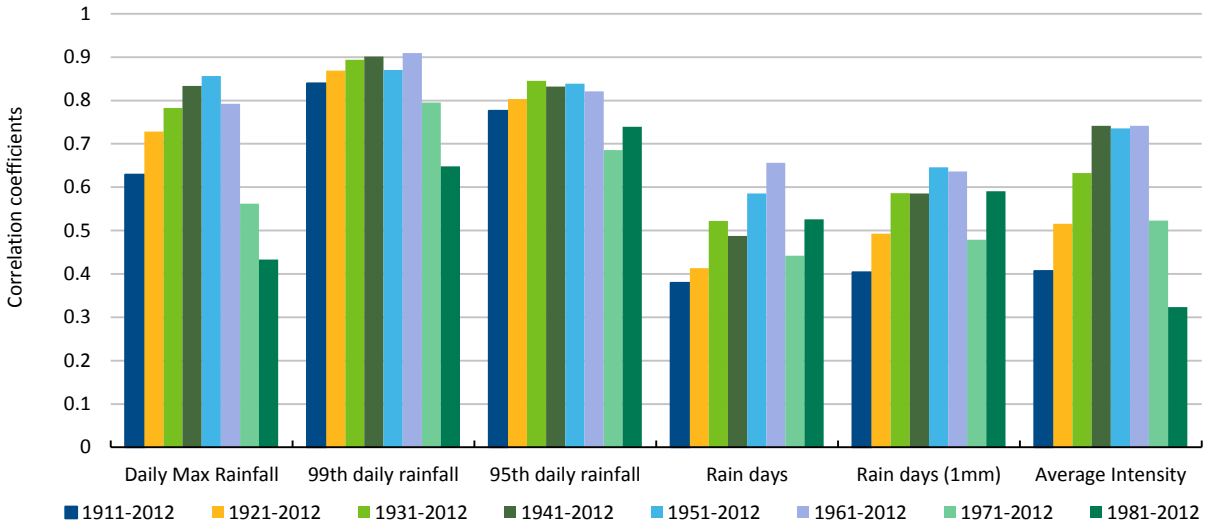

Figure 2.43 Correlation coefficients between spatial linear trends of annual rainfall and rainfall statistics for different periods

Temperature variability and trends

Both annual means of daily maximum and minimum temperature show a noticeable increasing trend for the last 100 years, especially since the late 1970s (Figure 2.44). It is also interesting to note that there was a relatively cooler period from the late 1940s to the late 1970s. The annual means of daily minimum and maximum temperature from 1947 to 1977 were about 0.44 and 0.23°C below the long-term means, respectively.

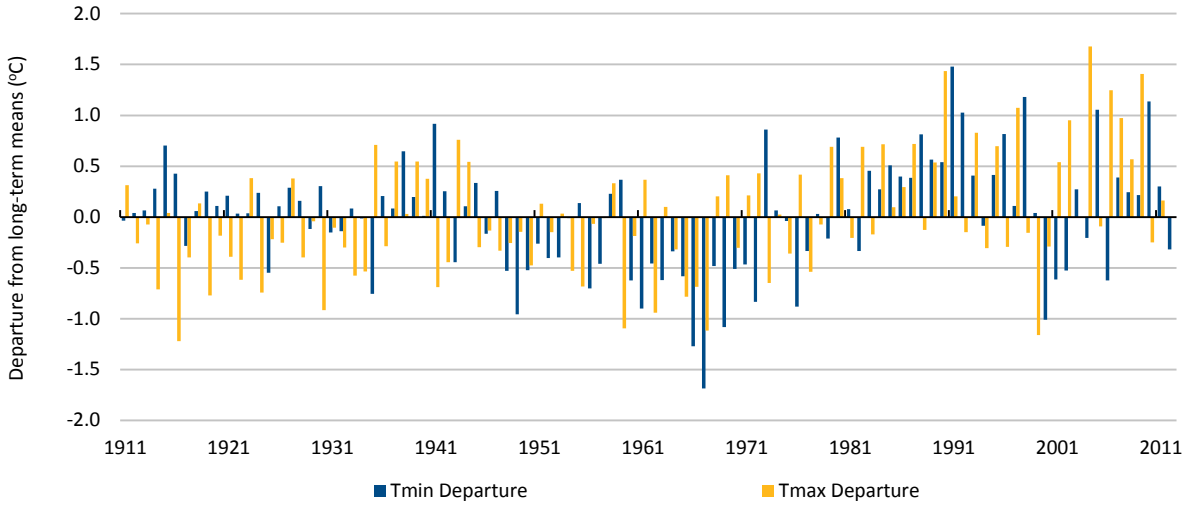

Figure 2.44 Time series of departure from long-term means for annual means of daily maximum and minimum temperature (°C)

Overall for the Assessment area, the trend magnitudes for the annual mean of daily maximum temperatures show greater increases than that of daily minimum temperatures overall (Figure 2.45 and Figure 2.46). In the last 30 years, most of the area shows a decreasing trend in mean daily minimum temperatures. This is because the mean daily minimum temperature for the entire study region reached a maximum value in 1991 (Figure 2.44), which was not the case for the annual mean daily maximum temperature.

The trends of monthly means of daily maximum and minimum temperatures are consistent in that for most months both maximum and minimum temperature trends are positive and the trends for the shorter recent period (1961-2012) are stronger than those of the full period (1911 to 2012) (Figure 2.47). There are some exceptions, with minimum temperature for the last 102 years showing slight decreasing trends for March, August, September and November and maximum temperature showing a decreasing trend in March for the last 52 years (Figure 2.47).

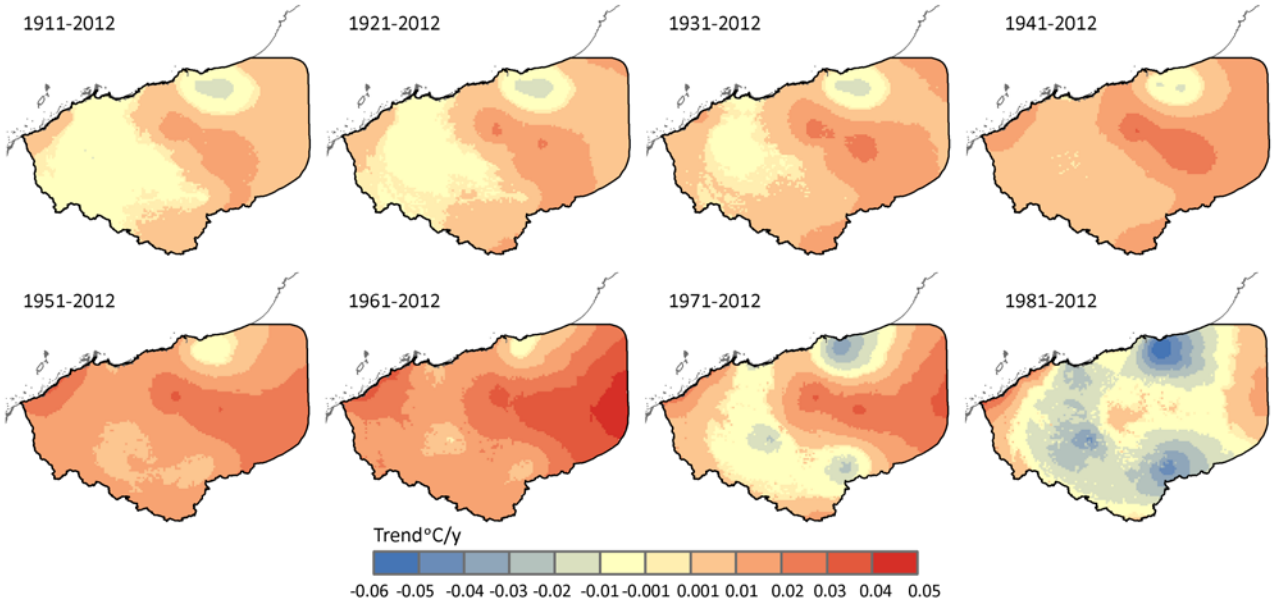

Figure 2.45 Trends in annual mean daily minimum temperatures (°C/year)

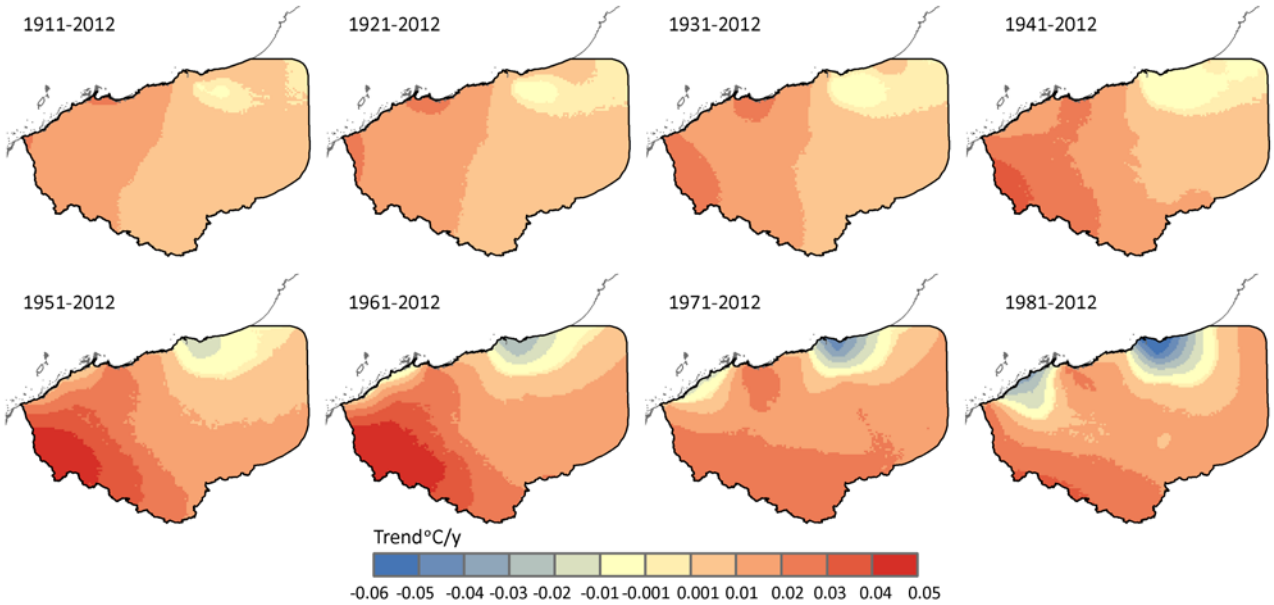

Figure 2.46 Trends in annual mean daily maximum temperatures (°C/year)

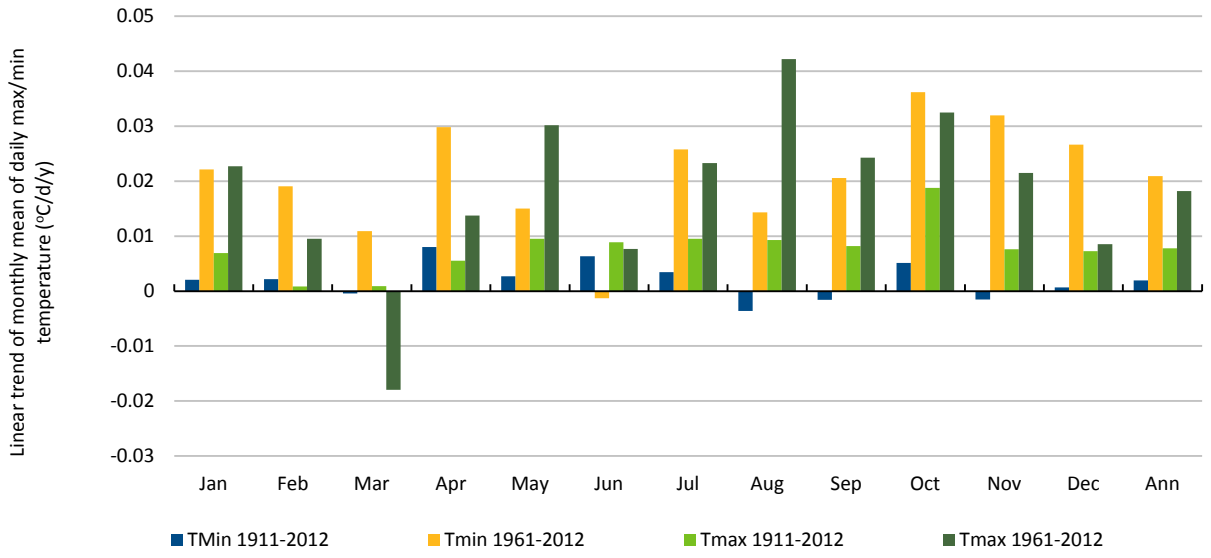

Figure 2.47 Trends in monthly mean daily maximum and minimum temperatures (°C/year)

Potential evaporation variability and trends

The Class A pan evaporation observations used as input to SILO are only available since 1970, thus the variability and trend analyses of potential evaporation are for water years 1971 to 2012 (i.e. 1st October 1970 to 30th September 2012). There is an important caveat given that the SILO Class A pan surface is interpolated from only a few stations that record Class A pan evaporation within the Assessment area (Jeffrey et al., 2001).

The time series show that pan evaporation in the last 40 years had a decreasing trend, with an apparent step-change in the mid-1990s that coincides with the wet seven-year period referred to earlier (Figure 2.48). However, neither the FAO56 (also SILO Data Drill interpolated) nor Morton's wet environment areal PE (derived from SILO Data Drill) show trends.

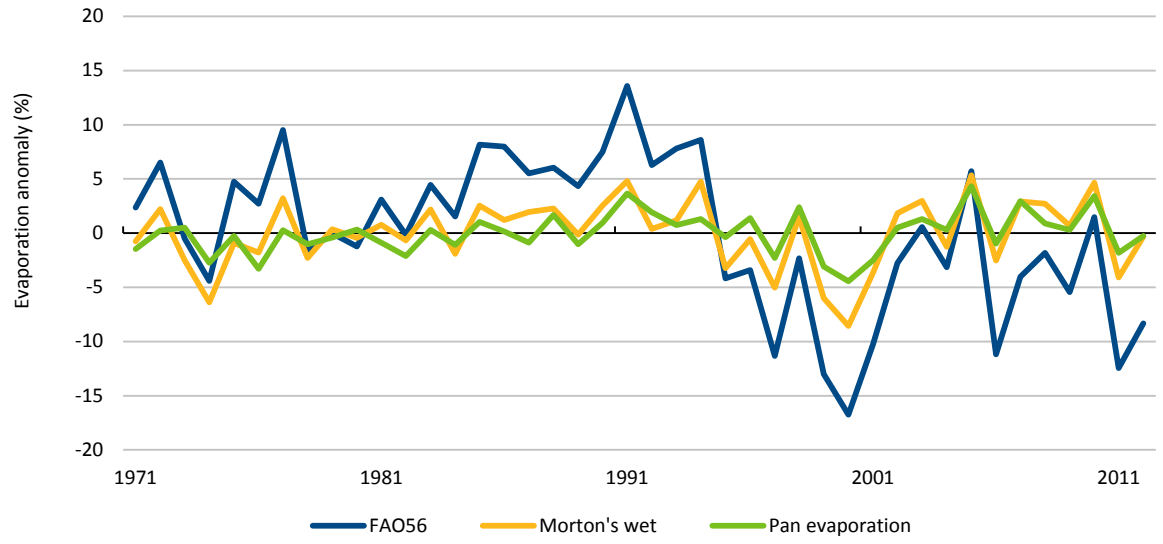

Figure 2.48 Time series of evaporation anomaly (%) for the 1971 to 2012 period

The spatial distributions of the trends for potential evaporation from the three methods show a contrast between the pan evaporation that has been decreasing across the entire area and Morton's wet environment areal PE that has increased in most of the area (Figure 2.49). The FAO56 reference evaporation falls in between these two estimates with mostly increasing but some decreasing near the coast. The number of cells with an increasing trend is larger than for those with a decreasing trend but they have a smaller magnitude. Given the annual totals from three potential evaporation estimates have different trend signs, it is not surprising that they also have differences at the monthly scale with consistency in direction, but not magnitude, in only a few months (Figure 2.50).

The increasing trends of calculated Morton's wet environment areal PE may be attributed to the increasing trends of solar radiation (Figure 2.51). The decreasing pan evaporation trend may be related to decreases in vapour pressure (Figure 2.51) and wind speed. For example, Roderick et al. (2007) concluded that the observed decreases in pan evaporation in Australia were mostly due to decreasing wind speed with some regional contributions from decreasing solar irradiance. Globally 36 studies confirmed wind speed importance when assessing evaporation trends (Fu et al., 2009; McVicar et al., 2012). Unfortunately, wind speed is not taken into account in Morton's equation. Pragmatic reasons based on the climate variables from historical records and GCM projections led to the choice of Morton's method for PE estimation. The sensitivity of hydrological modelling results to this choice of PE will be assessed in the respective components of the Assessment (e.g., rainfall-runoff modelling).

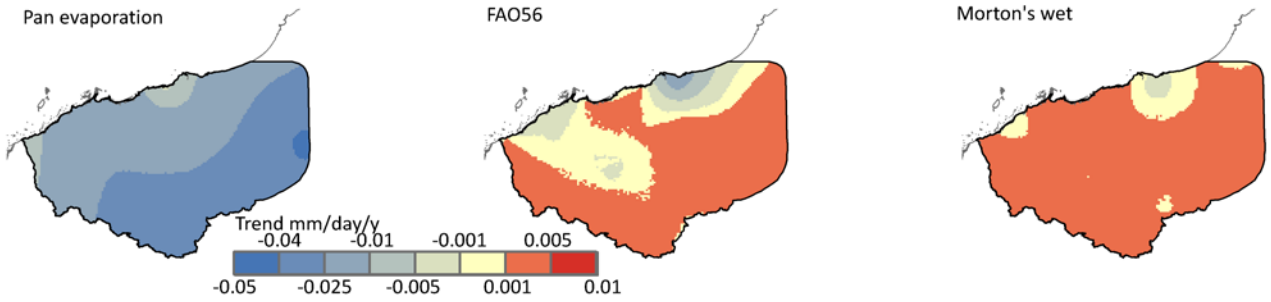

Figure 2.49 Trends in potential evaporation (mm/day/year) as estimated by three methods for the period 1971 to 2012

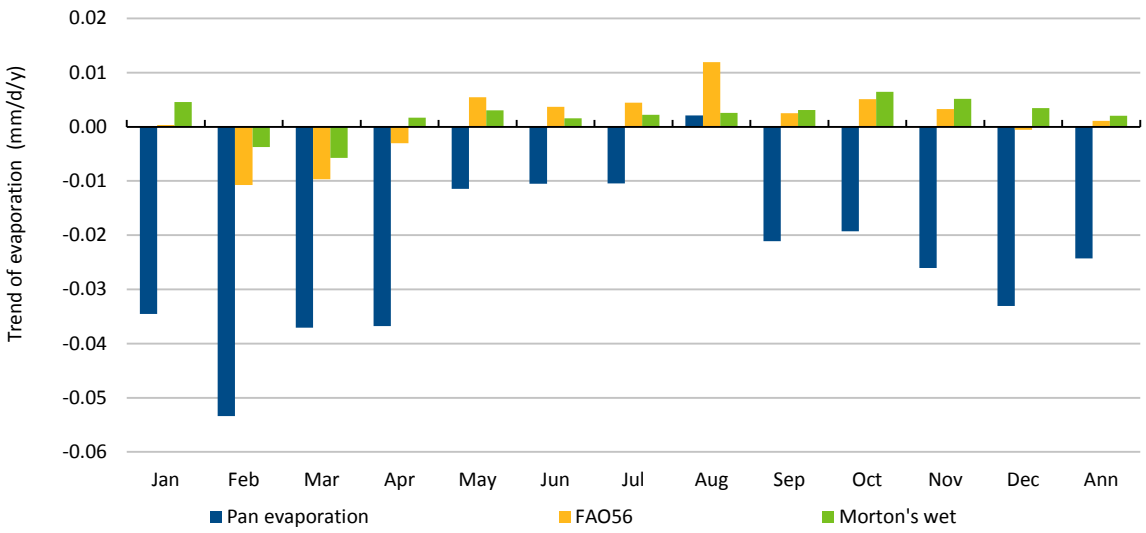

Figure 2.50 Monthly trends in daily potential evaporation (mm/day/year) for the period 1971 to 2012

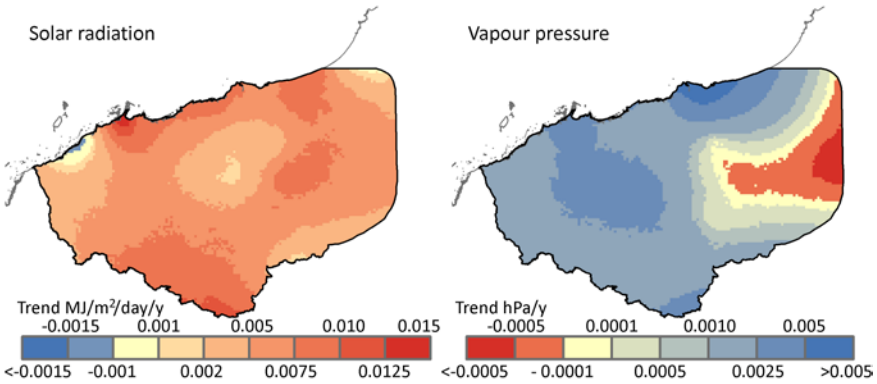

Figure 2.51 Trends in solar radiation (MJ/m^2/day/year) and vapour pressure (VP, hPa/year) for the period 1971 to 2012

2.2.4 Statistical downscaling

Statistical downscaling was applied in IOCI3 (IOCI, 2012) to provide projections at the station scale and to investigate historical atmospheric changes related to observed rainfall trends (IOCI, 2012). The non-homogeneous hidden Markov model (NHMM) statistical downscaling model was applied to a network of ten climate stations in the Pilbara (Table 2.3).

Table 2.3 Pilbara stations used for IOCI NHMM statistical downscaling

STATION NUMBER	BOM NUMBER	STATION NAME	LATITUDE (°S)	LONGITUDE (°E)	CURRENT STATUS
1	4020	Marble Bar Comparison	21.18	119.75	Closed 2006
2	4032	Port Hedland Airport	20.37	118.63	Open
3	5001	Coolawanyah	21.80	117.81	Open
4	5007	Learmonth Airport	22.24	114.10	Open
5	5008	Mardie	21.19	115.98	Open
6	5052	Karratha Station	20.88	116.67	Open
7	6011	Carnarvon Airport	24.89	113.67	Open
8	6050	Wandagee	23.76	114.55	Open
9	6072	Emu Creek Station	23.03	115.04	Open
10	7059	Mount Vernon	24.23	118.24	Open

Figure 2.52 Location of Pilbara stations listed in Table 2.3 and atmospheric predictor grid cells

The NHMM relates, on a seasonal basis, the dominant daily spatial rainfall patterns to their temporal sequencing through a set of distinct 'weather states'. For this 10-station Pilbara network NHMMs were calibrated to daily rainfall (using SILO patched point data, i.e. with missing days infilled) for summer (November to April) and winter (May to October) half-years.

The daily sequence of weather states was parameterised not only as a function of the spatial rainfall patterns but also as a function of a small set of atmospheric predictors representing the regional atmospheric characteristics of that day (e.g. surface air pressure, upper-air wind and moisture fields). Thus rainfall variability at daily to inter-decadal scales is accounted for through variability in the atmospheric predictor fields across the range of temporal scales (i.e. day-to-day changes, seasonal and year-to-year cycles, and long-term trends can all be accounted for). The predictors selected for the Pilbara summer and winter NHMMs are summarised in (IOCI, 2012) with their associated weather states shown in Figure 2.53 for summer and Figure 2.54 for winter. Although these figures show the predictors for the entire Australian region, the predictor inputs used for the NHMM were calculated over the Pilbara region as described in IOCI (2012). Both seasons have a predictor based on MSLP and dew-point temperature depression (DTD) at the 700 hPa level. DTD is the difference between air temperature and dew-point temperature (i.e. the temperature at which the air would need to be cooled to reach 100% relative humidity) and is thus a measure of the dryness of the atmosphere. Additionally the summer NHMM uses a predictor based on east-west wind speed (u-wind) at the 850 hPa level whereas the winter NHMM uses the same variable but for the 700 hPa level.

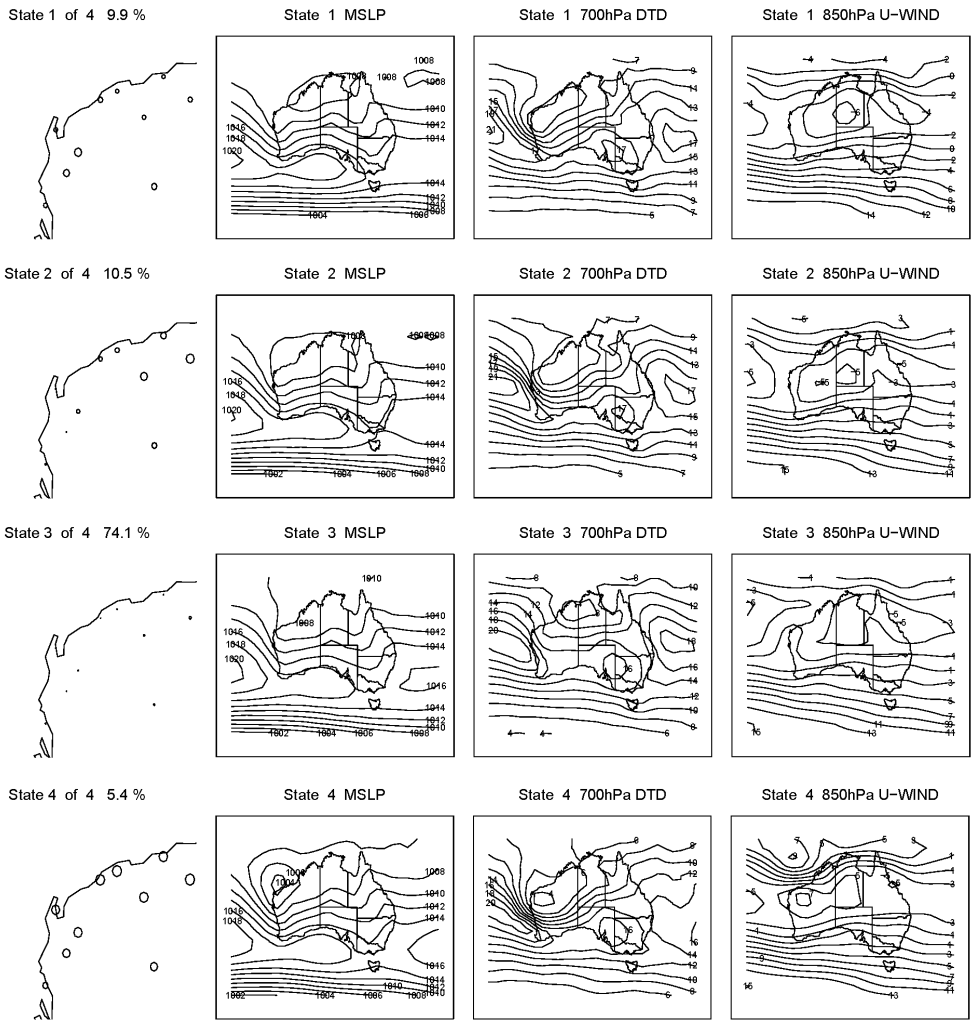

Figure 2.53 NHMM weather states for summer (November to April). Left-hand column maps represent the probability of precipitation as a circle. The other columns show the composite atmospheric predictor fields associated with each state

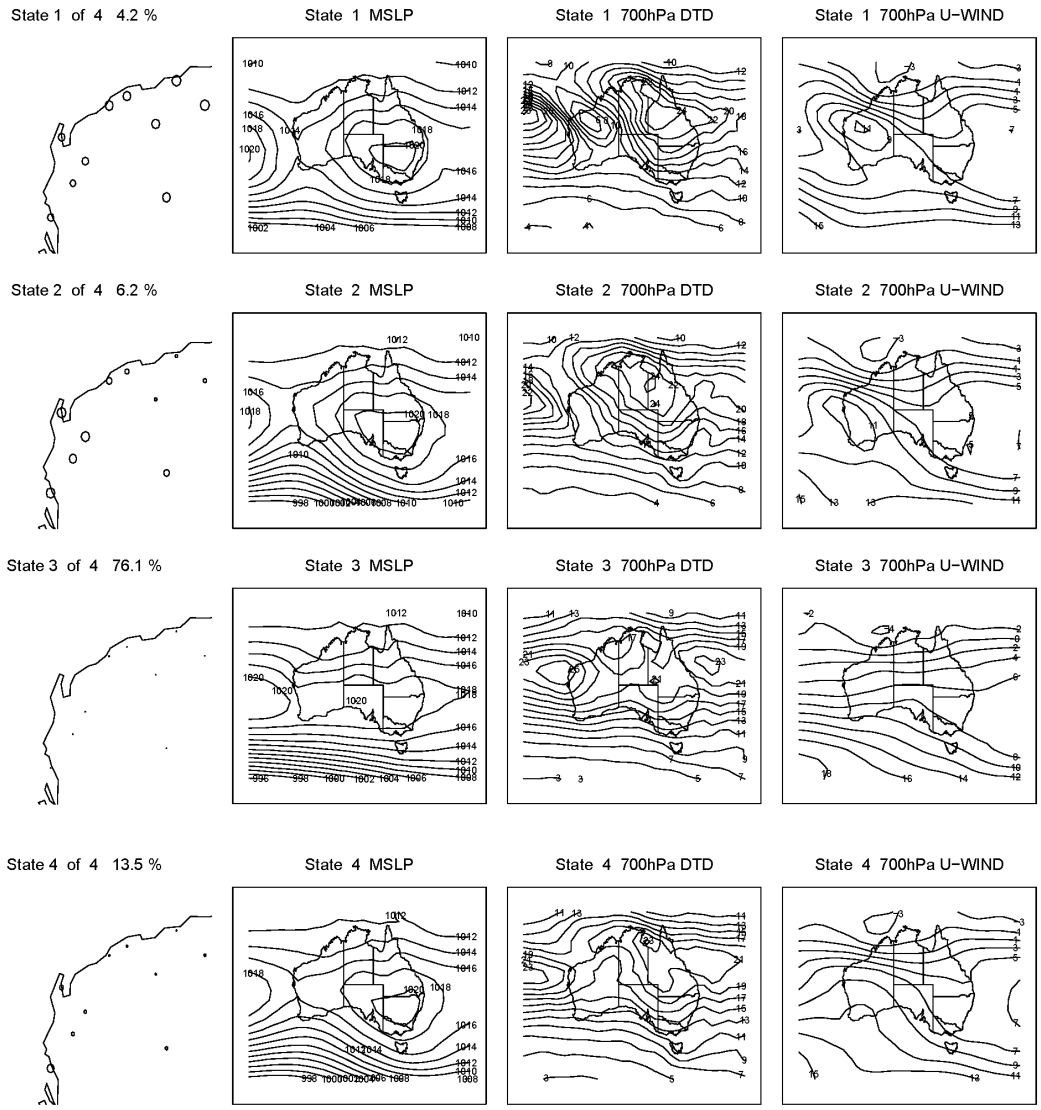

Figure 2.54 NHMM weather states for winter (May to October). Left-hand column maps represent the probability of precipitation as a circle. The other columns show the composite atmospheric predictor fields associated with each state

The inter-annual variability and long-term trends of the summer state frequencies are shown in Figure 2.55. An increasing trend is evident for State 2, which on average occurs on just over 10% of days and has a rainfall pattern indicating rainfall in the eastern Pilbara (Figure 2.53), which could be related to changes in a strengthening or more intense monsoon or it could be related to thunderstorms and a more active heat trough. The four eastern stations (1, 2, 3 and 10; Figure 2.52) receive a reasonable proportion of their annual rainfall in State 2 (14 to 30%; Table 2.4). Summer State 1 represents a pattern of wet southerly stations, with stations 8, 9 and 10 receiving 16 to 22% of their annual rainfall from this state (Table 2.4). This state has no long-term trend. Summer State 4 represents rainfall at all stations, and while occurring on only 5% of days it provides the largest proportion of annual rainfall for 9 out of the 10 stations (the exception being station 7, the most south-westerly and outside the Pilbara). These three wet patterns (states 1, 2 and 4) are all most frequent in the January to March period (Figure 2.56). In contrast the dry state 3, occurring in 74% of days, has the opposite seasonal cycle (Figure 2.56) and a slight decreasing trend (Figure 2.55).

In winter, wetter states include State 2 (Figure 2.54) which contributes a reasonable proportion of annual rainfall for stations 4, 7, 8 and 9 (15 to 44%; Table 2.4) which are the four most western stations (Figure 2.52). This state has an increasing trend (Figure 2.57) and is most frequent in May to July (Figure 2.58). State 3, which is dry across the entire Pilbara and occurs most frequently between August and October, is

the only winter state to have a decreasing trend (Figure 2.57). State 1 (4% of winter days) is wet across the Pilbara, has an increasing trend, and occurs mainly in May and June. This may correspond to the increased formation of NWCBs and intra-seasonal oscillations as inferred by (Frederiksen and Frederiksen, 2011; IOCI, 2012). It is very infrequent in August to October (Figure 2.58).

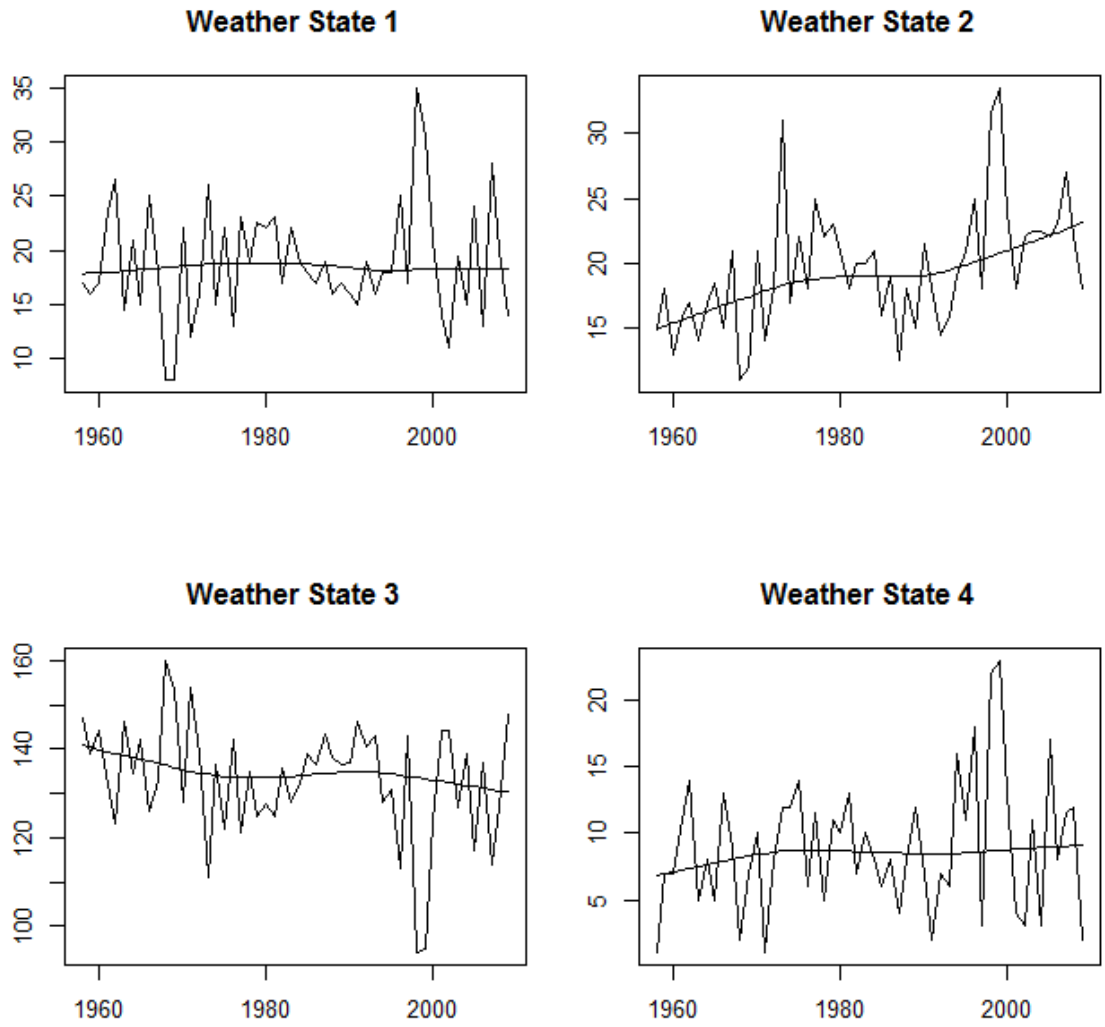

Figure 2.55 Time series of NHMM simulated frequency of summer weather states (days, season length is 181 days)

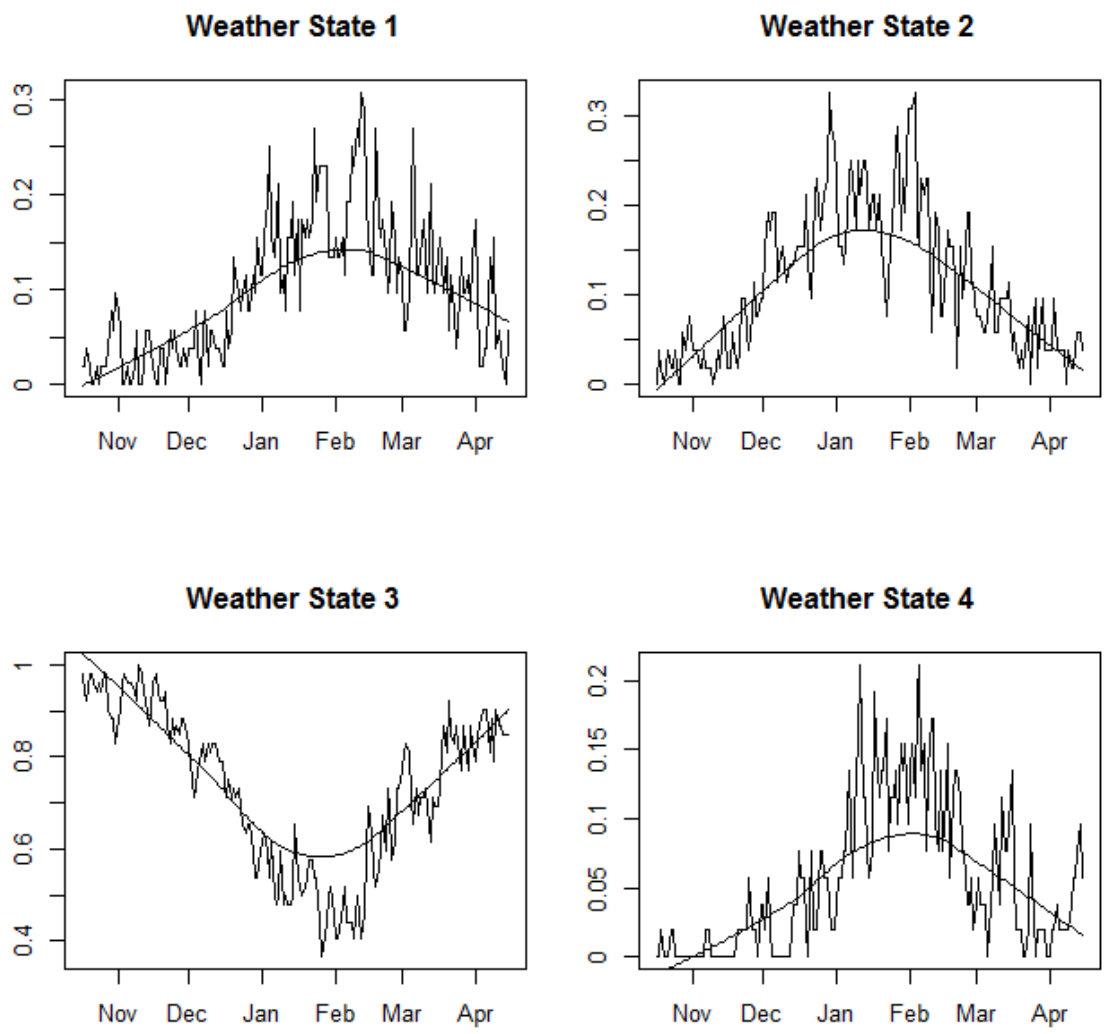

Figure 2.56 Seasonal cycle of NHMM simulated frequency of summer weather states

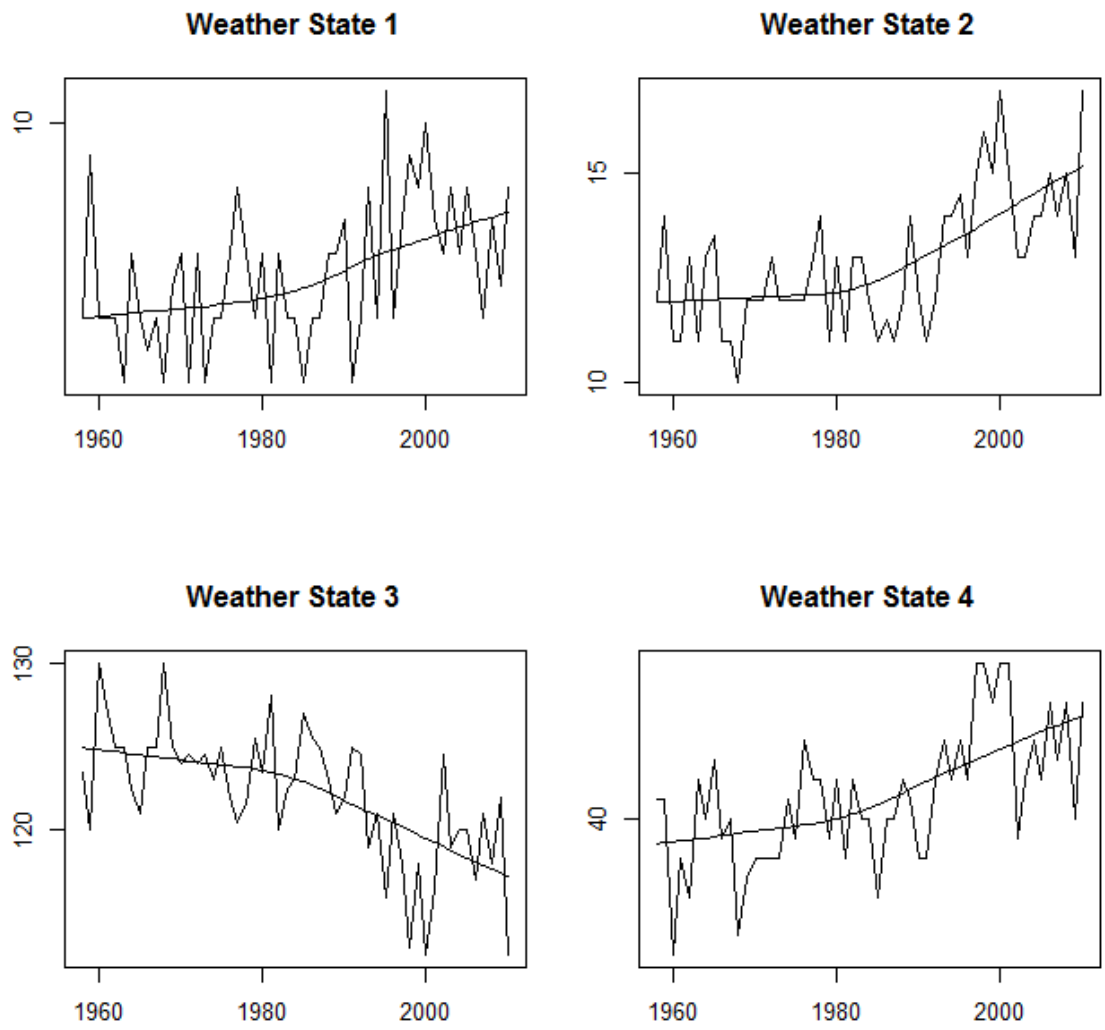

Figure 2.57 Time series of NHMM simulated frequency of winter weather states (days, season length is 184 days)

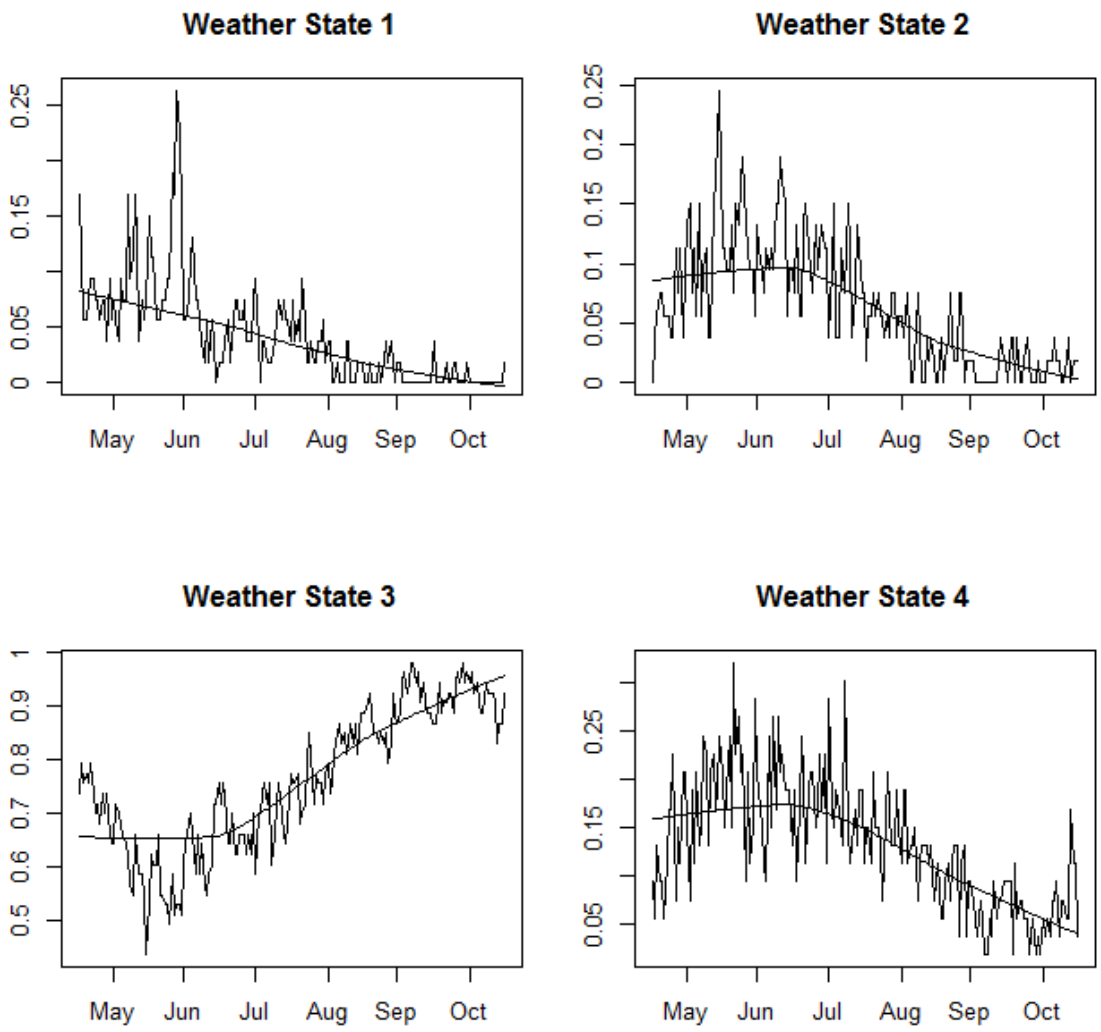

Figure 2.58 Seasonal cycle of NHMM simulated frequency of winter weather states

Table 2.4 Annual rainfall contribution by weather state (%)

STATION	SUMMER WEATHER STATES				WINTER WEATHER STATES			
	1	2	3	4	1	2	3	4
1	2.6	30.5	8.7	41.9	14.9	0.8	0.0	0.7
2	4.3	14.0	0.1	58.4	22.4	0.4	0.4	0.0
3	4.0	27.3	2.3	49.8	15.1	0.8	0.1	0.5
4	6.0	0.7	0.4	41.3	17.7	31.4	0.1	2.4
5	5.5	7.6	0.2	55.7	25.3	5.4	0.3	0.0
6	4.0	7.8	0.9	59.6	24.7	1.5	0.2	1.3
7	8.7	0.0	2.4	19.1	6.2	44.1	3.0	16.4
8	20.4	0.1	0.2	35.4	13.9	24.3	3.6	2.1
9	22.4	5.0	1.2	39.7	15.3	15.5	0.3	0.6
10	15.9	24.2	2.8	28.1	19.6	6.7	0.7	2.0

2.3 Hydroclimate extremes

IOCI researchers have developed techniques for simulating projected changes to extreme rainfall and intensity-frequency-duration (IFD) characteristics for the Pilbara by combining dynamically downscaled projections (CCAM) with a statistical model (IOCI, 2012). Prior to this research, only general assessments of how extremes may change had been undertaken. For example, Alexander and Arblaster (2009) examined trends in observed and modelled extremes across Australia. Precipitation indices they investigated were: (i) Heavy precipitation days [number of days with precipitation >= 10 mm]; (ii) Maximum 5-day precipitation; (iii) Simple daily intensity [ratio of annual total precipitation to number of days >= 1 mm]; (iv) Consecutive dry days [maximum number of consecutive days <1 mm]; and (v) Very heavy precipitation contribution [fraction of annual total precipitation due to events exceeding the 1961 to 1990 95th percentile]. They noted that most climate model projections indicate a decrease in heavy precipitation days over northwest Australia.

The IOCI downscaling based approach was applied to northwest Australia for periods centred on 2030 and 2070 under the SRES A2 emissions scenario. The statistical model incorporates covariates such as distance inland and height above sea level and so the sparse network for which observed data was available could be infilled to produce current and future maps of extreme 24-hr rainfall events with a 100-year return period.

Overall the Pilbara region shows decreases in extreme (24-hr 100-year return period) rainfall and IFD curves. Port Hedland shows an extreme rainfall decrease in the order of 10% and for Millstream little change (Figure 2.59). These results include the caveat that ‘these projections should be seen as initial estimates only’ given they are from only one GCM/CCAM simulation for only a single emissions scenario and so ‘should not be used for making impacts, vulnerability and risk assessments’ (IOCI, 2012).

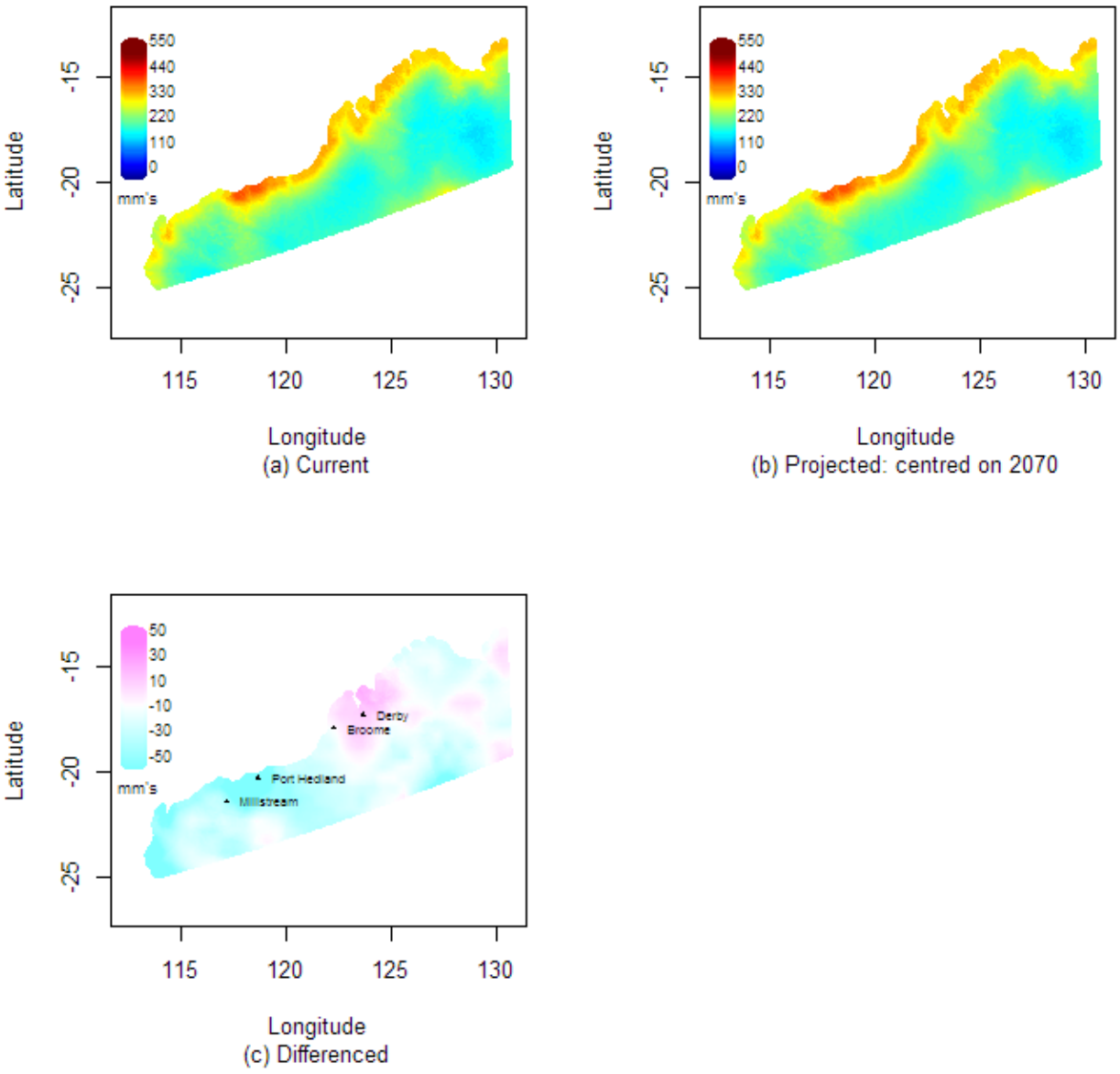

Figure 2.59 Extreme rainfall with a 100-year average recurrence interval under (a) the current climate, (b) projected climate at 2070 under a high (SRES A2) greenhouse gas emissions scenario, and (c) the difference between these two periods. Panels (a) & (b) show 24-hour return levels in millimetres; yellow to red areas indicate more intense extreme 24-hour rainfall, green to blue areas less intense. In (c) the magenta areas indicate areas where projected extreme 24-hour rainfall amounts are expected to increase by 2070; pale blue indicates areas of projected decrease

Source: (IOCI, 2012)

There is no research published on sub-daily rainfall trends in the Pilbara. As discussed in section 2.1.6, modelling studies indicate increases in sub-daily intensity from tropical cyclones in projected future climates, and the intensity of small-sale convective storms could also increase in a warmer and moister atmosphere (Allen et al., 2014b; Berg et al., 2013). Modelling of the historical relationship between sub-daily rainfall and changes in temperature and moisture across Australia suggests increasing temperature results in increased intensity of short duration rainfalls relative to daily rainfall amount, together with an increase in the fraction of each wet day with no rainfall (Westra et al., 2013).

Green and Johnson (2012) suggest that given '*the status of climate change science means that revised IFD estimates for future climate regimes will not be available for several years*' an interim approach is required to assess how climate change may impact IFD design rainfalls. They suggest assessing how risks would

change under 10, 20 and 30% increases in current IFDs. This would give practitioners and planners an understanding of how changes to design rainfalls translate into increased flood risk and severity of effects on infrastructure and the environment. Assessing vulnerabilities to possible climate change impacts on design rainfalls would indicate whether new risk and planning policies are required to control the increased risks.

In order to provide more reliable design flood information under climate change, including projections of IFD changes, Bates and Westra (2013) outline a comprehensive research plan for incorporating the most up-to-date climate change science into revisions of *Australian Rainfall and Runoff*, the national guideline document produce by Engineers Australia. The proposed research to quantify possible changes and uncertainties in IFD data under projected changed climates involves high spatial resolution (<5 km resolution) dynamical simulations from the Regional Atmospheric Modelling System (RAMS) and Weather Research and Forecasting (WRF) models at intervals down to five minutes duration. IFD uncertainty will be quantified by comparing the different model IFDs to radar/gauged data. The first stage of this research applies the techniques to the Greater Sydney region. On-going funding for the second stage could extend RAMS simulations to other regions of Australia, including to northwest Australia.

2.4 Paleoclimate

Pilbara ecosystems have evolved over millions of years under a variety of climates. Soil-landscapes and drainages have been shaped over this time period and there is also evidence that some aquifers across the Pilbara developed under climates very different to today (Skrzypek et al., 2013). To an extent this 'preconditioning' may be important to understanding how the Pilbara biota, especially of surface water and groundwater dependent ecosystems, may respond to a future climate regime. Hence knowledge of both past and future hydroclimatic scenarios is important for understanding the evolution of groundwater resources, risk management around mining operations and rural-based enterprises, as well as for indigenous use of the Assessment area. This section briefly summarises current understanding of the Pilbara palaeoclimate of the last hundred to several thousand years in order to place this Assessment of the 1910 to 2050 period into a broader context. Research on earlier periods (tens to hundreds of thousands of years BP) are not a focus given the desire to maintain context and relevance to modern climate.

Globally, records of climate fluctuations over recent millenia have increased significantly over the last few years as they provide appropriate context to evaluate the relative role of natural versus anthropogenic factors in generating climate shifts at decadal to centennial timescales (IPCC 2013). Palaeo studies have identified significant and largely coherent shifts in tropical hydroclimates across Africa (e.g. Thomas et al., 2009; Burrough and Thomas 2013), South America (Haug et al., 2001) and the Pacific (Sachs et al., 2009) during the late-Holocene (the last few thousand years). These hydrological changes are globally attributed to the precession-driven movement in the position of the Intertropical Convergence Zone (ITCZ), changes in strength of ENSO, or coupling of these two drivers (Sachs et al. 2009; Denniston et al. 2013). The pattern in tropical hydroclimate over recent millenia remains unclear in the Australasian region, which is largely attributable to a lack of sufficient data and imprecise or poorly resolved chronologies. However, recent reviews of the limited records from the Australian tropics and interior arid zone, including the Pilbara, have inferred increasingly arid conditions for the late-Holocene (Fitzsimmons et al. 2013; Reeves et al. 2013).

The links between terrestrial and marine systems for the north-eastern Indian Ocean rim remain poorly characterised. There have, however, been studies of the palaeoclimatic characteristics of the Leeuwin Current. For example, Gingele et al. (2001) hypothesised that changes in the clay mineral signature in sediments point to more outflow from Northwest Cape rivers hence more rainfall at the beginning of the Holocene (about 12,000 years ago). Spooner et al. (2011) also concluded that the Leeuwin Current was still active during the last five glacial periods going back 500k years based on the relative abundance of planktonic foraminifera, stable isotopic data, and temperature estimates of the upper part of the water column inferred from a high resolution ocean core taken off of the Northwest Cape.

The frequencies of tropical cyclones influencing south of the Pilbara from 6,000 to 500 years ago have been inferred from an assessment of shore parallel ridges between 3 and 6 m above mean sea level at Hamelin

Pool, Shark Bay. This study inferred a 1700 year long very dry period, with an absence of major tropical cyclones, between 5400 and 3700 years BP (Nott, 2011). Correspondingly a very dry 1200 year long period has been inferred in the Kimberley from a lack of Aboriginal rock art ending 3800 to 4000 years BP and this period has been linked to a failure of the monsoons related to changes in ENSO, magnified by land surface and aerosol loading changes (McGowan et al., 2012).

For the more recent past of the last hundred years or so, Pilbara climate has been assessed from the oxygen isotope chronology of *Callitris columellaris*, which was then compared to the observed records (Cullen et al., 2008; Cullen and Grierson, 2007). Tree-ring records from the Pilbara show summer rainfall, humidity and temperatures consistent with observational records, with a relatively dry and warm period from 1919 to 1955 followed by progressively wetter, more humid and cooler summers, with the 1980s and 1990s being the wettest and coolest of the last 80 years. A recent 210-year ring-width chronology from *C. columellaris* was highly correlated with summer-autumn (Dec-May) precipitation (r = 0.81) and revealed inter-annual to multi-decadal scale variation in hydroclimate across the Pilbara since at least 1800, typically showing periods of below average rainfall extending from one to three decades and periods of above average rainfall, which were often less than a decade. This study also demonstrates that the last two decades (1995-2012) have been unusually wet (average summer-autumn precipitation of 310 mm) compared to the previous two centuries (average summer-autumn precipitation of 229 mm), coinciding with both an anomalously high frequency and intensity of tropical cyclones in northwest Australia and the dominance of the positive phase of the Southern Annular Mode (O'Donnell et al. 2015).

This contrasts with the longer timescales, for which the Pilbara appears to have experienced glacial periods of extreme aridity when sea levels were lower and drainage lines were much longer than at present. However these periods would have been colder than at present, carbon dioxide levels would have been lower and growing seasons shorter. These arid periods may have enabled some plant and animal assemblages to adapt to extremely dry conditions. The recent drying period of the past 5000 to 6000 years needs to be placed into this longer context. As was shown in earlier sections of this chapter, there are also higher frequency wet and dry periods within these much longer climate sequences. While concentrating on rainfall is important for considering past and future climate the concurrent variability in temperature, potential evaporation (vapour pressure deficits) and carbon dioxide levels also play an important role in relation to how biota, industries, people and hydrology may be affected.

2.5 References

Abbs D (2012) The impact of climate change on the climatology of tropical cyclones in the Australian region. CSIRO Climate Adaptation Flagship Working paper No. 11.

Alexander LV and Arblaster JM (2009) Assessing trends in observed and modelled climate extremes over Australia in relation to future projections. International Journal of Climatology 29(3), 417-435. Doi: 10.1002/joc.1730.

Allen JT and Karoly DJ (2013) A climatology of Australian severe thunderstorm environments 1979–2011: inter-annual variability and ENSO influence. International Journal of Climatology, n/a-n/a. Doi: 10.1002/joc.3667.

Allen JT, Karoly DJ and Walsh KJ (2014a) Future Australian Severe Thunderstorm Environments. Part I: A Novel Evaluation and Climatology of Convective Parameters from Two Climate Models for the Late Twentieth Century. Journal of Climate 27(10), 3827-3847. Doi: 10.1175/JCLI-D-13-00425.1.

Allen JT, Karoly DJ and Walsh KJ (2014b) Future Australian Severe Thunderstorm Environments. Part II: The Influence of a Strongly Warming Climate on Convective Environments. Journal of Climate 27(10), 3848-3868. Doi: 10.1175/JCLI-D-13-00426.1.

Bates B and Westra S (2013) Australian Rainfall and Runoff Climate Change Research Plan Summary. Engineers Australia. Available online: <http://www.ncwe.org.au/arr/Website_links/ARRCCS_ResPlan_Summary_17Jan2013.pdf>.

Bell R, Strachan J, Vidale PL, Hodges K and Roberts M (2013) Response of Tropical Cyclones to Idealized Climate Change Experiments in a Global High-Resolution Coupled General Circulation Model. Journal of Climate 26(20), 7966-7980. Doi: 10.1175/JCLI-D-12-00749.1.

Berg P, Moseley C and Haerter JO (2013) Strong increase in convective precipitation in response to higher temperatures. Nature Geosci 6(3), 181-185. Doi: 10.1038/ngeo1731.

Berry G, Reeder MJ and Jakob C (2011) Physical Mechanisms Regulating Summertime Rainfall over Northwestern Australia. Journal of Climate 24(14), 3705-3717. Doi: 10.1175/2011jcli3943.1.

Bureau of Meteorology (2010) Australian Climate Influences. Viewed 15 April 2013, <http://www.bom.gov.au/watl/about-weather-and-climate/australian-climate-influences.shtml>.

Bureau of Meteorology (2012a) Average annual thunder-day and lightning flash density. Viewed 15 April 2013, <http://www.bom.gov.au/jsp/ncc/climate_averages/thunder-lightning/index.jsp>.

Bureau of Meteorology (2012b) Wind Roses for Selected Locations in Australia. Viewed 6 May 2013, <http://www.bom.gov.au/climate/averages/wind/selection_map.shtml>.

Bureau of Meteorology (2013a) About the Indian Ocean Dipole. Viewed 3 May 2013, <http://www.bom.gov.au/climate/IOD/about_IOD.shtml>.

Bureau of Meteorology (2013b) Western Australia Tropical Cyclone Season Summary 1998-99. Viewed 15 April 2013, <http://www.bom.gov.au/cyclone/history/wa/1999.shtml>.

Bureau of Meteorology (2013c) Western Australia Tropical Cyclone Season Summary 1999-2000. Viewed 15 April 2013, <http://www.bom.gov.au/cyclone/history/wa/2000.shtml>.

Bureau of Meteorology (2015) Madden-Julian Oscillation. Viewed 16 March 2015, <http://www.bom.gov.au/climate/mjo/#tabs=Regional-cloudiness>.

Cai W, Cowan T and Sullivan A (2009) Recent unprecedented skewness towards positive Indian Ocean Dipole occurrences and its impact on Australian rainfall. Geophysical Research Letters 36(11), L11705. Doi: 10.1029/2009GL037604.

Cai W, Cowan T, Sullivan A, Ribbe J and Shi G (2011a) Are Anthropogenic Aerosols Responsible for the Northwest Australia Summer Rainfall Increase? A CMIP3 Perspective and Implications. Journal of Climate 24(10), 2556-2564. Doi: 10.1175/2010jcli3832.1.

Cai W, van Rensch P, Cowan T and Hendon HH (2011b) Teleconnection Pathways of ENSO and the IOD and the Mechanisms for Impacts on Australian Rainfall. Journal of Climate 24(15), 3910-3923. Doi: 10.1175/2011JCLI4129.1.

Catto JL, Nicholls N and Jakob C (2012) North Australian Sea Surface Temperatures and the El Nino-Southern Oscillation in the CMIP5 Models. Journal of Climate 25(18), 6375-6382. Doi: 10.1175/jcli-d-12-00214.1.

Crosbie RS, Pollock DW, Mpelasoka FS, Barron OV, Charles SP and Donn MJ (2012) Changes in Köppen-Geiger climate types under a future climate for Australia: hydrological implications. Hydrol. Earth Syst. Sci. 16(9), 3341-3349. Doi: 10.5194/hess-16-3341-2012.

Cullen LE, Adams MA, Anderson MJ and Grierson PF (2008) Analyses of delta C-13 and delta O-18 in tree rings of Callitris columellaris provide evidence of a change in stomatal control of photosynthesis in response to regional changes in climate. Tree Physiology 28(10), 1525-1533.

Cullen LE and Grierson PF (2007) A stable oxygen, but not carbon, isotope chronology of Callitris columellaris reflects recent climate change in north-western Australia. Climatic Change 85(1-2), 213-229. Doi: 10.1007/s10584-006-9206-3.

Dare RA (2013) Seasonal Tropical Cyclone Rain Volumes over Australia. Journal of Climate 26(16), 5958-5964. Doi: 10.1175/JCLI-D-12-00778.1.

Dare RA, Davidson NE and McBride JL (2012) Tropical Cyclone Contribution to Rainfall over Australia. Monthly Weather Review 140(11), 3606-3619. Doi: 10.1175/MWR-D-11-00340.1.

Dowdy A and Kuleshov Y (2012) An analysis of tropical cyclone occurrence in the Southern Hemisphere derived from a new satellite-era data set. International Journal of Remote Sensing 33(23), 7382-7397. Doi: 10.1080/01431161.2012.685986.

Dowdy AJ (2014) Long-term changes in Australian tropical cyclone numbers. Atmospheric Science Letters 15(4), 292-298. Doi: 10.1002/asl2.502.

Dunstone NJ, Smith DM, Booth BBB, Hermanson L and Eade R (2013) Anthropogenic aerosol forcing of Atlantic tropical storms. Nature Geosci 6(7), 534-539. Doi: 10.1038/ngeo1854.

Emanuel KA (2013) Downscaling CMIP5 climate models shows increased tropical cyclone activity over the 21st century. Proceedings of the National Academy of Sciences. Doi: 10.1073/pnas.1301293110.

Fierro AO and Leslie LM (2012) Links between Central West Western Australian Rainfall Variability and Large-Scale Climate Drivers. Journal of Climate 26(7), 2222-2246. Doi: 10.1175/JCLI-D-12-00129.1.

Frederiksen C and Grainger S (2015) The role of external forcing in prolonged trends in Australian rainfall. Climate Dynamics, 1-14. Doi: 10.1007/s00382-015-2482-8.

Frederiksen C, Zheng X and Grainger S (2014) Teleconnections and predictive characteristics of Australian seasonal rainfall. Climate Dynamics 43(5-6), 1381-1408. Doi: 10.1007/s00382-013-1952-0.

Frederiksen JS and Frederiksen CS (2011) Twentieth century winter changes in Southern Hemisphere synoptic weather modes. Advances in Meteorology 2011, 1-16. Doi: 10.1155/2011/353829.

Fu G, Charles SP and Yu J (2009) A critical overview of pan evaporation trends over the last 50 years. Climatic Change 97(1-2), 193-214. Doi: 10.1007/s10584-009-9579-1.

Gingele FX, De Deckker P and Hillenbrand CD (2001) Late Quaternary fluctuations of the Leeuwin Current and palaeoclimates on the adjacent land masses: clay mineral evidence. Australian Journal of Earth Sciences 48(6), 867-874. Doi: 10.1046/j.1440-0952.2001.00905.x.

Gleixner S, Keenlyside N, Hodges K, Tseng W-L and Bengtsson L (2014) An inter-hemispheric comparison of the tropical storm response to global warming. Climate Dynamics 42(7-8), 2147-2157. Doi: 10.1007/s00382-013-1914-6.

Goebbert KH and Leslie LM (2010) Interannual Variability of Northwest Australian Tropical Cyclones. Journal of Climate 23(17), 4538-4555. Doi: 10.1175/2010jcli3362.1.

Green JH and Johnson FM (2012) Incorporation of Climate Change in Intensity-Frequency-Duration (IFD) Design Rainfall Estimates. In: Practical Responses to Climate Change National Conference 2012. Engineers Australia, 48-55.

Hall JD, Matthews AJ and Karoly DJ (2001) The modulation of tropical cyclone activity in the Australian region by the Madden-Julian oscillation. Monthly Weather Review 129(12), 2970-2982. Doi: 10.1175/1520-0493(2001)129<2970:tmotca>2.0.co;2.

Harper BA, Stroud SA, McCormack M and West S (2008) A review of historical tropical cyclone intensity in Northwestern Australia and implications for climate change trend analysis. Australian Meteorological Magazine 57(2), 121-141.

Hassim MEE and Walsh KJE (2008) Tropical cyclone trends in the Australian region. Geochemistry Geophysics Geosystems 9. Doi: 10.1029/2007gc001804.

Hendon HH, Lim E-P and Nguyen H (2014) Seasonal Variations of Subtropical Precipitation Associated with the Southern Annular Mode. Journal of Climate 27(9), 3446-3460. Doi: 10.1175/JCLI-D-13-00550.1.

Hung M-P, Lin J-L, Wang W, Kim D, Shinoda T and Weaver SJ (2013) MJO and Convectively Coupled Equatorial Waves Simulated by CMIP5 Climate Models. Journal of Climate. Doi: 10.1175/JCLI-D-12-00541.1.

IOCI (2012) Western Australia's Weather and Climate: A Synthesis of Indian Ocean Climate Initiative Stage 3 Research. Australia. Available online: <http://www.ioci.org.au/publications/ioci-stage-3/cat_view/17-ioci-stage-3/23-reports.html>.

Jeffrey SJ, Carter JO, Moodie KB and Beswick AR (2001) Using spatial interpolation to construct a comprehensive archive of Australian climate data. Environmental Modelling and Software 16, 309-330.

Jovanovic B, Collins D, Braganza K, Jakob D and Jones D (2011) A high-quality monthly total cloud amount dataset for Australia. Climatic Change 108(3), 485-517. Doi: 10.1007/s10584-010-9992-5.

Knutson TR, McBride JL, Chan J, Emanuel K, Holland G, Landsea C, Held I, Kossin JP, Srivastava AK and Sugi M (2010) Tropical cyclones and climate change. Nature Geosci 3(3), 157-163. Doi: 10.1038/ngeo779.

Kuleshov Y (2012) Southern Hemisphere Tropical Cyclone Climatology. In: Wang S-Y (ed.), Modern Climatology. InTech, Croatia.

Kuleshov Y, de Hoedt G, Wright W and Brewster A (2002) Thunderstorm distribution and frequency in Australia. Australian Meteorological Magazine 51(3), 145-154.

Kuleshov Y, Fawcett R, Qi L, Trewin B, Jones D, McBride J and Ramsay H (2010) Trends in tropical cyclones in the South Indian Ocean and the South Pacific Ocean. Journal of Geophysical Research: Atmospheres 115(D1), D01101. Doi: 10.1029/2009JD012372.

Lavender SL and Abbs DJ (2013) Trends in Australian rainfall: contribution of tropical cyclones and closed lows. Climate Dynamics 40(1-2), 317-326. Doi: 10.1007/s00382-012-1566-y.

Leslie LM, Abbey Jr RF, Speer MS and Skinner TCL (2002) Intense tropical cyclogenesis over the northwest Australian region in 1998/1999: Causal factors. Meteorology and Atmospheric Physics 80(1-4), 89-101. Doi: 10.1007/s007030200017.

Li X-F, Yu J and Li Y (2013) Recent Summer Rainfall Increase and Surface Cooling over Northern Australia since the Late 1970s: A Response to Warming in the Tropical Western Pacific. Journal of Climate 26(18), 7221-7239. Doi: 10.1175/JCLI-D-12-00786.1.

Lin ZD and Li Y (2012) Remote Influence of the Tropical Atlantic on the Variability and Trend in North West Australia Summer Rainfall. Journal of Climate 25(7), 2408-2420. Doi: 10.1175/jcli-d-11-00020.1.

Liu KS and Chan JCL (2012) Interannual variation of Southern Hemisphere tropical cyclone activity and seasonal forecast of tropical cyclone number in the Australian region. International Journal of Climatology 32(2), 190-202. Doi: 10.1002/joc.2259.

Madden RA and Julian PR (1972) Description of Global-Scale Circulation Cells in the Tropics with a 40–50 Day Period. Journal of the Atmospheric Sciences 29(6), 1109-1123. Doi: 10.1175/1520-0469(1972)029<1109:DOGSCC>2.0.CO;2.

McBride J (1998) Indonesia, Papua New Guinea, and Tropical Australia: The Southern Hemisphere Monsoon. In: Karoly DJ and Vincent DG (eds), Meteorology of the Southern Hemisphere. American Meteorological Society, Boston, Mass.

McGowan H, Marx S, Moss P and Hammond A (2012) Evidence of ENSO mega-drought triggered collapse of prehistory Aboriginal society in northwest Australia. Geophysical Research Letters 39(22), L22702. Doi: 10.1029/2012GL053916.

McVicar TR, Roderick ML, Donohue RJ, Li LT, Van Niel TG, Thomas A, Grieser J, Jhajharia D, Himri Y, Mahowald NM, Mescherskaya AV, Kruger AC, Rehman S and Dinpashoh Y (2012) Global review and synthesis of trends in observed terrestrial near-surface wind speeds: Implications for evaporation. Journal of Hydrology 416, 182-205. Doi: 10.1016/j.jhydrol.2011.10.024.

Morton FI (1983) Operational estimates of areal evapotranspiration and their significance to the science and practice of hydrology. Journal of Hydrology 66(1–4), 1-76. Doi: http://dx.doi.org/10.1016/0022-1694(83)90177-4.

Murakami H, Hsu P-C, Arakawa O and Li T (2014) Influence of Model Biases on Projected Future Changes in Tropical Cyclone Frequency of Occurrence*. Journal of Climate 27(5), 2159-2181. Doi: 10.1175/JCLI-D-13-00436.1.

Nott J (2011) A 6000 year tropical cyclone record from Western Australia. Quaternary Science Reviews 30(5-6), 713-722. Doi: 10.1016/j.quascirev.2010.12.004.

O'Donnell AJ, Cook ER, Palmer JG, Turney CSM, Page GFM and PF. G (2015 (submitted)) Tree-rings show recent summer-autumn precipitation in semi-arid northwest Australia is unprecedented within the last two centuries. PLoS ONE.

Ramsay HA, Leslie LM, Lamb PJ, Richman MB and Leplastrier M (2008) Interannual Variability of Tropical Cyclones in the Australian Region: Role of Large-Scale Environment. Journal of Climate 21(5), 1083-1103. Doi: 10.1175/2007JCLI1970.1.

Risbey JS, Pook MJ, McIntosh PC, Wheeler MC and Hendon HH (2009) On the Remote Drivers of Rainfall Variability in Australia. Monthly Weather Review 137(10), 3233-3253. Doi: 10.1175/2009MWR2861.1.

Roberts MJ, Vidale PL, Mizielinski MS, Demory M-E, Schiemann R, Strachan J, Hodges K, Bell R and Camp J (2015) Tropical Cyclones in the UPSCALE Ensemble of High-Resolution Global Climate Models. Journal of Climate 28(2), 574-596. Doi: 10.1175/JCLI-D-14-00131.1.

Roderick ML, Rotstayn LD, Farquhar GD and Hobbins MT (2007) On the attribution of changing pan evaporation. Geophysical Research Letters 34(17), L17403. Doi: 10.1029/2007GL031166.

Rotstayn LD, Jeffrey SJ, Collier MA, Dravitzki SM, Hirst AC, Syktus JI and Wong KK (2012) Aerosol- and greenhouse gas-induced changes in summer rainfall and circulation in the Australasian region: a study using single-forcing climate simulations. Atmospheric Chemistry and Physics 12(14), 6377-6404. Doi: 10.5194/acp-12-6377-2012.

Rouillard A, Skrzypek G, Dogramaci S, Turney C and Grierson PF (2014) Impacts of a changing climate on a century of extreme flood regime of northwest Australia. Hydrol. Earth Syst. Sci. Discuss. 11(10), 11905-11943. Doi: 10.5194/hessd-11-11905-2014.

Saji NH, Goswami BN, Vinayachandran PN and Yamagata T (1999) A dipole mode in the tropical Indian Ocean. Nature 401(6751), 360-363.

Schepen A, Wang QJ and Robertson D (2011) Evidence for Using Lagged Climate Indices to Forecast Australian Seasonal Rainfall. Journal of Climate 25(4), 1230-1246. Doi: 10.1175/JCLI-D-11-00156.1.

Scoccimarro E, Gualdi S, Villarini G, Vecchi GA, Zhao M, Walsh K and Navarra A (2014) Intense Precipitation Events Associated with Landfalling Tropical Cyclones in Response to a Warmer Climate and Increased CO2. Journal of Climate 27(12), 4642-4654. Doi: 10.1175/JCLI-D-14-00065.1.

Smith IN, Wilson L and Suppiah R (2008) Characteristics of the Northern Australian Rainy Season. Journal of Climate 21(17), 4298-4311. Doi: 10.1175/2008JCLI2109.1.

Spooner MI, De Deckker P, Barrows TT and Fifield LK (2011) The behaviour of the Leeuwin Current offshore NW Australia during the last five glacial-interglacial cycles. Global and Planetary Change 75(3-4), 119-132. Doi: 10.1016/j.gloplacha.2010.10.015.

Suppiah R (1992) The Australian summer monsoon: a review. Progress in Physical Geography 16(3), 283-318. Doi: 10.1177/030913339201600302.

Tapp RG and Barrell SL (1984) The north-west Australian cloud band: Climatology, characteristics and factors associated with development. Journal of Climatology 4(4), 411-424. Doi: 10.1002/joc.3370040406.

Taschetto AS and England MH (2009) An analysis of late twentieth century trends in Australian rainfall. International Journal of Climatology 29(6), 791-807. Doi: 10.1002/joc.1736.

Telcik N and Pattiaratchi C (2014) Influence of Northwest Cloudbands on Southwest Australian Rainfall. Journal of Climatology 2014, 11. Doi: 10.1155/2014/671394.

The Long Paddock (2011) Programmer notes. Viewed 15 April 2013, <http://www.longpaddock.qld.gov.au/silo/programmer_notes.html>.

Tory KJ, Chand SS, McBride JL, Ye H and Dare RA (2013) Projected Changes in Late-Twenty-First-Century Tropical Cyclone Frequency in 13 Coupled Climate Models from Phase 5 of the Coupled Model Intercomparison Project. Journal of Climate 26(24), 9946-9959. Doi: 10.1175/JCLI-D-13-00010.1.

Westra S, Evans JP, Mehrotra R and Sharma A (2013) A conditional disaggregation algorithm for generating fine time-scale rainfall data in a warmer climate. Journal of Hydrology 479(0), 86-99. Doi: http://dx.doi.org/10.1016/j.jhydrol.2012.11.033.

Wheeler MC and Hendon HH (2004) An All-Season Real-Time Multivariate MJO Index: Development of an Index for Monitoring and Prediction. Monthly Weather Review 132(8), 1917-1932. Doi: 10.1175/1520-0493(2004)132<1917:AARMMI>2.0.CO;2.

Wheeler MC, Hendon HH, Cleland S, Meinke H and Donald A (2009) Impacts of the Madden-Julian Oscillation on Australian Rainfall and Circulation. Journal of Climate 22(6), 1482-1498. Doi: 10.1175/2008jcli2595.1.

Wheeler MC and McBride JL (2005) Australian-Indonesian monsoon. In: Lau WKM and Waliser DE (eds), Intraseasonal Variability in the Atmosphere-Ocean Climate System Springer.

Wright WJ (1997) Tropical-extratropical cloudbands and Australian rainfall: I. Climatology. International Journal of Climatology 17, 807-829.

Zhang CD (2005) Madden-Julian oscillation. Reviews of Geophysics 43(2). Doi: 10.1029/2004rg000158.

3 Climate thresholds for hydrological response

This Assessment is evaluating possible impacts of climatic conditions in 2030 and 2050 on the area's hydrology, water yields and dependent ecosystems. It is therefore important to know which climate variables most impact on runoff, recharge and river pool permanence so that an estimate can be made of their change between the historical climate period and these future dates. A key component governing the hydrology of the Pilbara is the minimum rainfall required to initiate runoff which we refer to as a rainfall-runoff threshold. There are also rainfall thresholds to generate recharge to aquifers, flow thresholds for streams to recharge riparian and alluvial aquifers, and thresholds of flow to maintain ecosystem health. A comprehensive discussion of each of these thresholds is beyond the scope of this document, being primarily on climate processes. In this section we present some initial findings illustrating the issues of hydrological thresholds in the Assessment area, and further results and discussion will be presented in the regional reports at a later date.

This chapter illustrates an approach which is adopted by the project for an integrated analysis of climate characteristics and hydrological catchment responses, groundwater level fluctuation and river pools dynamics. This approach aims to define specific climate parameters and their thresholds, which are particularly significant for water resources assessment, for instance, a minimum rainfall triggering runoff from a catchment or groundwater recharge. In what follows the preliminary results of such analysis are presented for selected locations on the lower reaches of the De Grey River, upper reaches of the Fortescue River and in Weeli Wolli Creek, in the upper Fortescue catchment (Figure 3.1).

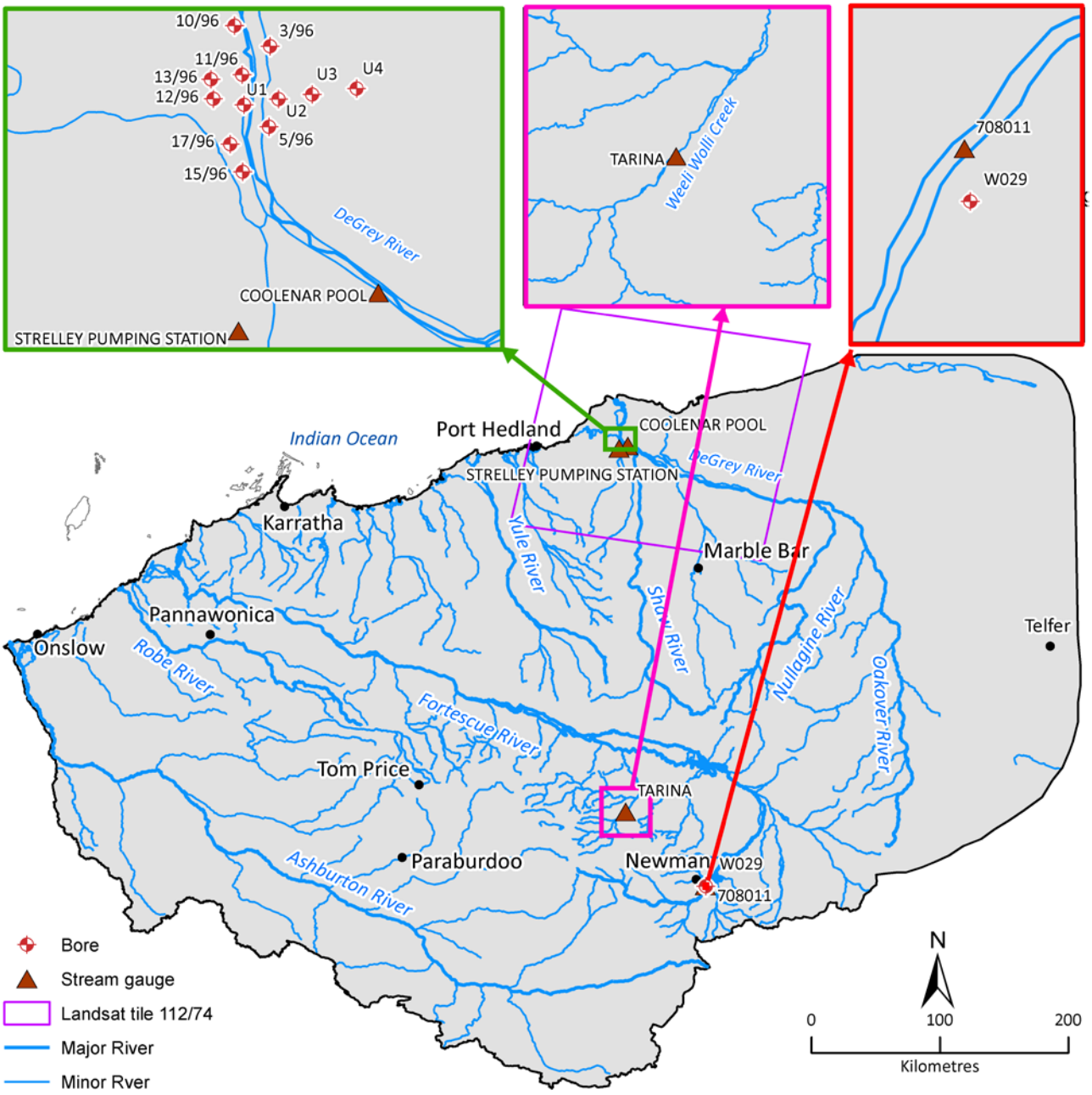

Figure 3.1 Map showing the location of gauging stations, groundwater bores and Landsat tile

3.1 Runoff thresholds

The changes in rainfall and other weather patterns due to future climate change have potential impact on runoff and other thresholds in catchments. The pre-threshold behaviour for a natural process (e.g. surface flow) usually is much different to the post threshold behaviour. For example until the threshold is reached a given large rainfall may not produce any runoff, while a relatively small rainfall can generate large runoff once the threshold is reached. Effects of climate change that are limited to below threshold behaviour may not be as severe as those changes that result in exceeding the threshold. Therefore the effect of climate change in relation to hydrologic threshold behaviour is essential to understand the hydrologic processes in the catchment. Thus there is a need to keep the threshold phenomenon in perspective while investigating climate change in an area.

Understanding the rainfall-runoff threshold helps us identify streamflow initiation processes and their consequential impact on stream water dependent ecosystems, including recharge of alluvial aquifers that support groundwater dependent ecosystems. Rainfall-runoff thresholds have never been thoroughly

studied in the Pilbara. The amount and intensity of rain required to initiate runoff depends on antecedent soil moisture conditions, the structure and texture of the soil, infiltration capacities, on vegetation, topography and surface properties such as micro-depressions that may impede overland flow reaching the stream. These thresholds, particularly in semi-arid areas such as the Pilbara, are strongly influenced by the fact that the potential evaporation over the region is much greater than rainfall over almost any time period other than around major rainfall events. The mean daily potential evaporation, as determined using Morton's wet environment algorithm (Figure 2.23) reaches a maximum of just over 7 mm/day in the summer months, substantially greater than the mean daily value of rainfall of less than 2 mm/day in January and just over 2 mm/day in February, the wettest months. Thus over almost all time periods a substantial soil moisture deficit accumulates and creates ample storage for water infiltration during rainfall events.

Averaged over the Assessment area, rainfall in excess of potential evaporation occurs for fewer than 20 days per year. However, as well as temporal variability, rainfall is highly variable spatially. The infiltration capacity of the soil is a significant determinant of runoff generation. Thus the texture and surface condition of the soil, land use and vegetation can all influence runoff generation thresholds, and consequently they may well be spatially and temporally variable.

As examples, daily rainfall and runoff sequences for Weeli Wolli Creek catchment at Tarina (station 708014), in the Upper Fortescue Basin, and De Grey River catchment at Coolenar Pool (710003) in the lower De Grey Basin are shown in to illustrate that frequent rainfall events may not produce streamflow.

(a)

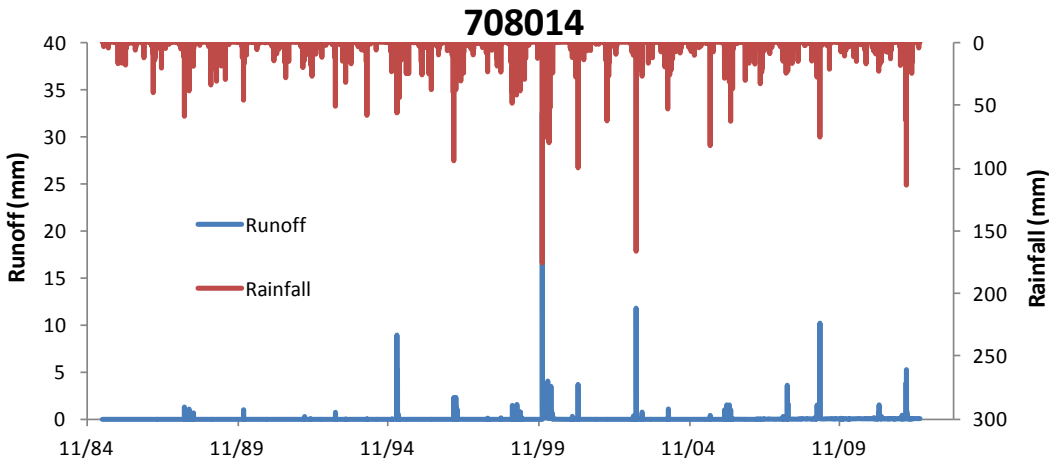

(b)

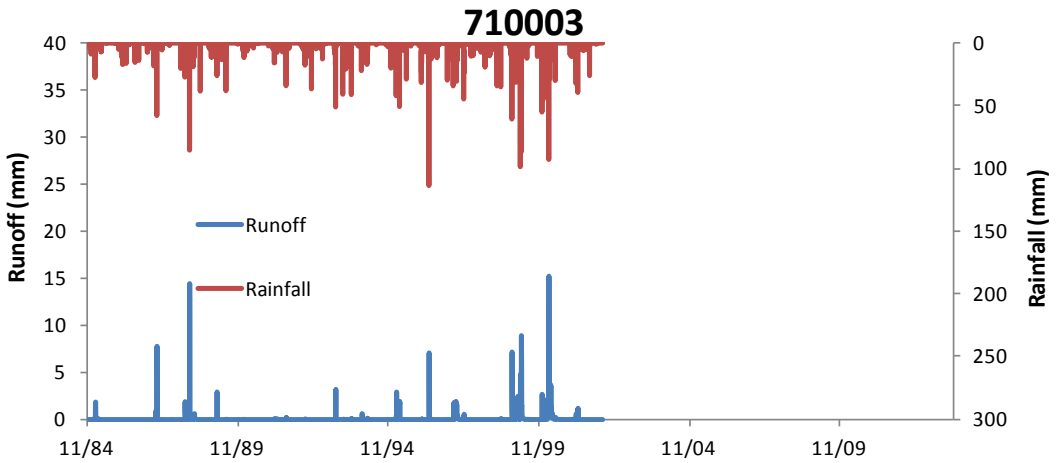

Figure 3.2 Daily rainfall and runoff for (a) Station 708014 (Tarina) and (b) 710003 (Coolenar Pool), and (c) and (d) the same stations showing only the 2000 water year

(c)

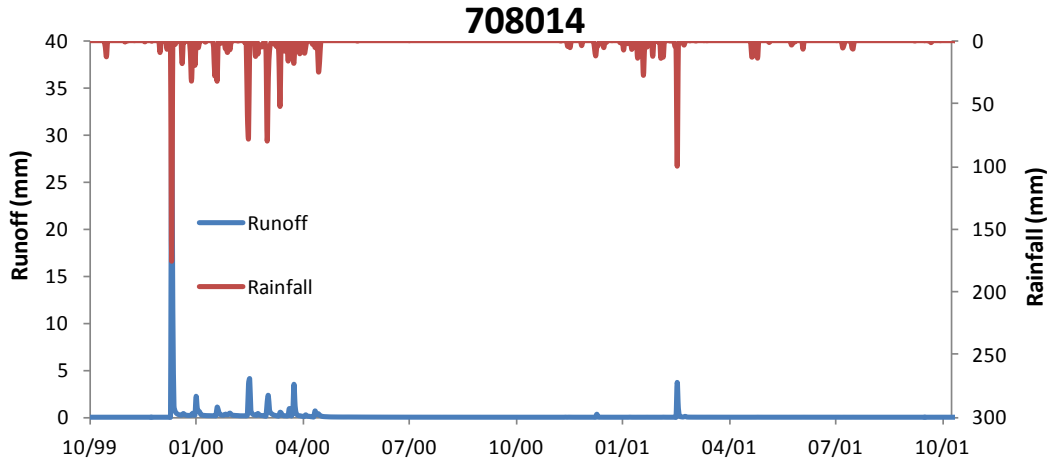

(d)

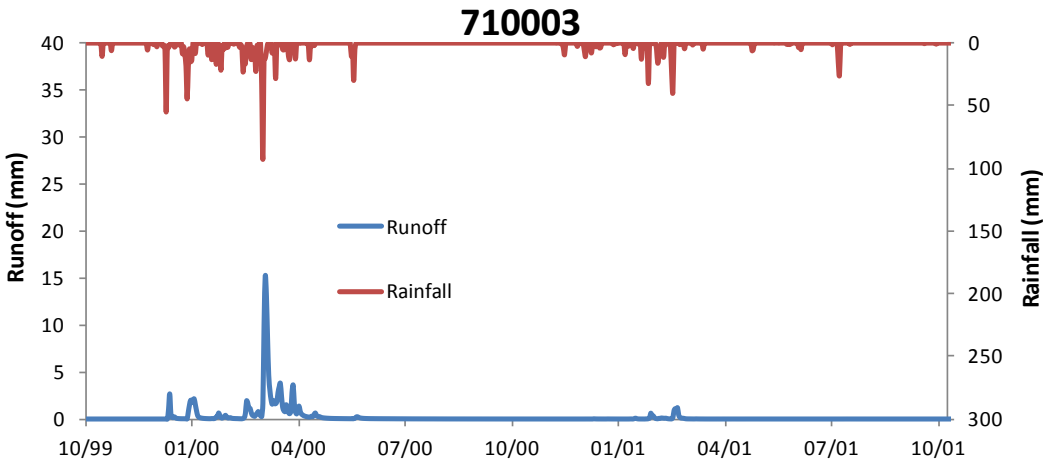

Figure 3.2 Daily rainfall and runoff for (a) Station 708014 (Tarina) and (b) 710003 (Coolenar Pool), and (c) and (d) the same stations showing only the 2000 water year (continued)

The threshold concept is illustrated in Figure 3.3 for the two stations, with annual, monthly and event-based runoff shown against rainfall for the same periods. For both sites, despite the large difference in catchment area and location, on an annual basis runoff generation thresholds are about 200 mm, and monthly thresholds are about 100 mm. No threshold appears in the event plot (Figure 3.3 c) because these only show data when there is flow. However, an event-based threshold can be determined by examining the rainfall sequence immediately prior to flow initiation. This analysis is summarised in Table 3.1. For this analysis we have chosen 0.002 mm as a minimum definition of an event at 710003 and 0.066 mm at 708014, approximately in proportion to their catchment areas and give a similar daily flow volume of approximately 3 GL/day, to remove insignificant and unreliable measurements.

Table 3.1 Mean annual statistics for stations 708014 (Weeli Wolli Creek at Tarina) and 710003 (De Grey River at Coolenar Pool)

DESCRIPTOR	708014 (TARINA, UPPER FORTESCUE)	710003 (COOLENAR POOL, DE GREY)
Catchment area (km^2)	1,512	50,007
Rainfall (mm)	393	359
Runoff (mm)	12	23
Mean annual flow days	88	82
Threshold (GL/day)(mm)	0.10GL, 0.066mm	0.10GL, 0.002mm
Number events (>0.2mm) per year	3.3	2.2
Mean rainfall for event (mm)	48.6	90.3
Mean rainfall in 2 days prior to event (mm)	30.2	20.0
Mean rainfall in 2 days prior to event plus 1st flow day (mm)	41.9	26.4
Mean runoff for event (mm)	2.98	10.80
Mean runoff coefficient per event	0.06	0.12
Mean rainfall threshold for runoff commencement (mm)	36	23
Number of days rain exceeds potential evaporation per year	21	13

While there are marked differences in rainfalls in flow events, and in the size of flow events, the rainfall required to stimulate flow is similar in the two catchments. Total rainfall each of two to five (*n*) days prior to the onset of flow was also calculated. For each of these periods, two statistics are given, the rainfall in the *n* days prior to flow onset and the rainfall in the *n* days prior to flow beginning plus the first day of flow. These values for 708014 and 710003 are given in Table 3.2. For each catchment, the average of these amounts gives an estimate of the threshold rainfall required to generate runoff. For this analysis the average rainfall across the catchment has been used.

Table 3.2 Total rainfall for 2 to 5 days prior to rainfall events

NUMBER OF DAYS, *N*, IN PERIOD BEFORE ONSET OF FLOW	TOTAL RAINFALL IN THE PERIOD BEFORE THE ONSET OF RUNOFF (mm)		TOTAL RAINFALL IN THE PERIOD BEFORE THE ONSET OF RUNOFF PLUS THE FIRST DAY (mm)		ESTIMATE OF RAINFALL THRESHOLD TO INITIATE RUNOFF (mm) (AVERAGE OF THE TWO COLUMNS TO THE LEFT)	
	GAUGING STATIONS		GAUGING STATIONS		GAUGING STATIONS	
	708014	710003	708014	708014	708014	708014
2	30	20	42	42	36	23
3	39	30	51	51	45	33
4	46	39	58	58	52	42
5	49	45	60	60	54	48

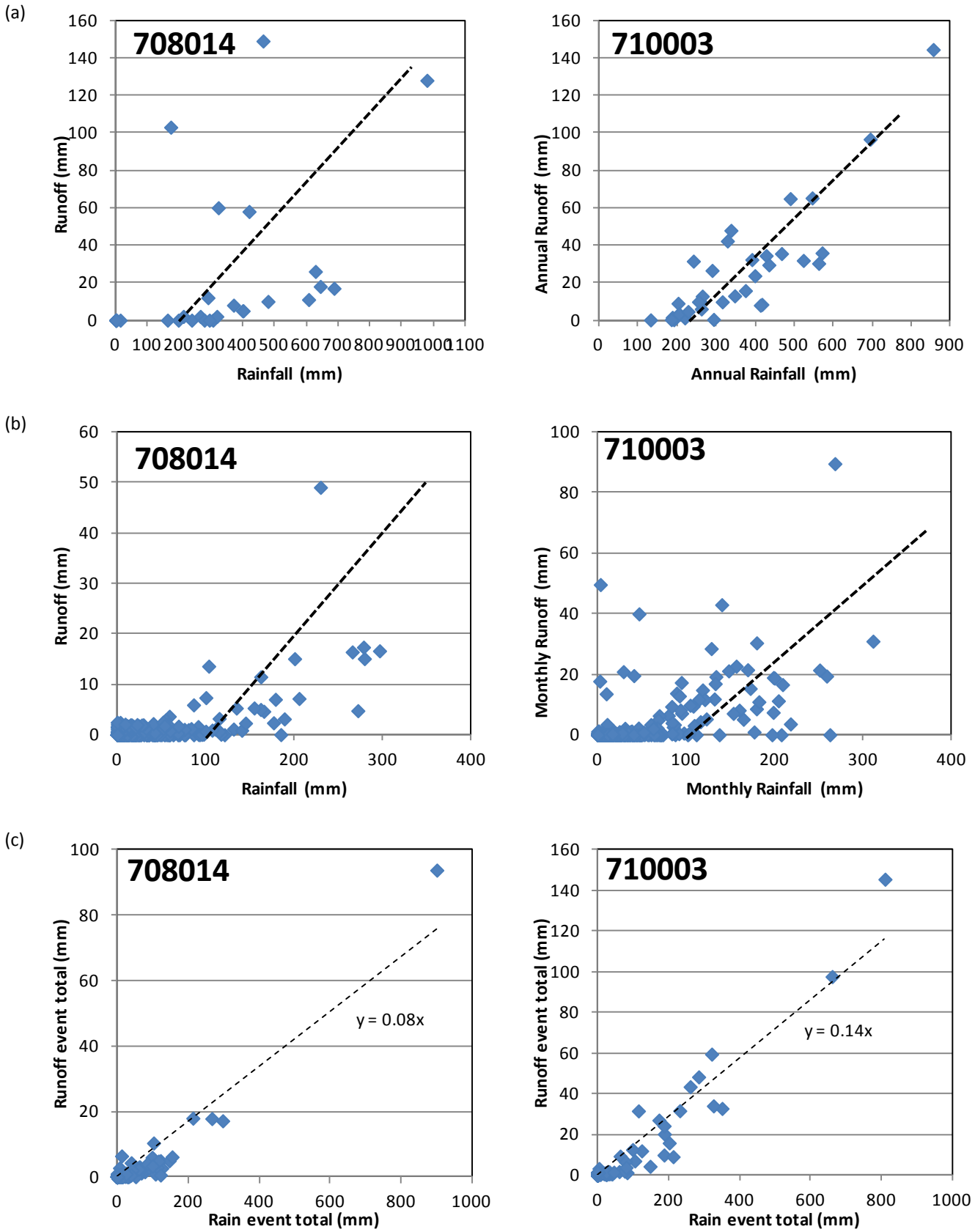

Figure 3.3 Runoff plotted against rainfall for (a) annual, (b) monthly and (c) events for the two stations indicated. The vertical axes are not to the same scale because this would conceal the relative rates of response

The number of flow days and runoff for the De Grey station (710003) (Figure 3.4) gives a sense of the rainfall threshold being about 100 mm in a year. Of course 100 mm would be a very dry year, but this site is near the outlet of the catchment, has a shallow regolith and a relatively high runoff coefficient (Table 3.1). Interestingly the number of flow days appears linearly related to annual rainfall, but this should be assessed cautiously as the minimum flow rate used to specify an event has a significant influence on the number of assessed flow days. Figure 3.5 shows the relationship between the number of flow days per year and the annual total runoff; not surprisingly, there is a close relationship.

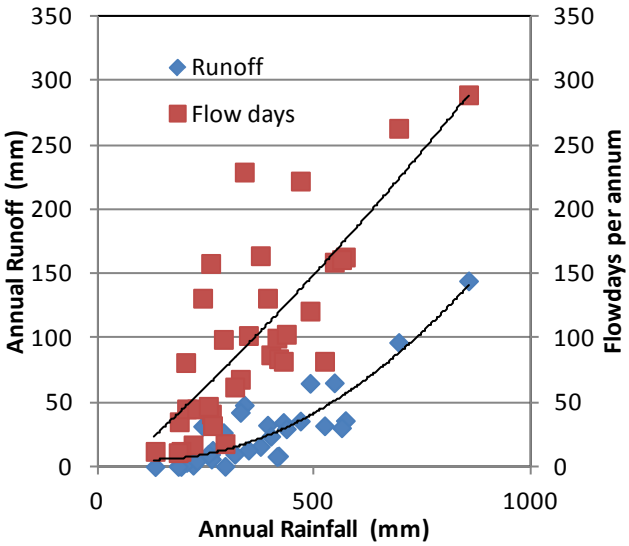

Figure 3.4 Runoff and number of flow days plotted against annual rainfall by water year at station 710003

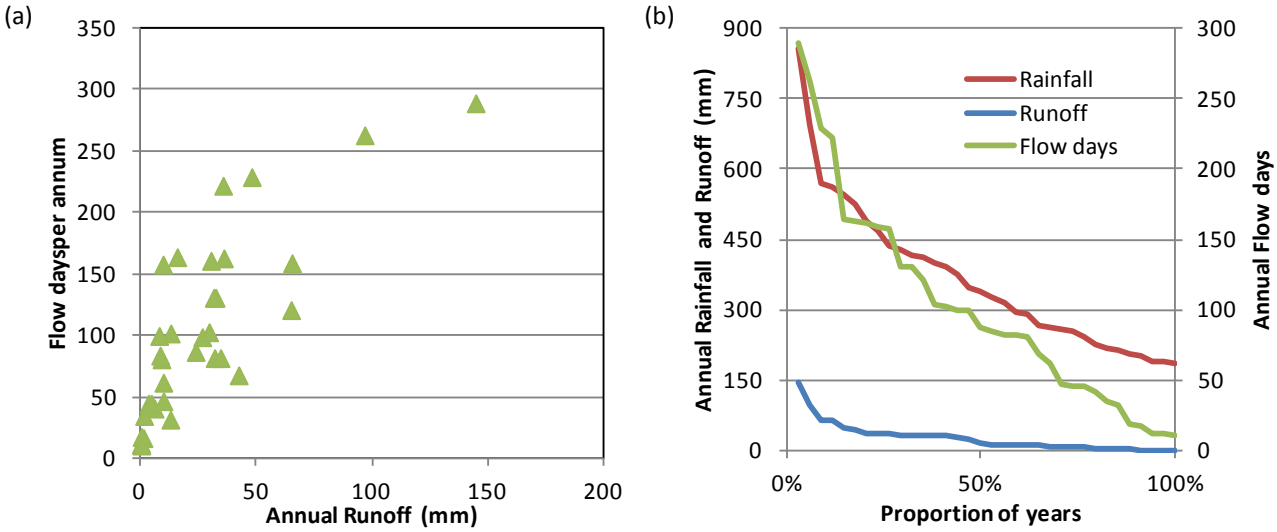

Figure 3.5 (a) Number of flow days per year plotted against annual total runoff, and (b) frequency distributions of annual flow days, total runoff and total rainfall per water year at 710003

Discussion of hydrological thresholds needs some context. In this section we have considered the relationship between rainfall and runoff generation, and the minimum rainfall needed to initiate streamflow. Obviously this depends on the condition of the catchment, both the soil surface condition and the antecedent soil moisture, which in turn depends on rainfall over the preceding days. We have attempted to account for this by including two to five days prior to flow commencing as a range of relevant rainfalls to the resultant streamflow. The rationale for these days is made on the basis that days of more rain than potential evaporation are few, and we expect soil within the surface layer to dry out relatively quickly once rain ceases. The drying out may take two to five days depending on the weather pattern during a given event.

In the next section, the relevance of rainfall amount to recharge and groundwater response is discussed. Conceptually this is similar to the threshold required to initiate runoff, but is dependent on surface conditions to a different extent, and has a longer timeframe for response, due to the slower infiltration process than the surface runoff response to rainfall. Finally thresholds relating streamflow levels to riverine pools and their significant ecological assets are assessed, and in particular the dependence of recharge and discharge connections between the stream and riparian aquifers.

3.2 Groundwater recharge thresholds

Recharge is the addition of water from an overlying unsaturated zone or surface water body to an aquifer (Scanlon et al. 2006). The replenishment of groundwater occurs through diffuse groundwater recharge or localised recharge. Diffuse recharge occurs from direct rainfall infiltration over large areas. Localised recharge occurs from surface topographic depressions such as streams and rivers, lakes, and playas or from artificial discharges such as agricultural drains, canals or industrial pumping. While often separated and active in different areas, there are some hydrological settings where both recharge processes are important. Recharge depends on the interaction between climate, geology, morphology, soil conditions and vegetation (de Vries and Simmers, 2002). One of the major challenges is uncertainty about recharge which is a major impediment to reliably quantifying groundwater resources and its allocation for use.

There are different aquifer systems or hydrological settings in the Assessment area. Fractured and sedimentary rock aquifers are mainly recharged by diffuse recharge and alluvial aquifers and valley-fill aquifers (which are also often topographic lows) are mainly recharged by localised recharge, mainly via leakage from streams during streamflow.

Factors affecting diffuse recharge include climate, rainfall intensity, duration and amount, soil properties and antecedent moisture conditions, topography, vegetation, and the aquifer extent and properties. The control parameters for localised recharge include climate, rainfall, flow rates, flow duration, aquifer extent and its hydrological setting, aquifer properties, and prior aquifer storage levels. The amount of recharge that occurs from a single rainfall or flow event therefore depends upon many factors. One conceptual model for the alluvial aquifers in the Pilbara is that the groundwater recharge is dominated by localised recharge via leakage through the river bed during times of flow (70-90%), with lesser contributions from broad-scale surface flooding (5-20%) and diffuse recharge from direct rainfall (5-20%) on alluvial soils (SKM, 2009). Careful measurement of groundwater levels adjacent to rivers during periods where cyclonic rainfall has caused streamflow through an area that has received no rainfall confirms streamflow as a major source of recharge. The percentages of each flow component are a summary of the results of groundwater models with streamflow, rainfall and flooding, against observed groundwater levels.

One of the objectives of this Assessment is to estimate thresholds, if any, and their spatial variation for diffuse and localised recharge rates for different aquifers in the Assessment area. This analysis is at a very early stage. To explore possible thresholds that exist in groundwater recharge and discharge processes for the alluvial aquifers in the Pilbara, we will focus where the bore and stream data are concentrated. Most bore data is centred on the alluvial aquifers which are recharged by river flow and have been used as a water source. Two examples are reported here for the alluvial aquifers at two locations where rainfall, streamflow data and groundwater monitoring data of sufficient length are available from nearby rainfall, river gauging station and groundwater bores, respectively. These data are used to estimate hydrological thresholds for localised recharge to the alluvial aquifers.

The first example is from the De Grey River gauge 710003 (Coolenar Pool) where a number of groundwater bores are located near the gauging station. The climate information is used from the Strelley Pumping Station (M004093) near the main area of groundwater abstraction and the streamflow gauge (Figure 3.1). Groundwater monitoring data from a number of bores was used to analyse thresholds for the localised recharge to the alluvial aquifer. Since groundwater levels from these bores are highly correlated (Figure 3.6) the threshold analysis is reported for one bore only (U2) from this location.

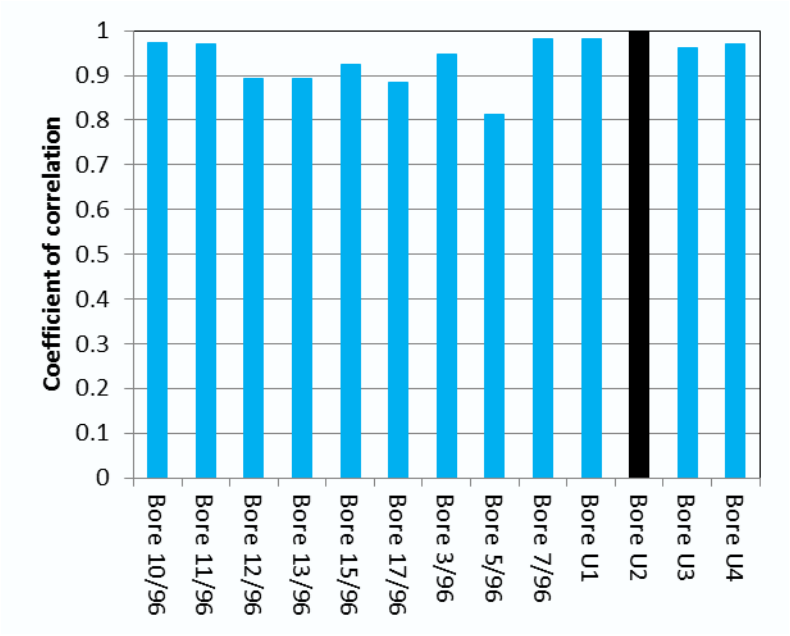

Figure 3.6 Correlation between U2 and other nearby groundwater monitoring bores groundwater level data

The distribution of annual streamflow measured at Coolenar Pool gauging station from 1975 to the present near the groundwater monitoring bore U2 is shown in Figure 3.7. There are three years from 1980 to 1982 where no flow records are available, and in 1986 there was no measured flow.

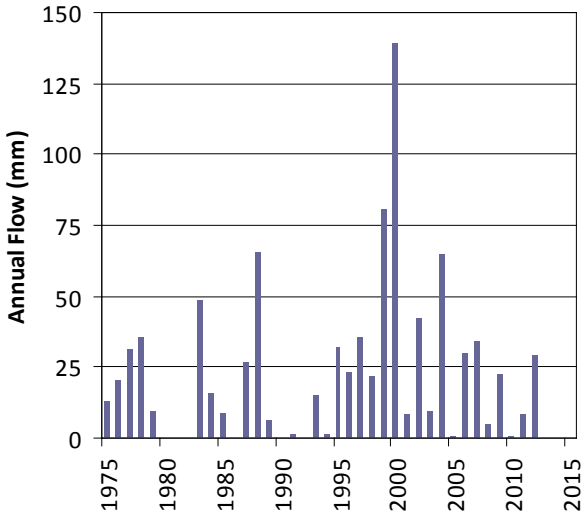

Figure 3.7 Annual flow expressed as runoff (mm) at gauge 710003 De Grey River at Coolenar Pool

Figure 3.8 shows the record of groundwater levels for all water years where there were six or more measurements taken and measured local rainfall against gauged streamflows. There are 11 years omitted from the bore hydrograph because they contain insufficient water level observations to be used, and there were no water levels recorded in water years 1999 to 2001. It is unfortunate that the years with the most groundwater data (29 readings in 1980 and 24 readings in 1981) do not have any streamflow records (b). This figure is somewhat misleading as rainfall across the entire catchment contributes to streamflow, and a rainfall event that misses a rain gauge may induce flow in another part of the catchment. The derived linear relationship between rainfall and flow therefore is not very strong, but is consistent with the concept that a minimum threshold amount of rain must fall before flow is generated. In this case it is approximately 116 mm. The straight line of best fit can be re-expressed as FLOW = 5.6 x (RAIN – 116).

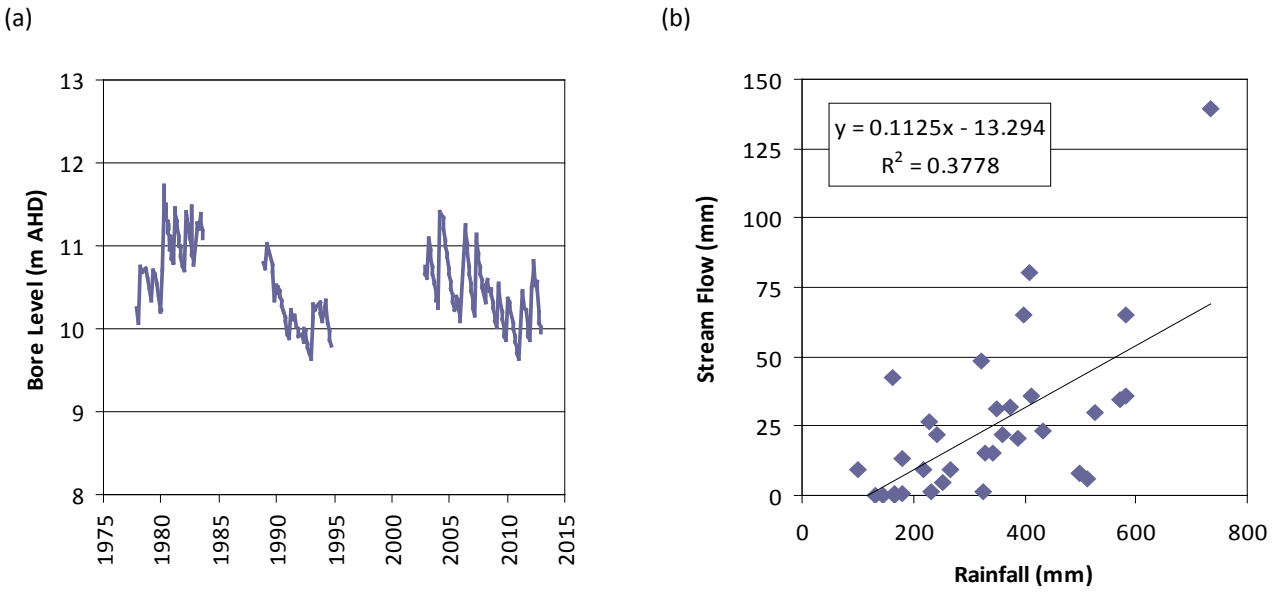

Figure 3.8 (a) Observed groundwater levels at bore U2 and (b) annual stream flow measured at Coolenar Pool regressed against local rainfall from Strelley Pumping Station

Figure 3.9 shows the relationship between the total streamflow (expressed as mm of runoff) and rise in groundwater levels in bore U2. The bore rise was estimated as the maximum recorded level minus the minimum level in each water year. There is a reasonable relationship between the two variables, with the slope indicating that each additional 1 mm of runoff results in a groundwater rise of 10.8 mm, and 433 mm is the mean minimum annual variation. Relating this value back to Figure 3.8b, this shows a minimum rainfall of 116 mm is required before streamflow is initiated, which would correspond to a fillable porosity of 27% if it is assumed that all rainfall infiltrates and none evaporates. Fillable, or drainable, porosity is the percentage of the bulk volume that can be filled or drained under the forces of gravity.

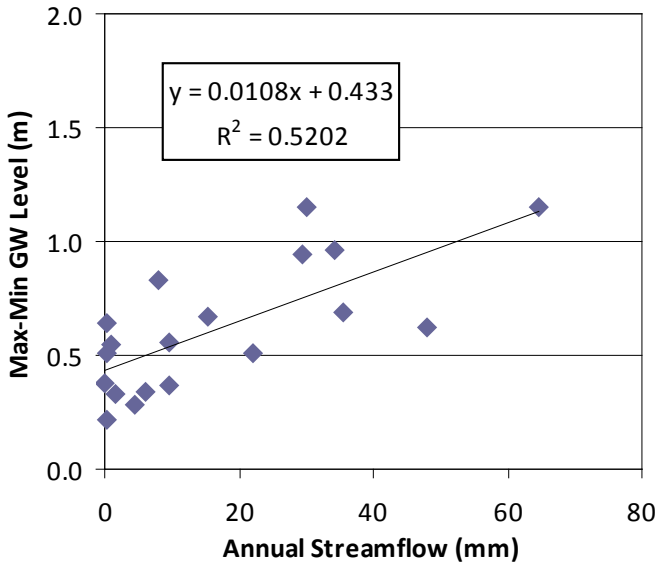

Figure 3.9 Rise in groundwater levels at bore U2 (m) plotted against annual stream flow (mm) for matching water years

Figure 3.10 shows rises in groundwater levels against the number of days of flow per year. The strength of linear relationship is moderate (R^2 = 0.4), with the slope of the regression implying that each day of flow results in a groundwater rise of 2 mm. The intercept is smaller than in Figure 3.9 and can be interpreted in two ways. Assuming it relates to infiltrated rainfall it implies a porosity of 39% when compared to the

116 mm threshold from Figure 3.8b, or it could be 80 mm of net recharge if associated with the 27% porosity estimated previously.

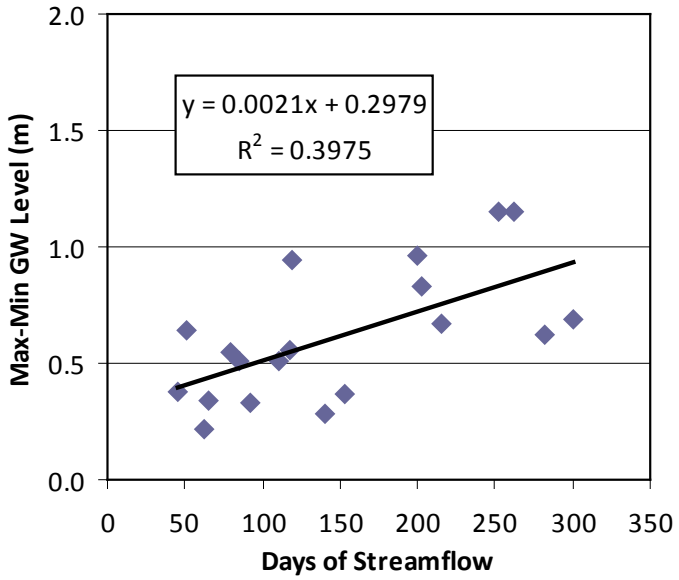

Figure 3.10 Rise in groundwater levels bore U2 (m) plotted against annual number of flow days for matching water years

The second example is from the Upper Fortescue River gauge 708011 near Newman where a relatively shallow (30 m) groundwater bore W029 is monitoring water levels in the alluvium deposits. The stream gauge has an excellent flow record from water year 1981 (01/10/1980) to present. As part of mining operations and monitoring BHP installed the bore W029 adjacent to the Fortescue River crossing on Great Northern Highway in 1998, and have monitored it between 6 and 12 times a year. The bore is located at about 200 m from the Fortescue River, and about 1 km upstream of the gauge site. Both the stream gauge and bore are several kilometres upstream of both mine pumping and the Ophthalmia Dam. Temporal variation in streamflow and flow days has a close relationship and typically follows each other (Figure3.11). The streamflow rates were largest during the water year 2000 due to tropical cyclones.

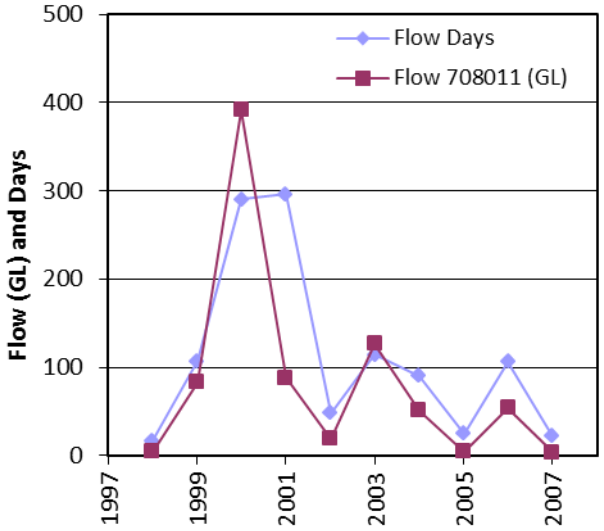

Figure 3.11 Temporal variation in streamflow and flow days at Newman stream gauging station (708011)

Temporal variation in groundwater levels at groundwater bore W029 is shown in Figure 3.12. Groundwater levels rose in response to tropical cyclones during the water year 2000 and slowly declined afterwards. There is still an annual rise and fall signal present due to streamflow and rainfall events post water year

2000. There is a noticeable decline in groundwater levels post 2004 with much less annual fluctuation which is mostly likely to lower rainfall and fewer streamflow events.

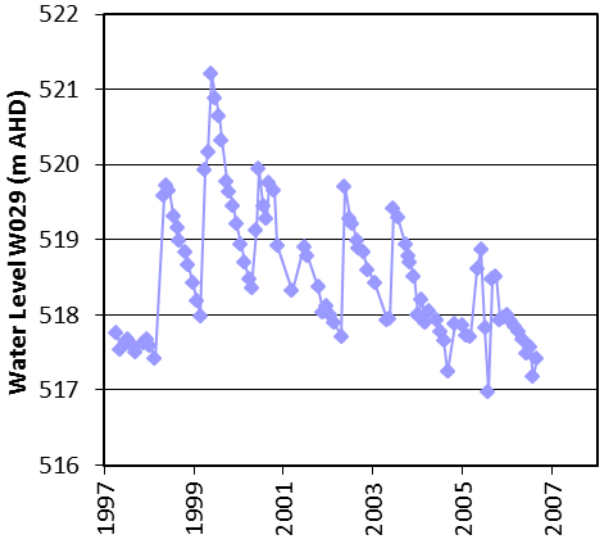

Figure 3.12 Temporal variation in groundwater levels at bore W029 near the Upper Fortescue River

There is a good relationship between streamflow and annual rise in groundwater levels at bore W029 (Figure 3.13a), with the slope indicating that each additional 1 mm of runoff results in a groundwater rise of 16.4 mm, and 1151 mm is the mean minimum annual variation. The response of groundwater level to streamflow events is greater at this location than at lower De Grey (Figure 3.9). Relatively large intercept of 1151 mm at this location compared to that at lower De Grey may be due to low storage capacity of the alluvium, greater proportion of diffuse rainfall recharge or a close linkage with the river stage.

There is also a moderate relationship between days of streamflow and annual rise in groundwater levels at bore W029 (Figure 3.13b). Every additional day of streamflow results in a rise of about 5 mm in groundwater level. The intercept is similar to annual streamflow and may have similar causes.

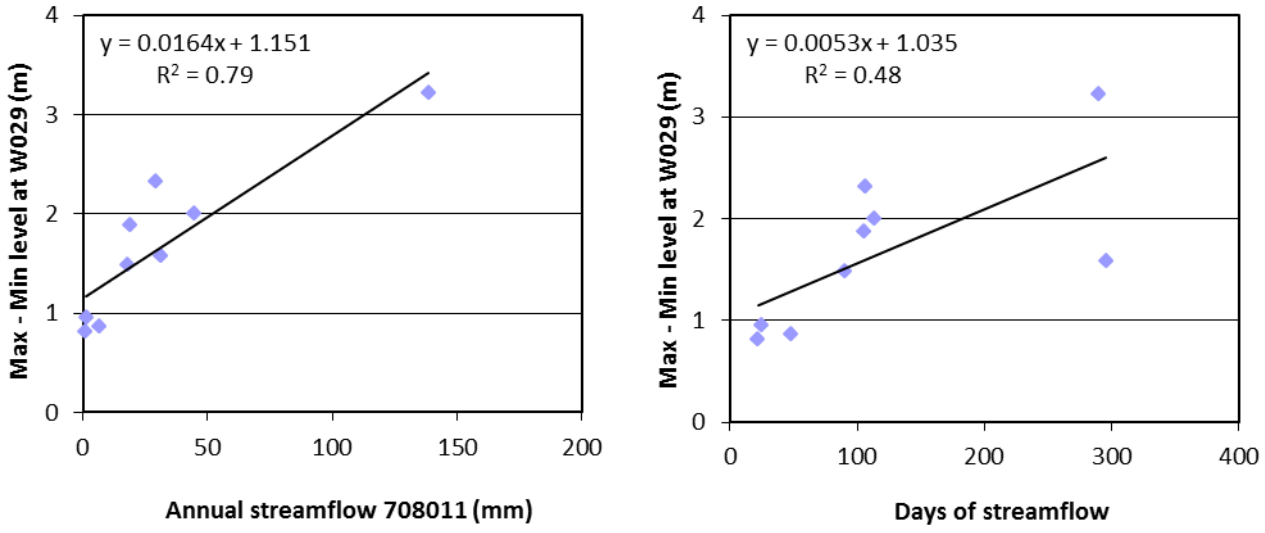

Figure 3.13 Relationship between annual groundwater level rise and (a) streamflow, and (b) flow days

Comparing the river stage to the annual rise there is a quite good relationship between the two variables (Figure 3.14), which may support the idea that the bore level is driven by river stage, with the actual recharge being the result of maintaining the appropriate head. It is a better relationship than for water

level rise against flow days. The least-squares linear fit of the stage-rise data is Rise= 0.72 x stage + 0.13, R^2=0.664, and is not a demonstrably better description than the line through the origin.

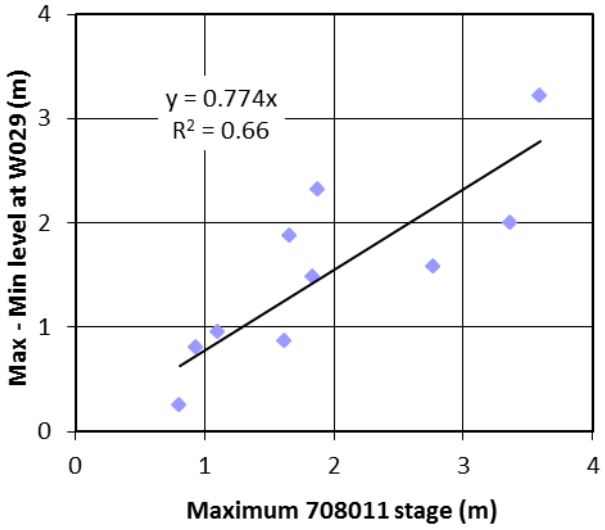

Figure 3.14 Relationship between river stage and groundwater level rise at bore W029

A comprehensive analysis of the rainfall, streamflow and groundwater data for selected and representative sections of alluvial aquifers will be conducted to estimate hydrological thresholds and this section of the report updated. Analysis of rainfall and diffuse recharge rates (using groundwater monitoring data) for other sedimentary and fractured rock aquifers will be undertaken and results about hydrological thresholds added to this section of the report.

3.3 Climate-related thresholds in ecological habitats

For the purpose of this project, groundwater dependent ecosystems (GDEs) are referred to as ecosystems associated with groundwater dependent terrestrial vegetation (GDV) and river pools. As such the ecohydrological conditions of GDEs are strongly related to both hydrological and groundwater regimes and therefore climate-related hydrological thresholds are likely to have important ecological implications.

This ecohydrological assessment is largely based on the identification of a series of metrics, derived using remote sensing techniques and the relationship between such metrics and variations in groundwater levels, streamflow as well as climatic conditions (rainfall or potential evaporation) (Close *et al*, 2012). A Landsat-based analysis was used to identify the presence of water and vegetation with frequent access to water (as well as their combination) along with the area occupied by such land classes. The relationship between the extent of river pools, vegetation and hydrological characteristics and thresholds, described above, will be used to estimate the impact of changed groundwater levels or flows under future climate scenarios on GDEs. Particular emphasis is made on 'key refugia' or areas where river pools are persistent in time.

This section illustrates some approaches which will be used to define the relationship between climate, hydrology and identified metrics responses to variation in climate and hydrology related parameters.

3.3.1 River pools

The seasonal variation in the areas of the pools is commonly dependent on pool morphology (especially their depth) and the relationship between inflow and outflow components of the water balance in the pool, including rainfall, river and groundwater inflow (as input parameters) and river and groundwater outflows, and potential evaporation (as output parameters).

For pools that are located within river channels it is likely that any river flow event will result in recovery of the water level in such pools. Hence, it is the frequency of streamflows which will define the frequency of

full water level recovery in a pool. This is illustrated by Figure 3.15, showing that despite declining groundwater levels, the water level in this pool (J96, DoW, 2012) (Figure 3.1) fully recovers during each of the considered flow/rainfall events within considered time periods (1, 2 and 3 as shown in Figure 3.15a). And this is despite the overall declining groundwater levels. As Figure 3.15b shows the maximum water level in the pool was reached when the groundwater level was at approximately 11 m and 10.2 m for 1 and 3 period respectively.

However the relative changes in the pool water level compared to changes in groundwater level is greatest during period '3', the driest period analysed (Figure 3.15b). This is either because of lower groundwater levels leading to less groundwater inflow to the pool after the period of river flow or greater losses of water from the pool to the adjacent aquifer. Groundwater levels appear to influence the dynamics of water level in this pool in the end of the dry periods, illustrated by the all three plots merging when groundwater level falls below 10 m.

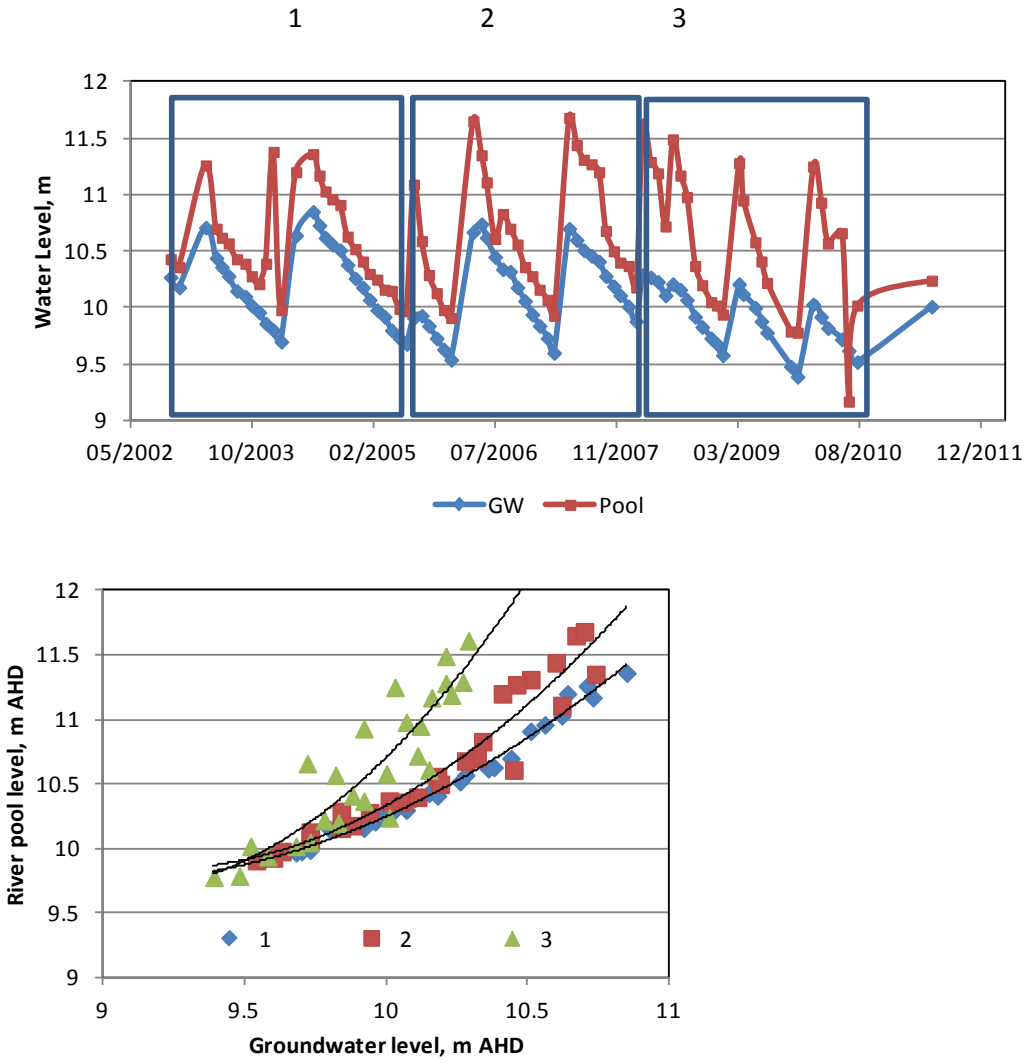

Figure 3.15 Temporal dynamics of water level in pools (J96) and groundwater (a) and relationship between them (b) for three periods (1, 2 and 3) as identified by boxes in (a) (monitoring data courtesy of the Water Corporation) (see Figure 3.1 for location)

The analysis undertaken so far illustrates that the persistency of river pools in identified river reaches (low De Grey area) is variable across the region. Figure 3.16 shows the river reaches (approximately 5 km long and inclusive of 1 km buffer along the river) where some extent of area cover with water occurs at various frequencies estimated based on 59 image-dates over the period from 2004 to 2011. Climatic and hydrological conditions in this region were adequate for river pools within some reaches of the De Grey River to be persistent during this entire period. There is also a relatively higher frequency of water occurrence in the river pools in the Coongan and Shaw Rivers.

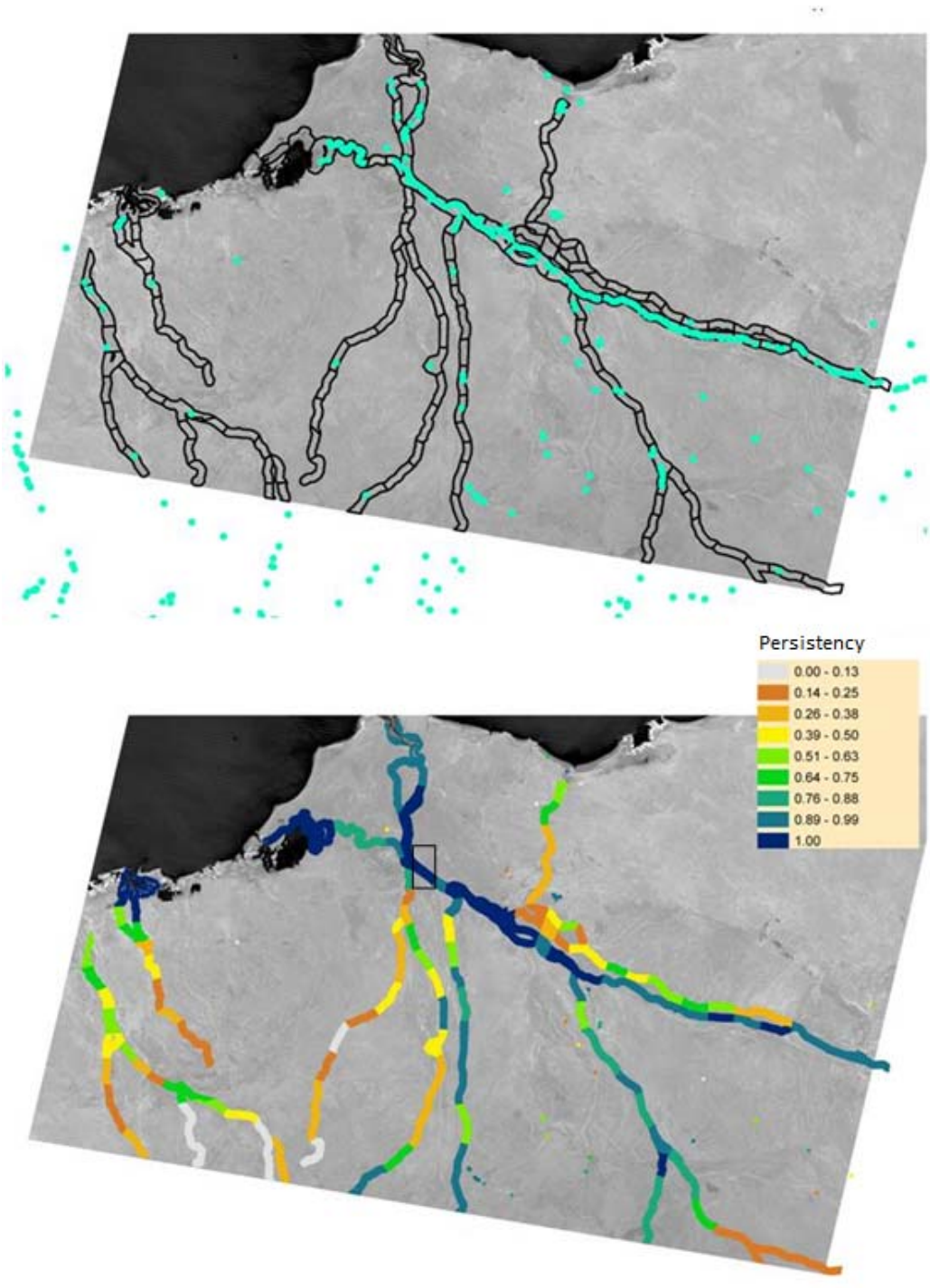

Figure 3.16 River reaches included in analysis and the known pools (a) and the results of the analysis of water persistency (as the river reaches where river pools occur under specified frequency or persistency) (see Figure 3.1 for the image location)

Analysis of data generated for each reach is illustrated in Figure 3.17 and Figure 3.18. Figure 3.17 shows a progressive reduction in the area covered by water during a dry period in 2008-09 in the proximity of Coolenar Pool, while the area covered by vegetation characterised by high greenness (NDVI>0.3) is relatively consistent. This is further illustrated by Figure 3.18, where the temporal changes in the areas covered by such vegetation and water is closely linked with streamflow/rainfall events (see for the gauging station 710003). The high values of the area covered by green vegetation are associated with the period of rain or high flow (most often both) and as such are most likely associated with annual vegetation. The lesser values of the area covered by green vegetation are relatively consistent and are likely to represent the riparian vegetation with consistent access to water (likely to be groundwater in this instance).

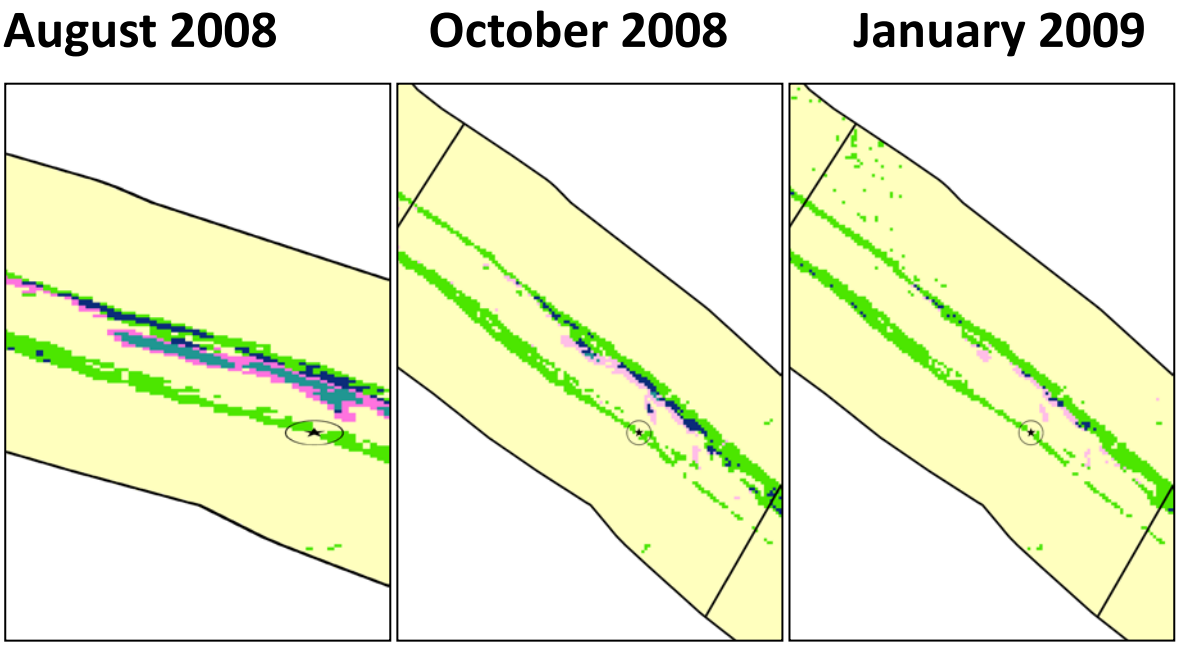

Figure 3.17 The results of classification analysis illustrated for a reach indicated by a small box in Figure 3.16 (Coolenar Pool); the extent of highly green vegetation (green), water (blue) and wet soil (pink) are shown for three dates; a location of the gauging station 710003 is shown

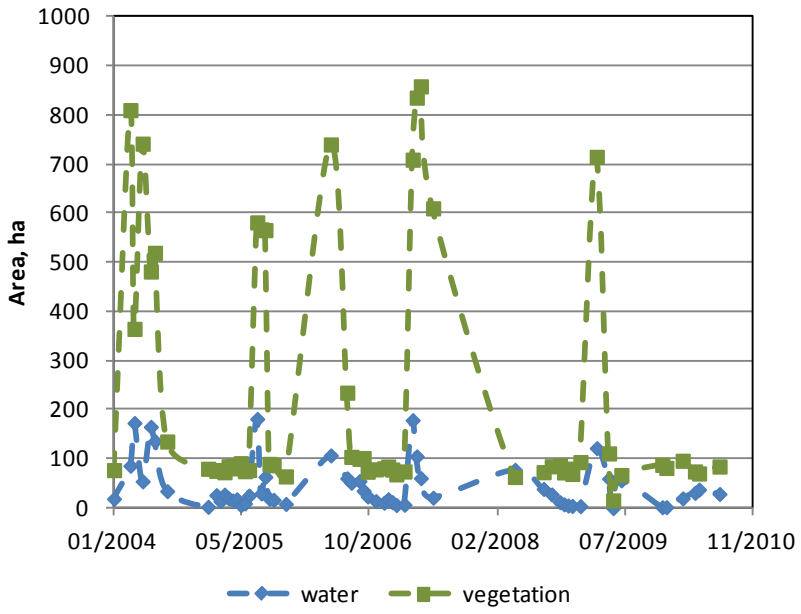

Figure 3.18 The temporal variation in the extents of highly green vegetation and water within the river reach shown in Figure 3.17

The relationship between the extent of the area covered with water or vegetation of a particularly high greenness and groundwater levels (as well as pan evaporation) could be further explored, as illustrated in Figure 3.19 and Figure 3.20 respectively. Figure 3.19 show a strong relationship between groundwater levels and the extent of water in the same river reach, indicating the presence of water at the surface is unlikely when groundwater falls below 14 mAHD. Under the climatic conditions of this period, groundwater levels ranged between 14.3 m and 17 m and the extent of green vegetation is below 100 ha for levels below about 15.5 m.

Evaporation from the water surface is one of the "discharge" components of the water balance in pools. Cumulative pan evaporation, estimated following the end of the wet season and river flow cessation for the period of 2006 to 2008, was plotted along with the area of water, estimated using RS analysis (Figure 3.20a and Figure 3.20b).

While the cumulative pan evaporation increases nearly linear over the period considered, the changes in the pool area appear to be more significant during the initial stage of the dry season despite the relatively low evaporation potential during this period. Afterward the changes in the pool area are less significant, which is likely due to the specifics of the pool geometry (i.e. it could be narrow and deep).

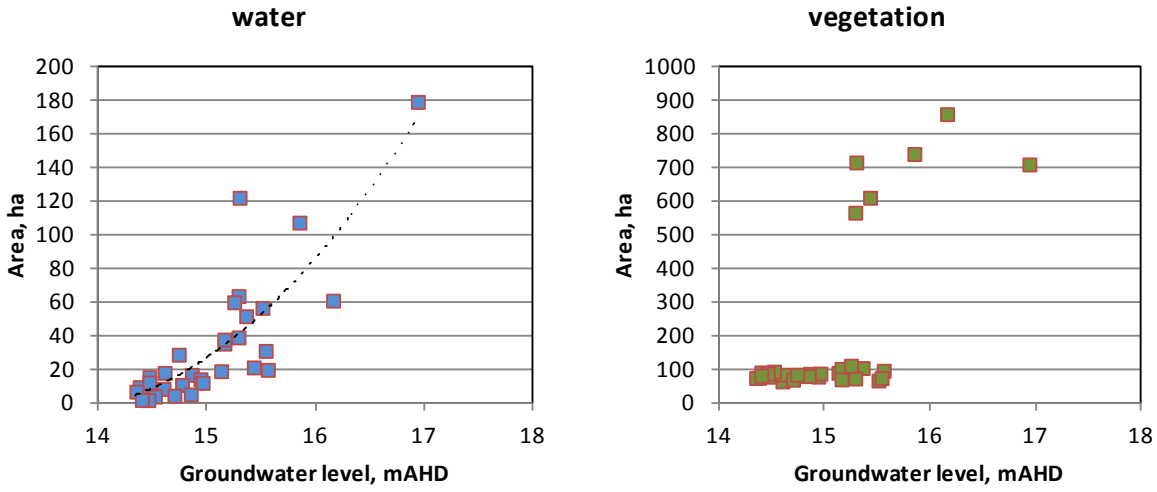

Figure 3.19 Relationship between groundwater levels in bore 07/04 (see Figure 3.1 for the bore location) and the extent of the water pool and vegetation

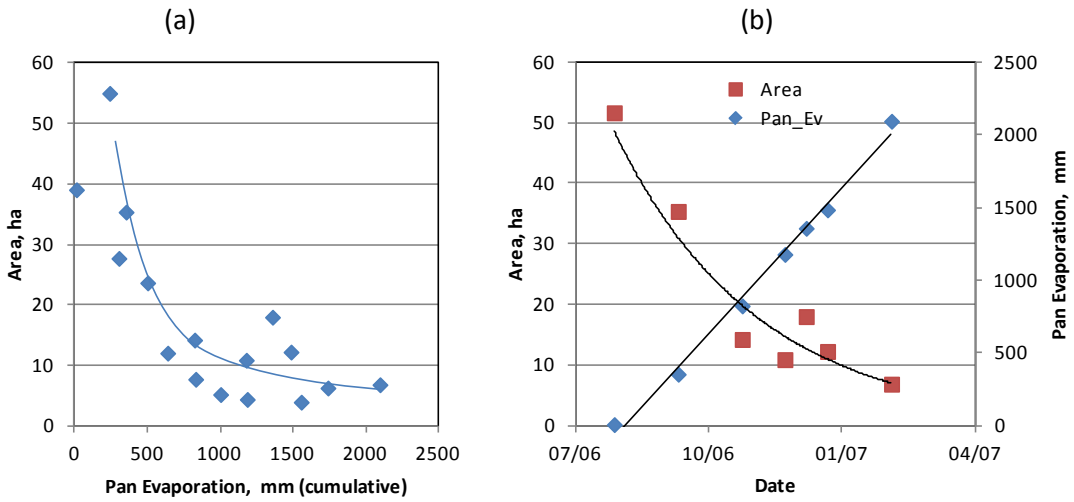

Figure 3.20 Relationship between cumulative pan evaporation and the extent of the water pool (a) and seasonal variation in pool area (b)

3.4 Summary

In summary, after preliminary analysis, there appear to be a number of climate thresholds that should be assessed under future climate scenarios as they seem to impact on the hydrology and dependent ecosystems in the Assessment area. It is anticipated that the climate parameter thresholds are also likely to be influenced by catchments characteristics, including their geological and geomorphological setting, as well as the variation in climate parameters across the region as discussed earlier.

Regional analyses are particularly useful for assessment of the future climate scenario's effects on regional water resources (both surface and groundwater) as well as GDEs in the Assessment area. There will be an iterative process in identifying these thresholds and reporting on how they may change over the course of the Assessment.

3.5 References

Close PG, Wallace J, Bayliss P, Bartolo R, Burrows D, Pusey BJ, Robinson CJ, McJannet D, Karim F, Byrne G, Marvanek S, Turnadge C, Harrington G, Petheram C, Dutra L, Dobbs R, Pettit N, Jankowski A, Wallington T, Kroon F, Schmidt D, Buttler B, Stock M, Veld A, Speldewinde P, Cook BA, Cook B, Douglas M, Setterfield S, Kennard M, Davies P, Hughes J, Cossart R, Conolly N and Townsend S (2012) Assessment of the likely impacts of development and climate change on aquatic ecological assets in Northern Australia. A report for the National Water Commission, Australia. Tropical Rivers and Coastal Knowledge (TRaCK) Commonwealth Environmental Research Facility, Charles Darwin University, Darwin. ISBN: 978-1-921576-66-9. 561pp

DoW (2012). Ecological water requirements of the Lower De Grey River. Environmental water report series, Department of Water, Report n 20.

De Vries JJ and Simmers I (2002) Groundwater recharge: an overview of processes and challenges. Hydrogeology Journal 10, 5–17.

Scanlon BR, Keese KK, Flint AL, Flint LE, Gaye CB, Simmers S and Edmunds WM (2006) Groundwater recharge in semiarid and arid regions. Hydrological Processes 20, 3335–3370.

SKM (2009). Millstream model recalibration, modelling report submitted to the Department of Water, Western Australia.

4 Hydroclimate modelling scenarios

4.1 Historical climate scenario

4.1.1 Climate data

As discussed in Chapter 2, analysis of Pilbara climate variability and trends used the SILO database Patched Point Data (PPD) and data drill gridded data, as produced by the Queensland Government Department of Science, Information Technology, Innovation and the Arts. The data drill gridded data is the basis for the scenario data described in this Chapter.

The trends in rainfall station coverage for the Pilbara are shown in Figure 4.1. This gives a visual summary of the quantity of station data that has been incorporated in the production of the data drill gridded datasets, showing the 1980s and 1990s had the best coverage with a decline since then. The reduction in station coverage in the 2000s is hypothesised to result from fewer working pastoral stations across the Pilbara in recent decades. While Chapter 2 showed the relationship between station and Assessment area average rainfall appears strong, it is likely that on a local scale there will be discontinuities in the SILO records caused by changes in the density of stations. These biases are not quantifiable, given the lack of independent data sets of sufficient record length to assess SILO against.

Figure 4.2, the corresponding maps of daily temperature records by decade across the Pilbara, clearly shows that a significantly lower density of stations record temperature than rainfall. This is not of major concern given these variables are more spatially homogeneous than rainfall. Daily temperature, incoming solar radiation and vapour pressure records are the input variables used to calculate Morton's wet areal PE (Morton, 1983) (Chiew and Leahy, 2003) using the method outlined in Li et al. (2009).

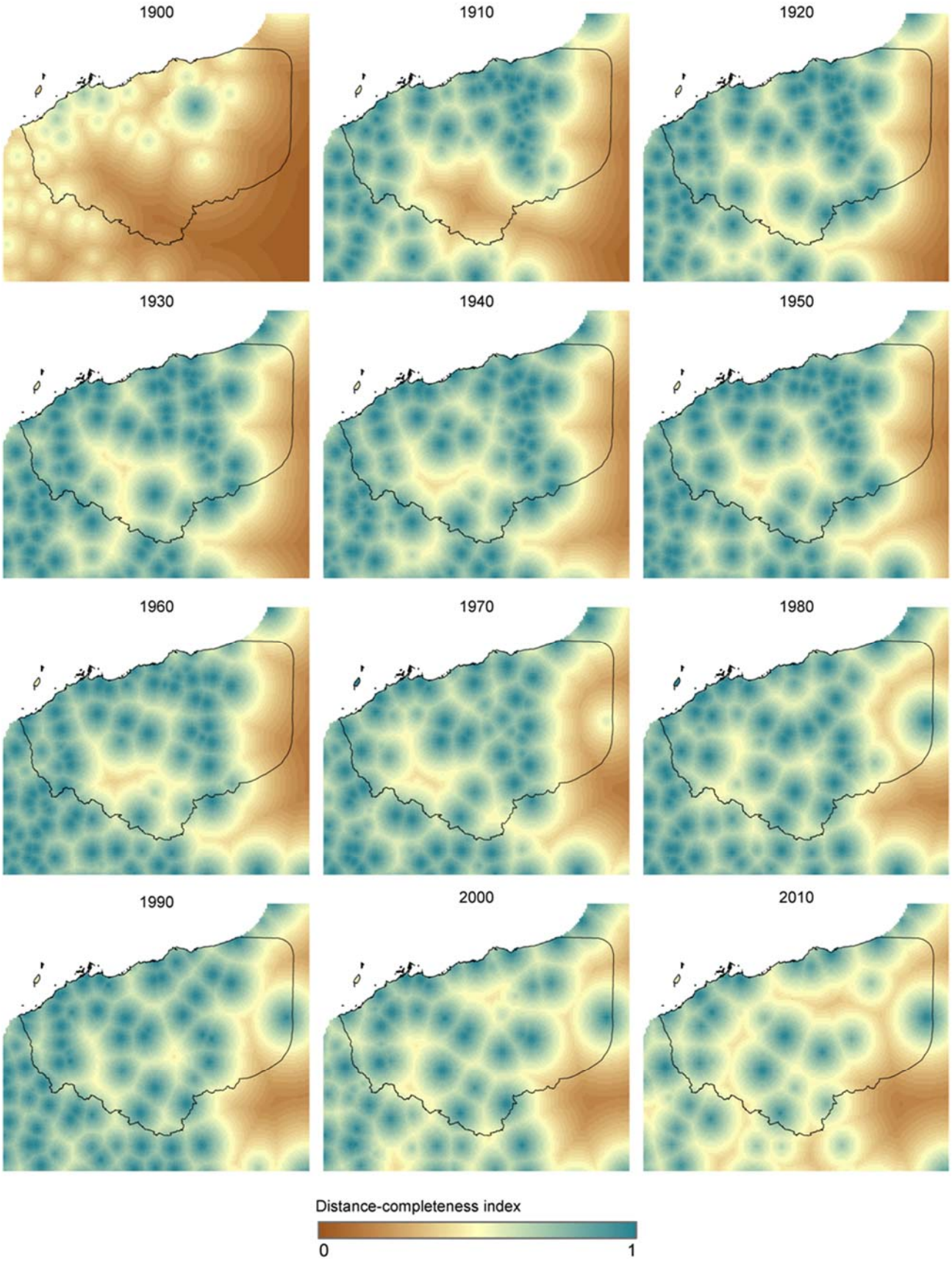

Figure 4.1 Daily rainfall distance-completeness index. A value of 1.0 means the location is a station with a complete rainfall record for the decade commencing 1 January of the labelled year, with the index decreasing with distance from a station and as the number of missing records increases (Li et al., 2009)

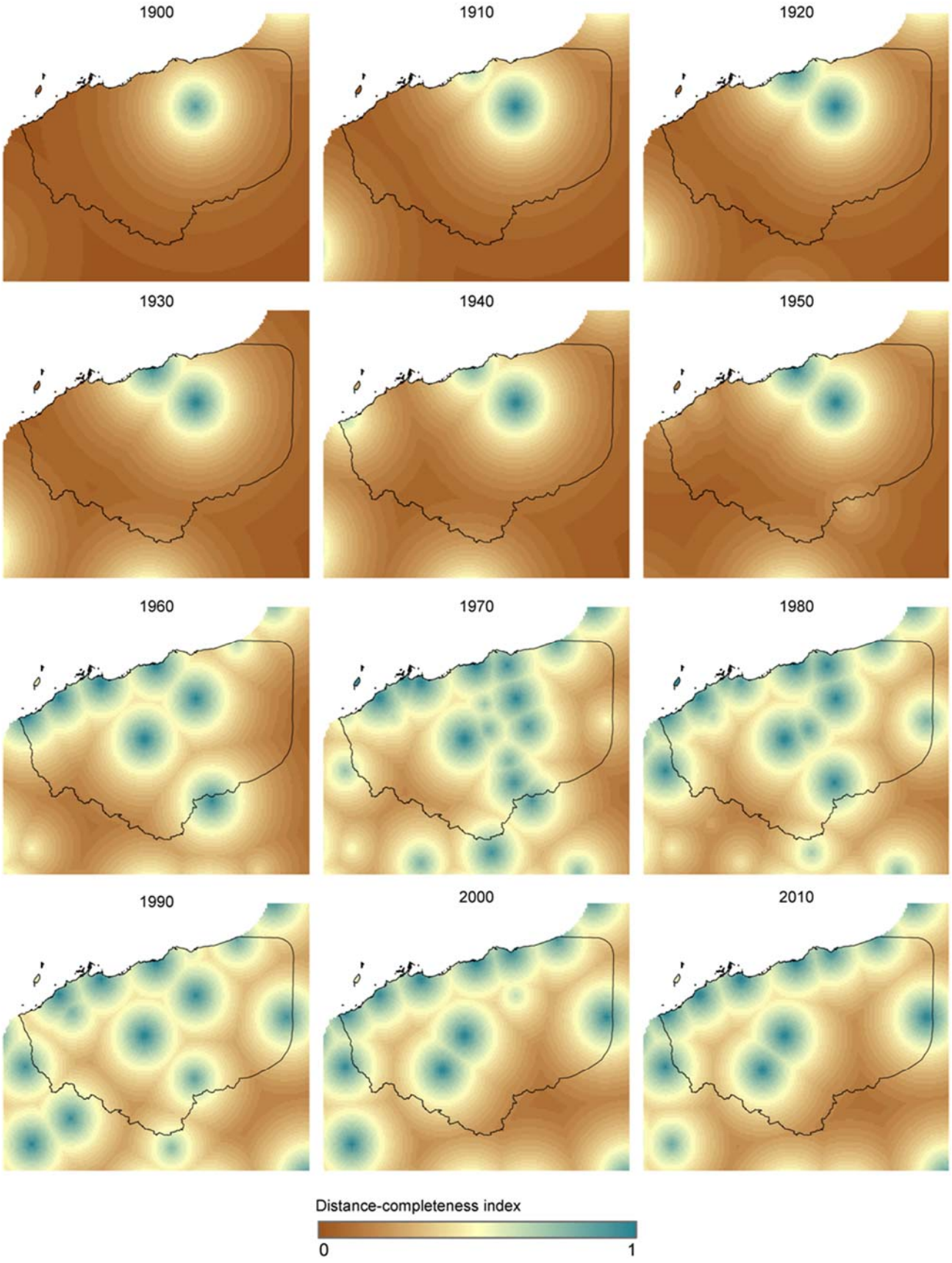

Figure 4.2 Daily temperature distance-completeness index (as an example of an input variable used in the calculation of areal PE) (Li et al., 2009)

4.1.2 Baseline selection

The selection of the baseline historical period needs to take account of region-wide rainfall and potential evaporation characteristics as well as how climate data will be used in the hydrological models and how the resulting data are analysed and portrayed. Most parts of the Pilbara are not expected to have systems with a long historical 'hydrological memory' in that the amount of runoff or recharge is not dependent on previous sequences of annual rainfall beyond a few years. This is in contrast to the south-west of Western Australia where thick weathered aquifers interact with streams in the Darling Range and aquifers in the Perth Basins can be very deep. Therefore statistical hydrologic parameters for the historical period can be compared with similar statistics for periods under a 2030 and 2050 climate regime – e.g. streamflows, probabilities of low or no flow periods, presence of river pools, amount of recharge etc.

Those parts of the Pilbara that do have a long memory include the West Canning Basin, and the fractured rock aquifers which in large part do not have regional models. Additionally, Millstream is an aquifer system with some longer term memory. The sequence of years in these areas will be influential and therefore a different approach which enables groundwater models (where available) to be run in pseudo-predictive mode will be adopted.

Figure 4.1 shows that rainfall over the Pilbara has been relatively well recorded through the last 100 years. As presented in Chapter 2, there are over 90 stations with reasonable records from 1910 to present. The Assessment uses a water year of 1 October to 30 September as this period corresponds (on average) with the end of the dry season and the start of the wet season. It is thus a more meaningful climatic period than the calendar year, which would 'split' the wet season. Analyses of regional average rainfalls[2] have shown that the 102 year record from 1911 to 2012 has several distinct characteristics. There has been a steady increase in annual rainfall averaged over the Assessment area through this period with an acceleration of the rate of increase from 1960, and this rate increasing further from the mid-1990s, as can be seen from the 11-year and 51-year moving average plotted (Figure 4.3a),

The first half of the record has an average rainfall of around 260 mm/year, and the latter half 330 mm/year. The major part of the increase commenced in the 1960s, with an increased rate of change in the 1970s and 1980s. The moving average trends in total rainfall illustrate apparently persistent periods of rainfall trend, with some step changes from 290 mm/year to 320 mm/year around 1980. Then, after a few drier years in the early 1990s, there was an accelerated rate of increase to 2000 followed by a fairly consistent period to the present, with the most recent decade (2003 to 2012) having an average of 350 mm/year.

[2] Rainfall trends differ across the Pilbara as shown in Chapter 2, but only one historical period will be used for the Assessment area

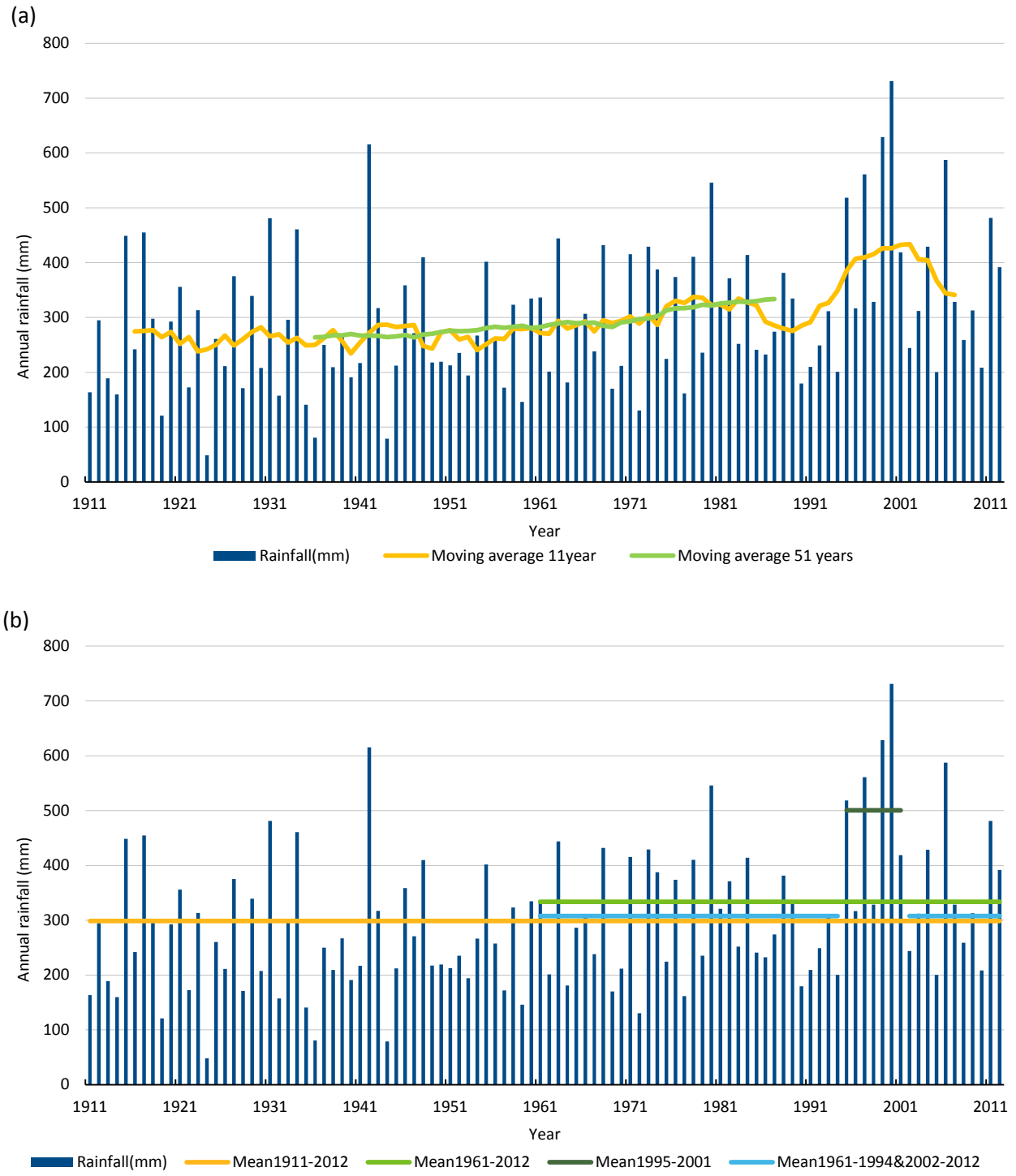

Figure 4.3 Average annual total rainfall for the Assessment area for the water years 1911 to 2012, with (a) 11-year and 51-year moving averages and (b) means for certain periods

The criteria used to select a baseline were thus as follows:

- As long a representative record as possible, including the period with hydrological records, to ensure a robust statistical representation of the historical climate.
- Include as many stations as possible with as near as complete records as possible for both precipitation and potential evaporation.
- Focus on the recent record as this is likely to be more representative of future climate than early records.
- Include the IPCC's (AR4) baseline climate period of 1961 to 1990.

A climatically 'stationary' historical record would make baseline selection straightforward; unfortunately, as shown above, this does not seem to be the case in the Pilbara. However, analysis of trends in annual rainfall against the average for the whole 102 year record (299 mm/year) shows that the period water years 1961 to 2012 has a similar mean rainfall to the full record (334 mm/year). The exceptional seven-year period between 1995 and 2001 has an average annual rainfall of 500 mm/year, while the mean for the rest of the 1961 to 2011 sequence is 308 mm/year (Figure 4.3b). Furthermore, we have no quantitative data on streamflow and groundwater levels to assess climate sensitivity prior to the 1950s, and very little prior to 1970.

Reiterating some of the findings of Chapter 2, for the 1961 to 2012 period the eastern parts of the Assessment Area show increasing linear trends for annual rainfall, 99th percentile daily rainfall (as an example of extremes), number of rain days, and rainfall intensity (i.e. rainfall amount per rain day), with opposing decreasing linear trends in the western parts of the region (Figure 4.4). The presence of the seven wet years towards the end of the record contributes to the region-averaged trends. For example, the mean 1961 to 2012 trend in annual rainfall, averaged across the Assessment area, is 2.2 mm/year/year with removal of the seven-year wet period reducing this to a 0.9 mm/year/year trend. The magnitudes of the trends in 99th percentile daily rainfall, number of rain days and rainfall intensity are small when averaged across the Assessment area, as the increasing trends in the east are mostly cancelled out by the decreasing trends in the west.

Given this, the Assessment has selected the 52 period of record from 1st October, 1960 to 30th September, 2012 as the baseline historical period. This period has an average rainfall over the Pilbara of 334 mm/year. The selected period includes the IPCC baseline period of 1961 to 1990, which will be useful for analysis of the results in comparison with other studies internationally. It also predates by a few years the installation of many groundwater monitoring bores, and most of the gauging stations. Thus this period ensures that the maximum use is made of the available data for hydrologic analyses and model calibrations.

Currently there is a MODFLOW model for the West Canning Basin for which the sequence of rainfall years will be important in estimating future groundwater levels. In this case the 18 year period 1st October 1995 to 30th September 2012 will be used as the historical period for comparing groundwater levels in 2030. Similarly the 38 year period 1st October 1975 to 30th September 2012 will be used for comparing levels in 2050. The model will also be calibrated against 2012 levels to enable future climate scenarios to evolve from the current baseline. Most interest will be on the Wallal Formation aquifer which is either semi-confined or confined where the impact of climate will be delayed, as was found for the Leederville and Yarragadee aquifers in the South-West Western Australia Sustainable Yields project (CSIRO, 2009). Thus, except for the West Canning Basin, the historical baseline scenario (Scenario A), against which all future scenarios will be compared, will be 1st October, 1960 to 30th September, 2012.

In some previous projects, a Scenario B 'Recent Climate' sequence was included but there is no reason for this to be applied in the Pilbara as, while 1995 to 2000 had higher rainfall than the earlier record, the most recent decade is not significantly different than the previous 52 years. However, particular attention will be given to the impact of the aforementioned seven-year wet period (1995 to 2001) on the runoff and recharge magnitudes as well as the drier period since. For example yields with and without this period will be compared for historical and future scenarios to assess overall results to this unusually wet period. As noted in the palaeoclimate review in Chapter 2, this period appears wetter than any decadal length period in the last 150 years at least.

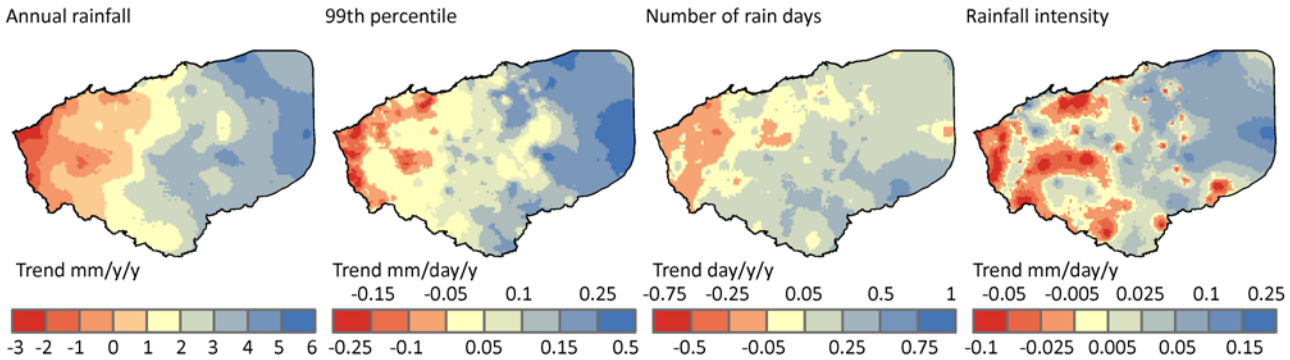

Figure 4.4 Trends for 1961 to 2012 (a) annual rainfall, (b) 99th percentile daily rainfall, (c) number of rain days > 1mm, and (d) rainfall intensity for the Assessment Area

4.2 Future climate scenarios

4.2.1 Global climate model projections

The fundamental scientific tool used to evaluate how the future climate will evolve in response to enhanced concentrations of atmospheric greenhouse gases (GHG) is the Global Climate Model (GCM). As the name implies these simulate the Earth's climate on a global scale, achieved by modelling the atmosphere and oceans as layers of grid cells at a spatial resolution that is a compromise between available computing power and the realistic incorporation of the processes that transfer mass and energy around the globe. Current generation GCMs typically have horizontal grid resolutions of between 100 and 250 km, which is too coarse to resolve regional-scale processes such as individual clouds, tropical cyclones and convective storms.

As climate science progresses there is a need to access the latest knowledge to inform adaptation to future anthropogenic climate change. Thus on a regular basis the global community of climate modelling research groups embark on 'Coupled Model Intercomparison Projects' to facilitate the incorporation of the most up-to-date science within the reports of the Intergovernmental Panel on Climate Change (IPCC). The current project, CMIP5 (Taylor et al., 2011), has recently provided GCM simulations that have been assessed for the IPCC Fifth Assessment Report (AR5) <www.ipcc.ch/report/ar5/>. The uncertainties in future climate conditions are quantified based on the range of projections from the many CMIP5 GCMs forced by a range of plausible scenarios of how GHG emissions will track throughout the 21st century. The emissions scenarios used in CMIP5 are referred to as 'representative concentration pathways' (RCPs) (Van Vuuren et al., 2011).

This Assessment has assessed GCM projections from 36 CMIP5 GCMs (Table 4.1). Of these 36 GCMs, 18 provide the full set of output variables required for calculation of daily scenarios for the two core CMIP5 scenarios RCP8.5 and RCP4.5 (Taylor et al., 2011). RCP8.5 is a high emissions scenario and RCP4.5 is a mid-range scenario, similar to IPCC Fourth Assessment Report A1FI and B1, respectively. The RCP numbers refer to the approximate radiative forcing levels by 2100, i.e. 8.5 W/m^2 and 4.5 W/m^2 corresponding to ~1370 ppm CO_2 and ~650 ppm CO_2, respectively.

Table 4.1 CMIP5 global climate models and institutions. Those in bold provide the output required for calculation of Scenario C

GLOBAL CLIMATE MODEL	INSTITUTION	INSTITUTION ID
ACCESS1.0 **ACCESS1.3**	Commonwealth Scientific and Industrial Research Organisation (CSIRO) and Bureau of Meteorology (BOM), Australia	CSIRO-BOM
BCC-CSM1.1 **BCC-CSM1.1(m)**	Beijing Climate Center, China Meteorological Administration	BCC
BNU-ESM	College of Global Change and Earth System Science, Beijing Normal University	GCESS
CanESM2	Canadian Centre for Climate Modelling and Analysis	CCCMA
CCSM4	National Center for Atmospheric Research	NCAR
CESM1(BGC) CESM1(CAM5)	Community Earth System Model Contributors	NSF-DOE-NCAR
CMCC-CM CMCC-CMS	Centro Euro-Mediterraneo per I Cambiamenti Climatici	CMCC
CNRM-CM5	Centre National de Recherches Meteorologiques / Centre Europeen de Recherche et Formation Avancees en Calcul Scientifique	CNRM-CERFACS
CSIRO-Mk3.6.0	Commonwealth Scientific and Industrial Research Organisation (CSIRO) in collaboration with Queensland Climate Change Centre of Excellence	CSIRO-QCCCE
FGOALS-g2	LASG, Institute of Atmospheric Physics, Chinese Academy of Sciences and CESS,Tsinghua University	LASG-CESS
FGOALS-s2	LASG, Institute of Atmospheric Physics, Chinese Academy of Sciences	LASG-IAP
FIO-ESM	The First Institute of Oceanography, SOA, China	FIO
GFDL-CM3 **GFDL-ESM2G** **GFDL-ESM2M**	NOAA Geophysical Fluid Dynamics Laboratory	NOAA GFDL
GISS-E2-H GISS-E2-R	NASA Goddard Institute for Space Studies	NASA GISS
HadGEM2-AO	National Institute of Meteorological Research/Korea Meteorological Administration	NIMR/KMA
HadGEM2-CC **HadGEM2-ES**	Met Office Hadley Centre	MOHC
INM-CM4	Institute for Numerical Mathematics	INM
IPSL-CM5A-LR **IPSL-CM5A-MR** **IPSL-CM5B-LR**	Institut Pierre-Simon Laplace	IPSL
MIROC-ESM **MIROC-ESM-CHEM**	Japan Agency for Marine-Earth Science and Technology, Atmosphere and Ocean Research Institute (The University of Tokyo), and National Institute for Environmental Studies	MIROC
MIROC5	Atmosphere and Ocean Research Institute (The University of Tokyo), National Institute for Environmental Studies, and Japan Agency for Marine-Earth Science and Technology	MIROC
MPI-ESM-LR MPI-ESM-MR	Max-Planck-Institut für Meteorologie (Max Planck Institute for Meteorology)	MPI-M

GLOBAL CLIMATE MODEL	INSTITUTION	INSTITUTION ID
MRI-CGCM3	Meteorological Research Institute	MRI
NorESM1-M NorESM1-ME	Norwegian Climate Centre	NCC

It is beyond the scope of this Assessment to determine which of these scenarios are more likely to occur. By 2030 and 2050 the multimodel ensemble ranges in the levels of atmospheric CO_2 concentrations and global surface warming overlap as they do not diverge significantly until after 2050 (Knutti and Sedlacek, 2013). Thus similar levels of mean change could be expected from the two scenarios for both 2030 and 2050, and the largest change by 2030 could come from either whereas by 2050 RCP8.5 has a larger range of change.

4.2.2 Global climate model selection and assessment

The selection of GCMs for this Assessment was limited to those that currently have all the required variables available to produce the scaling factors outlined in Section 4.3; namely, monthly and daily rainfall and monthly temperature, solar radiation, and relative humidity. While a formal validation of these GCMs' suitability for modelling the regional climatology of the Assessment area is not within scope, an initial assessment undertaken by CSIRO (Watterson, 2013, pers. comm.) using a skills score termed the M-statistic (Watterson et al., 2014) has assessed the performance 27 CMIP5 GCMs for Australia for temperature, precipitation and mean sea level pressure. One of the regions assessed was tropical Australia, relevant to the Assessment given the influence on tropical climatological processes on Pilbara rainfall, as was discussed in Chapter 2. Additionally, specific features of the climate were also assessed (Watterson et al., 2013). Of the specific features assessed, a 'monsoon onset test' is relevant to the tropical region.

Results for the M-statistic for the tropical region place the performance of the 18 GCMs used in this Assessment within the context of the 27 assessed by Watterson. The 18 include 3 of the top 4 and 13 of the top 15; that is our sample of 18 is weighted towards the top half of rankings for performance across tropical Australia. Only 20 of the 27 GCMs had the required data for the monsoon onset test, of which 14 are used in the Assessment including 6 of the top 9. Hence our selected GCMs are spread across the range of performance for this particular test. Additionally, CSIRO and Bureau of Meteorology (2015) assessed the full set of AR5 GCMs within an Australian context. An overall picture emerges that the GCMs projecting a drier future for the Pilbara region are more likely to be assessed poorer performers in terms of tropical climatology (monsoon, ENSO, MJO) compared to those that project wetter futures. However, there is still a role for assessing the full range of projected change, as is undertaken herein, while taking into account potential reduced confidence in those GCMs producing the dry scenarios. A cautionary note is that a link between the skills of GCMs in simulating mean climatological characteristics of recent decades and the reliability of their climate change projections is not well established.

4.3 Method for producing Scenario C

As proposed in CSIRO (2012), a scaling approach has been used that has modified the daily rainfall and areal PE data in the Scenario A series according to the changes simulated by the 18 GCMs for the two RCP scenarios. This approach is based on the 'daily scaling' methods outlined in Chiew et al. (2009) and Mpelasoka and Chiew (2009) as used in CSIRO Sustainable Yields projects in the Murray-Darling Basin, Northern Australia and South-western Western Australia. This approach has been found generally applicable to surface and groundwater climate change studies (Chiew et al., 2010; Crosbie et al., 2011). The approach scales daily areal PE according to GCM-projected seasonal changes (i.e. DJF, MAM, JJA and SON seasons) and daily rainfall according to GCM-projected changes to daily rainfall on a percentile-class basis (also by season). That is, the rainfall scaling takes into account that projected changes in the higher intensity daily rainfalls may differ from moderate and low intensity events, and so the percentage changes as projected by the GCMs for the different percentile-bins are applied to the Scenario A rainfall amounts in the equivalent percentile-bins. This allows high intensity daily rainfall to increase even in cases where mean rainfall decreases. A limitation of this method is that the Scenario C series maintain the sequence of rainfall events as given by the Scenario A series, thus potential event frequency changes are not assessed.

The scaling factors were originally calculated to represent the projected changes by 2030 and 2050 using the GCM rainfall and GCM-derived areal PE for 2021 to 2040 and 2041 to 2060 periods respectively, converted to % changes relative to the GCM's 1961 to 2000 climatology. Note that as only the mean changes are used, the GCM biases in daily absolute quantities or variability do not adversely influence these calculations. However multi-decadal variability in GCM simulated rainfall was found to produce large variations in decadal to decadal changes in rainfall, resulting in scaling factors that were not representing long-term trends due to climate change (not shown). Thus rather than rely on the changes for rainfall simulated in the 2021 to 2040 and 2041 to 2060 periods, instead the long-term trends were calculated for the GCM rainfall for the full period of simulation (i.e. to 2100) and the linear slope of these trends were used to determine the seasonal scaling factors for rainfall representative of the change between GCM baseline and 2030 and 2050 climates. These were used in conjunction with the originally calculated rainfall daily scaling factors and areal PE seasonal scaling factors, as these calculations were not unduly influenced by multi-decadal variability. In the case of areal PE, this is because the long-term trends in temperature increase due to climate change dominant the changes in the inputs to calculating areal PE future mean changes in 2021 to 2040 and 2041 to 2060, rather than multi-decadal variability.

Applying the scaling factor techniques to the Scenario A daily rainfall and areal PE time-series produces an ensemble of Scenario C time-series representing projected-2030 and -2050 climates of the Pilbara. For each of the 2030 and 2050 ensembles, the Scenario C ensemble members that produce the 10^{th}, 50^{th} and 90^{th} percentile rainfall totals (averaged over the Assessment area) are identified as the key Scenario C time-series for use in hydrological modelling. These are termed: C30dry, C30mid, and C30wet; and: C50dry, C50mid and C50wet for 2030 and 2050 respectively.

4.4 Scaling results

4.4.1 Rainfall

The long-term linear trends in GCM rainfall have been calculated on a seasonal basis and converted to percentage change in Assessment area rainfall for 2030 and 2050 (as shown in Table 4.2 and Table 4.3, for 2030 and 2050 respectively). The ranges emphasise the uncertainty in GCM changes for the Assessment area, and also emphasise the dominance of summer (DJF) changes in total annual rainfall.

The range of projected annual changes across the 18 GCMs for RCP4.5 is between -13 to 5% (median -0.1%) for 2030 and -18 to 7% (median -0.2%) for 2050. For RCP 8.5 these ranges are -16 to 6% (median -2%) for 2030 and -22 to 8% (median -2%) for 2050. In comparison, the ranges from the 36 GCMs are -13 to 6% (median 0.2%) for 2030 and -18 to 9% (median 0.2%) for 2050 for RCP4.5 and -16 to 13% (median -1%) for

2030 and -22 to 18% for 2050 (median -2%) for RCP8.5. The most noticeable difference between the distributions from the 18 and 36 GCMs is due to the model FGOALS-g2 projecting much wetter conditions than any of the 18 GCMs used for Scenario C. That is, the annual rainfall change from FGOALS-g2 for 2030 RCP4.5 is 6.5% and for RCP8.5 13.2% and for 2050 RCP4.5 9.1% and RCP8.5 18.5%. In contrast the wettest GCMs (which vary between periods and RCPs) from the set of 18 project increases of 5.3%, 5.6%, 7.4% and 7.8% for 2030 RCP4.5 and RCP8.5 and 2050 RCP4.5 and RCP8.5 respectively.

Table 4.2 Changes in Assessment area seasonal rainfall (%, relative to Scenario A) for 2030. GCMs in bold are those that have the required output for Scenario C production

GLOBAL CLIMATE MODEL	DJF		MAM		JJA		SON		Annual	
	RCP45	RCP85	RCP45	RCP85	RCP45	RCP85	RCP45	RCP85	RCP45	RCP85
ACCESS1.0	0.3	–2.5	–1.5	–1.7	0.8	–0.5	1.9	3.5	–0.1	–1.8
ACCESS1.3	1.2	0.5	–5.1	–6.7	–11.6	–12.1	–7.6	–13.5	–2.7	–3.8
BCC-CSM1.1	0.7	–4.0	2.7	4.5	–0.2	–1.1	–10.8	–10.5	0.8	–1.3
BCC-CSM1.1(m)	–5.0	–3.2	–2.1	–1.5	–8.4	–8.7	–5.8	–9.5	–4.6	–3.6
BNU-ESM	1.8	6.7	2.2	0.7	–4.1	–5.3	3.2	1.7	1.2	3.1
CanESM2	3.5	0.1	0.5	–2.2	–7.6	–15.5	–5.7	–7.2	0.8	–3.0
CCSM4	0.6	0.6	4.0	5.1	–7.7	–5.4	–1.7	–2.7	0.4	1.0
CESM1(BGC)	0.7	1.6	3.4	5.7	–0.7	–2.4	–2.9	1.0	1.2	2.3
CESM1(CAM5)	0.7	–0.2	–1.4	0.9	2.4	1.1	4.0	2.9	0.4	0.4
CMCC-CM	–0.7	2.7	–3.1	3.9	–1.8	3.9	–25.2	–32.9	–2.4	2.0
CMCC-CMS	1.3	–1.2	1.9	1.9	17.5	–9.1	–26.2	–32.6	2.7	–2.4
CNRM-CM5	2.5	6.3	3.7	8.4	3.2	–3.2	9.8	4.2	3.2	5.6
CSIRO-Mk3.6.0	–15.9	–18.3	–6.1	–8.1	–12.6	–18.7	–35.2	–39.4	–13.2	–16.0
FGOALS-g2	9.7	17.0	4.5	10.9	–1.5	2.7	4.1	16.3	6.5	13.2
FGOALS-s2	3.6	5.8	4.3	2.7	–1.3	–5.3	1.7	–2.3	3.1	3.1
FIO-ESM	2.2	2.2	6.0	7.7	–0.9	–4.5	6.5	4.3	3.1	3.0
GFDL-CM3	–2.7	–1.5	0.7	–0.9	–15.8	–18.7	–2.6	–5.8	–3.4	–3.7
GFDL-ESM2G	–0.2	–1.5	0.9	4.7	–3.3	0.4	–11.9	1.0	–0.7	0.7
GFDL-ESM2M	1.3	–2.0	0.4	–0.9	–4.7	–9.9	–11.2	–8.0	–0.2	–3.0
GISS-E2-H	–5.1	–6.0	–6.0	–6.2	–7.7	–12.6	0.1	2.6	–5.5	–6.6
GISS-E2-R	3.1	6.2	4.0	9.9	–3.5	–3.4	2.4	3.1	2.5	5.9
HadGEM2-AO	–6.4	–9.1	–4.3	–8.9	–2.3	–6.7	–5.9	–8.2	–5.2	–8.7
HadGEM2-CC	0.9	–3.8	–1.3	–1.2	–2.7	–5.8	–11.3	–14.0	–0.6	–3.6
HadGEM2-ES	1.4	–7.2	–11.1	–7.5	–11.2	–5.6	18.3	–13.6	–3.4	–7.3

GLOBAL CLIMATE MODEL	DJF		MAM		JJA		SON		Annual	
	RCP45	RCP85	RCP45	RCP85	RCP45	RCP85	RCP45	RCP85	RCP45	RCP85
INM-CM4	–5.7	–4.6	–7.5	–9.5	–6.7	–8.1	–4.5	–0.6	–6.3	–6.4
IPSL-CM5A-LR	4.6	3.0	–0.8	–3.0	–6.7	–13.4	–44.6	–33.7	–0.2	–2.3
IPSL-CM5A-MR	–4.6	–12.4	–0.7	–12.1	–7.3	–12.1	–16.9	–21.3	–4.2	–12.6
IPSL-CM5B-LR	2.9	6.9	1.3	4.2	–6.7	2.3	3.8	3.7	1.2	5.4
MIROC-ESM	–2.1	–2.6	3.8	4.3	–3.9	–5.3	–7.6	–17.3	–0.8	–1.4
MIROC-ESM-CHEM	–3.4	–5.1	–2.0	–0.3	–6.5	–7.8	–11.4	–18.5	–3.6	–4.5
MIROC5	5.9	4.9	5.9	4.0	–1.1	–0.2	14.4	13.2	5.3	4.2
MPI-ESM-LR	0.2	–0.1	2.9	0.9	4.2	1.0	–5.5	–10.9	1.3	0.0
MPI-ESM-MR	0.6	1.4	0.7	0.0	–10.2	–12.0	–33.6	–44.5	–2.0	–2.4
MRI-CGCM3	–3.5	1.5	5.0	4.1	6.4	18.1	8.6	9.7	0.8	4.8
NorESM1-M	1.3	4.4	1.6	4.0	–5.4	–3.9	0.8	7.7	0.5	3.3
NorESM1-ME	1.0	0.9	8.5	12.7	0.7	–1.1	10.2	14.9	3.5	4.7

Table 4.3 Changes in Assessment area seasonal rainfall (%, relative to Scenario A) for 2050. GCMs in bold are those that have the required output for Scenario C production

GLOBAL CLIMATE MODEL	DJF		MAM		JJA		SON		Annual	
	RCP45	RCP85	RCP45	RCP85	RCP45	RCP85	RCP45	RCP85	RCP45	RCP85
ACCESS1.0	0.4	–3.4	–2.1	–2.4	1.1	–0.7	2.7	5.0	–0.1	–2.5
ACCESS1.3	1.7	0.7	–7.1	–9.3	–16.3	–17.0	–10.6	–19.0	–3.8	–5.4
BCC-CSM1.1	0.9	–5.6	3.8	6.3	–0.2	–1.6	–15.1	–14.6	1.1	–1.8
BCC-CSM1.1(m)	–7.1	–4.5	–2.9	–2.1	–11.8	–12.1	–8.2	–13.2	–6.5	–5.1
BNU-ESM	2.6	9.4	3.1	1.0	–5.7	–7.5	4.4	2.3	1.7	4.4
CanESM2	4.9	0.1	0.6	–3.1	–10.6	–21.7	–8.0	–10.1	1.1	–4.2
CCSM4	0.9	0.8	5.6	7.1	–10.8	–7.6	–2.4	–3.8	0.6	1.4
CESM1(BGC)	1.0	2.3	4.8	8.0	–0.9	–3.4	–4.0	1.4	1.7	3.2
CESM1(CAM5)	1.0	–0.3	–2.0	1.2	3.4	1.5	5.6	4.0	0.6	0.6
CMCC-CM	–1.0	3.8	–4.3	5.4	–2.5	5.4	–34.7	–45.5	–3.4	2.8
CMCC-CMS	1.8	–1.7	2.7	2.6	24.5	–12.8	–36.6	–43.7	3.8	–3.3
CNRM-CM5	3.5	8.8	5.2	11.8	4.5	–4.5	13.7	5.9	4.5	7.8
CSIRO-Mk3.6.0	–22.2	–25.6	–8.5	–11.3	–17.6	–26.2	–49.2	–55.1	–18.4	–22.4
FGOALS-g2	13.6	23.8	6.3	15.2	–2.0	3.8	5.7	22.9	9.1	18.5

GLOBAL CLIMATE MODEL	DJF		MAM		JJA		SON		Annual	
	RCP45	RCP85	RCP45	RCP85	RCP45	RCP85	RCP45	RCP85	RCP45	RCP85
FGOALS-s2	5.0	8.2	6.0	3.7	–1.9	–7.4	2.4	–3.2	4.3	4.4
FIO-ESM	3.1	3.1	8.4	10.7	–1.3	–6.4	9.1	6.0	4.3	4.2
GFDL-CM3	–3.8	–2.0	1.0	–1.2	–22.1	–26.2	–3.7	–8.1	–4.8	–5.2
GFDL-ESM2G	–0.3	–2.1	1.2	6.5	–4.7	0.6	–16.6	1.5	–1.0	1.0
GFDL-ESM2M	1.8	–2.9	0.5	–1.3	–6.6	–13.8	–15.6	–11.2	–0.3	–4.2
GISS-E2-H	–7.1	–8.4	–8.5	–8.7	–10.8	–17.6	0.2	3.6	–7.7	–9.3
GISS-E2-R	4.4	8.6	5.6	13.8	–4.9	–4.7	3.4	4.4	3.5	8.2
HadGEM2-AO	–8.9	–12.7	–6.1	–12.4	–3.2	–9.3	–8.2	–11.5	–7.3	–12.1
HadGEM2-CC	1.3	–5.3	–1.8	–1.6	–3.7	–8.2	–15.8	–19.7	–0.9	–5.1
HadGEM2-ES	2.0	–10.0	–15.6	–10.6	–15.7	–7.9	25.6	–19.0	–4.8	–10.2
INM-CM4	–7.9	–6.5	–10.6	–13.4	–9.3	–11.4	–6.3	–0.8	–8.8	–9.0
IPSL-CM5A-LR	6.5	4.2	–1.1	–4.2	–9.4	–18.7	–61.7	–47.2	–0.3	–3.2
IPSL-CM5A-MR	–6.4	–17.3	–0.9	–16.9	–10.3	–17.0	–23.6	–25.7	–5.9	–17.4
IPSL-CM5B-LR	4.1	9.7	1.9	5.9	–9.3	3.2	5.4	5.1	1.7	7.5
MIROC-ESM	–3.0	–3.6	5.3	6.1	–5.5	–7.4	–10.6	–24.2	–1.1	–2.0
MIROC-ESM-CHEM	–4.7	–7.2	–2.7	–0.4	–9.1	–10.9	–16.0	–25.9	–5.1	–6.3
MIROC5	8.3	6.8	8.3	5.6	–1.5	–0.3	20.1	18.5	7.4	5.9
MPI-ESM-LR	0.3	–0.2	4.0	1.3	5.8	1.5	–7.6	–15.3	1.9	–0.1
MPI-ESM-MR	0.8	2.0	1.0	0.1	–14.3	–16.8	–47.0	–62.3	–2.8	–3.3
MRI-CGCM3	–5.0	2.1	7.0	5.7	9.0	25.3	12.0	13.6	1.1	6.7
NorESM1-M	1.8	6.2	2.2	5.6	–7.5	–5.5	1.1	10.8	0.6	4.6
NorESM1-ME	1.4	1.3	11.8	17.8	0.9	–1.6	14.3	20.8	4.9	6.5

4.4.2 Potential evaporation

The calculated Assessment area average seasonal areal PE scaling factors for the 2030 and 2050 periods are shown in Table 4.4 and Table 4.5 for the 18 GCMs that are available for Scenario C production. The areal PE changes are more consistent than those obtained for rainfall as they are a function of the consistently increasing trend in temperature projected by the GCMs, rather than the regional trend in rainfall that varies across a large range between the different GCMs. This is expected given areal PE is calculated as a function of temperature, solar radiation and relative humidity using Morton's wet areal formulation. A different formulation that accounts for wind speed may give a different result given observational studies indicate decreasing wind speeds may be a dominant factor in recent areal PE decreases (Donohue et al., 2010). Consistent with the differences in the two emissions scenarios discussed above, the upper bound of areal PE change is most often higher from RCP8.5 than from RCP4.5 for all seasons for 2050 whereas for 2030

this is not the case. The range of projected annual changes across the 18 GCMs for RCP4.5 is between 1.5 to 6% (median 3.4%) for 2030 and 3 to 6% (median 4.4%) for 2050. For RCP 8.5 these ranges are 2 to 5% (median 3.4%) for 2030 and 4 to 8% (median 6.5%) for 2050. There were large changes from the IPSL-CM5A-LR model for RCP8.5 due to unrealistically large projections of temperature increase and these are not reported or used in Scenario C selection.

Table 4.4 Changes in Assessment area seasonal areal PE (%, relative to Scenario A) for 2030

GLOBAL CLIMATE MODEL	DJF		MAM		JJA		SON		Annual	
	RCP45	RCP85	RCP45	RCP45	RCP85	RCP85	RCP45	RCP85	RCP45	RCP85
ACCESS1.0	3.0	2.8	3.5	2.2	3.5	3.9	3.2	3.8	3.2	3.1
ACCESS1.3	2.4	2.9	3.3	4.0	4.5	4.5	3.9	4.7	3.4	3.9
BCC-CSM1.1	2.8	3.1	3.6	4.1	5.4	5.5	3.8	4.0	3.7	3.9
CanESM2	4.2	4.1	4.4	5.5	3.7	5.9	4.6	4.5	4.3	4.8
CCSM4	3.1	2.9	4.2	4.4	5.2	5.5	4.0	4.1	3.9	4.0
CNRM-CM5	2.0	0.0	4.9	3.6	3.1	3.7	2.8	3.0	3.1	2.2
CSIRO-Mk3.6.0	3.1	4.0	3.5	4.9	4.1	4.4	4.1	3.7	3.6	4.2
GFDL-ESM2G	0.7	1.9	3.6	4.4	4.2	3.1	2.7	4.3	2.5	3.3
GFDL-ESM2M	5.8	4.5	10.4	6.1	3.6	4.4	3.9	4.5	6.0	4.8
HadGEM2-ES	3.1	3.4	6.4	6.0	4.1	4.7	3.8	3.3	4.2	4.2
IPSL-CM5A-LR	6.4	–	8.5	–	10.6	–	7.8	–	7.9	–
IPSL-CM5A-MR	3.2	2.9	4.0	4.4	4.8	4.6	3.8	3.8	3.8	3.8
IPSL-CM5B-LR	2.2	2.1	2.6	3.7	3.4	3.3	2.9	2.8	2.7	2.8
MIROC-ESM	4.2	2.0	6.5	2.2	8.1	4.0	5.1	2.7	5.6	2.5
MIROC-ESM-CHEM	2.7	1.2	1.0	0.4	3.8	3.4	6.0	3.0	3.4	1.9
MIROC5	3.4	2.9	3.6	3.7	3.0	2.6	3.4	4.2	3.4	3.4
MRI-CGCM3	4.2	0.8	2.1	2.3	2.9	3.0	2.2	2.7	3.0	2.0
NorESM1-M	0.0	1.8	0.4	1.3	3.5	4.9	3.2	3.3	1.5	2.6

Table 4.5 Changes in Assessment area seasonal areal PE (%, relative to Scenario A) for 2050

GLOBAL CLIMATE MODEL	DJF		MAM		JJA		SON		Annual	
	RCP45	RCP85	RCP45	RCP45	RCP85	RCP85	RCP45	RCP85	RCP45	RCP85
ACCESS1.0	4.3	6.2	5.7	6.7	4.9	7.1	4.3	6.8	4.7	6.6
ACCESS1.3	4.5	6.3	5.1	7.3	6.0	8.6	5.1	7.6	5.0	7.2
BCC-CSM1.1	3.4	5.1	4.8	6.2	9.0	7.3	4.1	5.7	4.8	5.9
CanESM2	5.5	8.0	6.1	8.8	6.6	8.5	5.5	7.6	5.8	8.1
CCSM4	1.3	5.9	4.5	7.2	6.0	8.1	4.7	6.7	3.7	6.8
CNRM-CM5	2.2	2.5	5.8	4.0	4.8	6.0	4.1	5.0	4.0	4.1
CSIRO-Mk3.6.0	5.5	6.5	6.7	8.0	6.0	7.8	5.1	6.2	5.7	7.0
GFDL-ESM2G	3.0	7.5	5.4	9.5	4.0	5.8	3.9	6.1	4.0	7.3
GFDL-ESM2M	–0.5	5.5	5.6	9.4	6.0	7.3	5.1	6.9	3.5	7.1
HadGEM2-ES	5.3	6.3	7.8	9.3	6.2	8.9	5.2	6.0	6.0	7.3
IPSL-CM5A-LR	6.7	–	8.6	–	9.2	–	7.6	–	7.8	–
IPSL-CM5A-MR	3.4	5.3	4.9	7.3	5.3	8.8	4.7	6.0	4.4	6.5
IPSL-CM5B-LR	4.5	5.1	5.5	5.6	4.1	6.2	3.5	4.5	4.4	5.2
MIROC-ESM	4.6	4.0	5.0	2.7	9.7	7.8	5.1	5.8	5.6	4.8
MIROC-ESM-CHEM	6.2	6.6	3.6	2.7	7.1	5.7	6.3	6.8	5.8	5.6
MIROC5	3.3	5.0	2.7	5.0	4.7	5.7	4.5	6.8	3.7	5.6
MRI-CGCM3	3.2	4.5	1.6	2.8	3.2	4.0	3.3	5.3	2.9	4.3
NorESM1-M	2.9	3.3	2.7	6.3	5.2	7.8	3.3	4.6	3.3	5.0

4.4.3 Scenario C selection

The selection of the C30 and C50 wet, mid and dry scenarios is based on the whole of Assessment area mean annual rainfall changes obtained from applying the scaling methodology to the 18 GCMs rainfall. Figure 4.5 summarises the projected Assessment area mean annual rainfall % changes obtained from the 18 GCMs with each coloured bar giving the range between the RCP4.5 and RCP8.5 scenarios, for 2030 (left) and 2050 (right). Overall the majority of GCMs project changes within 5% of the current climate mean for both 2030 and 2050.

The ensemble members that produced the 90th, 50th and 10th percentile rainfall changes for the Assessment area were initially identified as the Cwet, Cmid and Cdry scenarios (Figure 4.5). Evaluation of the spatial patterns associated with each of these initially selected scenarios determined cases where the initial selection had a spatial pattern that would not produce consistent results across the four reporting regions (not shown). For example, a Scenario Cmid selected on the basis that it produced the 50th percentile rainfall change when averaged over the entire Assessment area could have a spatial pattern consisting of two large opposing changes that cancel each other out to produce a small overall change. Thus selection of a different GCM with a more consistent spatial pattern and a similar overall rainfall

change to that which was initially chosen was undertaken. This approach resulted in the selection of the CNRM-CM5 GCM scenarios for Cwet, the ACCESS 1.0 GCM scenarios for the Cmid, and the IPSL-CM5A-MR GCM scenarios for the Cdry (for both RCP8.5 and RCP4.5 in each case).

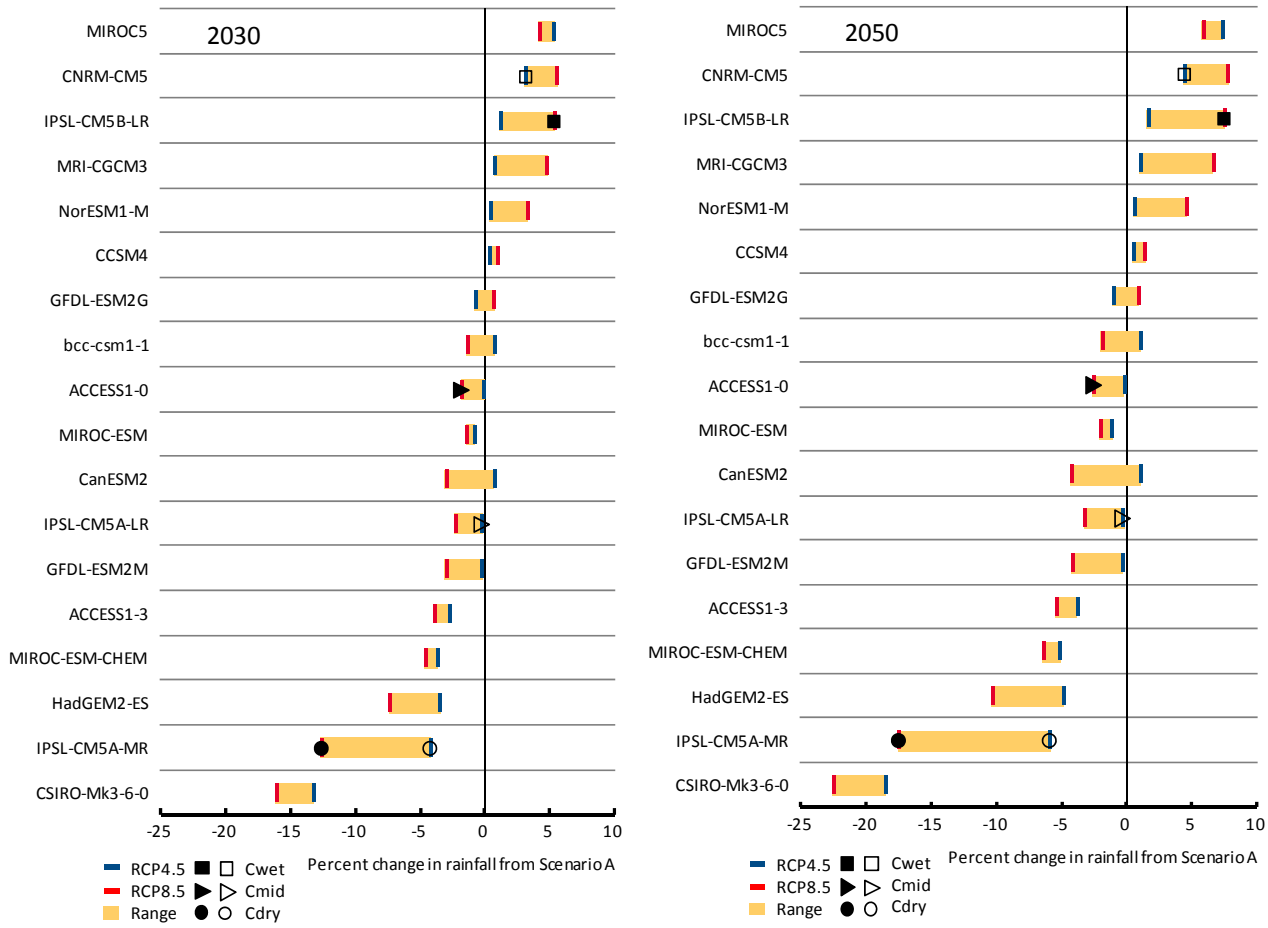

Figure 4.5 Assessment area mean annual rainfall change (%, relative to Scenario A) for RCP4.5 and RCP8.5 projections from 18 CMIP5 GCMs for 2030 and 2050. The second wettest (driest) scenarios from RCP4.5 and RCP8.5 are designated Cwet (Cdry). The median, selected from the 9th and 10th ranked GCM closest to the respective RCP4.5 and RCP8.5 mean, is designated Cmid. Solid symbols are used for RCP8.5, open symbols for RCP4.5

The resulting Scenario C rainfall changes are summarised in Table 4.5, with the associated areal PE changes summarised in Table 4.6. While rainfall in the future scenarios falls each side of a continuation of the current historical rainfall, the magnitude of change for the dry projections are up to 10% greater than those of the wet projections (i.e. the largest increase is 7.8% in contrast to the largest decrease of –17.4%). In addition, the across-the-board increases in areal PE mean that even the Cwet and Cmid scenarios experience increased annual rainfall deficits.

The spatial patterns of projected mean annual rainfall and areal PE change, for the Cwet, Cmid and Cdry scenarios, are shown in Figure 4.6 and Figure 4.8 respectively. The strong correlation between annual and extreme daily rainfall, as outlined in Chapter 2, is maintained in the scenarios with the projected changes to 99th percentile daily rainfall (Figure 4.7) of similar magnitude to the annual changes (Figure 4.6). The spatial discontinuities seen in the scenario maps are a result of the changes in scaling factors across GCM grid boundaries.

Table 4.6 Assessment area mean annual rainfall changes (relative to Scenario A) under Cwet, Cmid and Cdry future climate scenarios from 18 GCM's RCP4.5 and RCP8.5 emissions scenario projections for 2030 and 2050

Period	Scenario C	RCP4.5 emissions scenario		RCP8.5 emissions scenario	
		(%)	(mm)	(%)	(mm)
2030	C30wet	3.2	11	5.6	19
2030	C30mid	–0.1	0	–1.8	–6
2030	C30dry	–4.2	–14	–12.6	–42
2050	C50wet	4.5	15	7.8	26
2050	C50mid	–0.1	0	–2.5	–8
2050	C50dry	–5.9	–20	–17.4	–58

Table 4.7 Assessment area mean annual areal PE changes (relative to Scenario A) under Cwet, Cmid and Cdry future climate scenarios from 18 GCM's RCP4.5 and RCP8.5 emissions scenario projections for 2030 and 2050

Period	Scenario C	RCP4.5 emissions scenario		RCP8.5 emissions scenario	
		(%)	(mm)	(%)	(mm)
2030	C30wet	3.0	57	2.2	42
2030	C30mid	3.2	60	3.1	59
2030	C30dry	3.8	72	3.8	72
2050	C50wet	4.0	76	4.1	77
2050	C50mid	4.7	89	6.6	125
2050	C50dry	4.4	83	6.5	123

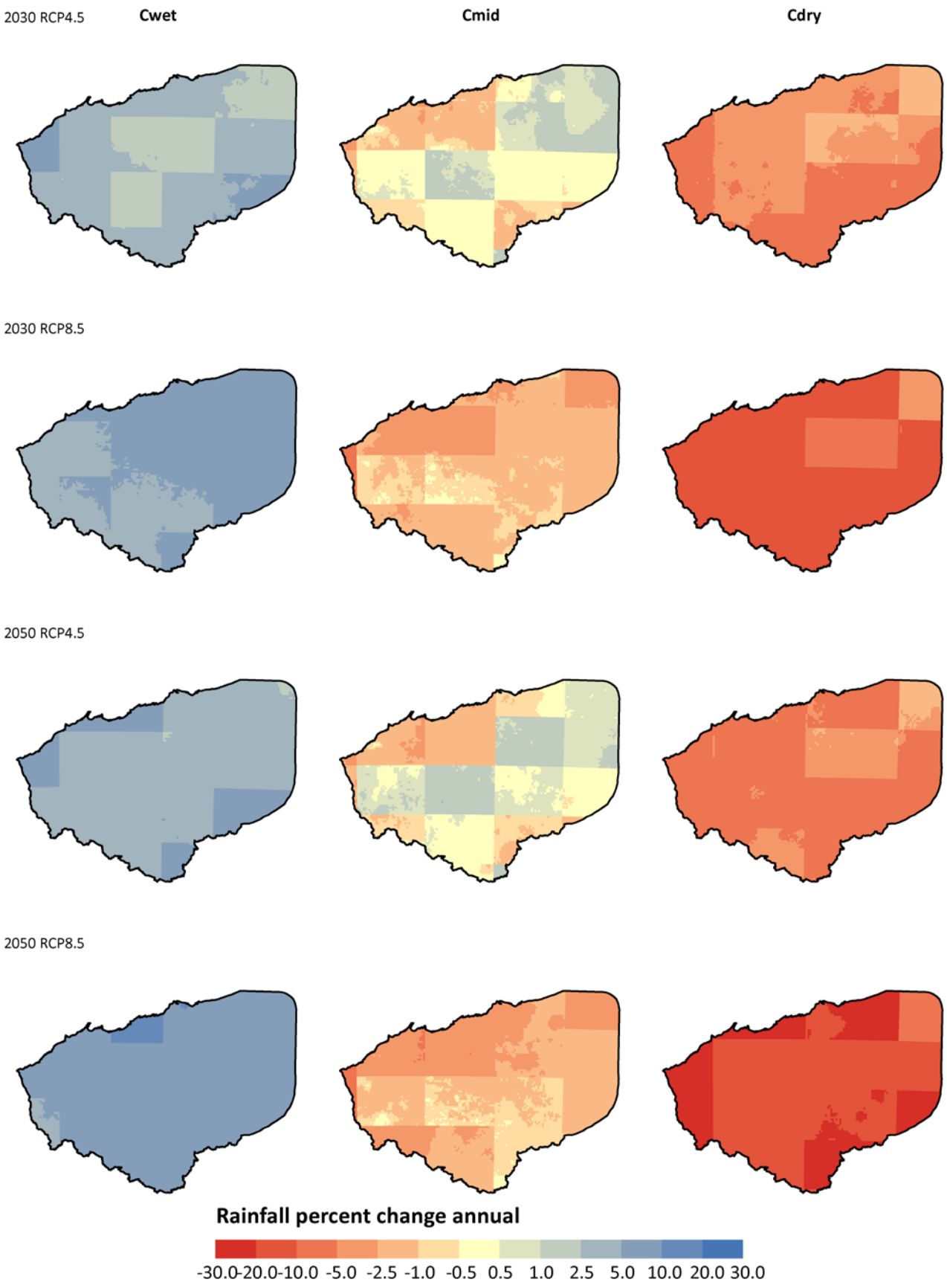

Figure 4.6 Mean annual rainfall change (percentage, relative to Scenario A) for 2030 and 2050 RCP4.5 and RCP8.5 projections for Cwet, Cmid and Cdry scenarios for the Assessment Area

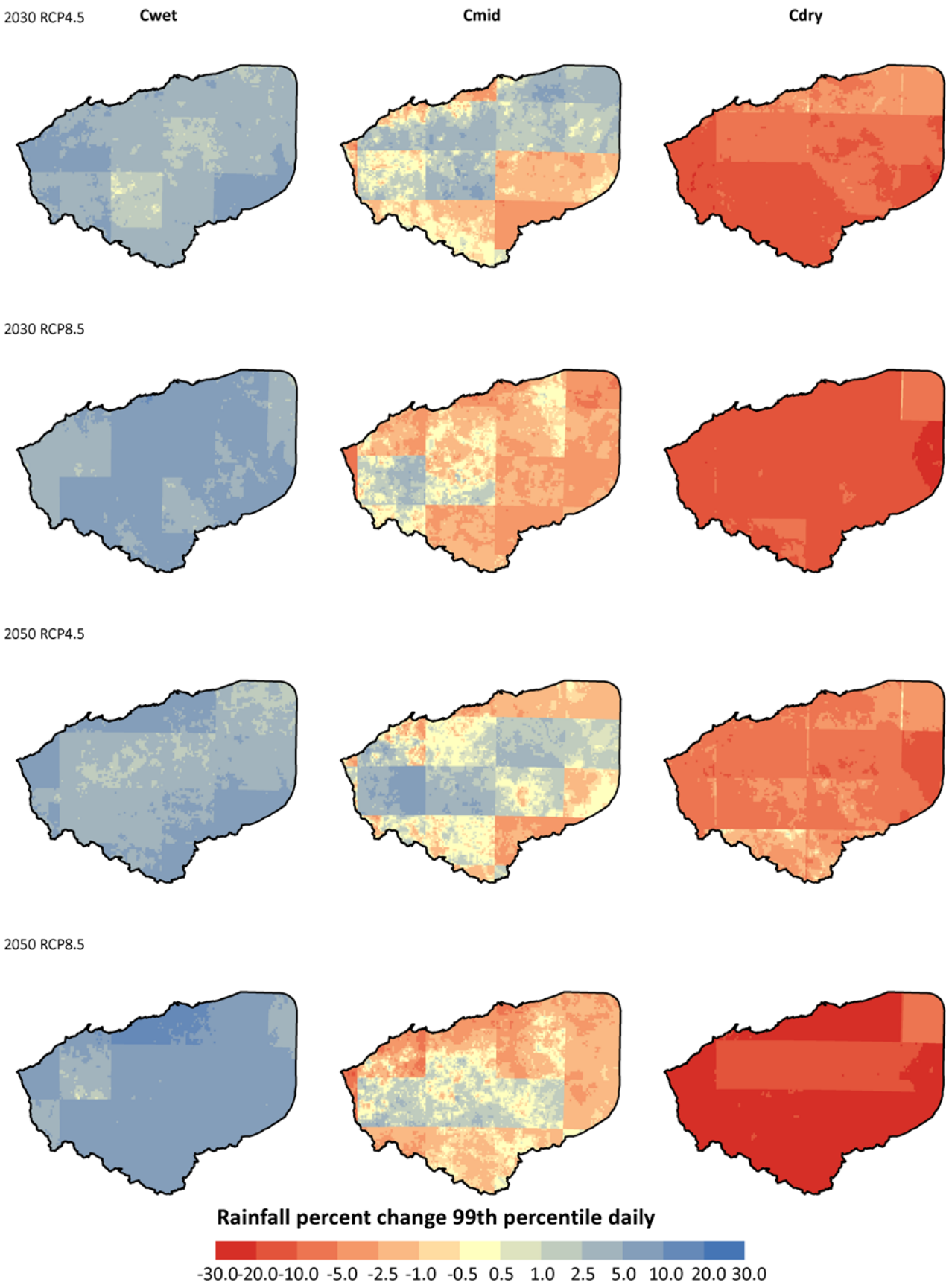

Figure 4.7 99th percentile daily rainfall change (percentage, relative to Scenario A) for 2030 and 2050 RCP4.5 and RCP8.5 projections for Cwet, Cmid and Cdry scenarios for the Assessment Area

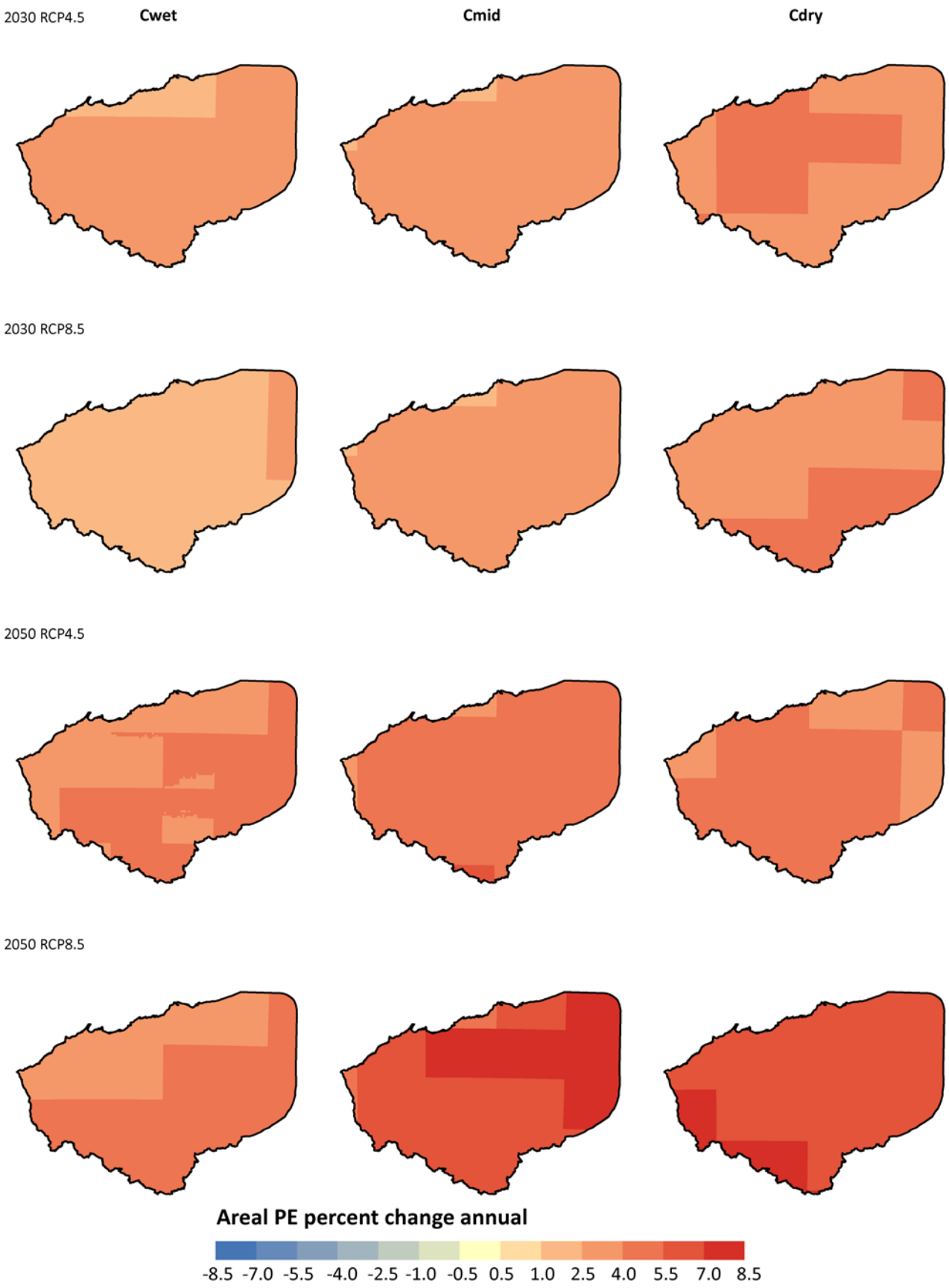

Figure 4.8 Mean annual areal PE change (percentage, relative to Scenario A) for 2030 and 2050 RCP4.5 and RCP8.5 projections for Cwet, Cmid and Cdry scenarios for the Assessment Area

The median and 10th to 90th percentile range of monthly rainfall from the Scenario C ensemble for RCP8.5 are shown for 2030 in Figure 4.9, for 2030, and Figure 4.10, for 2050. The Scenario Cdry is dominated by the relatively large reductions in January and February rainfall, the wettest months. RCP4.5 ensemble ranges (not shown) are smaller.

The monthly mean, median and range of the scaled 1911 to 2012 series (this period allows direct comparison with Figure 2.4 in Section 2.2) for the RCP8.5 2050 Cwet and Cdry scenarios are shown in Figure 4.11 and Figure 4.12, respectively. These plots also highlight that the largest projected absolute changes are for the wetter summer months.

Monthly projected areal PE results for the RCP8.5 Scenario C ensemble are shown in Figure 4.13 and Figure 4.14, for 2030 and 2050 respectively. The increase between 2030 and 2050 is driven predominantly by the continued warming in the GCM simulations. The equivalent plots for the RCP4.5 scenario are not shown as they are similar but with smaller ranges and the changes between 2030 and 2050 are less.

While on balance future projections indicate a slightly higher likelihood that the future climate will be both hotter and drier, with rainfall deficits and therefore soil moisture deficits correspondingly higher, the wet scenarios should not be discounted given that there is possibly lower confidence in the performance of the GCMs projecting a drier future (CSIRO and Bureau of Meteorology, 2015). Consideration of the wet scenarios is also important given observed trends of increased summer rainfall in the north-west of Australia (as discussed in Chapter 2).

An additional caveat applies to confidence in the areal PE projections, given that the Morton's areal PE formulation used does not take account of wind speed changes and thus is not considered a physically based method by, for example, McVicar et al. (2012). The impact of the Scenario C projected rainfall and areal PE changes on modelled surface water and groundwater changes is covered in other reports.

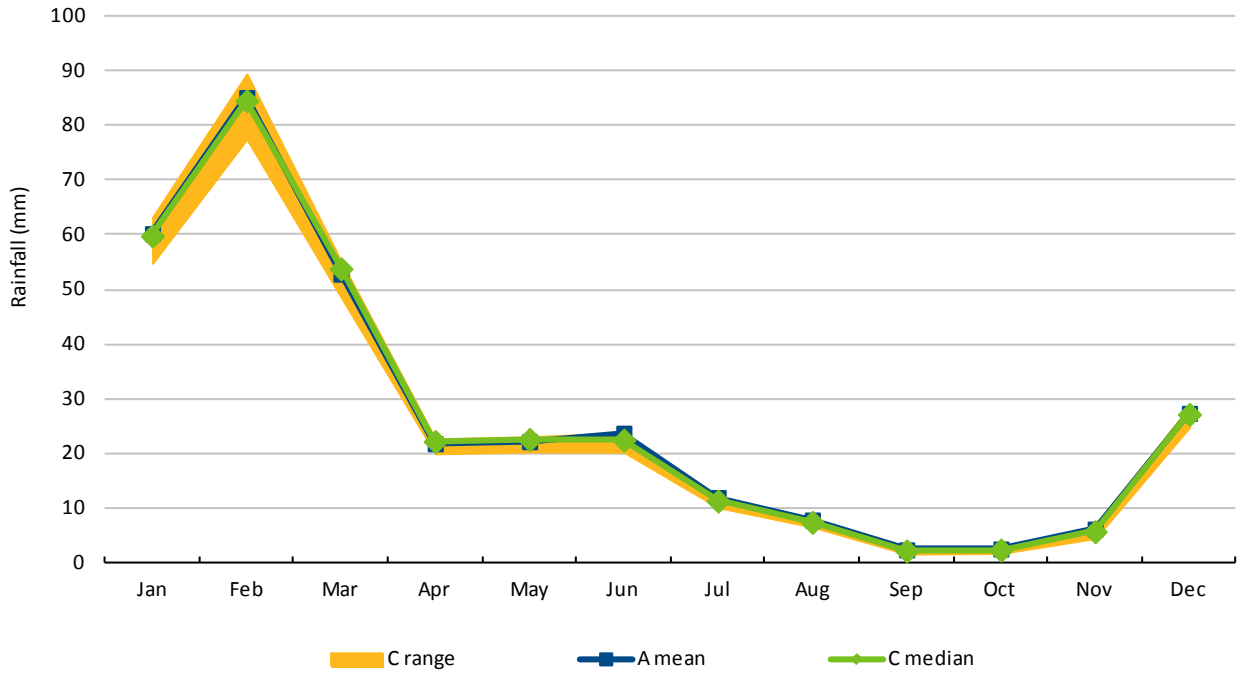

Figure 4.9 Assessment area mean monthly rainfall for Scenario A (A mean) and 2030 RCP8.5 Scenario C median (C median) and range (C range, from 10th to 90th percentile seasonal changes of 18 GCMs)

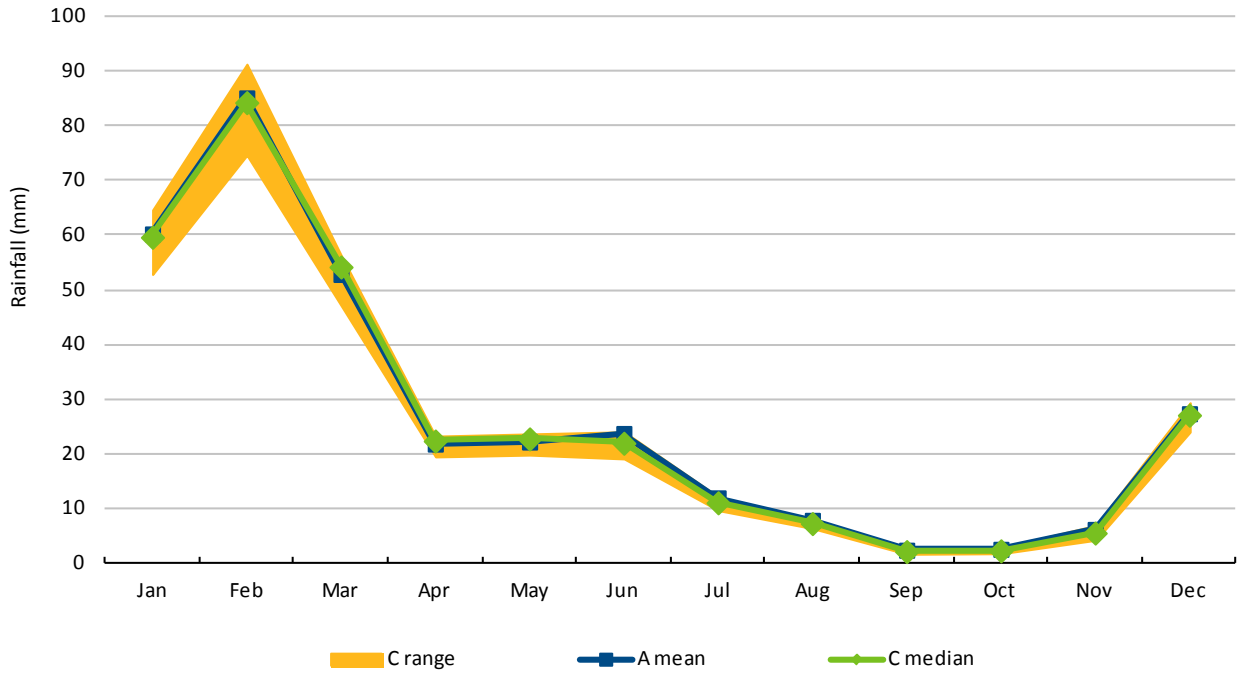

Figure 4.10 Assessment area mean monthly rainfall for Scenario A (A mean) and 2050 RCP8.5 Scenario C median (C median) and range (C range, from 10th to 90th percentile seasonal changes of 18 GCMs)

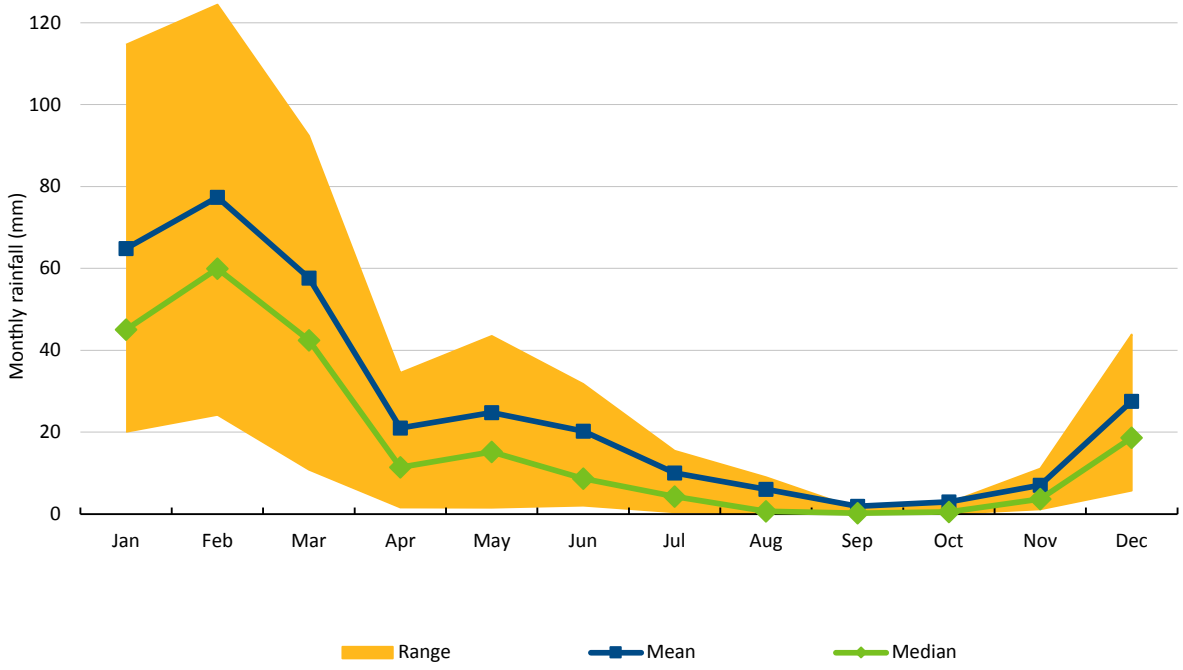

Figure 4.11 Assessment area Scenario Cwet 2050 RCP8.5 monthly rainfall (mean, median and 20th to 80th percentile monthly rainfall range)

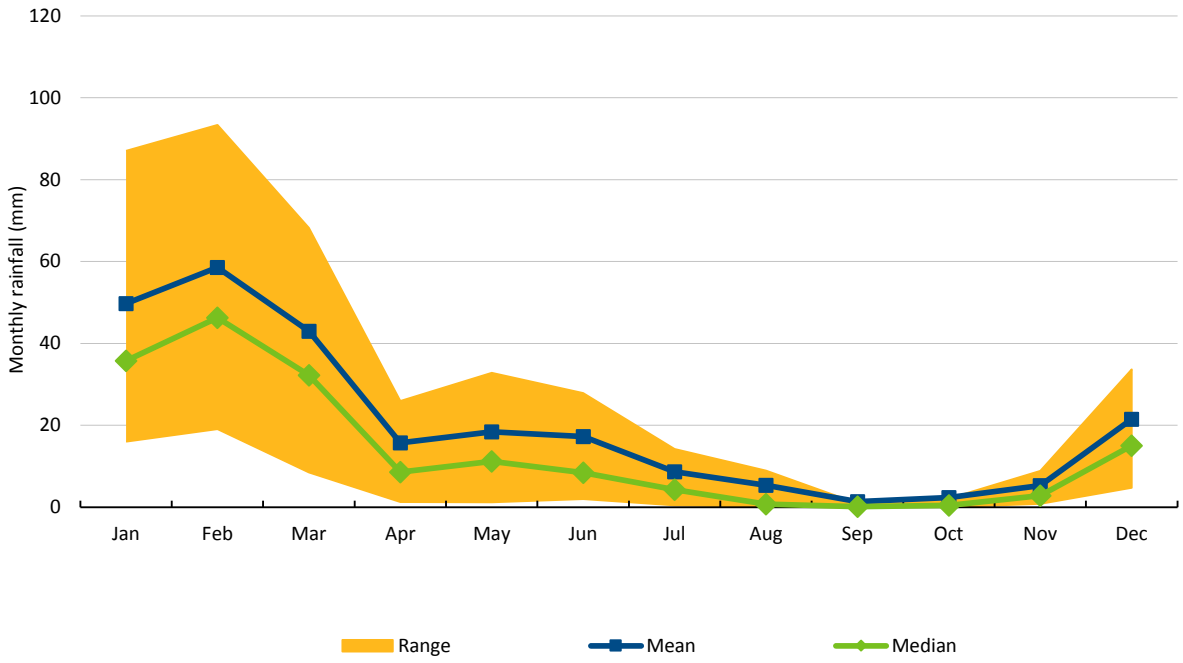

Figure 4.12 Assessment area Scenario Cdry 2050 RCP8.5 monthly rainfall (mean, median and 20th to 80th percentile monthly rainfall range)

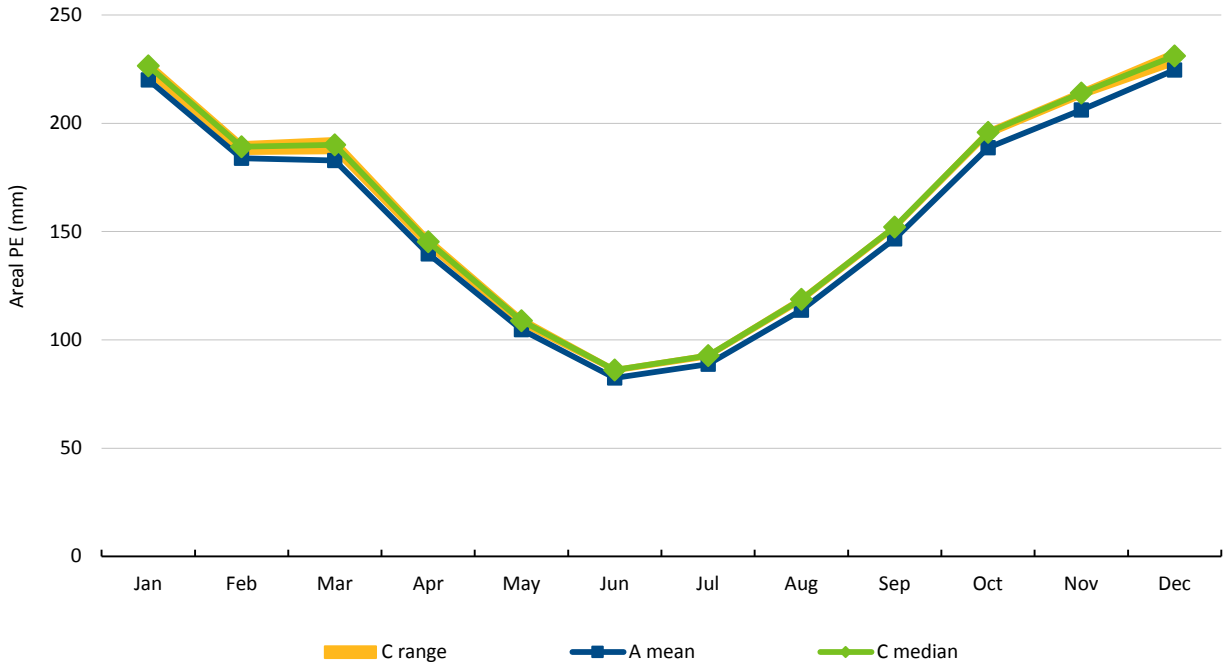

Figure 4.13 Assessment area mean monthly areal PE for Scenario A (A mean) and 2030 RCP8.5 Scenario C median (C median) and range (C range, from 10th to 90th percentile seasonal changes of 18 GCMs)

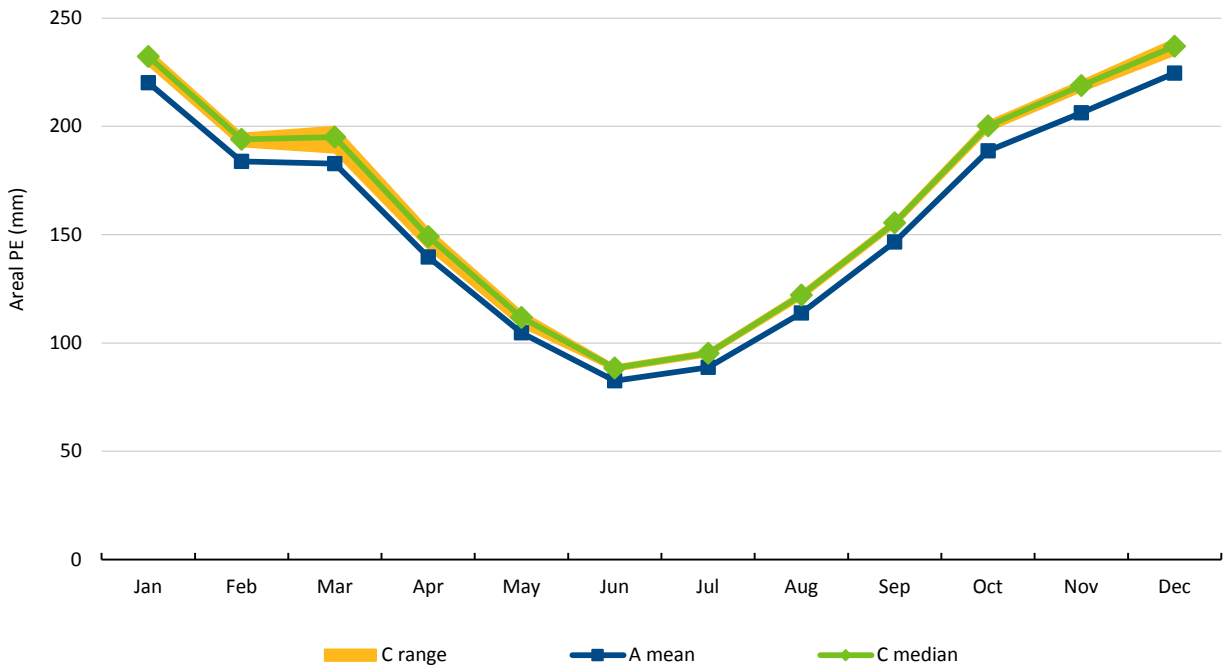

Figure 4.14 Assessment area mean monthly areal PE for Scenario A (A mean) and 2050 RCP8.5 Scenario C median (C median) and range (C range, from 10th to 90th percentile seasonal changes of 18 GCMs)

4.5 References

Chiew FHS, Kirono DGC, Kent DM, Frost AJ, Charles SP, Timbal B, Nguyen KC and Fu G (2010) Comparison of runoff modelled using rainfall from different downscaling methods for historical and future climates. Journal of Hydrology 387(1-2), 10-23.

Chiew FHS and Leahy C (2003) Comparison of evapotranspiration variables in Evapotranspiration Maps of Australia with commonly used evapotranspiration variables. Australian Journal of Water Resources 7, 1-11.

Chiew FHS, Teng J, Vaze J, Post DA, Perraud JM, Kirono DGC and Viney NR (2009) Estimating climate change impact on runoff across southeast Australia: method, results, and implications of the modeling method. Water Resources Research 45(10), W10414. Doi: 10.1029/2008WR007338.

Crosbie RS, Dawes WR, Charles SP, Mpelasoka FS, Aryal S, Barron O and Summerell GK (2011) Differences in future recharge estimates due to GCMs, downscaling methods and hydrological models. Geophys. Res. Lett. 38(11), L11406. Doi: 10.1029/2011gl047657.

CSIRO (2009) Groundwater yields in south-west Western Australia. A report to the Australian Government from the CSIRO South-West Western Australia Sustainable Yields Project. CSIRO Water for a Healthy Country Flagship, Australia.

CSIRO (2012) Proposed project methods. A report to the West Australian Government and industry partners from the CSIRO Pilbara Water Resource Assessment. CSIRO Water for a Healthy Country, Australia.

CSIRO and Bureau of Meteorology (2015) Climate Change in Australia: Projections for Australia's Natural Resource Management Regions: Technical Report. CSIRO and Bureau of Meteorology, Australia.

Donohue RJ, McVicar TR and Roderick ML (2010) Assessing the ability of potential evaporation formulations to capture the dynamics in evaporative demand within a changing climate. Journal of Hydrology 386(1-4), 186-197. Doi: 10.1016/j.jhydrol.2010.03.020.

Knutti R and Sedlacek J (2013) Robustness and uncertainties in the new CMIP5 climate model projections. Nature Climate Change 3(4), 369–373. Doi: 10.1038/NCLIMATE1716.

Li L, Donohue R, McVicar T, Van Niel T, Teng J, Potter N, Smith I, Kirono D, Bathols J, Cai W, Marvanek S, Gallant S, Chiew F and Frost A (2009) Climate data and their characterisation for hydrological scenario modelling across northern Australia. A report to the Australian Government from the CSIRO Northern Australia Sustainable Yields Project. CSIRO Water for a Healthy Country Flagship, Australia.

McVicar TR, Roderick ML, Donohue RJ, Li LT, Van Niel TG, Thomas A, Grieser J, Jhajharia D, Himri Y, Mahowald NM, Mescherskaya AV, Kruger AC, Rehman S and Dinpashoh Y (2012) Global review and synthesis of trends in observed terrestrial near-surface wind speeds: Implications for evaporation. Journal of Hydrology 416, 182-205. Doi: 10.1016/j.jhydrol.2011.10.024.

Morton FI (1983) Operational estimates of areal evapotranspiration and their significance to the science and practice of hydrology. Journal of Hydrology 66(1–4), 1-76. Doi: http://dx.doi.org/10.1016/0022-1694(83)90177-4.

Mpelasoka FS and Chiew FHS (2009) Influence of rainfall scenario construction methods on runoff projections. Journal of Hydrometeorology 10(5), 1168–1183. Doi: 10.1175/2009JHM1045.1.

Taylor KE, Stouffer RJ and Meehl GA (2011) An Overview of CMIP5 and the Experiment Design. Bulletin of the American Meteorological Society 93(4), 485-498. Doi: 10.1175/BAMS-D-11-00094.1.

Van Vuuren DP, Edmonds J, Kainuma M, Riahi K, Thomson A, Hibbard K, Hurtt GC, Kram T, Krey V, Lamarque JF, Masui T, Meinshausen M, Nakicenovic N, Smith SJ and Rose SK (2011) The representative concentration pathways: an overview. Climatic Change 109(1–2), 5–31. Doi: 10.1007/s10584-011-0148-z.

Watterson IG, Bathols J and Heady C (2014) What influences the skill of climate models over the continents? Bulletin of the American Meteorological Society 95, 689-700. Doi: http://dx.doi.org/10.1175/BAMS-D-12-00136.1.

Watterson IG, Hirst AC and Rotstayn LD (2013) A skill-score based evaluation of simulated Australian climate. Australian Meteorological and Oceanographic Journal 63, 181-190.

5 Conclusions

Chapter 2 reviewed the large-scale atmospheric and oceanic processes which interact to influence the hydroclimate of the Pilbara, including tropical, sub-tropical and mid-latitude weather systems. These processes, together with local-scale climate (e.g. sea-breezes and thunderstorms) and geographic influences (e.g. distance inland and orography) result in significant climatic gradients across the Assessment area. The Assessment area experiences a large annual rainfall deficit as a result of relatively low but highly variable mean rainfall combined with continuously high potential evaporation (PE).

The mean annual rainfall averaged across the Assessment area for the 1911 to 2012 period is 299 mm, with an overall north to south gradient from 300 to 350 mm in the coastal north to less than 250 mm in the south, and up to 500 mm over parts of the Hamersley Ranges. There is strong seasonality with January to March producing 60% of annual rainfall. Year to year rainfall variability is high, ranging from 48 mm in 1924 to 731 mm in 2000 averaged across the Assessment area. Locally the range is much higher, an extreme example being a coastal location that had only 0.4 mm in its driest year (i.e. a virtually rain free year) and 737 mm in its wettest year.

There are long-term trends in rainfall that vary spatially, with a general increasing trend for the 1911 to 2012 period. The increasing trend is greater in the east for the 1961 to 2012 period, with a corresponding decreasing trend in the far west. A significantly wetter period of seven years from 1995 to 2001 has an annual average rainfall of 500 mm. Occurring towards the end of the record, this period contributes to increasing trends. This period had higher than average numbers of Tropical Cyclones (TC), with TC frequency more prevalent during La Niña phases. The largest positive trends in monthly rainfall, for the 1961 to 2012 period, occur in the months of February, March and December. These months coincide with the seasonality of peak TC frequency.

Trends in the characteristics of annual extreme rainfall (annual daily maximum, 99th and 95th percentile rainfall amount), number of rain days and average rain-day intensity were examined spatially and correlated with annual rainfall to ascertain how they relate to the trends in annual rainfall. It appears the intensity of extreme daily rainfall (particularly 99th percentile) has a higher correlation with annual rainfall trends than number of rain days or average intensity characteristics. As the most extreme rainfall is often produced by TCs, this may also relate to the higher number of TCs in the 1995 to 2001 period.

Morton's wet areal formula gives an annual average PE that ranges from 1700 mm in the south-east to over 2000 mm in the northern coastal parts of the Assessment area. The seasonal cycle varies from an average 7.3 mm/day maximum in December and January to a 2.8 mm/day minimum in June and July. The resulting annual average rainfall deficit (i.e. annual rainfall minus PE) has a minimum of approximately 1200 mm around the Hamersley Ranges and a maximum up to 1750 mm along the Pilbara coastline and the eastern inland parts of the Assessment area.

Chapter 3 encompassed analyses of methods to quantify climate thresholds for runoff generation and groundwater recharge. Remotely sensed metrics of river pools and vegetation are related to these climate-related hydrological thresholds to aid ecological assessment under changing flow regimes and groundwater levels. Impacts of projected future climate on groundwater-dependent ecosystems (GDEs) have been investigated further based upon understandings of thresholds on a regional basis developed during the course of the Assessment (separate report).

Chapter 4 presented the methods used for future climate scenario generation and projected 2030 and 2050 changes calculated from a set of 18 CMIP5 GCMs, for medium (RCP4.5) and high (RCP8.5) scenarios being used in the IPCC Fifth Assessment Report. These results indicate the largest magnitude changes are projected to result from decreases in December to February rainfall under the high emissions scenario.

The median projected changes in annual rainfall are small, with little change by 2030 or 2050 for the RCP4.5 scenario and reductions of 1.8% for 2030 and 2.5% for 2050 for the RCP8.5 scenario. Whilst the median changes are small, there is a large variation across the 18 GCMs with projections ranging from -18% to +7% for 2030 and -22% to +8% for 2050. About 60% of the GCMs project drier conditions. These rainfall changes will have larger proportional impacts on hydrology when combined with the projected higher temperatures and PE. All models project increases in PE, driven mainly by temperature increases. The median projected changes to annual PE are an increase of 3% for 2030 and 5 to 7% for 2050. These median rainfall and PE projections suggest the Pilbara will become slightly drier by 2030 and 2050. Whilst a slight majority of models project drier and warmer conditions, several indicate that the Pilbara could become wetter and warmer. These wetter models should not be discounted, even though they are in the minority, as they are better at reproducing some of the large-scale climate processes influencing Pilbara hydroclimate compared to the drier models (see the GCM evaluation in: www.climatechangeinaustralia.gov.au/en/publications-library/technical-report/). As well as using the median scenarios in hydrological modelling, drier and wetter scenarios have also been used to assess the range of possible impacts.

There is limited information on future rainfall intensity changes because development of the fine-scale modelling required is a rapidly developing area of research that is still in its infancy. Thus it is not possible, based on current knowledge, to provide projections of sub-daily IFD changes suitable for flood modelling.

CONTACT US

t 1300 363 400
+61 3 9545 2176
e enquiries@csiro.au
w www.csiro.au

AT CSIRO WE INVENT THE FUTURE

We do this by using science and technology to solve real issues. Our solutions make a difference to industry, people and the planet.
As Australia's national science agency we've been pushing the edge of what's possible for almost 90 years. Today we have thousands of talented people working across Australia and internationally. Our people work closely with industry and communities to leave a lasting legacy. Collectively, our innovation and excellence places us in the top ten applied research agencies in the world.
We collaborate to innovate.

FOR FURTHER INFORMATION

CSIRO Land and Water
Dr Steve Charles
t +61 8 9333 6795
e Steve.Charles@csiro.au
w www.csiro.au/en/Research/LWF

For an electronic version of this report and other materials pertaining to the Pilbara Water Resource Assessment visit http://www.csiro.au/Pilbara-water-assessment.